

AD-A092 720

POLYTECHNIC INST OF NEW YORK FARMINGDALE MICROWAVE R--ETC F/G 4/1  
IONOSPHERIC SCINTILLATION (U)

SEP 80 D M WU

N00014-76-C-0176

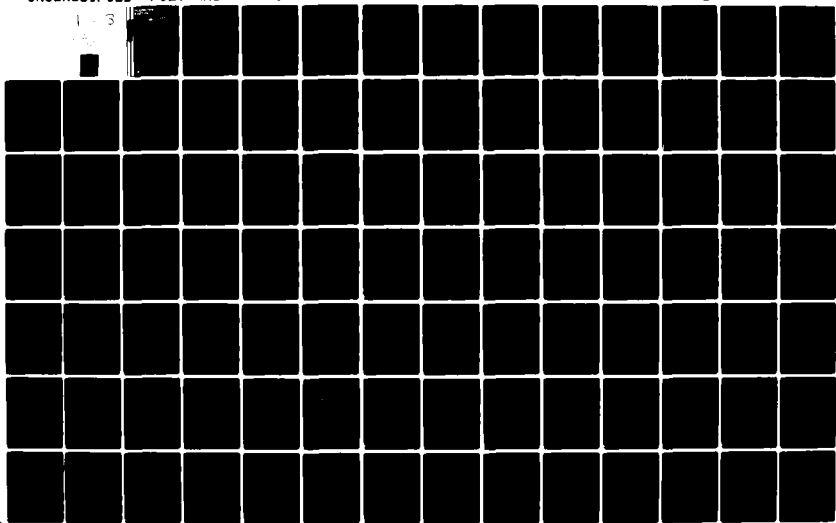
UNCLASSIFIED

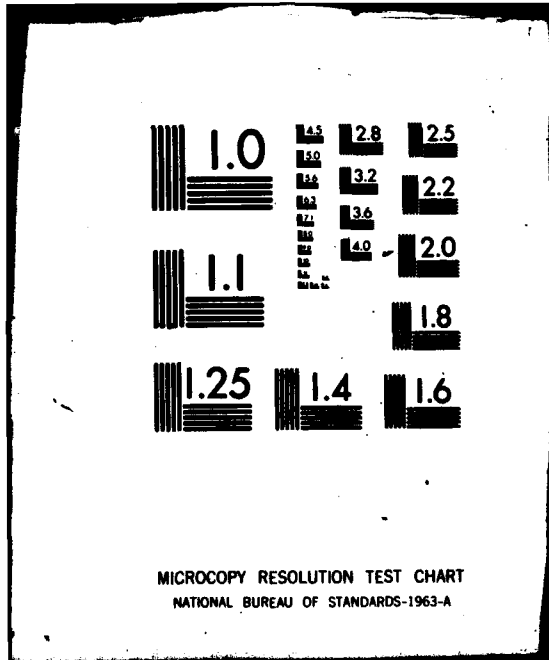
POLY-MRI-1410-80

NL

1-3

1-3





MICROCOPY RESOLUTION TEST CHART  
NATIONAL BUREAU OF STANDARDS-1963-A

**Polytechnic  
Institute**

**of New York**

**MRI**

**LEVEL II**

6

POLY-MRI-1410-80  
September 1980

**IONOSPHERIC SCINTILLATION**

by

*David M. Wu*

**SDTIC  
ELECTE  
DEC 0 4 1980  
E**

**DISTRIBUTION STATEMENT A**

**Approved for public release;  
Distribution Unlimited**

Prepared for

**OFFICE OF NAVAL RESEARCH**

Contract No. N00014-76-C-0176

**80 11 24 052**

AD A092720

**DDC FILE COPY**

UNCLASSIFIED

SECURITY CLASSIFICATION OF THIS PAGE (When Data Entered)

REPORT DOCUMENTATION PAGE		READ INSTRUCTIONS BEFORE COMPLETING FORM
1. REPORT NUMBER	2. GOVT ACCESSION NO. AD-A092 720	3. RECIPIENT'S CATALOG NUMBER
4. TITLE (and Subtitle) IONOSPHERIC SCINTILLATION		5. TYPE OF REPORT & PERIOD COVERED
6. AUTHOR(s) David M./Wu		7. PERFORMING ORG. REPORT NUMBER POLY-MRI-1418-80
8. PERFORMING ORGANIZATION NAME AND ADDRESS Polytechnic Institute of New York Microwave Research Institute Route 110, Farmingdale, NY 11735		9. CONTRACT OR GRANT NUMBER(s) N00014-76-C-0176
10. CONTROLLING OFFICE NAME AND ADDRESS Office of Naval Research 800 N. Quincy Street Arlington, VA 22217		11. PROGRAM ELEMENT, PROJECT, TASK AREA & WORK UNIT NUMBERS
12. MONITORING AGENCY NAME & ADDRESS (if different from Controlling Office)		13. REPORT DATE September 1980
		14. NUMBER OF PAGES 230
		15. SECURITY CLASS. (of this report) Unclassified
		16. DECLASSIFICATION/DOWNGRADING SCHEDULE
17. DISTRIBUTION STATEMENT (of this Report) Approved for public release; distribution unlimited.		
18. DISTRIBUTION STATEMENT (of the abstract entered in Block 20, if different from Report)		
19. SUPPLEMENTARY NOTES		
20. KEY WORDS (Continue on reverse side if necessary and identify by block number) Scintillations Ionosphere Turbulence		
21. ABSTRACT (Continue on reverse side if necessary and identify by block number) A renormalization technique, employed in the spirit of the formal theory of scattering, is applied to the problem of ionospheric scintillation. Using the forward scattering approximation for wave propagation and a Markov approximation for ionospheric fluctuations, one derives renormalized moment equations descriptive of the wave statistics.  The propagation of the two and four point wave statistics through the ionosphere are obtained using a slow quasiparticle distribution function $S$ . For the case of an ionospheric structure function $H(\ell) = a \ell^{-\alpha}$ , where $\ell$ is a		

DD FORM 1 JAN 73 1473

UNCLASSIFIED  
SECURITY CLASSIFICATION OF THIS PAGE (When Data Entered)

412081 685

UNCLASSIFIED

SECURITY CLASSIFICATION OF THIS PAGE (When Data Entered)

20. ABSTRACT - Continued

transverse distance, one can obtain exact analytical solutions for the wave statistics. For an arbitrary fluctuation spectrum, one can evaluate the S function along a quasiparticle trajectory and thereby infer second moments exactly and fourth moments approximately. Knowledge of the S function enables one to ascertain statistical properties, such as average intensity, two point intensity correlation and the scintillation index  $S_4$ .

The Scintillation index for the case of a plane wave propagating through the ionosphere is studied for the case of an arbitrary power spectrum of ionospheric fluctuations. Peaks superposed on a power law spectrum are found to increase the value of  $S_4$ . A focusing effect on the  $S_4$  vs. z variation is observed in the strong scintillation limit.

An experimental power spectrum, corresponding to relative density fluctuations of about 20% as obtained from in situ measurements by the Atmospheric Explorer-E satellite, is used to calculate the corresponding  $S_4$  for night time equatorial scintillations. For an ionospheric slab model with a thickness of 200 Km and an altitude of 300 Km numerical calculations yield, in approximate agreement with Dr. Basu, an almost saturated scintillation index  $S_4$  of about 1.1.



UNCLASSIFIED

SECURITY CLASSIFICATION OF THIS PAGE (When Data Entered)

### ACKNOWLEDGMENT

The research reported herein has been supported by the Office of Naval Research under Contract No. N00014-76-C-0176.

This work is a portion of a Ph. D. thesis in Electrophysics at the Polytechnic Institute of New York.

The author wishes to express his gratitude to Professor N. Marcuvitz, for his guidance and encouragement. He is also indebted to Dr. S. Barone and Dr. S. Basu for their helpful discussions and criticisms.

Accession For	
NTIS GRA&I	<input checked="" type="checkbox"/>
DDC TAB	<input type="checkbox"/>
Unannounced	<input type="checkbox"/>
Justification	
By _____	
Distribution/	
Availability Codes	
Dist	Avail and/or special
A	

## TABLE OF CONTENTS

	<u>Page</u>	
Chapter 1	INTRODUCTION	1
	I. Motivation	1
	II. General Introduction and Review	2
Chapter 2	THEORETICAL ANALYSIS	7
	I. Problem Description	7
	II. Theory of Multiple Scattering	11
	III. Markov Approximation	21
	IV. The Equation for the Mean Field	23
	V. Parabolic Equation for the Mutual Coherence Function	27
	VI. The Equation for Fourth Order Moment	30
Chapter 3	SOLUTIONS FOR THE MUTUAL COHERENCE FUNCTION	34
	I. "Slow" and "Fast" Quasiparticle Distribution Functions	34
	II. Exact Solution of Mutual Coherence Function for the Case $H(f) = a f^2$	40
	III. Numerical Evaluation of Mutual Coherence Function for a Complicated Power Spectrum	55
	IV. Conclusion and Discussion	93
Chapter 4	THE FOURTH MOMENT AND INTENSITY FUNCTION	101
	I. Formulation of the Fourth Moment Equation	101
	II. The Exact Solution for the Case $H(f) = a f^2$	103
	III. Approximate Solution for the Fourth Moment	110
	IV. The Boundary Conditions and Steady State Solution for Plane Wave Case	116
	V. Numerical Solution for $M_4$ in Plane Wave Case	121
	VI. Discussion and Conclusion	128
Chapter 5	THE INTENSITY FLUCTUATION AND SCINTILLATION INDEX	145
	I. Definition of Intensity Correlation Function and Scintillation Index	145
	II. Numerical Solution of Scintillation Index for Arbitrary Power Spectrum	148
	III. Application and Discussion	158
Appendix 1	Renormalization Methods	161
Appendix 2	Convergent Series for $V_c G$	171
Appendix 3	The Limit of Application of the Markov Approximation	181
Appendix 4	Convergence of the Green's Function	185
Appendix 5	Limits of Application of the Parabolic Equation	200
Appendix 6	Numerical Scheme for Solving $M_4$	208
Bibliography		210

TABLE OF FIGURES

<u>Fig. No.</u>		<u>Page</u>
1	Mutual Coherence Function at $z = 0$ .	52
1a	Amplitude of MCF at $z = 0.5$ ; free space.	53
1b	Amplitude of MCF at $z = 1$ ; free space.	53
1c	Amplitude of MCF at $z = 1.5$ ; free space.	54
1d	Amplitude of MCF at $z = 2$ ; free space.	54
2a.	Amplitude of MCF at $z = 0.5$ ; $H(\xi) = a\xi^2$ , $a = 1$ .	56
2b	Amplitude of MCF at $z = 1$ ; $H(\xi) = a\xi^2$	56
2c	Amplitude of MCF at $z = 1.5$ ; $H(\xi) = a\xi^2$	57
2d	Amplitude of MCF at $z = 2$ ; $H(\xi) = a\xi^2$	57
3	Normalized MCF vs. $\xi$ for different values of $z$ ; collimated beams in free space.	58
4	Normalized MCF vs. $\xi$ for different values of $z$ ; focused beams in free space.	58
5	Normalized MCF vs. $\xi$ for different values of $z$ ; collimated beam; $H(\xi) = a\xi^2$ , $a=1$ .	59
6	Normalized MCF vs. $\xi$ for different values of $z$ ; focused beam; $H(\xi) = a\xi^2$ , $a=1$ .	59
7	Normalized MCF vs. $\xi$ for different values of $a$ ; $H(\xi) = a\xi^2$ ; collimated beam.	60
8	Normalized MCF vs. $\xi$ for different values of $a$ ; $H(\xi) = a\xi^2$ ; focused beam.	60
9a	Normalized MCF vs. $\xi$ for different values of beam width $b$ ; collimated beam.	61
9b	Normalized MCF vs. $\xi$ for different values of beam width $b$ ; focused beam.	61

<u>Fig. No.</u>		<u>Page</u>
10	Initial slow q.p. distribution function for collimated beam.	63
11	Collimated beam propagating in free space, $z = 0.75$ .	63
12	$z = 1.5$	64
13	MCF vs. $\xi$ at different values of $z$ ; free space; $x = 0$ .	64
14	Initial slow q.p. distribution function for focused beam.	65
15	Focused beam propagating in free space, $z = 0.75$ .	65
16	$z = 1.5$ .	66
17	MCF vs. $\xi$ at different values of $z$ ;	66
18	Intensity function vs. $x$ ; collimated beam propagating in free space.	66b
19	Intensity function vs. $x$ ; focused beam propagating in free space.	66
20a	Power spectrum vs. $k$	70
20b	Structure functions vs. $\xi$	70
21a	$H(\xi)$ vs. $\xi$ for spectrum (c).	71
21b	$H(\xi)$ vs. $\xi$ for spectrum a,b,c.	71
22a	S function for a collimated beam, $z=0$ .	73
22b	S function for a focused beam, $z=0$ .	73
23a	S function for a focused beam; $z=0.4375$ ; power law spectrum with $p = 4$ .	74
23b	$z = 0.875$	75
23c	$z = 1.3125$ .	75
23d	$z = 1.75$ .	75

<u>Fig. No.</u>		<u>Page</u>
24a	S function for a focused beam; $z = 0.4375$ ; power law spectrum with peaks;	77
24b	$z = 0.875$ .	77
24c	$z = 1.3125$ .	77
24d	$z = 1.75$ .	77
25a	S function for a collimated beam; $z=0.4375$ ; power law spectrum with peaks. $k'=1$ .	79
25b	$z = 0.875$ .	80
25c	$z = 1.3125$ .	80
25d	$z = 1.75$ .	80
26a	S function for a collimated beam; $z = 0.4375$ ; power law spectrum with peaks, $k'=3$ .	81
26b	$z = 0.875$ .	81
26c	$z = 1.3125$ .	82
26d	$z = 1.75$ .	82
27a	$z = 0.4375$ , $k' = 4$ .	83
27b	$z = 0.875$ , $k' = 4$ .	83
27c	$z = 1.3125$ , $k' = 4$ .	84
27d	$z = 1.75$ , $k' = 4$ .	84
28a.	$(2\pi)^{\frac{1}{2}}$ vs. $z$ dotted line; $I(0,z)$ vs. $z$ solid line; collimated beam; $H=a\xi^2$ .	86
28b	$(2\pi)^{\frac{1}{2}}$ vs. $z$ ; $I(0,z)$ vs. $z$ , focused beam.	86
29a	$(2\pi)^{\frac{1}{2}}$ vs. $z$ ; $I(0,z)$ vs. $z$ ; Gaussian spectrum; collimated beam.	87
29b	Focused beam case.	87

<u>Fig. No.</u>		<u>Page</u>
30a	$(2\pi)^{\frac{1}{2}} I$ vs. $z$ ; $I(0,z)$ vs. $z$ ; collimated beam; power law spectrum, $p = 4$ .	88
30b	Focused beam case.	88
31a	$(2\pi)^{\frac{1}{2}} I$ vs. $z$ ; $I(0,z)$ vs. $z$ ; Power law spectrum with peaks, $k' = 1$ . collimated beam.	90
31b	focused beam case.	90
32a	$(2\pi)^{\frac{1}{2}} I$ vs. $z$ ; $I(0,z)$ vs. $z$ ; collimated beam; power law spectrum with peaks.	91
32b	focused beam case. $k' = 1$ .	91
33a	Collimated beam case, $k' = 3$ .	92
33b	Focused beam case; $k' = 3$ .	92
34	Quantitative representation of S function; collimated beam case.	94
35	Focused beam case.	94
36	Quantitative plot of structure function in phase space.	97
37	S function of a collimated beam moving in a random medium characterized by H.	97
38	Focused beam case.	97
39a	Quasiparticle density function, at $x = 0$ , in $\xi$ space. collimated beam case.	98
39b	Normalized $M(0, \xi, z)$ vs. $\xi$ and $z$ ; collimated beam case..	98
40a	Quasiparticle density function; focused beam case.	99
40b	Normalized $M(0, \xi, z)$ vs. $\xi$ and $z$ ; focused beam case.	99

<u>Fig. No.</u>		<u>Page</u>
41	$f(r_1, r_2)$ vs. $r_1$ and $r_2$ ; power spectrum with $p = 4$ .	126
42	$M_4$ vs. $r_1$ and $r_2$ ; plane wave case; power spectrum with $p = 4$ , $z = 0.1125$ .	126
43	$z = 0.1725$ .	127
44	$z = 0.24$ .	127
45	$M_4$ vs. $r_1$ and $r_2$ ; $z = 0.4275$ from the bottom of the random slab, $L = 0.24$ .	129
46	$z = 0.6525$ .	129
47.	$z = 0.8775$ .	130
48	$z = 1.1025$ .	130
49	(1) $\langle \hat{I} \rangle$ vs. $z$ ; (2) $\langle \hat{I}^2 \rangle$ vs. $z$ ; (3) $S_4$ vs. $z$ ; collimated beam, $H = a \xi^2$ .	133
50	$a = 5$ .	133
51	Focused beam case, $a = 1$ .	134
52	$a = 5$ .	134
53	A modulated collimated beam propagating in free space; $L = 0.25$ , $a = 5$ ;	135
54	A modulated focused beam case.	135
55	A modulated collimated beam case; $a=10$ .	137
56	A modulated focused beam case; $a =10$ .	137
57	$S_4$ vs. $z$ for $a = 2$ to 16 with a step of 2; collimated beam in free space.	138
58	Focused beam case.	138
59	(1) $\langle \hat{I} \rangle$ vs. $z$ ; (2) $\langle \hat{I}^2 \rangle$ vs. $z$ ; (3) $S_4$ vs. $z$ ; a modulated collimated beam; $L = 0.5$ , $a = 5$ .	139
60	Focused beam case.	139

<u>Fig. No.</u>		<u>Page</u>
61	A modulated collimated beam propagating in free space, $L=0.5$ , $a=10$ .	140
62	A modulated focused beam case.	140
63	$S_4$ vs. $z$ for $a = 2$ to $16$ , in step of $2$ ; collimated beam case, $L=0.5$ .	141
64	Focused beam case.	141
65	$S_4$ vs. $z$ for $L=0.125$ to $1$ , in step of $0.125$ ; collimated beam; $a = 10$ .	143
66	Focused beam case.	143
67	$S_4$ vs. $z$ ; approximated solution.	144
68	$S_4$ vs. $z$ ; $L = 0.24$ .	144
69	$S_4$ vs. $z$ ; Gaussian spectrum with $\mathcal{T} = 10$ ;	150
70	$S_4$ vs. $z$ ; Gaussian spectrum with $L=0.06$ .	150
71	$f(r_1, r_2)$ vs. $r_1$ and $r_2$ ; power law spectrum, $p = 4$ .	152
72	$f(r_1, r_2)$ vs. $r_1$ and $r_2$ ; Von Karmann spectrum with $p = 11/3$ .	152
73	$f(r_1, r_2)$ vs. $r_1$ and $r_2$ ; Von Karmann spectrum with a Gaussian peak, $k=2$ .	153
74	$f(r_1, r_2)$ vs. $r_1$ and $r_2$ ; Von Karmann spectrum with a Gaussian peak, $k=3$ .	153
75	$S_4$ vs. $z$ ; power law spectrum and Gaussian spectrum..	155
76	$S_4$ vs. $z$ ; Von Karmann spectrum.	155
77	$S_4$ vs. $z$ ; Von Karmann spectrum with a Gaussian peak.	156
78	$S_4$ vs. $z$ ; $L=0.12$ , $\mathcal{T} = 15$ ; Von Karmann spectrum and Von Karmann spectrum with a Gaussian peak.	156

<u>Fig. No.</u>		<u>Page</u>
79	$S_4$ vs. $z$ ; Von Karman spectrum with a Gaussian peak; $L = 0.12$ , $\gamma = 5, 15$ .	157
80	$S_4$ vs. $z$ for power law spectrum.	157
81	In situ power spectrum.	160b
82	$S_4$ vs. $z$ for a power spectrum in Fig. 81.	160b
A2.1	$V_C g$ vs. $g^2 \langle \tilde{V}^2 \rangle$ ; expansion a, b.	177
A2.2	$V_C g$ vs. $g^2 \langle \tilde{V}^2 \rangle$ ; expansion c.	177
A2.3	$V_C g$ vs. $g^2 \langle \tilde{V}^2 \rangle$ ; Gaussian random variable.	179
A2.4	$V_C g$ vs. $g^2 \langle \tilde{V}^2 \rangle$ ; $\tilde{V}$ is a truncated Gaussian.	179
A2.5	Same as A2.4; ratio = 3.623.	180
A2.6	Same as A2.4; ratio = 3.05.	180
A4.1	$g_{kr}$ vs. $B$ ; $\tilde{V}$ is uniformly distributed.	188
A4.2	The exact solution of $g_{kr}$ ; $\tilde{V} = 0.333$ .	188
A4.3	$g_{kr}$ vs. $B$ ; $\tilde{V}$ is uniformly distributed over $(-a, +a)$ ; $\langle \tilde{V}^2 \rangle = 2.083$ .	189
A4.4	Exact solution; $\langle \tilde{V}^2 \rangle = 2.083$ .	189
A4.5	$g_{kr}$ vs. $B$ ; $\tilde{V}$ is uniformly distributed over $(-a, +a)$ ; $\langle \tilde{V}^2 \rangle = 8.333$ .	190
A4.6	Exact solution; $\langle \tilde{V}^2 \rangle = 8.333$ .	190
A4.7	$g_{kr}$ vs. $B$ ; $\tilde{V}$ is Gaussian; $\langle \tilde{V}^2 \rangle = 1$ .	194
A4.8	$V_C g$ vs. $B$ ; $\tilde{V}$ is Gaussian; $\langle \tilde{V}^2 \rangle = 1$ .	194
A4.9	1st approximation of Fig. A4.8.	195
A4.10	2nd approximation of Fig. A4.8.	195

<u>Fig. No.</u>		<u>Page</u>
A4.11	$V_{cg}$ vs. B; $\tilde{v}$ is Gaussian; $\langle \tilde{v}^2 \rangle = 0.25$ .	196
A4.12	1st approximation of Fig. A4.11.	196
A4.13	2nd approximation of Fig. A4.11.	197
A4.14	$V_{cg}$ vs. B; $\tilde{v}$ is uniformly distributed over a range (-0.5, +0.5); $\langle \tilde{v}^2 \rangle = 0.083$ .	198
A4.15	1st approximation of Fig. A4.14.	198
A4.16	2nd approximation of Fig. A4.14.	199

## Chapter 1 INTRODUCTION

### I. Motivation

Wave propagation in random media has been studied over the last two decades. Heightened interest in this problem has been mainly due to the large number of problems that arise in radio physics, acoustics, plasma studies and certain other branches of physics. From the physical viewpoint random wave propagation can be analyzed at two levels: macroscopic, concerned with propagation in continuous random media such as turbulent fluids and microscopic, concerned with the scattering of waves by randomly distributed scatterers such as electrons, molecules, rain, blood cells. Wave propagation in continuous random media, applies to such problems as the scattering of sound and ultrasound waves in sea water, light scattering in the atmosphere, radio waves scattering in the ionosphere and the twinkling of stellar images. Wave propagation in discrete random media is of considerable interest for such problems as molecular scattering of light, wave scattered by the rain, and bioengineers may use the fluctuation and scattering characteristics of a sound wave as a diagnostic tool. The abundance and variety of such problems has stimulated development and refinement of statistical methods for calculating wave propagation in a random medium. This paper is mainly concerned with the wave propagation through an ionospheric random layer.

When a random wave from an extraterrestrial source, such as a radio star or an artificial satellite, passes through the ionosphere, its wavefront and amplitude will be distorted by the density fluctuation in the ionosphere plasma. On propagating to the ground, the resulting phase variations cause interference to occur and a diffraction pattern is set up across the ground. The resulting random variations

of the electromagnetic field are termed scintillations. In consequence, satellite based communications exhibit serious performance degradation, the degradation being most serious for propagation paths which transit the auroral and equatorial ionosphere. The importance of a thorough investigation of this problem is obvious.

## II. General Introduction and Review

Propagation models are required to provide satellite communication system and radar system designers with a means to translate the available ionospheric statistics into constraints for the specific systems that are being designed. Approximate models have been proposed that apply under restrictive conditions. Analyses of propagation effects generally start with the scalar wave equation. If the dominant scattering irregularities have dimensions much larger than a wavelength, depolarization effect can be neglected (1, 2). Let the wave field be represented by  $E = E \exp(-i\omega t)$ , where  $\omega = 2\pi f$ ,  $f$  is the carrier frequency,  $t$  is the time,  $E$  is the electric field vector and  $u$  is a component of  $E$ . If the dielectric properties of the medium change slowly in time in comparison with  $1/f$  and slowly in space in comparison with the wavelength  $\lambda$ , then with a monochromatic source, the propagation of the wave through a random irregularity region is governed by the scalar wave equation

$$\nabla^2 \hat{u} + k^2 \hat{\epsilon} \hat{u} = 0$$

(1.1)

where  $k = \frac{2\pi}{\lambda}$ ,  $\hat{\epsilon}$  is the dielectric constant and both  $\hat{u}$  and  $\hat{\epsilon}$  are random variables.  $\hat{\epsilon}$  enters as a coefficient of the unknown wave function  $\hat{u}$ . This is the root of all the mathe-

mathematical difficulties of the theory, since we don't know how to find an exact solution of such a wave equation. It is necessary to apply certain approximations that make use of the small parameters such as the fluctuation of  $\hat{\epsilon}$ , i.e. the deviation from the mean value. It can also be the smallness of the wavelength in comparison with the dimension of the inhomogeneities. In practice, two types of problems arise; the direct problem, in which one has to find the statistics of waves propagating in the medium from the known statistics of the medium, and the inverse problem wherein one draws conclusions about the properties of random inhomogeneities from the measured moments of the field. Actually, these two problems are equivalent, i.e. one needs to find the relation between the statistic of the medium and the wave field.

We shall assume for simplicity that the medium is on the average homogeneous and stationary. Removing these two restrictions does not give rise to any difficulties in principle. Under conditions usually encountered in ionospheric propagation, the energy is scattered into the forward direction and (1.1) can be replaced by the parabolic equation:

$$2ik_0 \frac{\partial \hat{U}}{\partial z} + \nabla_p^2 \hat{U} + k_0^2 \tilde{\epsilon} \hat{U} = 0 \quad (1.2)$$

where  $k_0 = k^2 \langle \hat{\epsilon} \rangle$ ,  $\hat{u} = \hat{U} \exp(ik_0 z)$ ,  $z$  is the direction of propagation, and  $\nabla_p^2 = \frac{\partial^2}{\partial x^2} + \frac{\partial^2}{\partial y^2}$ , the transverse Laplacian. Both the wave equation (1.1) and the parabolic equation (1.2) are stochastic. The wave properties of interest are the average, variance, and higher moment of  $\hat{U}$ . If  $\tilde{\epsilon}$  and  $\hat{U}$  were uncorrelated, these equations could be

solved easily. However,  $\tilde{\epsilon}$  and  $\hat{U}$  are generally correlated, the approximations used to provide solutions to (1.1) and (1.2) are all directed towards modeling the statistical relationship between  $\tilde{\epsilon}$  and  $\hat{U}$ . If  $\tilde{\epsilon}$  is small enough, then we can naturally resort to the method of perturbations, and expand in a power series in  $\tilde{\epsilon}$ , or more exactly in  $(\tilde{\epsilon}^2)^{1/2}$ .

A perturbation series solution to (1.2) can be formed that separates  $\tilde{\epsilon}$  and  $\tilde{U}$  where  $\tilde{U}$  describes the fluctuation in  $\hat{U}$ ,  $\hat{U} = \langle \hat{U} \rangle + \tilde{U}$ . The first term in the perturbation series for  $\tilde{U}$  is the Born or single-scattering approximation, which applies only when both  $\tilde{\epsilon}$  and  $\tilde{U}$  are small. When  $\tilde{U}$  is not small, a large number of terms in the perturbation series must be summed. The nth term of the series describes the n-fold scattering and contains the n-fold product  $\tilde{\epsilon}(r_1) \dots \tilde{\epsilon}(r_n)$ . Thus, in calculating the average  $\langle \hat{U} \rangle$ , we have to know the moments  $\langle \tilde{\epsilon}(r_1) \dots \tilde{\epsilon}(r_n) \rangle$  of  $\tilde{\epsilon}$  of all orders. The renormalization schemes of multiple-scattering theory attempt to solve this problem by a selective summation technique that leads to readily evaluated expressions for the moment of  $\tilde{U}$  of interest.

The Born approximation is shown to be valid when  $k_0 l$  is small, where  $l$  is the characteristic scale of the turbulent medium. As  $k_0 l$  increases, we must either take into account the higher order terms in the perturbation series or go over to other approximate methods which deal with multiple scattering to some extent. Rytov proposed that an equation for  $\hat{\psi} = \ln \hat{U}$  be used in place of (1.2). The equation for  $\hat{\psi}$  is then given by

$$-2k_0 \frac{\partial \hat{\psi}}{\partial z} + \nabla_r^2 \hat{\psi} + (\nabla_r \hat{\psi})^2 + k_0^2 \tilde{\epsilon} = 0$$

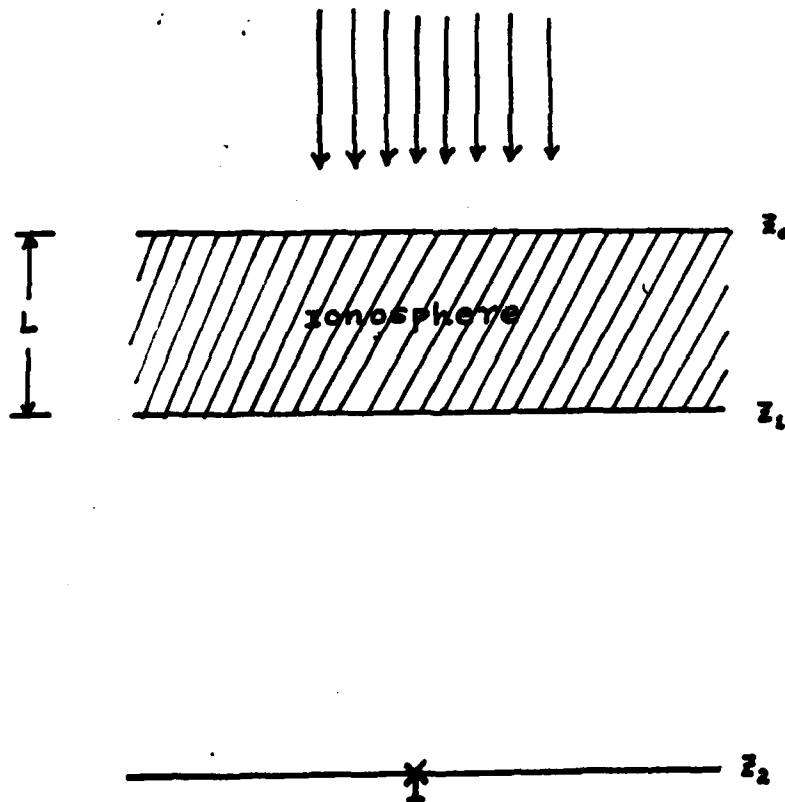
the equation has separated  $\hat{\Psi}$  and  $\tilde{\epsilon}$  so that the correlation between  $\hat{\Psi}$  and  $\tilde{\epsilon}$  is not explicit. A perturbation series expansion for  $\tilde{\Psi}$ , representing the fluctuation in  $\hat{\Psi}$ , can be formed to solve the nonlinear equation ( in  $\nabla_r \hat{\Psi}$  ). The zeroth order equation represents free space propagation. The 1st order equation for  $\tilde{\Psi}$  can be solved yielding the Rytov approximation, which is also called the method of smooth perturbations. The Rytov approximation is a weak scintillation approximation that hold for small  $\langle \tilde{\chi}^2 \rangle$ , where  $\tilde{\chi}$  is the fluctuation of the logarithm of the amplitude, it has a wider range of validity than the Born approximation.

The generally accepted model for ionospheric propagation thru a turbulent ionosphere has been the thin phase diffraction screen model (3). The ionospheric irregularities perturb the phase of the field at the layer and their effect upon the wave beyond the layer can be computed using diffraction theory. Mercier (4) and Briggs and Parkin (5) introduced a Gaussian correlation function to describe the phase fluctuation at the screen and related all higher moments to the second moment. Spectral analyses of observed phase and amplitude fluctuations have shown that the electron-density irregularities have a power spectrum that may be characterized by a power law shape. Rufenach (6) extended the phase-screen theory using a power law spectral shape for the irregularities.

For the weak scintillation case, the Born, Rytov and the thin phase screen approximations are all applicable. For strong scintillation and a thick layer, the effect of multiple scattering on transionospheric signals has to be taken into account.

Several techniques have been proposed to deal with the

strong fluctuation problem. They are the diagram method (DeWolf 1968, 1977; Tatarski 1971; Frisch 1968) (1, 7, 8) the integral equation method (Brown 1971, 1972), (9,10), including the Dyson and the Bethe-Salpeter equations, the extended Huygens-Fresnel principle (Kon 1970; Clifford 1974) (11, 12), and the parabolic equation method (Tatarski 1971; Furustsu 1972) (1, 13). In this paper, we shall apply the parabolic equation method to the case of radio wave on propagation through an ionospheric slab. First the statistical moments of waves are obtained inside the random slab. Then the free space propagation of resulting randomly modulated waves is analyzed from the bottom of the slab to a ground receiver. The geometry of this problem is shown in Fig. 1.



Chapter 2 THEORETICAL ANALYSIS

I. Problem Description

Ionospheric scintillation has been observed at frequencies ranging from 10 MHz to 6 GHz. The irregularities in the ionosphere which produce the fluctuations are believed to be mainly in the F-region, the layer of strong irregularities is often 100-500 km thick ranging from 200-700 km in altitude. The electron density fluctuations are often of the order of a few tens of per cent and can be as high as 70 per cent. The F-region irregularities are usually regarded as a stochastic process and characterized by three dimensional random functions which are assumed spatially and temporally stationary over the increments of interest. One defines the spatial correlation function  $B_N(\underline{r}'')$  of the density function by

$$B_N(\underline{r}'') = \frac{\langle \tilde{N}(\underline{r}_1) \tilde{N}(\underline{r}_2) \rangle}{\langle \tilde{N}^2 \rangle^{1/2}} \quad (2.1)$$

where  $\underline{r} = (x, y, z)$  is the position vector,  $\underline{r}'' = \underline{r}_1 - \underline{r}_2$  is the correlation lag vector,  $\langle \tilde{N}^2 \rangle^{1/2}$  is the rms density fluctuation, and  $\langle \rangle$  denotes the ensemble average. The relationship between the three dimensional power spectrum of the density fluctuation  $\Phi_N(\underline{k})$  and the density correlation function is given by the Fourier transform pair:

$$\Phi_N(\underline{k}) = \frac{\langle \tilde{N}^2 \rangle^{1/2}}{(2\pi)^3} \iiint_{-\infty}^{+\infty} B_N(\underline{r}'') e^{-i \underline{k} \cdot \underline{r}''} d\underline{r}'' \quad (2.2)$$

$$B_N(\underline{r}''') = \frac{1}{\langle \tilde{N}^2 \rangle} \iiint_{-\infty}^{+\infty} \Phi_N(\underline{k}) e^{i \underline{k} \cdot \underline{r}'''} d\underline{k} \quad (2.3)$$

the power spectrum is often characterized by a wide range of wave numbers, and hence designated as a wide-band process, whereas a narrow range of wave numbers associated with a Gaussian spectrum is designated narrow-band process. The wide-band process is important since it is inferred from the in-situ results. In the F-region, the wide range of wavenumbers corresponds to dimensions ranging from a few meters to hundreds of kilometers. If a Gaussian spectral shape is assumed, it is characterized by one dominant scale approximately equal to the Fresnel wave number. (about  $2\text{km}^{-1}$ ) (Brigg and Parkin 1963).

Referring to Fig. 1, let us consider a time harmonic radio wave incident on a region of ionospheric irregularities at  $z = z_0$ .  $L$  is the thickness of the slab. Inside the irregular region, the relative dielectric permittivity is given by

$$\hat{\epsilon}(\underline{r}) = \epsilon_0(z) [1 + \tilde{\epsilon}(\underline{r})] \quad (2.4)$$

where one models a collisionless ionospheric plasma by

$$\epsilon_0(z) = 1 - \frac{\omega_{p_0}^2(z)}{\omega^2} \quad (2.5)$$

$$\tilde{\epsilon}(\underline{r}) = - \frac{\omega_{p_0}^2 / \omega^2}{1 - \omega_{p_0}^2 / \omega^2} \left[ \frac{\tilde{N}(\underline{r})}{N_0} \right] \quad (2.6)$$

$\omega_{p_0}(\underline{z})$  is the plasma frequency for the background electron density profile,  $\tilde{N}(\underline{r})/N_0$  is the percentage fluctuations of the electron density. In the following, we shall assume that  $\tilde{N}(\underline{r})$  is a homogeneous, isotropic random field while  $N_0$  is taken as constant.

The wave first travels through the ionospheric slab of length  $L$ , at  $z = z_1$  the modulated wave enters the free region, and it is detected at  $z = z_2$ . Therefore, there are two regions: in the first region, the incident wave at  $z_0$  is deterministic and the outgoing wave at  $z_1$  becomes stochastic. In the second region, the entering wave at  $z_1$  has a stochastic modulation but the medium is deterministic.

Writing the scalar wave field as

$$\hat{E} = \hat{u}(\underline{r}) e^{i k_0 z} \quad (2.7)$$

where the  $\exp(-i\omega t)$  dependence is omitted,  $k^2 \epsilon_0 \rightarrow k_0$ , and  $\hat{u}(\underline{r})$  is the complex amplitude of the wave. Substituting (2.7) into the wave equation (1.1), we obtain an equation for  $\hat{u}(\underline{r})$

$$2ik_0 \frac{\partial \hat{u}}{\partial z} + \nabla^2 \hat{u} + k_0^2 \tilde{\epsilon}(r) \hat{u} = 0 \quad (2.8)$$

where  $\nabla_p^2 \equiv \nabla^2 - \frac{\partial^2}{\partial z^2}$ . If the complex amplitude  $\hat{u}$  varies markedly over distances of the order of the inhomogeneity scale  $l$ , the second derivative  $\partial^2 \hat{u} / \partial z^2$  is of the order of  $\hat{u}/l^2$ . On the other hand, the term  $2ik_0 \partial \hat{u} / \partial z$  in (2.8) is of the order of  $\hat{u}/\lambda$ . Therefore, for  $\lambda \ll l$ , the term  $\partial^2 \hat{u} / \partial z^2$  is small compared to the first term in (2.8). Thus, one can replace  $\nabla^2 \hat{u}$  in (2.8) by the transverse Laplacian  $\nabla_p^2 \hat{u}$  and obtain the parabolic equation

$$2ik_0 \frac{\partial \hat{u}}{\partial z} + \nabla_p^2 \hat{u} + k_0^2 \tilde{\epsilon}(r) \hat{u} = 0 \quad (2.9)$$

This is the starting point of our analysis, in the later sections, we shall examine the statistical properties of  $\hat{u}$ ; they are specified by the infinite set of correlation functions

$$\begin{aligned} & \Gamma_{mn} (z, \rho_1, \rho_2, \dots, \rho_m; \rho'_1, \rho'_2, \dots, \rho'_n) \\ & = \langle \hat{u}(z, \rho_1) \dots \hat{u}(z, \rho_m) \hat{u}^*(z, \rho'_1) \dots \hat{u}^*(z, \rho'_n) \rangle \end{aligned} \quad (2.10)$$

The problem is to manipulate equation (2.9) to obtain equations for  $\Gamma_{mn}$  in terms of the statistical properties of  $\tilde{\epsilon}(\underline{r})$ .

## II. Theory of Multiple Scattering

The general theory of multiple scattering has been developed by many authors. (Bourret 1961, Apresyan 1973, Tatarski 1971, Marcuvitz 1974, DeWolf 1979). The Green's function method, which had previously been investigated in quantum field theory, was applied to the problem of wave propagation in a random medium. People have used the Dyson equation for the average field, and the Bethe-Salpeter equation for the covariance  $B = \langle \hat{u}(\underline{r}_1) \hat{u}^*(\underline{r}_2) \rangle$ . However, one cannot derive such closed equations by averaging the original differential equations for the field because moments of different orders are coupled together. Bourret (14) was the first person to apply the graph technique to scattering of waves in a continuous fluctuating medium. He assumed that the parameters of the medium fluctuate according to a normal law and are statistically independent of the sought field. This led to an approximate expression for the effective average dielectric constant proportional to the correlation function  $\langle \tilde{\epsilon}(\underline{r}_1) \tilde{\epsilon}(\underline{r}_2) \rangle$  of the medium. A more detailed derivation of the equations for the average and 2 point correlation assuming a normal law for a fluctuating medium is due to Tatarski, and to Frisch who admitted deviations from the normal law.

The utility of series representations is dependent on the rapidity of convergence. Operator techniques employed in the spirit of the formal theory of scattering was shown by Marcuvitz (1974), to provide alternative and formally exact representations of turbulent field quantities and their n-point ensemble averages. In appropriate parametric ranges these formally exact expressions are expandable into rapidly

convergent series. In this section, we shall apply this technique to the average equation and investigate its convergence.

In abstract the wave equation (2.9) can be written as

$$(L_0 - \tilde{V}) \hat{f} = 0 \quad (2.11)$$

where, in a  $\rho, z$  space the unperturbed operator  $L_0$  and the perturbation  $\tilde{V}$ , whose average  $\langle \tilde{V} \rangle = 0$ , are represented by

$$\begin{aligned} L_0 &\longrightarrow 2ik_0 \frac{\partial}{\partial z} + \frac{\partial^2}{\partial \rho^2} \\ \tilde{V} &\longrightarrow -k_0^2 \tilde{\epsilon} \end{aligned} \quad (2.12)$$

equation (7) is a generic operator equation for the field, with the initial condition acting as a impulsive source applied at  $z = 0$ . It is convenient to define a stochastic Green's function such that

$$(L_0 - \tilde{V}) \hat{G} = \underline{1} \quad (2.13)$$

where in  $\rho, z$  space

$$\begin{aligned} \hat{G} \hat{f} &\longrightarrow \int \hat{g}(\rho, z; \rho', z') \hat{f}(\rho', z') d\rho' dz' \\ \underline{1} &\longrightarrow \delta(\rho - \rho') \delta(z - z') \end{aligned} \quad (2.14)$$

and  $\delta(x)$  is the Dirac delta function. For uniqueness,  $G$  will be distinguished by the requirement

$$\hat{g}(p, z, p', z') = 0 \quad (z < z') \quad (2.15)$$

If we introduce  $G_0$  as unperturbed operator inverse to the operator  $L_0$ , and defined by

$$L_0 G_0 = \underline{1} \quad (2.16)$$

where the domain of  $L_0$  is such that

$$G_0 \longrightarrow g_0(p, z, p', z') = 0 \quad (2.17)$$

as is the case for  $\hat{G}$ .

The ensemble average  $G$  of  $\hat{G}$  is taken to satisfy

$$(L_0 - V_C) G = \underline{1} \quad (2.18)$$

and depends on the "smoothed" scattering operator  $V_C$  defined below. Eq. (2.18) provides a nonlinear defining equation for  $G$ , the nonlinearity arising from the dependence of  $V_C$  on  $G$ .

A stochastic operator  $T_c$ , with zero ensemble average, is defined by

$$\hat{G} = G + G \tilde{T}_c G \quad (2-19)$$

which represents the multiple scattering in the smoothed background  $G$ . One can derive the expression for  $\tilde{T}_c$  in terms of  $G$  and a power series in  $\tilde{V}$  to 4th order in  $\tilde{V}$ : (Appendix 2)

$$\begin{aligned} \tilde{T}_c = & \tilde{V} + \tilde{V} G \tilde{V} - \langle \tilde{V} G \tilde{V} \rangle + \tilde{V} G \tilde{V} G \tilde{V} \\ & - \langle \tilde{V} G \tilde{V} G \tilde{V} \rangle - \langle \tilde{V} G \tilde{V} \rangle G \tilde{V} \\ & - \tilde{V} G \langle \tilde{V} G \tilde{V} \rangle + \tilde{V} G \tilde{V} G \tilde{V} G \tilde{V} \\ & - \langle \tilde{V} G \tilde{V} G \tilde{V} G \tilde{V} \rangle - \tilde{V} G \langle \tilde{V} G \tilde{V} \rangle G \tilde{V} \\ & + \langle \tilde{V} G \langle \tilde{V} G \tilde{V} \rangle G \tilde{V} \rangle - \langle \tilde{V} G \tilde{V} \rangle G \tilde{V} G \tilde{V} \quad (2.20) \\ & - \tilde{V} G \tilde{V} G \langle \tilde{V} G \tilde{V} \rangle + 2 \langle \tilde{V} G \tilde{V} \rangle G \langle \tilde{V} G \tilde{V} \rangle \\ & - \langle \tilde{V} G \tilde{V} G \tilde{V} \rangle G \tilde{V} - \tilde{V} G \langle \tilde{V} G \tilde{V} G \tilde{V} \rangle \\ & + \dots \end{aligned}$$

and correspondingly the operator  $V_c = \langle \tilde{V} G \tilde{T}_c \rangle$  is represented as

$$\begin{aligned} V_c = & \langle \tilde{V} G \tilde{V} \rangle + \langle \tilde{V} G \tilde{V} G \tilde{V} \rangle + \langle \tilde{V} G \tilde{V} G \tilde{V} G \tilde{V} \rangle \\ & - \langle \tilde{V} G \langle \tilde{V} G \tilde{V} \rangle G \tilde{V} \rangle \quad (2.21) \\ & - \langle \tilde{V} G \tilde{V} \rangle G \langle \tilde{V} G \tilde{V} \rangle + \dots \end{aligned}$$

the expansions are in terms of the average operator  $G$ , which in contrast to  $G_0$  is nonsingular. They are more rapidly convergent than the perturbative expansions in terms of  $G_0$ .

As a simple example, used to study wave propagation in a one dimensional random medium, let us consider a differential equation of the following type:

$$i \frac{d \hat{\psi}(z)}{d z} = \tilde{V}(z) \hat{\psi}(z) \quad (2.22)$$

If  $\tilde{V}(z) = \nu_0 (1 + \tilde{v}(z))$ , where  $\nu_0$  is a real mean frequency and  $\tilde{v}(z)$  is a centered stationary and Gaussian random function of  $z$ , then it represents a randomly modulated oscillator whose correlation function is

$$B(z-z') = \langle \tilde{v}(z) \tilde{v}(z') \rangle \quad (2.23)$$

The model will be used as a check for the approximate expansion in equation (2.21).

The Generic stochastic Green's function for (2.22) is defined by

$$i \frac{d \hat{G}(z, z')}{d z} - \tilde{V}(z) \hat{G}(z, z') = \delta(z-z') \quad (2.24)$$

To find the average Green's function, we must calculate

$$G(\beta, \beta') = -i \left\langle e^{-i \int_{\beta'}^{\beta} \tilde{v}(z) dz} \right\rangle U(\beta - \beta') \quad (2.25)$$

where  $U(u)$  is the step function to insure the uniqueness of  $G$ . Here  $\int_{\beta'}^{\beta} \tilde{v}(z) dz$ , being a linear functional of the centered Gaussian random function  $\tilde{v}(z)$ , is a centered random variable  $\tilde{y}$ , hence

$$\langle e^{-i\tilde{y}} \rangle = e^{-\frac{1}{2} \langle \tilde{y}^2 \rangle} \quad (2.26)$$

Since

$$\begin{aligned} \langle \tilde{y}^2 \rangle &= \left\langle \left( \int_{\beta'}^{\beta} \tilde{v}(z) dz \right)^2 \right\rangle \\ &= \int_{\beta'}^{\beta} \int_{\beta'}^{\beta} B(z-z') dz dz' \end{aligned} \quad (2.27)$$

We obtain the final result

$$G(\beta, \beta') = -i e^{-\frac{1}{2} \int_{\beta'}^{\beta} \int_{\beta'}^{\beta} B(z-z') dz dz'} U(\beta - \beta') \quad (2.28)$$

If we use the correlation function

$$B(\bar{z}-\bar{z}') = A \delta(\bar{z}-\bar{z}') \quad (2.29)$$

the integration in Eq. (2.28) can be performed exactly to give

$$G(\bar{z}, \bar{z}') = -i e^{-\frac{A}{2}(\bar{z}-\bar{z}')} U(\bar{z}-\bar{z}') \quad (2.30)$$

If we approximate  $V_c G$  by taking the 1st term in eq. (2.21), i.e.

$$V_c G \cong \langle \tilde{V} G \tilde{V} \rangle G \quad (2.31)$$

or

$$V_c G = \int B(\bar{z}-\bar{z}) G(\bar{z}, \bar{z}) G(\bar{z}, \bar{z}') U(\bar{z}-\bar{z}) U(\bar{z}-\bar{z}') d\bar{z} \quad (2.32)$$

Substitute eq. (2.30) into (2.32), one obtains

$$V_c G = \frac{A}{2} G(\bar{z}, \bar{z}) G(\bar{z}, \bar{z}') U(\bar{z}-\bar{z}') \quad (2.33)$$

since

$$G(\beta, \beta) = -i \tag{2.34}$$

therefore

$$V_c G = -\frac{i}{2} A G(\beta, \beta') U(\beta - \beta') \tag{2.35}$$

the solution of eq. (2.24) can be easily obtained to give

$$G(\beta, \beta') = -i e^{-\frac{A}{2}(\beta - \beta')} U(\beta - \beta') \tag{2.36}$$

which is identical with the exact solution (2.30). It is an interesting result and leads to the conclusion that : If  $\tilde{V}$  is a centered stationary and Gaussian random function, with a correlation function defined by (2.29), the first term in eq. (2.21) gives the exact expression for  $V_c G$  . i.e. the higher moments terms do not contribute to the expansion. Furthermore, since

$$\begin{aligned} \langle \tilde{V} G \tilde{V} \rangle &= \langle \tilde{V} G_0 \tilde{V} \rangle + \langle \tilde{V} G_0 \tilde{V} G_0 \tilde{V} G_0 \tilde{V} \rangle \\ &+ \dots \end{aligned} \tag{2.37}$$

it can be shown that in this particular case

$$\langle \tilde{V} G \tilde{V} \rangle = \langle \tilde{V} G_0 \tilde{V} \rangle \quad (2.38)$$

Let us consider a more complicate correlation functions

$$B(\beta - \beta') = \epsilon^2 e^{-\frac{|\beta - \beta'|}{T}} \quad (2.39)$$

the integration in eq. (2.28) can be evaluated exactly to give

$$\begin{aligned} & \int_{\beta'}^{\beta} \int_{\beta'}^{\beta} e^{-\frac{|\tau - \tau'|}{T}} d\tau d\tau' \\ &= 2T^2 \left[ e^{-\frac{\beta - \beta'}{T}} - 1 + \frac{\beta - \beta'}{T} \right] \end{aligned} \quad (2.40)$$

for short-range correlation,

$$\begin{aligned} & e^{-\frac{1}{2} \int_{\beta'}^{\beta} \int_{\beta'}^{\beta} B(\tau - \tau') d\tau d\tau'} \\ &= e^{-\epsilon^2 T^2 \left[ e^{-\frac{\beta - \beta'}{T}} - 1 + \frac{\beta - \beta'}{T} \right]} \\ &\approx e^{-\epsilon^2 T (\beta - \beta')} \end{aligned} \quad (2.41)$$

Therefore

$$G(z, z') \cong -i e^{-\epsilon^2 T (z - z')} U(z - z') \quad (2.42)$$

One can examine the 1st approximation in eq. (2.31) by substituting (2.42) into the expression for  $V_C G$ :

$$\begin{aligned} V_C G &= \int \langle \tilde{v}(z) \tilde{v}(\bar{z}) \rangle G(z, \bar{z}) G(\bar{z}, z') \\ &\quad U(z - \bar{z}) U(\bar{z} - z') d\bar{z} \\ &= -\epsilon^2 T e^{-\epsilon^2 T (z - z')} \left[ 1 - e^{-\frac{z - z'}{T}} \right] \quad (2.43) \end{aligned}$$

while the exact solution for  $G$  gives rise to the expression

$$\begin{aligned} V_C G &= i \frac{dG}{dz} - \delta(z - z') \\ &= -\epsilon^2 T e^{-\epsilon^2 T (z - z')} \quad (2.44) \end{aligned}$$

Compare (2.43) to (2.44), one observes that  $V_C G \cong \langle \tilde{v} \tilde{v} \rangle$  is a good approximation when the correlation range is small.

Thus, one concludes that for a centered Gaussian random variable  $\tilde{v}$  with a delta correlated 2-point correlation function,  $V_C G$  can be exactly expressed by the 1st term of the series expansion (2.21), i.e.  $V_C G = \langle \tilde{v} \tilde{v} \rangle G = \langle \tilde{v} G, \tilde{v} \rangle G$ . For

small range correlation function,  $V_{CG} = \langle \tilde{V}G \tilde{V} \rangle G$  is a good approximation. The representation (2.31) can also be applied to the case of large scale correlation, but then the fluctuation  $\tilde{V}$  must be small. Otherwise, the higher moment terms have to be summed to get a good expansion.

### III. Markov Approximation

In order to proceed further, additional approximations for the random medium statistics must be considered. A very useful approximation is the Markov approximation which gives correct results in cases of interest even in the limit of strong scintillations. The mathematical representation and physical interpretation of the Markov approximation is based on the following observation: the correlation of the dielectric constant in the transverse direction  $\rho$  has a direct bearing on the transverse correlation of the field but the correlation of the dielectric constant in the direction of the wave propagation has little effect on the fluctuation characteristic of the wave. Hence, one can assume that  $\tilde{\epsilon}(\underline{r})$  is delta correlated in the direction of propagation,

$$\langle \tilde{\epsilon}(z, \rho) \tilde{\epsilon}(z', \rho') \rangle = \delta(z-z') A(\rho-\rho') \quad (2.45)$$

i.e. one can treat wave propagation in a random medium as a Markov random process. It is equivalent to assume that the turbulent eddies are like flat disks oriented normally to the propagation path. Tatarski (1971) gives a derivation of this approximation which provides the limits of applicability of the Markov approximation. For typical ionospheric parameters,

these conditions are generally satisfied for an incident wave with frequency about twice the maximum plasma frequency or higher.

The relationship between the function  $A(\underline{r} - \underline{r}')$  and the power spectrum  $\Phi(\underline{k})$  is given by the following:

$$A(\underline{r} - \underline{r}') = 2\pi \int \Phi(\underline{k}) e^{i \underline{k} \cdot (\underline{r} - \underline{r}')} d\underline{k} \quad (2.46)$$

If the turbulence is isotropic, i.e.  $\Phi(\underline{k}) = \Phi(k)$ , then we get

$$A(\underline{r} - \underline{r}') = (2\pi)^2 \int_0^{\infty} J_0(k \cdot (\underline{r} - \underline{r}')) \Phi(k) k dk \quad (2.47)$$

$A(\underline{r})$  is also related to the correlation function  $B(z, \underline{r})$  through

$$A(\underline{r} - \underline{r}') = \int_{-\infty}^{\infty} B(z, \underline{r} - \underline{r}') dz \quad (2.48)$$

The limit of application of the Markov approximation was investigated by Tatarski (1971) via variational techniques. We derived identical results using the operator method as present in Appendix 3.

#### IV. Equation for the Mean Field

In summary, our analysis of strong scintillations will be based on the following assumptions:

- (1) The parabolic approximation. (limits of applicability of the parabolic approximations will be derive in Appendix 4).
- (2)  $\tilde{\epsilon}(\underline{r})$  is delta correlated in the direction of propagation.

Let us take the ensemble average of parabolic equation (2.9)

$$2ik_0 \frac{\partial \langle \hat{\psi} \rangle}{\partial z} + \nabla_{\rho}^2 \langle \hat{\psi} \rangle + k_0^2 \langle \tilde{\epsilon} \hat{\psi} \rangle = 0 \quad (2.49)$$

The last term in (2.49) will be expressed as follows:

$$\langle \tilde{\epsilon}(\underline{r}) \hat{\psi}(\underline{r}) \rangle = V_c(\underline{r}) \langle \hat{\psi}(\underline{r}) \rangle$$

which is valid if the incident field at  $z = 0$  is deterministic. One notes that  $\tilde{\epsilon}(\underline{r}) = 2\tilde{n}(\underline{r})$  is the fluctuation of the refractive index. To get a differential equation for  $\langle \hat{\psi}(\underline{r}) \rangle$ , under the assumptions (1) - (2), one obtains the following expression for  $V_c$ :

$$V_c = \langle \tilde{V} G \tilde{V} \rangle = \langle \tilde{V} G_0 \tilde{V} \rangle \quad (2.50)$$

If the fluctuation  $\tilde{\xi}(\underline{r})$  is a centered Gaussian random field and characterized completely by the correlation function  $\langle \tilde{\xi}(\underline{r}_1) \tilde{\xi}(\underline{r}_2) \rangle$ , then (2.50) is exact.

To ascertain  $V_C$ , the unperturbed operator  $G_0$  must be found. Therefore, we have to find the Green's function for the homogeneous equation

$$i \frac{\partial \hat{\psi}}{\partial \underline{z}} + \frac{1}{2k_0} \frac{\partial^2 \hat{\psi}}{\partial \underline{p}^2} = 0 \quad (2.51)$$

Setting

$$\hat{\psi}(\underline{p}, \underline{z}) = \int_{-\infty}^{+\infty} \hat{\psi}(\underline{k}, \underline{z}) e^{-i\underline{k} \cdot \underline{p}} d\underline{k} \quad (2.52)$$

One can write equation (2.51) as

$$i \frac{\partial \hat{\psi}(\underline{k}, \underline{z})}{\partial \underline{z}} - \frac{k^2}{2k_0} \hat{\psi}(\underline{k}, \underline{z}) = 0 \quad (2.53)$$

From (2.51), we define  $G_0$  by

$$i \frac{\partial G_0}{\partial \underline{z}} + \frac{1}{2k_0} \frac{\partial^2 G_0}{\partial \underline{p}^2} = \delta(\underline{r} - \underline{r}') \quad (2.54)$$

Setting

$$G_0(\underline{r}, \underline{z}, \underline{r}', \underline{z}') = \int \underline{g}_{\underline{k}}(\underline{z}, \underline{z}') e^{i \underline{k} \cdot (\underline{r} - \underline{r}')} \frac{d\underline{k}}{(2\pi)^2} \quad (2.55)$$

where

$$G_0(\underline{r}, \underline{z}, \underline{r}', \underline{z}') = 0 \quad \underline{z} < \underline{z}' \quad (2.56)$$

From (2.55), we obtain

$$i \frac{\partial \underline{g}_{\underline{k}}}{\partial \underline{z}} - \frac{\underline{k}^2}{2k_0} \underline{g}_{\underline{k}} = \delta(\underline{z} - \underline{z}') \quad (2.57)$$

$$\underline{g}_{\underline{k}}(\underline{z}, \underline{z}') = 0 \quad \underline{z} < \underline{z}' \quad (2.58)$$

For  $z > z'$ , we note that

$$\underline{g}_{\underline{k}}(\underline{z}, \underline{z}') = A e^{-i \frac{\underline{k}^2}{2k_0} (\underline{z} - \underline{z}')} \quad (2.59)$$

Using (2.57) and (2.58), one sees that

$$\underline{g}_{\underline{k}}(\underline{z}, \underline{z}') = -i \quad \text{as } \underline{z} \rightarrow \underline{z}' \quad (2.60)$$

One then observes from (2.59) and (2.60) that  $A = -i$  and

$$g_k(z, z') = -i e^{-\frac{k^2}{2k_0}(z-z')} \quad (2.61)$$

From (2.54), one sees that for  $z \rightarrow z'$

$$G_0(\rho, z, \rho', z') \cong -i \delta(\rho - \rho') \quad (2.62)$$

the above is also a good approximation provided  $k^2|z-z'|/2k_0 \ll 1$ . Therefore, by using (2.50), we obtain

$$\begin{aligned} V_c &= -i k_0^2 \iint_{-\infty}^{\infty} \int_{-\infty}^{\infty} \langle \tilde{n}(\rho, z) \tilde{n}(\rho', z') \rangle \delta(\rho - \rho') d\rho' dz' \\ &= -i k_0^2 \int_{-\infty}^{\infty} \langle \tilde{n}(\rho, z) \tilde{n}(\rho, z') \rangle dz' \end{aligned} \quad (2.63)$$

where  $\tilde{n} = \tilde{\epsilon}/2$ . Setting  $z - z' = \eta$ , we obtain

$$V_c = -i k_0^2 \int_0^{\infty} \langle \tilde{n}(\rho, z) \tilde{n}(\rho, z-\eta) \rangle d\eta \quad (2.64)$$

Applying the Markov approximation, one obtains

$$V_c = -i k_0^2 \int_0^\infty \delta(\eta) A(z, 0) d\eta \quad (2.65)$$

Therefore, the average equation (2.49) becomes

$$i \frac{\partial \langle \hat{\psi} \rangle}{\partial z} + \frac{1}{2k_0} \frac{\partial^2 \langle \hat{\psi} \rangle}{\partial \rho^2} + \frac{i k_0^2}{2} A(z, 0) \langle \hat{\psi} \rangle = 0 \quad (2.66)$$

#### V. Parabolic Equation for the Mutual Coherence Function

The parabolic equation (2.9) and its conjugate can be written as:

$$\left[ i \frac{\partial}{\partial z} + \frac{1}{2k_0} \frac{\partial^2}{\partial \rho^2} + k_0 \tilde{n}(r) \right] \hat{\psi}(z, \rho) = 0 \quad (2.67)$$

$$\left[ -i \frac{\partial}{\partial z} + \frac{1}{2k_0} \frac{\partial^2}{\partial \rho'^2} + k_0 \tilde{n}(r') \right] \hat{\psi}^*(z, \rho') = 0 \quad (2.68)$$

Multiplying (2.67) by  $\hat{\psi}^*(z, \rho')$  and (2.68) by  $\hat{\psi}(z, \rho)$  and subtracting the second equation from the first, we obtain:

$$\left[ i \frac{\partial}{\partial z} + \frac{1}{2k_0} (\nabla_\rho^2 - \nabla_{\rho'}^2) + k_0 (\tilde{n}(z, \rho) - \tilde{n}(z, \rho')) \right] \hat{\psi} \hat{\psi}'^* = 0 \quad (2.69)$$

The mutual coherence function,  $\langle \hat{\psi}(z, \underline{r}) \hat{\psi}^*(z, \underline{r}') \rangle$  is defined as the cross-correlation function of the fields  $\hat{\psi}$  and  $\hat{\psi}^*$  in a direction transverse to the direction of propagation.

Using the operator notation described in section II, we rewrite  $\hat{M} = \hat{\psi} \hat{\psi}'^*$  in the form:

$$(L_0 - \tilde{V}) \hat{M} = 0 \quad (2.70)$$

where

$$\begin{aligned} L_0 &\longrightarrow i \frac{\partial}{\partial \bar{z}} + \frac{1}{2k_0} (\nabla_{\underline{r}}^2 - \nabla_{\underline{r}'}^2) \\ \tilde{V} &\longrightarrow -k_0 [\tilde{n}(z, \underline{r}) - \tilde{n}(z, \underline{r}')] \\ \hat{M} &\longrightarrow \hat{\psi}(z, \underline{r}) \hat{\psi}'^*(z, \underline{r}') \end{aligned} \quad (2.71)$$

An unperturbed Green's function may be defined as

$$\begin{aligned} & \left[ i \frac{\partial}{\partial \bar{z}} + \frac{1}{2k_0} (\nabla_{\underline{r}}^2 - \nabla_{\underline{r}'}^2) \right] G_0(\underline{r}, \underline{r}', \bar{z}; \bar{r}, \bar{r}', \bar{z}) \\ & = \delta(\underline{r} - \bar{r}) \delta(\underline{r}' - \bar{r}') \delta(\bar{z} - \bar{z}) \end{aligned} \quad (2.72)$$

Applying the same analysis as described in section IV, one finds approximately that

$$G_0(\underline{r}, \underline{r}', \underline{z}; \underline{\bar{r}}, \underline{\bar{r}}', \underline{\bar{z}}) \cong -i \delta(\underline{r} - \underline{\bar{r}}) \delta(\underline{r}' - \underline{\bar{r}}') \quad (2.73)$$

The smoothed scattering operator for the ensemble averaged Green's function, defined as in (2.38) can be expressed by

$$V_c = \langle \tilde{V} G \tilde{V} \rangle = \langle \tilde{V} G_0 \tilde{V} \rangle \quad (2.74)$$

and written as:

$$\begin{aligned} V_c &\cong -i k_0^2 \int_{-\infty}^{+\infty} \int_{-\infty}^{\bar{z}} \langle [\tilde{n}(\underline{r}, \underline{z}) - \tilde{n}(\underline{r}', \underline{z})] \delta(\underline{r} - \underline{\bar{r}}) \\ &\quad \delta(\underline{r}' - \underline{\bar{r}}') [\tilde{n}(\underline{\bar{r}}, \underline{\bar{z}}) - \tilde{n}(\underline{\bar{r}}', \underline{\bar{z}})] \rangle d\underline{\bar{r}} d\underline{\bar{r}}' d\underline{\bar{z}} \\ &= -i k_0^2 \int_{-\infty}^{\bar{z}} 2 \left[ \langle \tilde{n}(\underline{r}, \underline{z}) \tilde{n}(\underline{r}, \underline{\bar{z}}) \rangle - \langle \tilde{n}(\underline{r}, \underline{z}) \tilde{n}(\underline{r}', \underline{\bar{z}}) \rangle \right] d\underline{\bar{z}} \end{aligned} \quad (2.75)$$

Setting  $z - \bar{z} = \eta$ , one obtains

$$V_c = -i k_0^2 \int_0^{\infty} [\delta(\eta) A(\bar{z}, 0) - \delta(\eta) A(\bar{z}, \underline{r} - \underline{r}')] d\eta \quad (2.76)$$

Applying the Markov approximation, one obtains

$$V_c = -\frac{i k_0^2}{2} [A(z, 0) - A(z, \underline{\rho} - \underline{\rho}')] \quad (2.77)$$

Equation (2.70) then becomes

$$\left\{ i \frac{\partial}{\partial z} + \frac{1}{2k_0} (\nabla_{\underline{\rho}}^2 - \nabla_{\underline{\rho}'}^2) + \frac{i k_0^2}{2} [A(z, 0) - A(z, \underline{\rho} - \underline{\rho}')] \right\} M_2 = 0 \quad (2.78)$$

where

$$M_2(z, \underline{\rho}, \underline{\rho}') = \langle \hat{\psi}(z, \underline{\rho}) \hat{\psi}^*(z, \underline{\rho}') \rangle \quad (2.79)$$

#### VI. The Equation for Fourth Order Moment

On considering the parabolic equation for  $\hat{\psi}(z, \underline{\rho}_1)$ ,  $\hat{\psi}(z, \underline{\rho}_2)$ ,  $\hat{\psi}^*(z, \underline{\rho}_3)$ ,  $\hat{\psi}^*(z, \underline{\rho}_4)$ , respectively, we can obtain an equation for

$$\hat{M}_4 = \hat{\psi}(z, \underline{\rho}_1) \hat{\psi}(z, \underline{\rho}_2) \hat{\psi}^*(z, \underline{\rho}_3) \hat{\psi}^*(z, \underline{\rho}_4) \quad (2.80)$$

as in the form

$$[L_0 - \tilde{V}] \hat{M}_4 = 0 \quad (2.81)$$

where

$$L_0 \longrightarrow i \frac{\partial}{\partial \bar{z}} + \frac{1}{2k_0} [\nabla_{\underline{p}_1}^2 + \nabla_{\underline{p}_2}^2 - \nabla_{\underline{p}_3}^2 - \nabla_{\underline{p}_4}^2]$$

$$\tilde{V} \longrightarrow -k_0 [\tilde{n}(z, \underline{p}_1) + \tilde{n}(z, \underline{p}_2) - \tilde{n}(z, \underline{p}_3) - \tilde{n}(z, \underline{p}_4)] \quad (2.82)$$

as before one defines an unperturbed Green's function defined by

$$[i \frac{\partial}{\partial \bar{z}} + \frac{1}{2k_0} (\nabla_{\underline{p}_1}^2 + \nabla_{\underline{p}_2}^2 - \nabla_{\underline{p}_3}^2 - \nabla_{\underline{p}_4}^2)] G_0(\underline{p}_1, \underline{p}_2, \underline{p}_3, \underline{p}_4, \bar{z}; \underline{\bar{p}}_1, \underline{\bar{p}}_2, \underline{\bar{p}}_3, \underline{\bar{p}}_4, \bar{z}) = \delta(\underline{p}_1 - \underline{\bar{p}}_1) \delta(\underline{p}_2 - \underline{\bar{p}}_2) \delta(\underline{p}_3 - \underline{\bar{p}}_3) \delta(\underline{p}_4 - \underline{\bar{p}}_4) \delta(\bar{z} - \bar{z}) \quad (2.83)$$

Applying the same analysis as described in section IV, one sees that  $G_0$  can be approximated as:

$$G_0 \cong -i \delta(\underline{p}_1 - \underline{\bar{p}}_1) \delta(\underline{p}_2 - \underline{\bar{p}}_2) \delta(\underline{p}_3 - \underline{\bar{p}}_3) \delta(\underline{p}_4 - \underline{\bar{p}}_4) \quad (2.84)$$

Therefore, the operator  $V_c$  for this case can be approximated as

$$\begin{aligned}
 V_c &\cong \langle \tilde{V} G_0 \tilde{V} \rangle \\
 &= -i k_0^2 \int \langle [\tilde{n}(\tilde{z}, \underline{p}_1) + \tilde{n}(\tilde{z}, \underline{p}_2) - \tilde{n}(\tilde{z}, \underline{p}_3) - \tilde{n}(\tilde{z}, \underline{p}_4)] \\
 &\quad \delta(\underline{p}_1 - \underline{\bar{p}}_1) \delta(\underline{p}_2 - \underline{\bar{p}}_2) \delta(\underline{p}_3 - \underline{\bar{p}}_3) \delta(\underline{p}_4 - \underline{\bar{p}}_4) \\
 &\quad [\tilde{n}(\tilde{z}, \underline{\bar{p}}_1) + \tilde{n}(\tilde{z}, \underline{\bar{p}}_2) - \tilde{n}(\tilde{z}, \underline{\bar{p}}_3) - \tilde{n}(\tilde{z}, \underline{\bar{p}}_4)] \rangle \quad (2.85) \\
 &\quad d\underline{\bar{p}}_1 d\underline{\bar{p}}_2 d\underline{\bar{p}}_3 d\underline{\bar{p}}_4 d\tilde{z}
 \end{aligned}$$

Upon application of the Markov approximation, one obtains

$$\begin{aligned}
 V_c &= -i k_0^2 [2A(\tilde{z}, 0) - A(\tilde{z}, \underline{p}_1 - \underline{p}_3) - A(\tilde{z}, \underline{p}_1 - \underline{p}_4) \\
 &\quad - A(\tilde{z}, \underline{p}_2 - \underline{p}_4) - A(\tilde{z}, \underline{p}_2 - \underline{p}_3) + A(\tilde{z}, \underline{p}_2 - \underline{p}_1) \\
 &\quad + A(\tilde{z}, \underline{p}_4 - \underline{p}_3)] \quad (2.86)
 \end{aligned}$$

By (2.28), one then obtains the equation for the fourth moment  $M_4 = \langle \hat{\psi}(z, \underline{p}_1) \hat{\psi}(z, \underline{p}_2) \hat{\psi}^*(z, \underline{p}_3) \hat{\psi}^*(z, \underline{p}_4) \rangle$  as:

$$\left\{ i \frac{\partial}{\partial \tilde{z}} + \frac{1}{2k_0} [\nabla_{\underline{p}_1}^2 + \nabla_{\underline{p}_2}^2 - \nabla_{\underline{p}_3}^2 - \nabla_{\underline{p}_4}^2] + i k_0^2 f \right\} M_4 = 0 \quad (2.87)$$

where

$$\begin{aligned} f &= f(\underline{z}, \underline{p}_1, \underline{p}_2, \underline{p}_3, \underline{p}_4) \\ &= 2A(\underline{z}, 0) - A(\underline{z}, \underline{p}_1 - \underline{p}_3) - A(\underline{z}, \underline{p}_1 - \underline{p}_4) \\ &\quad - A(\underline{z}, \underline{p}_2 - \underline{p}_4) - A(\underline{z}, \underline{p}_2 - \underline{p}_3) + A(\underline{z}, \underline{p}_2 - \underline{p}_1) \quad (2.88) \\ &\quad + A(\underline{z}, \underline{p}_4 - \underline{p}_3) \end{aligned}$$

and

$$A(\underline{z}, \underline{z}_x) = 2\pi \int_{-\infty}^{\infty} \underline{\Phi}(\underline{z}, \underline{k}_x) e^{i \underline{k}_x \cdot \underline{z}_x} d \underline{k}_x \quad (2.89)$$

Chapter 3 SOLUTIONS FOR THE MUTUAL COHERENCE  
FUNCTION

I. "Slow" and "Fast" Quasiparticle Distribution Functions

Equation (2.78) is a single mode type of wave problem dependent on the statistics of the random medium. In order to obtain the solutions for the mutual coherence function, we shall define the following Fourier transform with respect to the "fast" variable  $\xi = x_1 - x_2$ , and the "slow" variable  $x = x_1 + x_2/2$ . They are so called "quasiparticle distribution function" or "Wigner distribution function" described independently by Marcuvitz (74) and Bremmer (34). One introduces the double Fourier representation.

$$\langle \hat{\psi}_1 \hat{\psi}_2^* \rangle = \iint \langle \hat{\phi}_1 \hat{\phi}_2^* \rangle e^{i(k_1 x_1 - k_2 x_2)} \frac{dk_1 dk_2}{(2\pi)^2} \quad (3-1)$$

where  $\hat{\phi}_1 = \hat{\phi}(k_1, z)$  and  $\hat{\phi}_2 = \hat{\phi}(k_2, z)$  are, respectively, the Fourier amplitudes of  $\hat{\psi}_1 = \hat{\psi}(x_1, z)$  and  $\hat{\psi}_2 = \hat{\psi}(x_2, z)$ . Defining the "slow" ( $x$  or  $k$ ) and "fast" ( $\xi$  or  $k$ ) spatial and wave number variables via

$$x = \frac{x_1 + x_2}{2}, \quad k = k_1 - k_2$$

and

$$\xi = x_1 - x_2, \quad k = \frac{k_1 + k_2}{2} \quad (3.2)$$

whence

$$k_1 x_1 - k_2 x_2 = k \varepsilon + k x$$

and

$$dk_1 dk_2 = dk dk$$

(3.3)

One rewrites equation (3.1) as

$$\langle \hat{\psi}_1 \hat{\psi}_2^* \rangle = \int F(k, x, \varepsilon) e^{i k \varepsilon} \frac{dk}{2\pi} \quad (3.4)$$

where

$$F(k, x, \varepsilon) = \int \langle \hat{\phi}_1 \hat{\phi}_2^* \rangle e^{i k x} \frac{dk}{2\pi} \quad (3.5)$$

is called the "fast" quasiparticle distribution function.

Alternatively, one writes equation (3.1) as

$$\langle \hat{\psi}_1 \hat{\psi}_2^* \rangle = \int S(k, \varepsilon, \varepsilon) e^{i k \varepsilon} \frac{dk}{2\pi} \quad (3.6)$$

where

$$S(k, \varepsilon, \varepsilon) = \int \langle \hat{\phi}_1 \hat{\phi}_2^* \rangle e^{i k \varepsilon} \frac{dk}{2\pi} \quad (3.7)$$

and termed the "slow" quasiparticle distribution function also called the ambiguity function.

The reality property  $F(k,x,z) = F^*(k,x,z)$  of the fast quasiparticle d.f. follows readily from eq.(3.5); however, positive definiteness is not in general assured.  $S(K, \bar{E}, \bar{z})$  is only real when  $\hat{\Psi}(x)$  is an even function which can be proved using eq. (3.6).  $S(K, \bar{E}, \bar{z})$ , just as  $F(k,x,z)$ , can be negative for some value of  $K$  and  $\bar{E}$ . However, it should be noticed that integrals of  $\int F(k,x,z) \frac{dk}{2\pi}$ ,  $\int S(K, \bar{E}, \bar{z}) \frac{dK}{2\pi}$  is always positive.

It is interesting to observe the following properties of  $F(k,x,z)$  and  $S(K, \bar{E}, \bar{z})$ :

(a) one notes that from eq.(3.4) and (3.6)

$$S(K, \bar{E}, \bar{z}) = \int F(k,x,z) e^{i k \bar{E} - i k x} \frac{dk dx}{2\pi} \quad (3.8)$$

which suggests that  $S(K, \bar{E}, \bar{z})$  can be treated as a characteristic function of  $F(k,x,z)$ , in  $k,x$  space, and vice versa. The use of  $S(K, \bar{E}, \bar{z})$  or  $F(k,x,z)$  mainly dependent on the nature of the problem to be solved.

(b) for  $\bar{E} = 0$  and  $K = 0$  equations (3.4) and (3.5) yield

$$\langle |\hat{\Psi}(x, \bar{z})|^2 \rangle = \int F(k,x,z) \frac{dk}{2\pi} \quad (3.9a)$$

$$\langle |\hat{\phi}(k, z)|^2 \rangle = \int F(k, x, z) dx \quad (3.9b)$$

whence one infers that

$$\begin{aligned} \int \langle |\hat{\psi}(x, z)|^2 \rangle dx &= \int \langle |\hat{\phi}(k, z)|^2 \rangle \frac{dk}{2\pi} \\ &= \int F(k, x, z) \frac{dk dx}{2\pi} \end{aligned} \quad (3.10)$$

which suggests the identification of  $F(k, x, z)$  as a number density of "fast" quasiparticles in  $k, x$  phase space.

(c) Similarly, for  $x = 0$  and  $k = 0$  and  $\hat{\psi}(x)$  is even, equations (3.6), and (3.7), give

$$\langle |\hat{\psi}(\frac{\epsilon}{2}, z)|^2 \rangle = \int S(k, \epsilon, z) \frac{dk}{2\pi} \quad (3.11a)$$

$$\langle |\hat{\phi}(\frac{k}{2}, z)|^2 \rangle = \int S(k, \epsilon, z) d\epsilon \quad (3.11b)$$

which also suggests the identification of  $S(k, \epsilon, z)$  as a number density of "slow" quasiparticle in  $k, \epsilon$  space.  
also,

$$\begin{aligned} \int \langle |\hat{\psi}(\frac{\epsilon}{2}, z)|^2 \rangle d\epsilon &= \int \langle |\hat{\phi}(\frac{\kappa}{2}, z)|^2 \rangle \frac{d\kappa}{2\pi} \\ &= \int S(\kappa, \epsilon, z) \frac{d\kappa d\epsilon}{2\pi} \end{aligned} \quad (3.12)$$

(d) One notes that

$$\int F(\kappa, x, z) \frac{d\kappa dx}{2\pi} = S(0, 0, z) \equiv N_f(z) \quad (3.13a)$$

$$\int S(\kappa, \epsilon, z) \frac{d\kappa d\epsilon}{2\pi} = F(0, 0, z) \equiv N_s(z) \quad (3.13b)$$

where  $N_f(z)$  and  $N_s(z)$  denote the total number of "fast" and "slow" quasiparticles respectively. Both  $N_f(z)$  and  $N_s(z)$  can be obtained from information about  $F$  or  $S$ .

(e) A coarser description of the dynamics of a quasiparticle system views the overall system as a single Macro-particle. It is of interest to find the average position, momentum, size, etc., of the overall system. The average coordinates of quasiparticles are defined, in terms of the distribution functions  $F$  in  $\kappa, x$  space, by

$$\bar{x}(z) = \frac{1}{N_f(z)} \iint x F(\kappa, x, z) \frac{d\kappa dx}{2\pi} \quad (3.14a)$$

$$\bar{k}(\beta) = \frac{1}{N_f(\beta)} \iint k F(k, x, \beta) \frac{dk dx}{2\pi} \quad (3.14b)$$

and in terms of S function in  $K, \xi$  space

$$\bar{\xi}(\beta) = \frac{1}{N_s(\beta)} \iint \xi S(k, \xi, \beta) \frac{dk d\xi}{2\pi} \quad (3.15a)$$

$$\bar{k}(\beta) = \frac{1}{N_s(\beta)} \iint k S(k, \xi, \beta) \frac{dk d\xi}{2\pi} \quad (3.15b)$$

Similarly, the higher moment averages

$$\overline{k^m x^n} = \frac{1}{N_f(\beta)} \iint k^m x^n F(k, x, \beta) \frac{dk dx}{2\pi} \quad (3.16a)$$

$$\overline{k^m \xi^n} = \frac{1}{N_s(\beta)} \iint k^m \xi^n S(k, \xi, \beta) \frac{dk d\xi}{2\pi} \quad (3.16b)$$

It can be easily proved that

$$\overline{k^m x^n} = \frac{\partial^{m+n}}{\partial (i\xi)^m \partial (-ik)^n} S(k, \xi, \beta) \Big|_{k=\xi=0} \quad (3.17a)$$

$$\overline{k^m \xi^n} = \frac{\partial^{m+n}}{\partial (-ix)^m \partial (ik)^n} F(k, x, \beta) \Big|_{k=x=0} \quad (3.17b)$$

Therefore, a macro-description of the overall system can be found if either F or S is known.

II. Exact Solution of Mutual Coherence Function for the Case  
 $H(\xi) = a \xi^2$  (cf. Furutsu, 13)

The defining equation for the Mutual coherence function has been derived in section (2.V). Introducing the "fast" and "slow" coordinates

$$\tilde{x} = \frac{\tilde{\rho}_1 + \tilde{\rho}_2}{2}, \quad \tilde{\xi} = \tilde{\rho}_1 - \tilde{\rho}_2$$

one obtains

$$\left\{ \frac{\partial}{\partial \beta} - \frac{i}{k_0} \nabla_{\tilde{x}} \cdot \nabla_{\tilde{\xi}} + \frac{k_0^2}{4} [A(0) - A(\tilde{\xi})] \right\} M_2 = 0 \quad (3.18)$$

where  $M_2(\underline{x}, \underline{\xi}, \underline{z}) = \langle \hat{\psi}(\underline{p}_1, \underline{z}) \hat{\psi}^*(\underline{p}_2, \underline{z}) \rangle$ .

We now consider the Fourier transform with respect to  $\underline{x}$ , which is exactly the "slow" quasiparticle d.f. defined in section I. The resulting differential equation for  $S(\underline{k}, \underline{\xi}, \underline{z})$  becomes

$$\frac{\partial S}{\partial \underline{z}} + \frac{\underline{k}}{k_0} \cdot \frac{\partial S}{\partial \underline{\xi}} + H(\underline{\xi}) S = 0 \quad (3.19)$$

where

$$H(\underline{\xi}) = \frac{k_0^2}{4} [A(0) - A(\underline{\xi})] \quad (3.20)$$

Equation (3.19) has the form of a collisional "kinetic" equation indicative of a distribution of "slow quasiparticle" in  $\underline{k}, \underline{\xi}$  space at a plane  $\underline{z}$ . The "Characteristic" trajectory along which the "particles" move is defined by

$$\frac{d \underline{\xi}}{d \underline{z}} = \frac{\underline{k}}{k_0}, \quad \frac{d \underline{k}}{d \underline{z}} = 0 \quad (3.21)$$

On a quasiparticle trajectory, one observes that

$$\frac{d S(\underline{k}, \underline{\xi}, \underline{z})}{d \underline{z}} = -H(\underline{\xi}) S(\underline{k}, \underline{\xi}, \underline{z}) \quad (3.22)$$

or

$$S(\underline{k}, \underline{\xi}(z), z) = S(\underline{k}, \underline{\xi}(0), 0) e^{-\int_0^z H(\underline{\xi}(z')) dz'} \quad (3.23)$$

This implies that the number density of such "slow particles" per unit volume of the phase space  $\underline{k}, \underline{\xi}$  decays along the trajectory defined by equation (3.23).

For waves propagation in free space, the defining equation for  $S$  becomes

$$S(\underline{k}, \underline{\xi}(z), z) = S(\underline{k}(0), \underline{\xi}(0), 0) \quad (3.24)$$

which provides the constancy of  $S$  on a quasiparticle trajectory.

To illustrate the applicability of the slow  $q, p$  view we shall consider wave propagation through a random medium characterized by  $H(\underline{\xi}) = a \underline{\xi}^2$ . As an initial condition, we choose for analytical purposes a planar beam of the simple form

$$\psi(x, 0) = e^{-\frac{x^2}{2b^2}} \quad (3.25)$$

The slow quasiparticle distribution function at  $z = 0$  follows from the transform relation (3.6) as

$$\begin{aligned}
 S(\kappa, \xi, 0) &= \int e^{-\frac{1}{2b^2}(x_1^2 + x_2^2)} e^{-i\kappa x} dx \\
 &= \int e^{-\frac{1}{2b^2}(2x^2 + \frac{\xi^2}{2}) - i\kappa x} dx \\
 &= \sqrt{\pi} b e^{-\frac{\xi^2}{4b^2}} e^{-\frac{\kappa^2 b^2}{4}} \quad (3.26)
 \end{aligned}$$

At a subsequent distance  $z$  the  $S$  function follows from (3.21) and (3.23) as

$$\begin{aligned}
 S(\kappa, \xi, z) &= S(\kappa, \xi(0), 0) e^{-a \int_0^z \xi^2(z') dz'} \\
 &= S(\kappa, \xi(0), 0) e^{-a \int_0^z [\xi(0) + \kappa z']^2 dz'} \\
 &= S(\kappa, \xi - \kappa z, 0) e^{-a \int_0^z [\xi - \kappa(z - z')]^2 dz'} \\
 &= \sqrt{\pi} b e^{-\frac{(\xi - \kappa z)^2}{4b^2}} e^{-\frac{\kappa^2 b^2}{4}} \times \quad (3.27) \\
 &\quad e^{-\frac{1}{3} a [3\xi^2 z - 3\xi\kappa z^2 + \kappa^2 z^3]} \\
 &= \sqrt{\pi} b e^{-\kappa^2 (\frac{z^2}{4b^2} + \frac{b^2}{4} + \frac{1}{3} a z^3)} \\
 &\quad e^{-\xi^2 (\frac{1}{4b^2} + a z) + 2\xi\kappa (\frac{z}{4b^2} + \frac{a z^2}{2})}
 \end{aligned}$$

For the beam wave case, the wave at the aperture  $z=0$  can be assumed to have a Gaussian amplitude distribution with the beam size  $W_0$  and radius of curvature  $R_0$  for the wave front. Thus, at  $z=0$  the wave is given by

$$\psi(x, 0) = e^{-\frac{1}{2} k_0 (\alpha_r + i \alpha_i) x^2} \quad (3.28)$$

where

$$\alpha_r = \frac{\lambda}{\pi W_0^2}, \quad \alpha_i = \frac{1}{R_0} \quad (3.29)$$

Introducing the normalized coordinates

$$\bar{x} = \frac{x}{l}, \quad \bar{\alpha}_r = \frac{2}{\left(\frac{W_0}{l}\right)^2}, \quad \bar{\alpha}_i = \frac{1}{\left(\frac{R_0}{k_0 l^2}\right)}$$

one rewrites (3.28) as

$$\psi(x, 0) = e^{-\frac{1}{2} (\bar{\alpha}_r + i \bar{\alpha}_i) x^2} \quad (3.30)$$

Substituting into (3.6), one obtains (for simplicity, we will drop the bars)

$$\begin{aligned}
 S(k, \xi, 0) &= \int e^{-\frac{1}{2}\alpha_r(x_1^2+x_2^2) - \frac{1}{2}i\alpha_i(x_1^2-x_2^2)} \\
 &\quad e^{-ikx} dx \\
 &= \int e^{-\frac{1}{2}\alpha_r(2x^2 + \frac{\xi^2}{2}) - i\alpha_i x \xi - ikx} dx \\
 &= e^{-\frac{1}{4}\alpha_r \xi^2} e^{-\frac{(k + \alpha_i \xi)^2}{4\alpha_r}} \sqrt{\frac{\pi}{\alpha_r}}
 \end{aligned} \tag{3.31}$$

Using equation (3.23), one finds

$$\begin{aligned}
 S(k, \xi, \beta) &= \sqrt{\frac{\pi}{\alpha_r}} e^{-\frac{1}{4}\alpha_r(\xi - k\beta)^2} e^{-\frac{[k + \alpha_i(\xi - k\beta)]^2}{4\alpha_r}} \\
 &\quad e^{-a(\xi^2\beta - \xi k\beta^2 + \frac{1}{3}k^2\beta^3)}
 \end{aligned} \tag{3.32}$$

note that (3.32) can be reduced to (3.27) by setting  $\alpha_r = \frac{1}{b^2}$  and  $\alpha_i = 0$ .

The Mutual coherence function at  $z$  can be calculated via (3.6)

$$\begin{aligned}
 M_2(x, \xi, \beta) &= \int S(k, \xi, \beta) e^{ikx} \frac{dk}{2\pi} \\
 &= \int e^{-Ak^2 - B\xi^2 + C\xi k + ikx} \sqrt{\frac{\pi}{\alpha_r}} \frac{dk}{2\pi}
 \end{aligned} \tag{3.33}$$

where

$$\begin{aligned}
 A &= \frac{\alpha_r \beta^2}{4} + \frac{1}{4\alpha_r} (1 + \alpha_i^2 \beta^2 - 2\alpha_i \beta) + \frac{1}{3} a \beta^3 \\
 B &= \frac{1}{4} \alpha_r + \frac{1}{4} \frac{\alpha_i^2}{\alpha_r} + a \beta \\
 C &= \frac{\beta \alpha_r}{2} - \frac{1}{2} \frac{\alpha_i}{\alpha_r} (1 - \alpha_i \beta) + a \beta^2
 \end{aligned} \tag{3.34}$$

whence on integration of (3.33), one obtains

$$M_2(x, \xi, \beta) = \frac{1}{2} \sqrt{\frac{1}{\alpha_r A}} e^{-\xi^2 B} e^{\frac{(ix + \xi C)^2}{4A}} \tag{3.35}$$

where A, B and C are defined by (3.34).

Equation (3.35) is the exact solution for the Mutual coherence function at a distance z. It is of interest to consider as a function of Z the beam size ratio, axial intensity ratio, and the normalized MCF at x = 0 for the following cases:

(case a) For collimated beams ( $\alpha_i = 0$ ) propagating in free space, one obtains from equation (3.34)

$$\begin{aligned}
 A &= \frac{\alpha_r \beta^2}{4} + \frac{1}{4\alpha_r} \\
 B &= \frac{1}{4} \alpha_r, \quad C = \frac{1}{2} \beta \alpha_r
 \end{aligned} \tag{3.36}$$

Then the beam size ratio ( $\xi=0$ ) is defined by

$$\frac{W_0^2(z)}{W_0^2(0)} = \frac{4A}{1/\alpha_r} = 1 + z^2 \alpha_r^2 \quad (3.37)$$

increases with  $z$ .

The axial intensity ratio, defined as the intensity of the wave at  $x = \xi = 0$ , becomes

$$\frac{I(0, z)}{I(0, 0)} = \frac{M_2(0, 0, z)}{M_2(0, 0, 0)} = \frac{1}{(1 + z^2 \alpha_r^2)^{1/2}} \quad (3.38)$$

and decreases with  $z$ .

The normalized Mutual Coherence function (NMCF) is an important function for the measurement of coherence. The integral of NMCF,  $\int \frac{M_2(0, \xi, z)}{M_2(0, 0, z)} d\xi$ , gives the value of correlation scale. At  $x = 0$ , it is give by:

$$\frac{M_2(0, \xi, z)}{M_2(0, 0, z)} = e^{-\frac{\alpha_r \xi^2}{4} \left( \frac{1}{1 + z^2 \alpha_r^2} \right)} \quad (3.39)$$

(case b) For a focused beam ( $\alpha_i > 0$ ) and a divergent beam ( $\alpha_i < 0$ ) propagating in free space, one has

$$\begin{aligned} A &= \frac{\alpha_r \bar{z}^2}{4} + \frac{1}{4\alpha_r} (1 - \alpha_i \bar{z})^2 \\ B &= \frac{1}{4} \alpha_r + \frac{1}{4} \frac{\alpha_i^2}{\alpha_r} \\ C &= \frac{\bar{z} \alpha_r}{2} - \frac{1}{2} \frac{\alpha_i}{\alpha_r} (1 - \alpha_i \bar{z}) \end{aligned} \tag{3.40}$$

The beam size ratio is then

$$\frac{W_0^2(\bar{z})}{W_0^2(0)} = \frac{\alpha_i \bar{z}^2 + \frac{(1 - \alpha_i \bar{z})^2}{\alpha_r}}{\frac{1}{\alpha_r}} = \alpha_r^2 \bar{z}^2 + (1 - \alpha_i \bar{z})^2 \tag{3.41}$$

Whence for the focused beam, a minimum beam size occurs at a distance  $z = z'$  such that

$$\frac{d}{d\bar{z}} \left[ \frac{W_0^2(\bar{z})}{W_0^2(0)} \right]_{\bar{z}=\bar{z}'} = 0 \tag{3.42}$$

Applying equation (3.41), one obtains

$$\bar{z}' = \frac{\alpha_i}{\alpha_r^2 + \alpha_i^2} \tag{3.43}$$

and thus

$$\left[ \frac{W_0^2(z)}{W_0^2(0)} \right]_{\min} = \frac{(\alpha_i \alpha_r)^2}{(\alpha_r^2 + \alpha_i^2)^2} + \left( 1 - \frac{\alpha_i^2}{\alpha_r^2 + \alpha_i^2} \right)^2 \quad (3.44)$$

Using equation (3.33) and (3.38), we have for the axial intensity ratio

$$\frac{I(z)}{I(0)} = \frac{1}{2} \sqrt{\frac{1}{\alpha_r A}} = \left( \frac{1}{\alpha_r^2 z^2 + (1 - \alpha_i z)^2} \right)^{\frac{1}{2}} \quad (3.45)$$

and the normalized MCF ( $x = 0$ ) is then

$$\begin{aligned} \frac{M_2(0, \xi, z)}{M_2(0, 0, z)} &= e^{-\xi^2 \left( B - \frac{C^2}{4A} \right)} \\ &= e^{-\frac{\alpha_r \xi^2}{4} \left[ \frac{1}{\alpha_r^2 z^2 + (1 - \alpha_i z)^2} \right]} \quad (3.46) \end{aligned}$$

We note that the correlation width,  $\left[ \frac{2}{\alpha_r} (\alpha_r^2 z^2 + (1 - \alpha_i z)^2) \right]^{\frac{1}{2}}$ , is minimum when  $z = z' = \frac{\alpha_i}{\alpha_r + \alpha_i}$ , which implies that the correlation length of a focussed beam reduces to a minimum at the focal point and retains its coherence beyond the focal distance.

(case c) In the presence of turbulent medium,  $a > 0$ , the beam size ratio becomes

$$\frac{W_0^2(z)}{W_0^2(0)} = \alpha_r^2 z^2 + (1 - \alpha_i z)^2 + \frac{4}{3} a \alpha_r z^3 \quad (3.47)$$

where "a" measures the strength of turbulence. For the collimated beam,  $\alpha_i = 0$ , the beam size ratio reduces to  $1 + \alpha_r^2 z^2 + \frac{4}{3} a \alpha_r z^3$ , which implies a broadening of beam size with increasing distance. If  $\alpha_i > 0$ , indicative of focused beams, the minimum values of (3.47) will occur at

$$z = z' = \frac{-(\alpha_r^2 + \alpha_i^2) + [(\alpha_r^2 + \alpha_i^2) + 8 a \alpha_r \alpha_i]^{\frac{1}{2}}}{4 a \alpha_r} \quad (3.48)$$

If  $\alpha_i < 0$ , the beam focuses at negative values of z, i.e. it diverges with increasing z. The axial intensity ratio is

$$\frac{I(z)}{I(0)} = \frac{1}{2} \sqrt{\frac{1}{\alpha_r A}} = \left[ \alpha_r^2 z^2 + (1 - \alpha_i z)^2 + \frac{4}{3} a \alpha_r z^3 \right]^{-\frac{1}{2}} \quad (3.49)$$

For a divergent beam,  $\alpha_i < 0$ , the axial intensity ratio decays with increasing turbulent strength or increasing z. For a focused beam,  $\alpha_i > 0$ ,  $I(z)/I(0)$  will reach a minimum value at  $z = z'$  given by equation (3.48).

The normalized MCF given by at  $x = 0$  is equal to

$$\frac{M_2(0, \xi, \zeta)}{M_2(0, 0, \zeta)} = e^{-\xi^2 \left( B^2 - \frac{c^2}{A} \right)}$$

$$= e^{-\frac{1}{4} a_r \xi^2 \left[ \left( 1 + \frac{a_i^2}{a_r^2} + a_r \zeta \right) - \frac{\left[ a_r \zeta - \frac{a_i}{a_r} (1 - a_i \zeta) + 2a \zeta^2 \right]^2}{a_r^2 \zeta^2 + (1 - a_i \zeta)^2 + \frac{4}{3} a_r \zeta^3} \right]} \quad (3.50)$$

We observe that for collimated beams propagating in a random medium, wherein  $a_i = 0$  and  $a > 0$ , the wave will lose its coherence (the correlation length reduces) with increasing  $z$ .

For  $a_i > 0$ , the focused beam will reduce its correlation length before the focal point. After passing the focal distance, it broadens until turbulent effects dominate at which point the beam again loses its coherence. For the divergent beam case, the wave will increase its correlation length and then lose its coherence when the turbulent effect dominates.

To illustrate the evolution of Mutual Coherence Function, plots of  $M(x, \xi, \zeta)$  in the  $x, \xi$  space, for the case  $a_r = a_i = 1$ ,  $a = 0$  representation of a focused beam propagating in free space, are shown in Fig. 3.1a-3.1b at distance  $z = 0.5, 1, 1.5, 2$ . For a initial MCF depicted in Fig. 1, the focusing effect at  $z = 0.5$  is apparent.

Figs. 2a-2b display the Mutual Coherence Function for a focused beam in a random medium with  $a = k g = 1$ ,  $a_r = a_i = 1$ , the beam assumes a minimum width in  $x$  at  $z'$  according to equation (3.48) and then spreads in the  $x$  direction. Because of the turbulent effect, the MCF decorrelates as the wave is propagated and the width in  $\xi$  space is reduced. The amplitude of



dist= 5.00000e-01 kg= 0.0  
kb= 1.00000 kb= 1.00000  
Mutual coh. function

Kg= 5.00000e-01

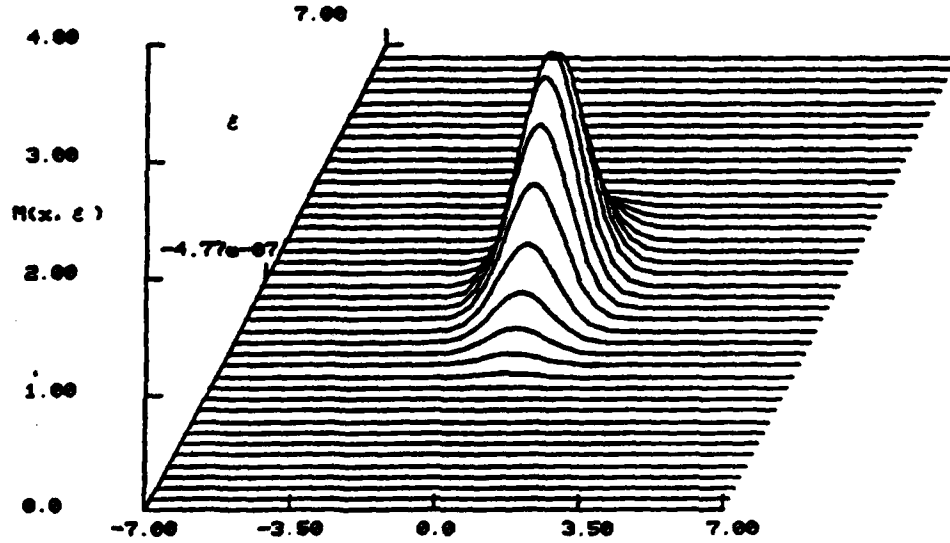


Fig. 1a. Amplitude of MCF at  $z = 0.5$ ; a focused beam propagating in free space;  $\alpha_r = \alpha_i = 1$ .

dist= 1.00000 kg= 0.0  
kb= 1.00000 kb= 1.00000  
Mutual coh. function

Kg= 5.00000e-01

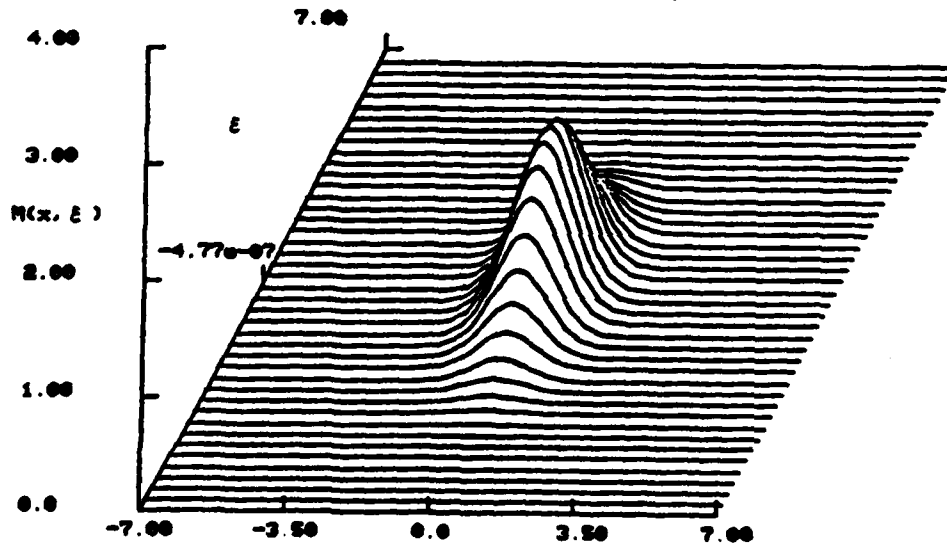


Fig. 1b. Amplitude of MCF at  $z = 1$ ; a focused beam propagating in free space;  $\alpha_r = \alpha_i = 1$ .

dist= 1.50000      kg= 0.0      Kg= 5.00000e-01  
ka= 1.00000      kb= 1.00000  
Mutual coh. function

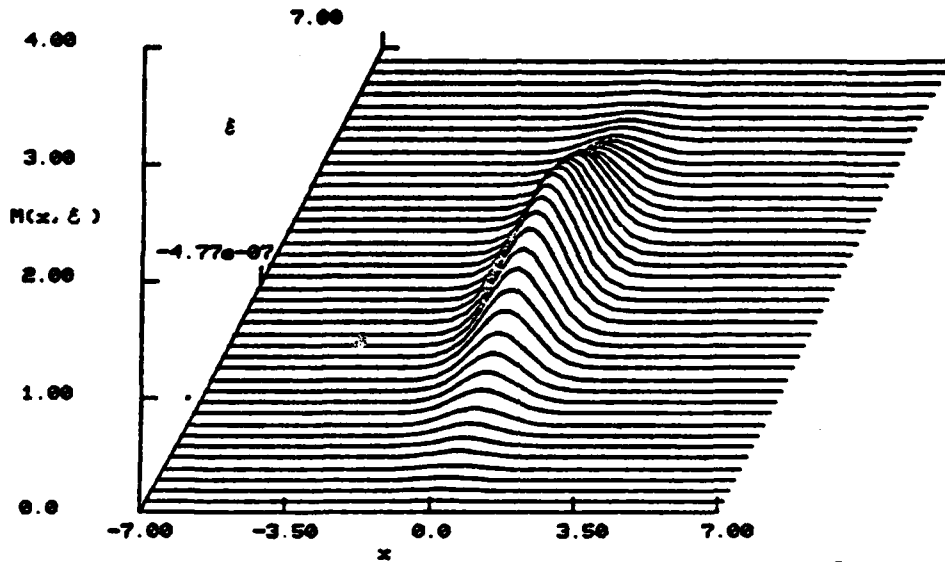


Fig. 1c. Amplitude of MCF at  $z = 1.5$ ; a focused beam propagating in free space;  $\alpha_r = \alpha_\lambda = 1$ .

dist= 2.00000      kg= 0.0      Kg= 5.00000e-01  
ka= 1.00000      kb= 1.00000  
Mutual coh. function  
x

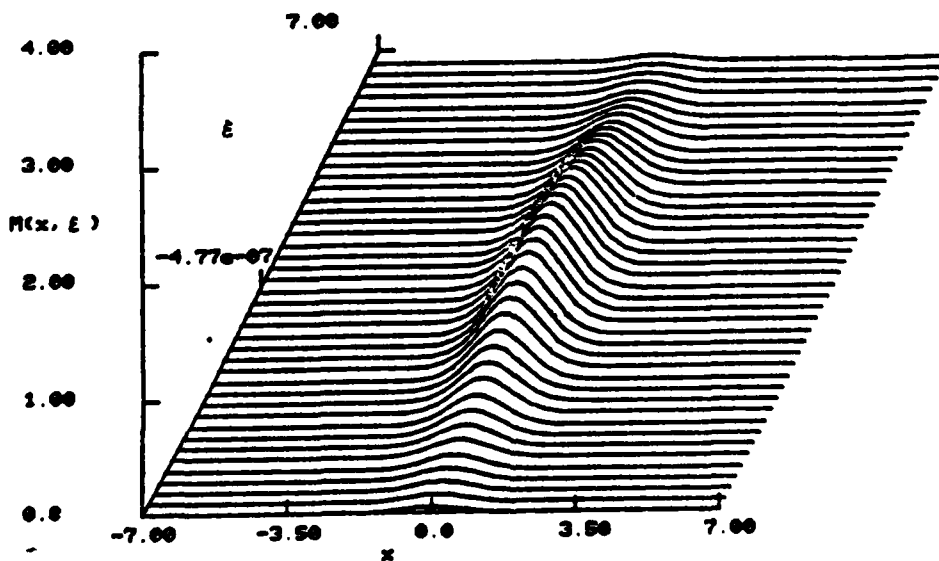


Fig. 1d. Amplitude of MCF at  $z = 2$ ; a focused beam propagating in free space;  $\alpha_r = \alpha_\lambda = 1$ .

the MCF decays with increasing  $z$ . Normalized MCFs calculated by use of equations (3.38) (3.45)-(3.50) are depicted in Figs. 3-9. For the case of a collimated beam in free space, the normalized MCF is broadened with increasing  $z$  (Fig.3). For the focused beam, the correlation length reduces to a minimum value at  $z = 0.5$ . Beyond the focal point, the beam starts to spread and increases its correlation length (Fig.4). Fig. 5 displays the normalized MCF for a collimated beam in a medium with the turbulent strength  $a = 1$ ; the correlation length decreases as  $z$  increases. The same case for a focused beam is depicted in Fig. 6. Due to focusing, the width of normalized MCF becomes narrower for small  $z$ , it then broadens for some distance because of the diffraction effect, finally, turbulent effects reduces its coherence length. Fig. 7 and 8 shows the MCF different values of "a" for a collimated beam and a focused beam respectively. In both cases, the MCF become more decorrelated as the turbulence becomes stronger. The effects of turbulence for different initial beam sizes are shown in Fig. 9a-9b for collimated beam and focused beam. The correlation length is larger for a wider beam size, as one expects.

### III. Numerical Evaluation of MCF for a Complicated Power Spectrum

To obtain MCF for an arbitrary power spectrum, one can apply the same procedure as described in section II. However, because of the complicate integration involved in evaluating the function  $H(\xi)$ , it is not realistic to solve the problem analytically. A numerical procedure via the quasiparticle distribution function approach will be used to find the disire information.

It is necessary to developpe a numerical scheme which calculates the slow quasiparticle distribution function  $S(K, \epsilon, \delta)$

dist= 5.00000e-01 kg= 1.00000 Kg= 5.00000e-01  
ka= 1.00000 kb= 1.00000  
Mutual coh. function

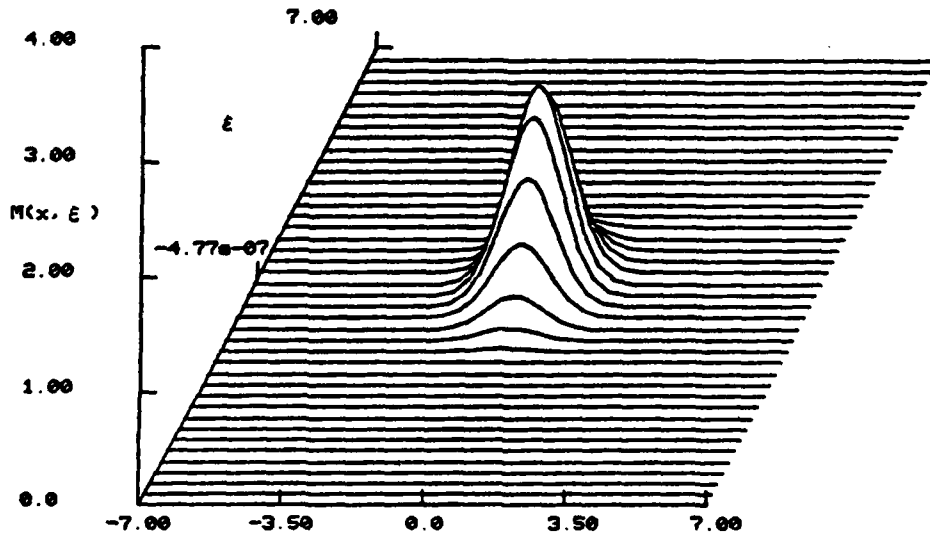


Fig. 2a. Amplitude of MCF at  $z = 0.5$ ; a focused beam propagating in a random medium with  $H(\xi) = a\xi^2$ ;  $a = 1$ ,  $\alpha_i = \alpha_r = 1$ .

dist= 1.00000 kg= 1.00000 Kg= 5.00000e-01  
ka= 1.00000 kb= 1.00000  
Mutual coh. function

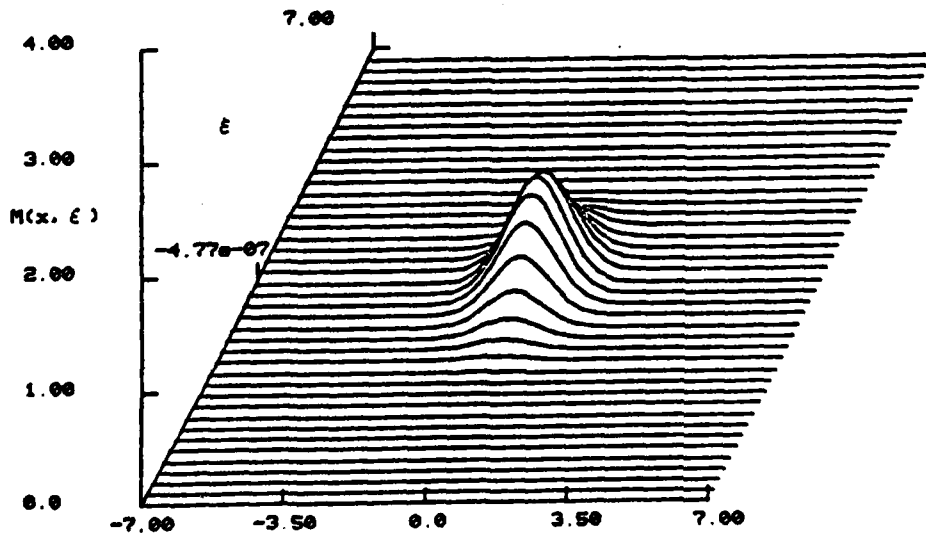


Fig. 2b. Amplitude of MCF at  $z = 1$ ; a focused beam propagating in a random medium with  $H(\xi) = a\xi^2$ ;  $a = 1$ ,  $\alpha_r = \alpha_i = 1$ .

dist= 1.50000      kg= 1.00000      Kg= 5.00000e-01  
ke= 1.00000      kb= 1.00000  
Mutual coh. function

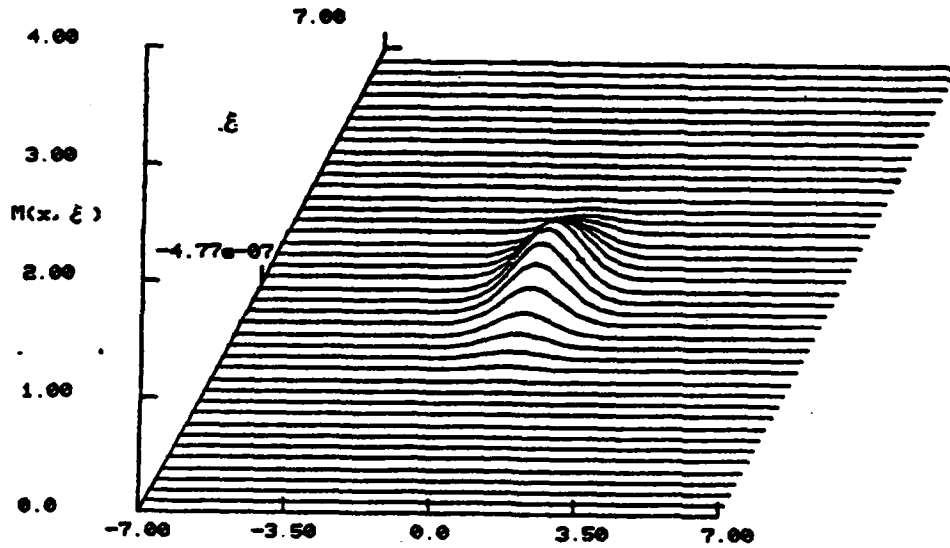


Fig. 2c.       $z = 1.5$ .

dist= 2.00000      kg= 1.00000      Kg= 5.00000e-01  
ke= 1.00000      kb= 1.00000  
Mutual coh. function  
x

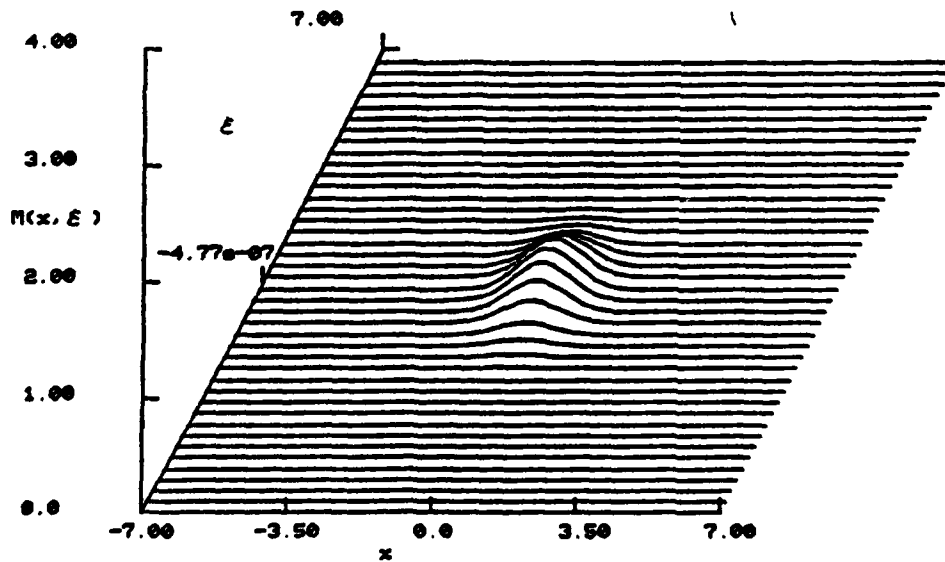


Fig. 2d.       $z = 2$ .

$k_g = 0.0$        $k_t = 2.50000$        $K_t = 2.50000 \times 10^{-1}$   
 $k_a = 0.0$        $k_b = 1.00000$   
 Mutual coh. function       $t \leftrightarrow z$

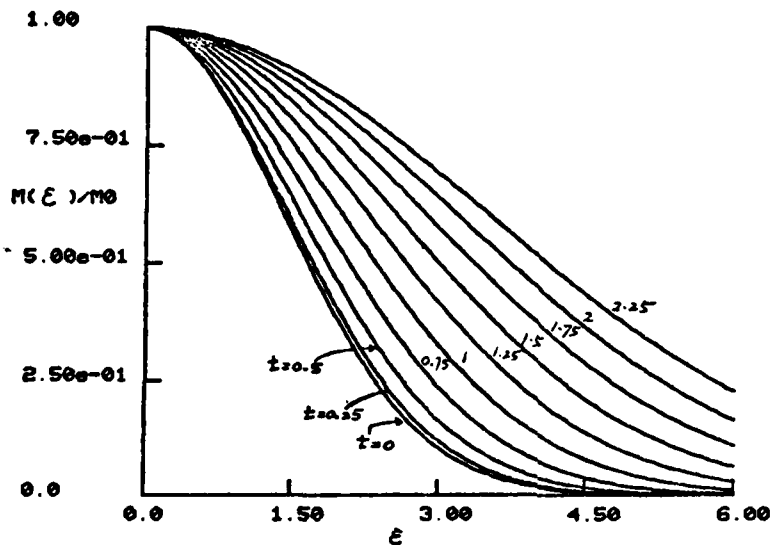


Fig. 3. Normalized MCF vs.  $\xi$  for different values of  $z$ ; a collimated beam propagating in free space.

$k_g = 0.0$        $k_t = 2.50000$        $K_t = 2.50000 \times 10^{-1}$   
 $k_a = 1.00000$        $k_b = 1.00000$   
 Mutual coh. function       $t \leftrightarrow z$

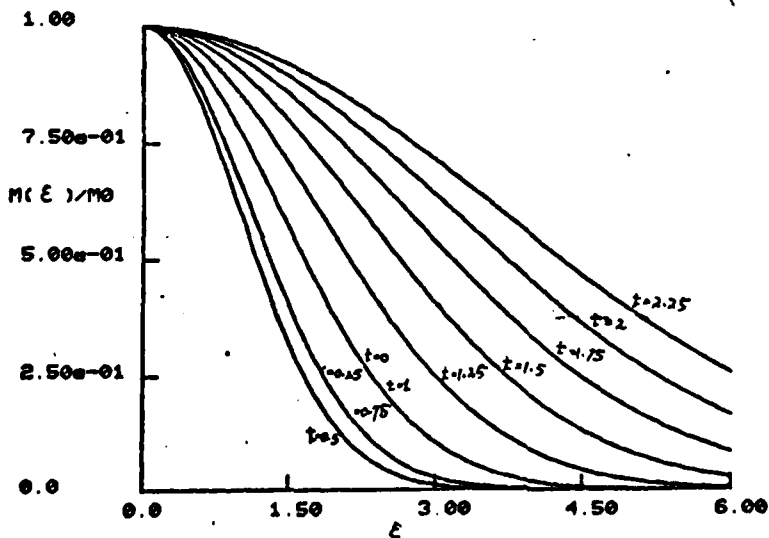


Fig. 4. Normalized MCF vs.  $\xi$  for different values of  $z$ ; a focused beam propagating in free space.

kg= 1.00000      kt= 4.00000      Kt= 5.00000e-01  
ka= 0.0           kb= 1.00000  
Mutual coh. function

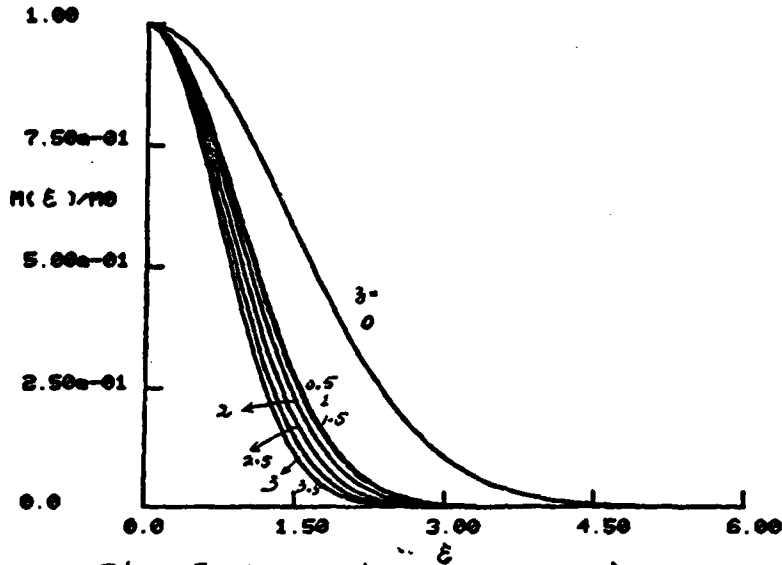


Fig. 5. Normalized MCF vs.  $\xi$  for different values of  $z$ ; a collimated beam propagating in a random medium with  $H(\xi) = a \xi^2$ ,  $a = 1$ .

kg= 1.00000      kt= 4.00000      Kt= 5.00000e-01  
ka= 1.00000      kb= 1.00000  
Mutual coh. function

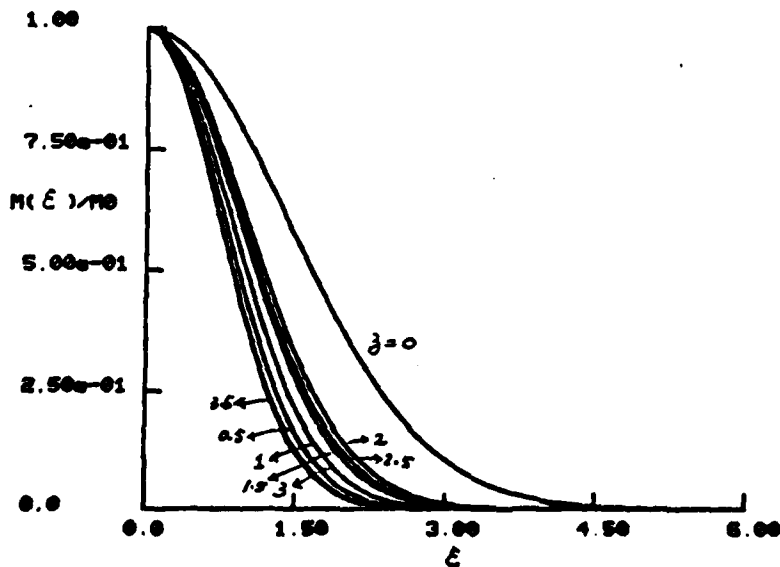


Fig. 6. Normalized MCF vs.  $\xi$  for different values of  $z$ ; a focused beam propagating in a random medium with  $H(\xi) = a \xi^2$ ,  $a = 1$ .

dist= 1.00000 kg= 3.00000 Kg= 5.00000e-01  
ka= 0.0 kb= 1.00000  
Mutual coh. function

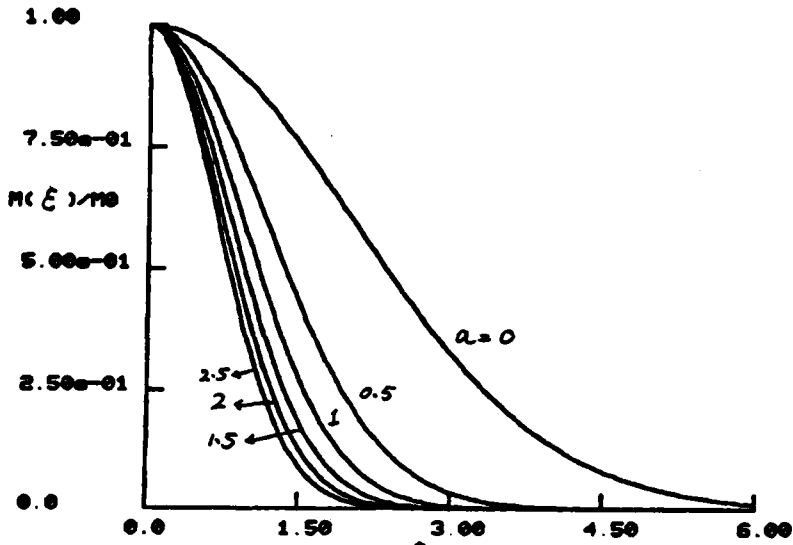


Fig. 7. Normalized MCF vs.  $\xi$  for different values of  $a$ ; a collimated beam propagating in a random medium with  $H(\xi) = a \xi^2$ .

dist= 1.00000 kg= 3.00000 Kg= 5.00000e-01  
ka= 1.00000 kb= 1.00000  
Mutual coh. function for

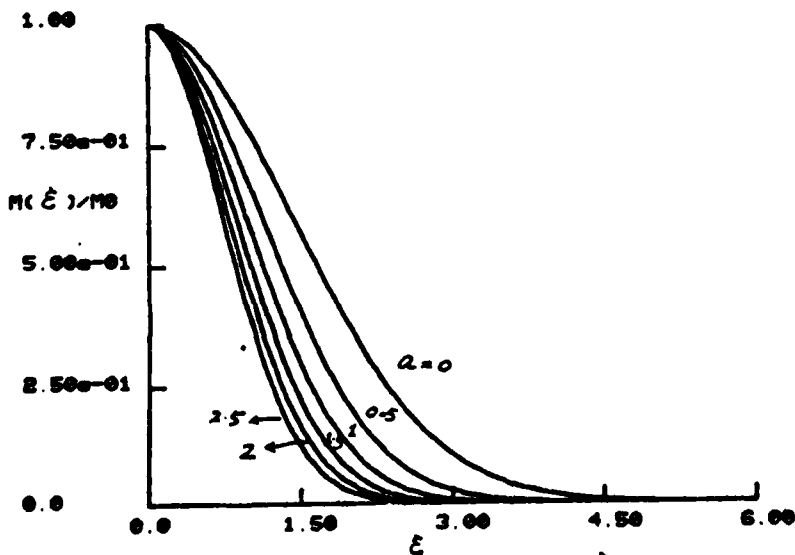


Fig. 3. Normalized MCF vs.  $\xi$  for different values of  $a$ ; a focused beam propagating in a random medium with  $H(\xi) = a \xi^2$ .

kg= 1.00000      dist= 5.00000e-01   kb= 11.0000  
ka= 0.0           Kb= 1.00000  
Mutual coh. function

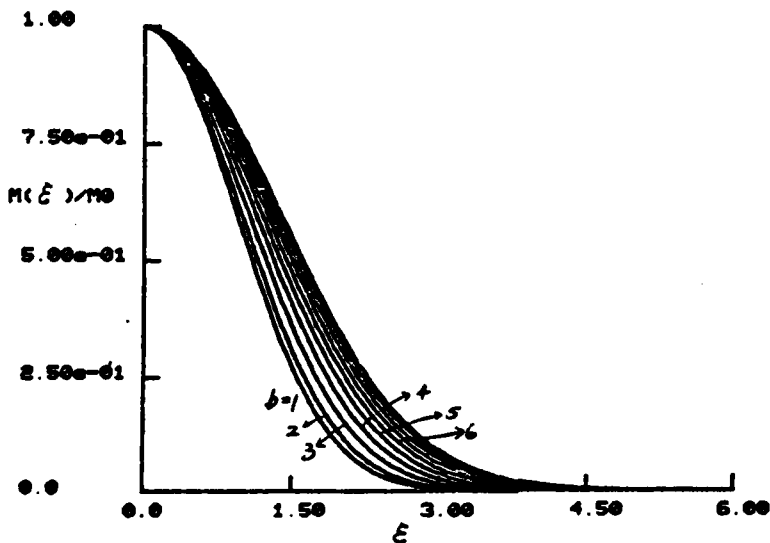


Fig. 9a. Normalized MCF vs.  $\xi$  for different values of beam width  $b$ ; a collimated beam propagating in a random medium with  $H(\xi) = a\xi^2$ ,  $a = 1$ .

kg= 1.00000      dist= 5.00000e-01   kb= 11.0000  
ka= 1.00000      Kb= 1.00000  
Mutual coh. function

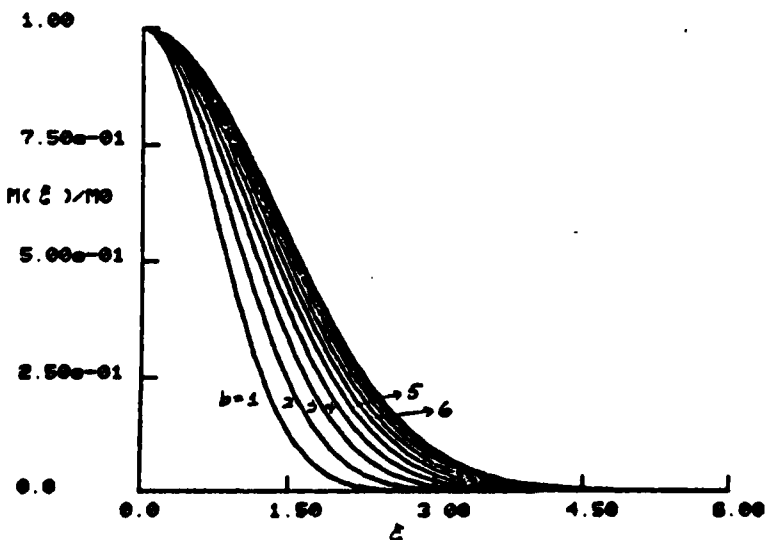


Fig. 9b. Normalized MCF vs.  $\xi$  for different values of beam width  $b$ ; a focused beam propagating in a random medium with  $H(\xi) = a\xi^2$ ,  $a = 1$ .

for a given  $S(\kappa, \xi, 0)$ . The corresponding results for intensity, beam size ratio and normalized MCF can then be obtained via equations (3.6) and (3.11). We shall first examine the case of a collimated beam propagating in free space to check the accuracy of the algorithm being used. The  $z = 0$  quasiparticle distribution function which follows from equation (3.31), i.e.

$$S(\kappa, \xi, 0) = \sqrt{\frac{\pi}{\alpha_r}} e^{-\frac{1}{4}\alpha_r \xi^2} e^{-\frac{(\kappa + \alpha_i \xi)^2}{4\alpha_r}} \quad (3.51)$$

is depicted in Fig. 10 for the case  $\alpha_r = 1$ ,  $\alpha_i = 0$ . The quasiparticles are evenly distributed in the intervals  $-7 < \xi < +7$ ,  $-7 < \kappa < +7$ . At a subsequent distance  $z$  the distribution function follows from (3.24) and (3.21) as

$$S(\kappa, \xi, \xi') = S(\kappa, \xi - \kappa \xi', 0) \quad (3.52)$$

i.e. the quasiparticle density is redistributed when evolves in  $\xi'$ , as the quasiparticle spread in  $\xi$  the probability distribution function (d.f.) with coordinates  $S(\kappa, \xi - \kappa \xi', 0)$ , at  $z = 0$  "moves" to the new location  $S(\kappa, \xi, \xi')$  at  $z = z'$ . The redistribution phenomena enable us to interpolate every point in  $\kappa, \xi$  space from the initial d.f. to the final d.f. at  $z = z'$  numerically. Figs. 11-12 display the  $S$  function at  $z = 0.75$ , 1.5 respectively. The quasiparticles with higher  $\kappa$  "move" faster than those with smaller  $\kappa$ . The resulting d.f. thus spreads along  $\xi$  directions. The MCF at  $x = 0$  as a function of  $\xi$  for distances  $z$  corresponding to the associated  $S(\kappa, \xi, \xi')$

DIST= 0.0      KE= 2.00000      KB= 1.00000E-01      #WIDTH= 1.00000  
# OF INTER= 40.0000      KC= 0.0      KT= 9.37500E-03  
KE= 0.0

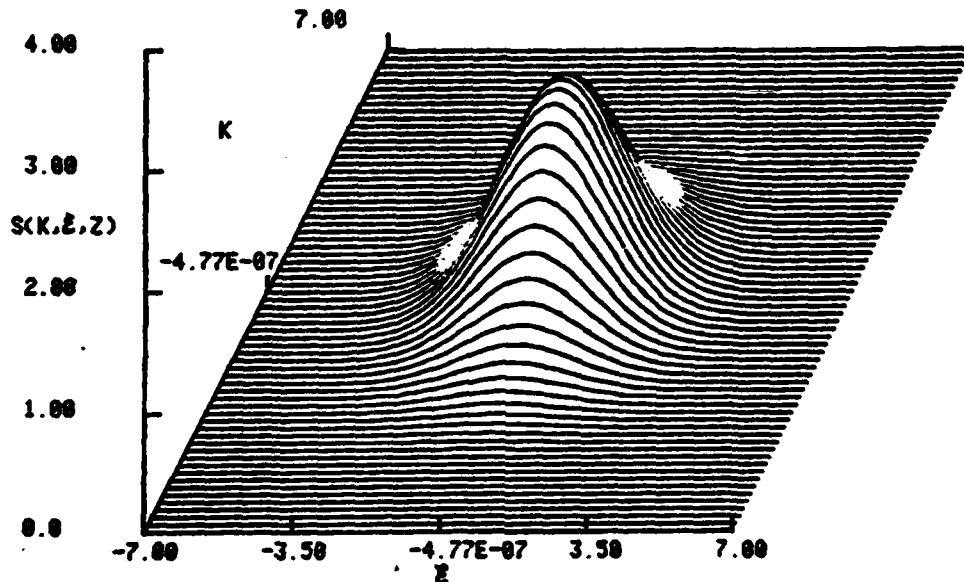


Fig. 10. Initial slow quasiparticle distribution function for collimated beam with  $\alpha_V = 1$ ;  $z = 0$ .

DIST= 7.50000E-01      KE= 2.00000      KB= 1.00000E-01      #WIDTH= 1.00000  
# OF INTER= 40.0000      KC= 0.0      KT= 9.37500E-03  
KE= 0.0

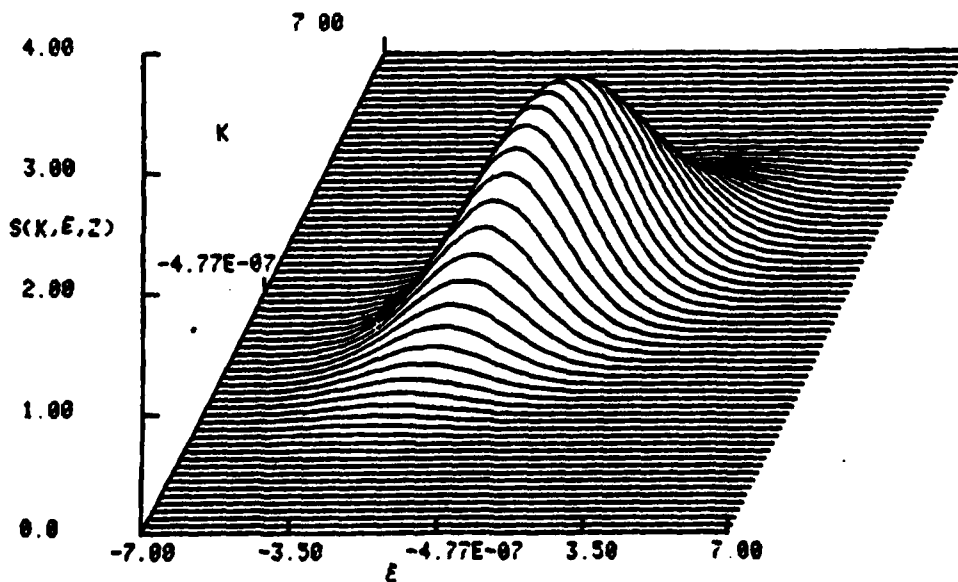


Fig. 11.  $S$  function in  $K, E$  space;  $z = 0.75$ . a collimated beam propagating in free space.

DIST= 1.50000      KE= 2.00000      KB= 1.00000E-01      #WIDTH= 1.00000  
KE= 0.0      # OF INTER= 40.0000      KC= 0.0      KT= 9.37500E-03

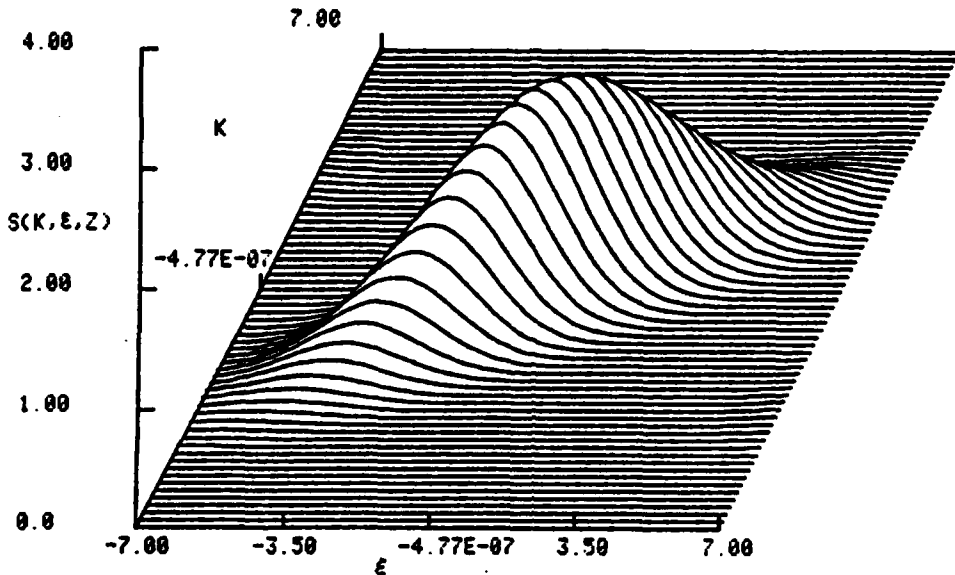


Fig. 12. S function in K , ε space; z = 1.5.  
a collimated beam propagating in free space.

DIST= 1.50000      KE= 2.00000      KB= 1.00000E-01      #WIDTH= 1.00000  
KE= 0.0      # OF INTER= 40.0000      KC= 0.0      KT= 9.37500E-03

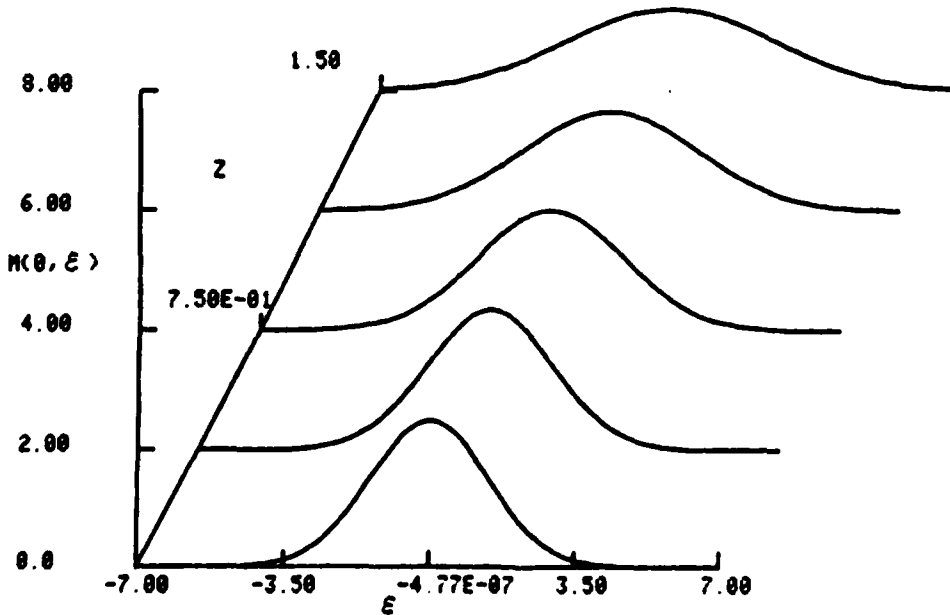


Fig. 13. MCF vs. ε at x = 0; a collimated beam  
propagating in free space.

DIST= 0.0      KE= 2.00000      KB= 1.00000E-01      #WIDTH= 1.00000  
\*      KE= 1.00000      # OF INTER= 40.0000      KC= 0.0      KT= 9.37500E-03

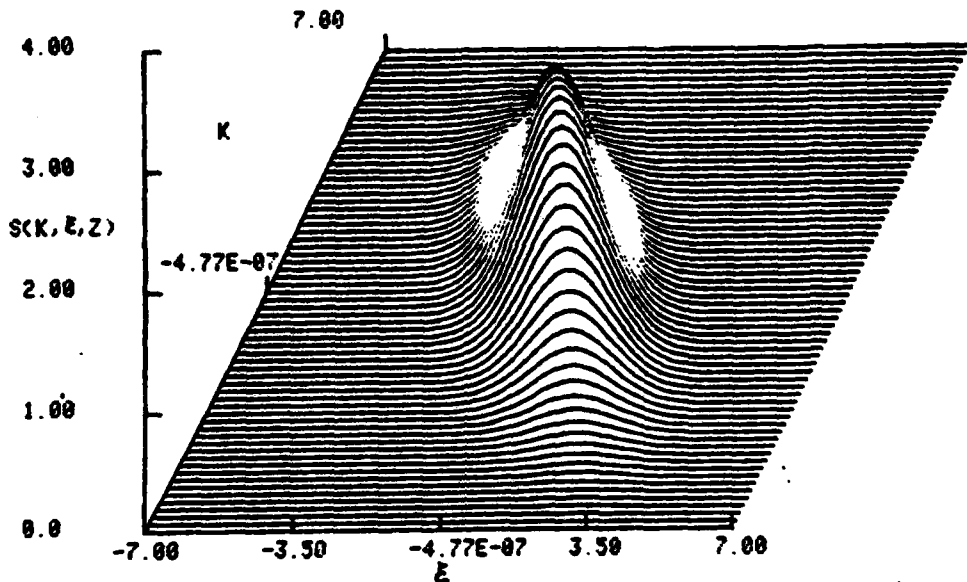


Fig. 14. Initial slow quasiparticle distribution function for focused beam with  $\alpha_v = \alpha_\lambda = 1$ ;  $z = 0$ .

DIST= 7.50000E-01      KE= 2.00000      KB= 1.00000E-01      #WIDTH= 1.00000  
\*      KE= 1.00000      # OF INTER= 40.0000      KC= 0.0      KT= 9.37500E-03

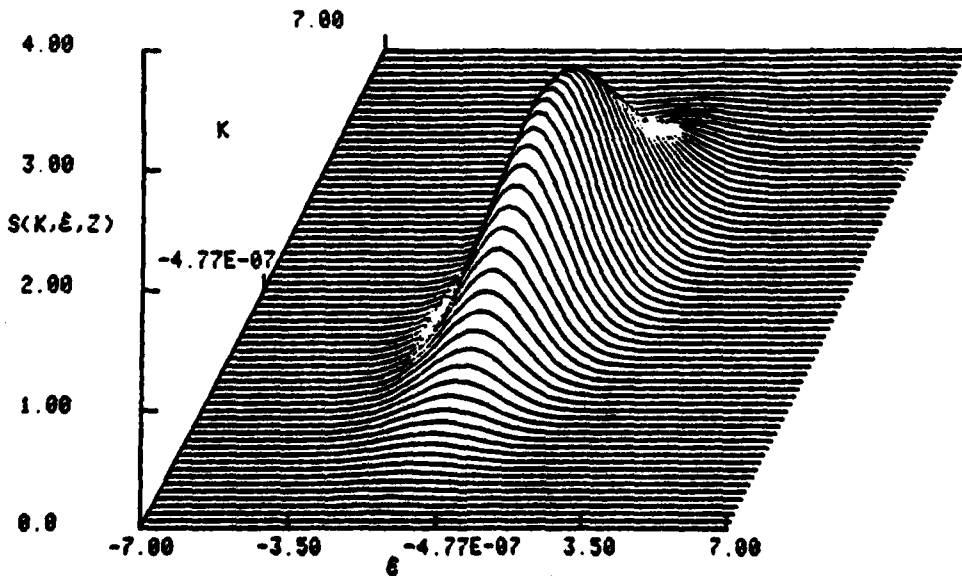


Fig. 15. S function in K, z space;  $z = 0.75$ , a focused beam propagating in free space.

DIST= 1.50000    KE= 2.00000    KB= 1.00000E-01    #WIDTH= 1.00000  
KE= 1.00000    # OF INTER= 40.0000    KC= 0.0    KT= 9.37500E-03

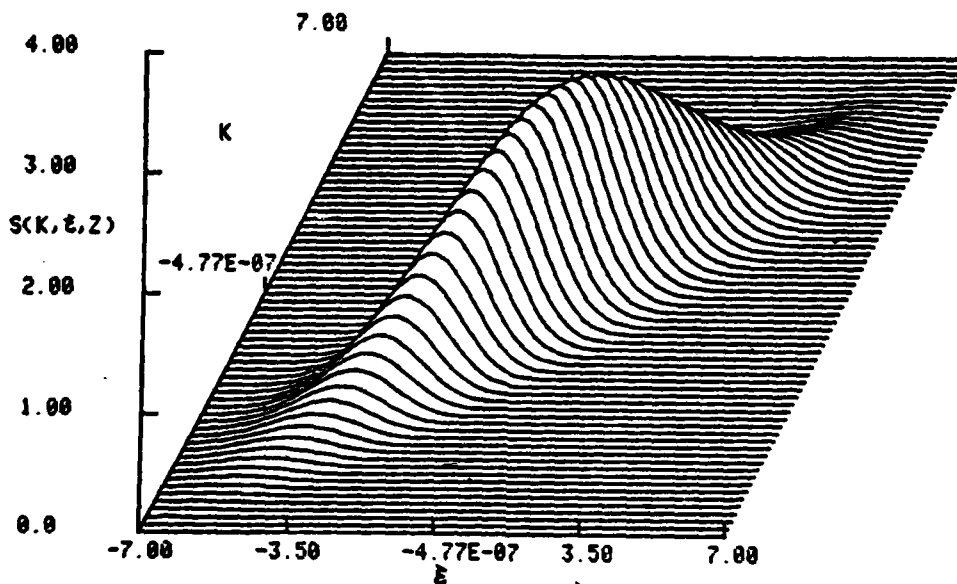


Fig. 16. S function in  $K, \xi$  space;  $z = 1.5$ , a focused beam propagating in free space.

DIST= 1.50000    KE= 2.00000    KB= 1.00000E-01    #WIDTH= 1.00000  
KE= 1.00000    # OF INTER= 40.0000    KC= 0.0    KT= 9.37500E-03

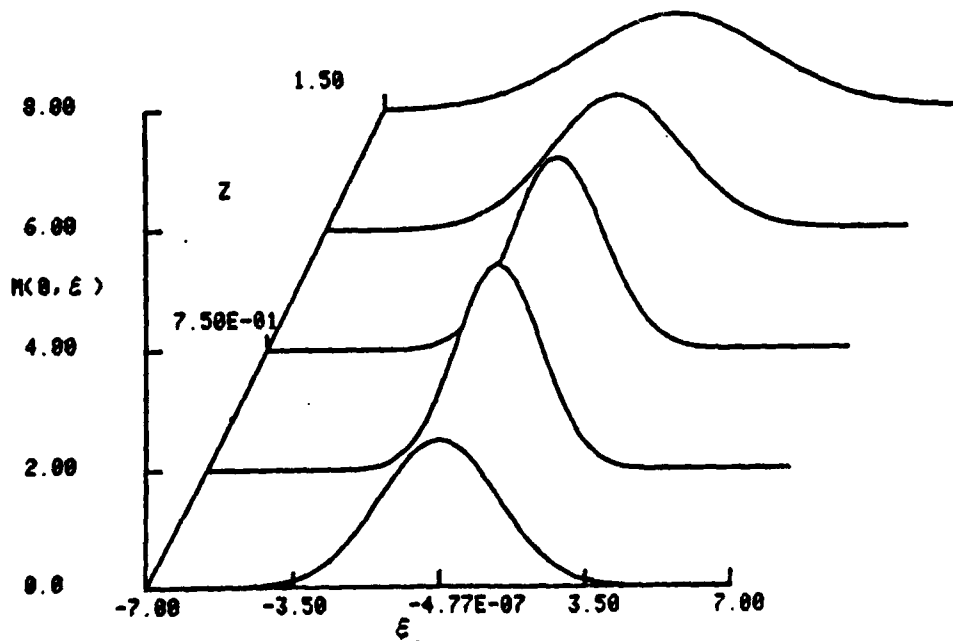


Fig. 17. MCF vs.  $\xi$  at  $x = 0$ ; a focused beam propagating in free space.

DIST= 1.00000 KE= 2.00000 KB= 1.00000E-01 #WIDTH= 1.00000  
KE= 0.0 # OF INTER= 20.0000 KG= 1.00000E-01 KT= 1.25000E-02

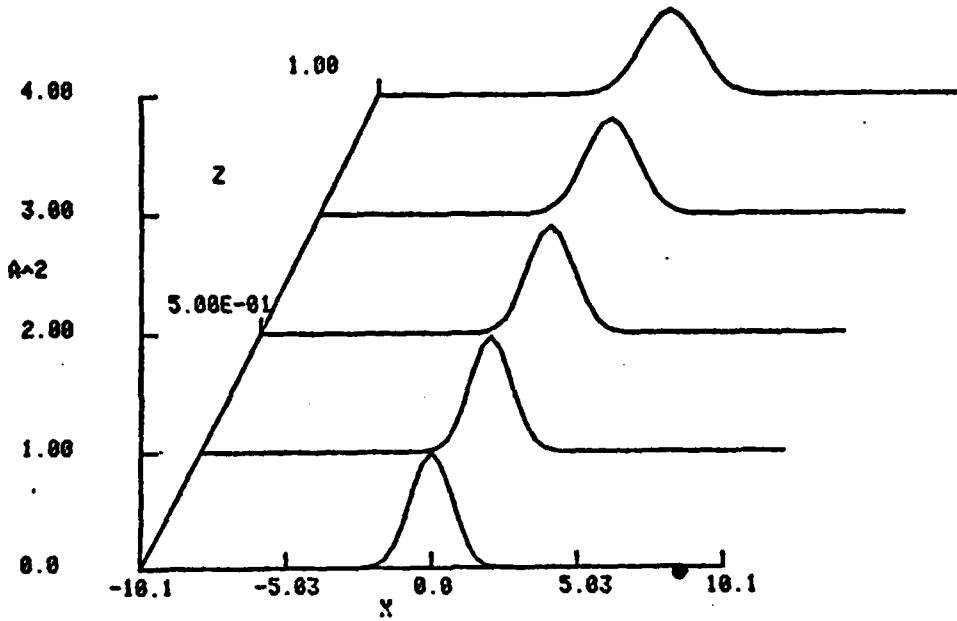


Fig. 18. intensity function  $I(x,z)$  vs.  $x$ ;  
a collimated beam propagating in free space.

DIST= 1.00000 KE= 2.00000 KB= 2.00000E-01 #WIDTH= 1.00000  
KE= 1.00000 # OF INTER= 20.0000 KG= 1.00000E-01 KT= 1.25000E-02

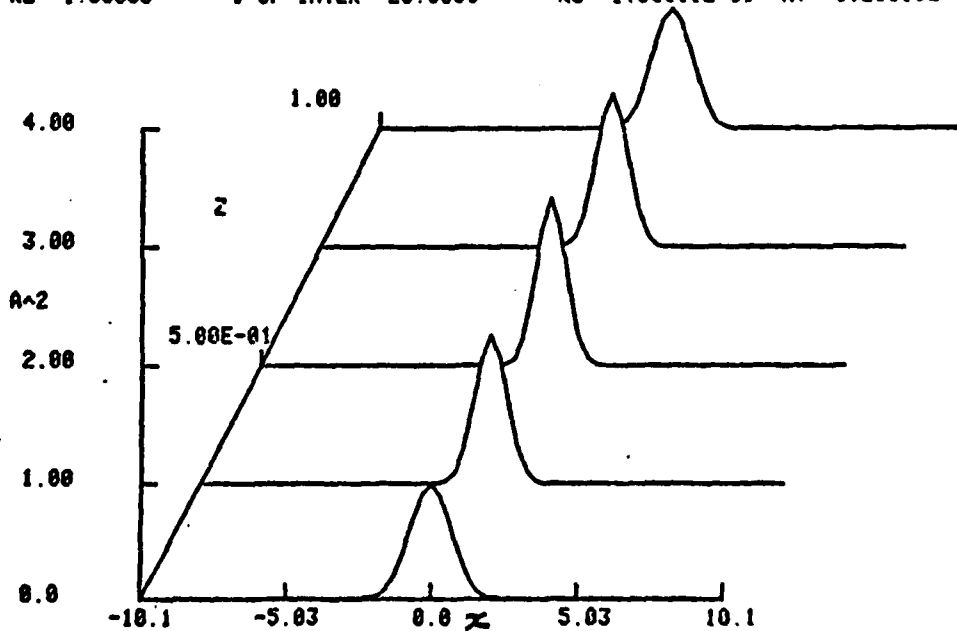


Fig. 19. Intensity function  $I(x,z)$  vs.  $x$ ;  
a focused beam propagating in free space.

are displayed in Fig. 13. The spreading effect increases the coherence length as  $z$  increases. Fig. 14 depicts the initial condition described by equation (3.51) with  $\alpha_r = \alpha_i = 1$ ,  $a = 0$  i.e. focused beam in free space at  $z < 0.5$ , the field reduce its coherence length because of the focusing effect, it then spreads as  $z = 0.5$ , as described in section II. The S function at  $z = 0.75, 1.5$  are shown in Fig. 15, 16. Fig. 17 displays the MCF as a function of  $\xi$  and  $z$ . The above exact results have been used to check the accuracy of the algorithm and found to be very good.

The Fourier transform of  $S(k, \xi, z)$  gives the MCF  $M(x, \xi, z)$ . Setting  $\xi = 0$ , one obtains the intensity,  $I(x, z) = M(x, 0, z)$  as a function of  $x$  and  $z$ . Figs. 18 and 19 depict the intensity function for collimated and focused beams propagating in free space. In the first case the intensities spreads in the  $x$  direction as  $z$  evolves. The focusing effect is observed in the second case and is shown in Fig.19.

For a wave propagating thru a random medium, characterized by a power spectrum  $\Phi(k)$ , the evolution of the S function can be obtained from the relation:

$$S(k, \xi, z) = S(k, \xi(0), 0) e^{-\int_0^z H(\xi(0) + k z') dz'} \quad (3.53)$$

where, for the one dimensional case,  $H(\xi)$  can be represented as

$$H(\xi) = \int_{-\infty}^{\infty} 2\pi (1 - \cos k\xi) \Phi(k) dk \quad (3.54)$$

Along the quasiparticle trajectory, one can rewrite (3.53) as

$$S(k, \xi, \beta) = S(k, \xi - k\beta, 0) e^{-\int_0^\beta H[\xi - k(\beta - \beta')] d\beta'} \quad (3.55)$$

From knowledge of the power spectrum and the initial distribution function, one can interpolate the S function along the trajectory in accordance with (3.55). That is, the S function spreads in  $\xi$  space and decays along the trajectory with a structure function  $H(\xi)$  dependence.

One finds equation (3.55) is different from eq. (3.52) by a collisional (decaying) term  $\exp -\int_0^\beta H[\xi - k(\beta - \beta')] d\beta'$ . It is thus important to observe the behavior of the H function for an arbitrary power spectrum. We shall choose three different kinds of power spectrum and study the resulting behavior of the H function:

(a) Gaussian spectrum

$$\Phi(k) = A_g e^{-\frac{(k - k')^2}{2b^2}} \quad (3.56)$$

where  $k'$  is the center of the Gaussian spectrum and  $b$  is the width

(b) Power law spectrum with spectral index  $P$

$$\Phi(k) = A_p \left(1 + \frac{k^2}{k_{L_0}^2}\right)^{-\frac{P}{2}} \quad (3.57)$$

where  $k_{L_0} = 1/L_0$  is the wavenumber associate with the outer scale  $L_0$  and  $P$  is the spectral index.

(c) Compound spectrum

$$\Phi(k) = A_c \left[ \frac{1}{\left(1 + \frac{k^2}{k_{L_0}^2}\right)^{P/2}} + a e^{-\frac{(k-k')^2}{2b^2}} \right] \quad (3.58)$$

is the superposition of spectrum (a) and (b).

The power spectrum and associated H function are shown in Figs. 20a and 20b. Curve 1 in Figs. 20a, b represents  $\Phi(k)$  and  $H(\xi)$  for spectrum type (b). The Gaussian bump power spectrum and corresponding H function are depicted in curves 2,3,4 with  $k'$  equal to 1,2,3 respectively, and with  $a = 0.3$ ,  $b = 0.2$ . One observes that the additive Gaussian bump contributes an oscillatory structure to the power spectrum. For instance,  $k' = 3$  imposes an oscillatory structure with three peaks located at  $\xi = \pi/3, \pi, 5\pi/3$ .

The oscillatory behavior implies a higher randomness in the medium. As a result, the wave is more decorrelated by the random field and a stronger scattering effect is encountered. Fig. 21a displays the Amplitude dependence of the Gaussian bump for  $a = 0.3, 0.5$  and  $0.7$  from lower curve to higher curve. The superposed behavior of spectrum (a) and (b) is shown in Fig. 21b for the case  $k' = 1, a = 0.3, b = 0.2$ .

It is of interest to evaluate numerically the S function at a distance  $z$  using equation (3.55). Once the S function is obtained, one can easily find the intensity function  $I(x,z)$  and correlation function  $M(0, \xi, z)$  at  $x = 0$  from

DIST= 2.13281      WIDTH= 1.00000      AI= 1.00000      GAMMA= 1.00000  
GCTR= 3.00000      GWID= 2.00000E-01      GAMP= 3.00000E-01      INDEX= 2.00000  
POWER SPECTRUM WITH A GAUSSIAN BUMP

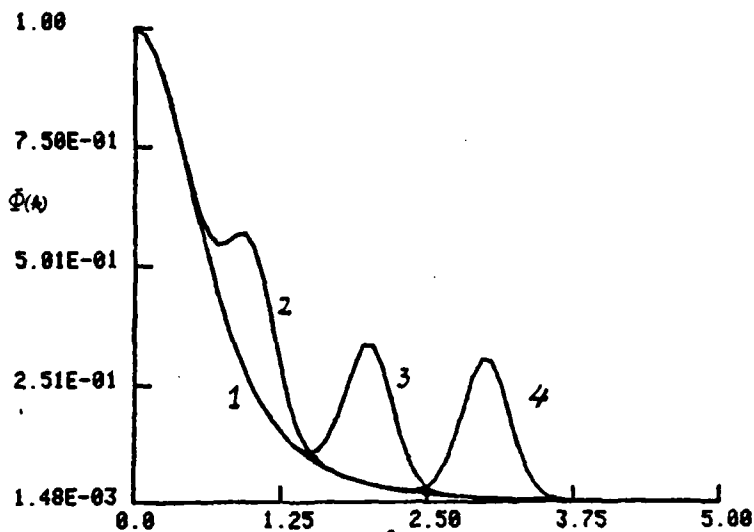


Fig. 20a.  $\Phi(k)$  vs.  $k$ ; curve 1. stands for spectrum (b) curves 2,3,4. for spectrum (c) with  $k' = 1,2,3$  respectively;  $p = 4$ ,  $a = 0.3$ ,  $b = 0.2$ .

DIST= 2.13281      WIDTH= 1.00000      AI= 1.00000      GAMMA= 1.00000  
GCTR= 3.00000      GWID= 2.00000E-01      GAMP= 3.00000E-01      INDEX= 2.00000  
POWER SPECTRUM WITH A GAUSSIAN BUMP

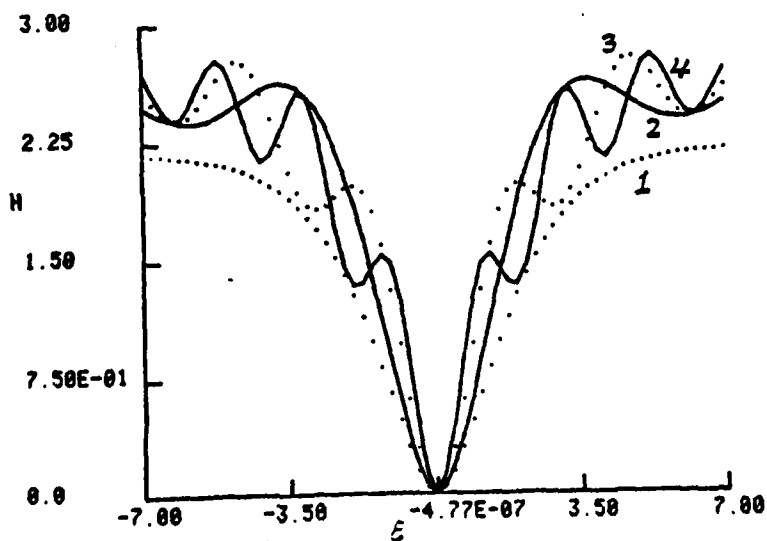


Fig. 20b.  $H(\xi)$  vs.  $\xi$ ; Curve 1,2,3,4 correspond to  $\Phi(k)$  of Fig. 20a.

DIST= 2.13281      WIDTH= 1.00000      AI= 1.00000      GAMMA= 1.00000  
GCTR= 2.00000      GWID= 2.00000E-01      GAMP= 7.00000E-01      INDEX= 2.00000

POWER SPECTRUM WITH A GAUSSIAN BUMP

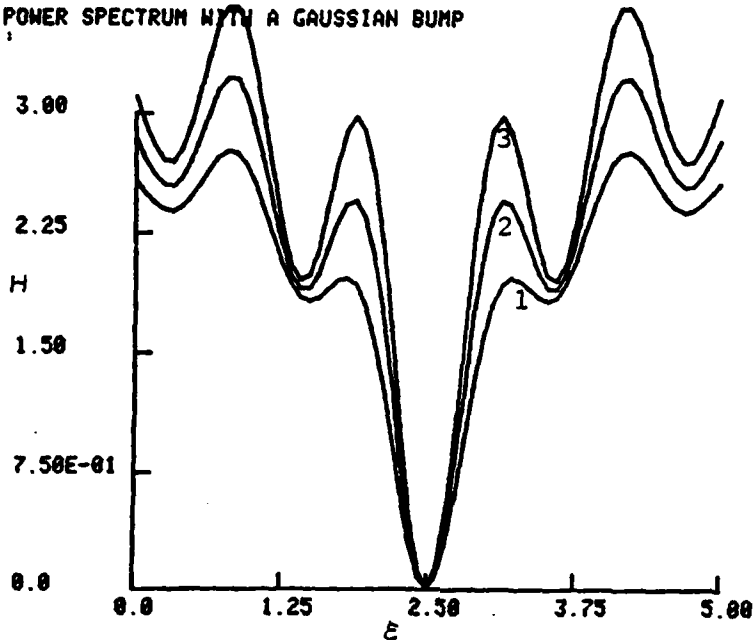


Fig. 21a.  $H(\xi)$  vs.  $\xi$  ; spectrum (c) with  $a = 0.3$  (curve 1),  $a = 0.5$  (curve 2),  $a = 0.7$  (curve 3).

DIST= 2.13281      WIDTH= 1.00000      AI= 1.00000      GAMMA= 1.00000  
GCTR= 1.00000      GWID= 2.00000E-01      GAMP= 3.00000E-01      INDEX= 2.00000

POWER SPECTRUM WITH A GAUSSIAN BUMP

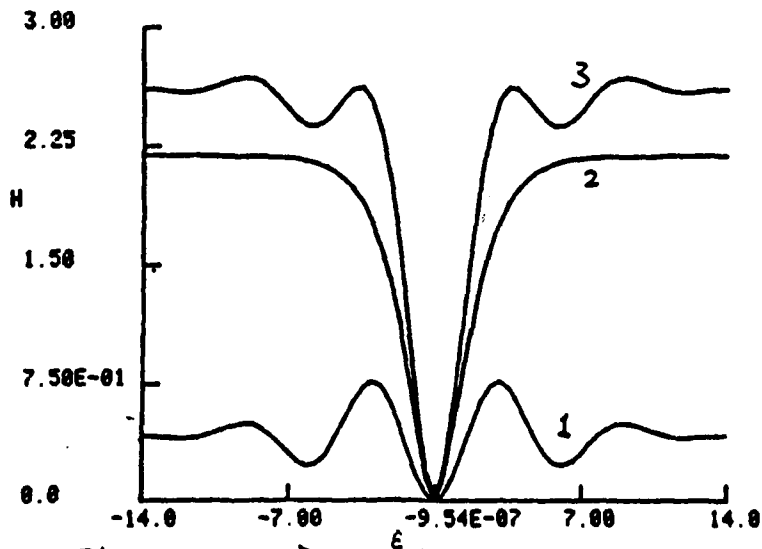


Fig. 21b.  $H(\xi)$  vs.  $\xi$  ; curve 1 for spectrum (a), curve 2 for spectrum (b), curve 3 for spectrum (c).

$$\begin{aligned}
 I(x, z) &= M(x, 0, z) \\
 &= \int S(k, 0, z) e^{ikx} \frac{dk}{2\pi} \quad (3.59)
 \end{aligned}$$

$$M(0, \xi, z) = \int S(k, \xi, z) \frac{dk}{2\pi} \quad (3.60)$$

The correlation scale  $l$  of the field is defined by

$$l = \int \frac{M(0, \xi, z)}{M(0, 0, z)} d\xi \quad (3.61)$$

and hence the knowledge of  $M(0, \xi, z)$  permits one to evaluate the correlation scale  $l$ . We shall first present some numerical evaluations of the  $S$  function by means of eq. (3.55). The significance of intensity and correlation length for both focused and collimated beams will be discussed later.

In the following numerical evaluations, we have used the normalized quantities:  $z \rightarrow z/k_0 L_0^2$ ,  $x \rightarrow x/L_0$ ,  $\gamma = \frac{1}{2} k_0^2 L_0^2 A(0)$ , where  $k_0$  is the wavenumber of the incident field and  $L_0$  is the outer scale of the random field. Figs. 22a and 22b depict the  $S$  function at the boundary  $z = 0$  for the collimated beam and focused beam, respectively. Figs. 23a-d depict the  $S$  func-

DIST= 0.0      WIDTH= 1.00000      AI= 0.0      GAMMA= 1.00000  
CTR= 0.0      GWID= 1.00000      GAMP= 1.00000      INDEX= 2.00000  
GAUSSIAN SPECTRUM

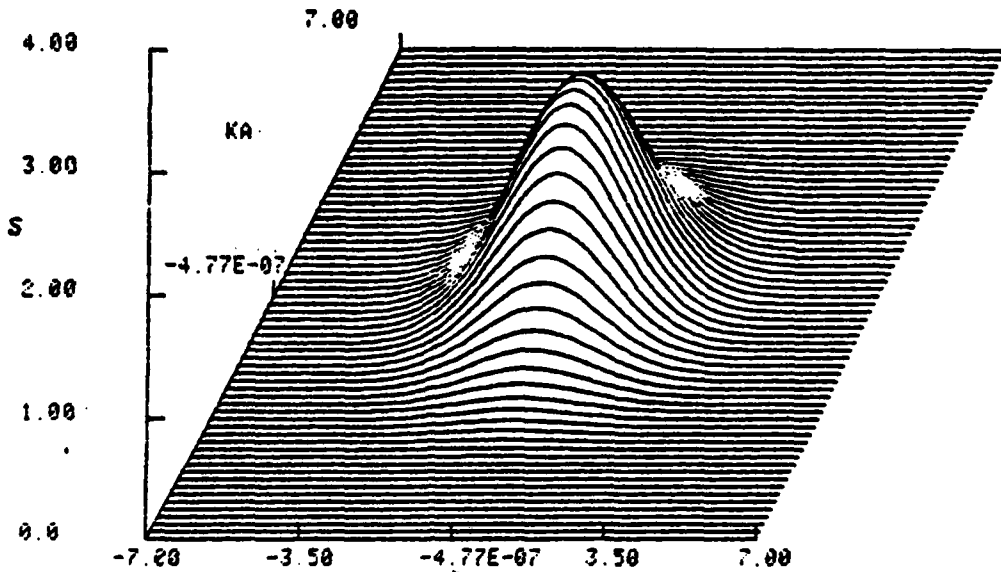


Fig. 22a. S function  $\xi$  for a collimated beam with  $\alpha_r = 1$ ;  $z = 0$ .

DIST= 0.0      WIDTH= 1.00000      AI= 1.00000      GAMMA= 10.0000  
CTR= 3.00000      GWID= 2.00000E-01      GAMP= 3.00000E-01      INDEX= 2.00000  
POWER SPECTRUM WITH A GAUSSIAN BUMP

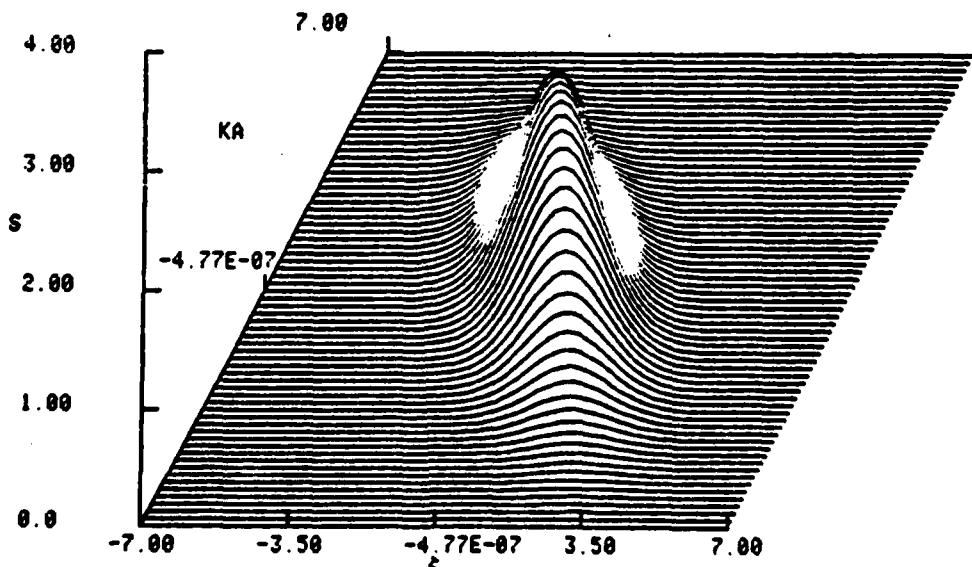


Fig. 22b. S function  $\xi$  for a focused beam with  $\alpha_r = \alpha_\lambda = 1$ ;  $z = 0$ .

DIST= 4.37500E-01 WIDTH= 1.00000 AI= 1.00000 GAMMA= 10.0000  
SCTR= 3.00000 GWID= 2.00000E-01 GAMP= 3.00000E-01 INDEX= 2.00000  
POWER LAW SPECTRUM

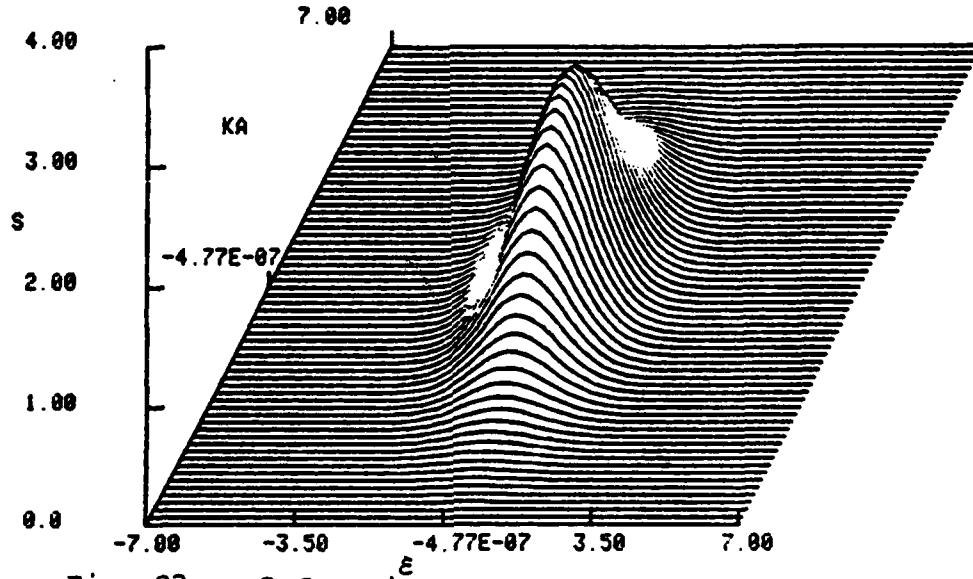


Fig. 23a. S function for a focused beam propagates thru a random medium with a power law spectrum,  $p = 4$ ,  $\gamma = 10$ ,  $\alpha_r = \alpha_s = 1$ ;  $z = 0.4375$ .

DIST= 9.75000E-01 WIDTH= 1.00000 AI= 1.00000 GAMMA= 10.0000  
SCTR= 3.00000 GWID= 2.00000E-01 GAMP= 3.00000E-01 INDEX= 2.00000  
POWER LAW SPECTRUM

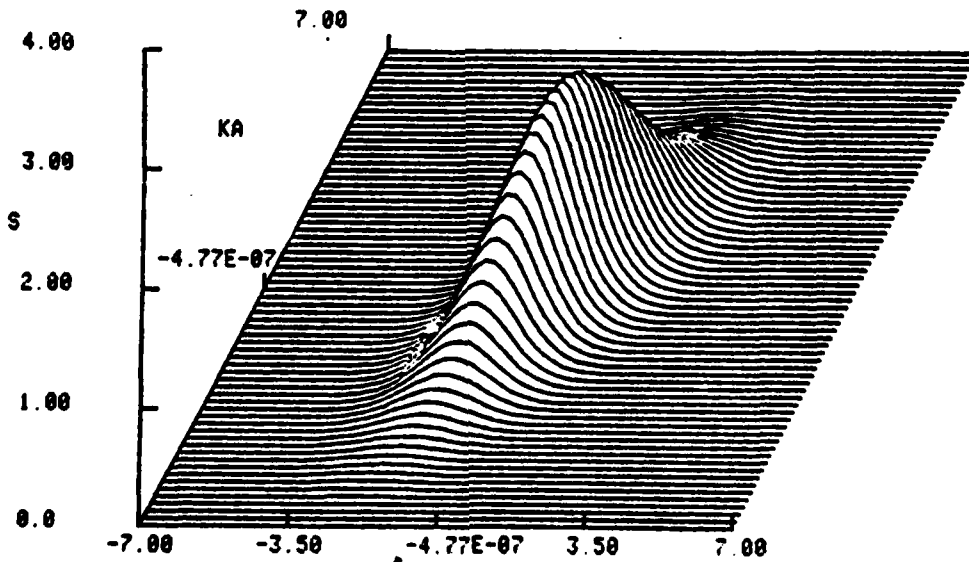


Fig. 23b.  $z = 0.875$ .

DIST= 1.31250    WIDTH= 1.00000    AI= 1.00000    GAMMA= 10.0000  
ECTR= 3.00000    GWID= 2.00000E-01    GAMP= 3.00000E-01    INDEX= 2.00000  
POWER LAW SPECTRUM

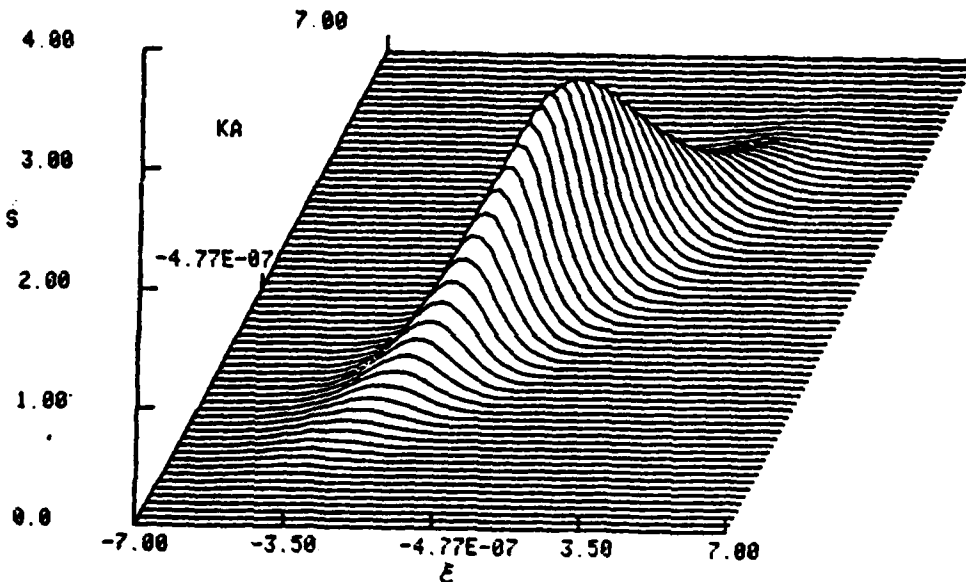


Fig. 23c.                    z = 1.3125.

DIST= 1.75000    WIDTH= 1.00000    AI= 1.00000    GAMMA= 10.0000  
ECTR= 3.00000    GWID= 2.00000E-01    GAMP= 3.00000E-01    INDEX= 2.00000  
POWER LAW SPECTRUM

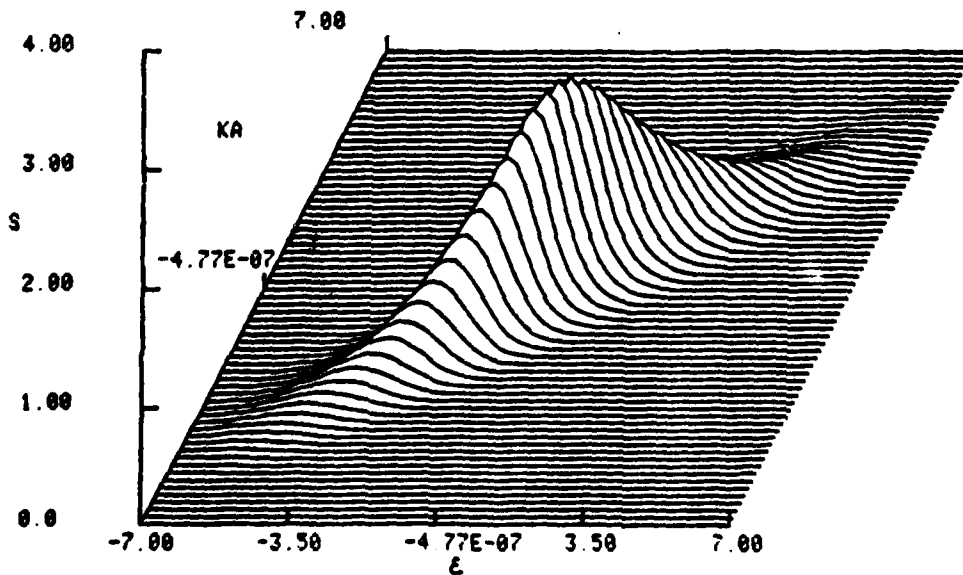


Fig. 23d.                    z = 1.75.

tion at  $z = 0.4375, 0.875, 1.3125, 1.75$  for focused beam propagating thru a random medium with power law spectrum defined by the spectral index  $p = 4$ ,  $\gamma = 10$ ,  $d_r = 1$ . One observes that the quasiparticle d.f. spreads in the  $\xi$  direction and decays according to the H function as it redistributes. If a Gaussian bump is imposed with its center located at  $k' = 3$ (GCTR), width  $b = 0.2$ (GWID), amplitude  $a = 0.3$  (GAMP), the S function is distorted and sharpened compared to the case of the simple power law spectrum. These effects are displayed in Figs. 24a-24d. As discussed earlier, the location of the Gaussian bump determines the number of peaks in the H function. In order to illustrate the effect of these peaks on the S function, we shall examine the case of a collimated beam propagating thru a random medium with the composite spectrum (c). The center of the bump is chosen to be located at  $k' = 1, 3, 4$ , respectively. For  $\gamma = 10$ , GWID = 0.2, GAMP = 0.3,  $p = 4$ , one displays the numerical solutions in Figs. 25a-25d, figs. 26a-26d and figs. 27a-27d. At  $z = 0.4375$ , the S function is less distorted for  $k'=1$  than it is for  $k' = 3$  and 4. At  $z = 1.75$ , the S function for  $k' = 3$  and 4 clearly shows the effects of the H function peaks. One observes that the presence of these peaks in the H function greatly reduces the correlation length in the  $\xi$  direction.

It is easier and clearer to discuss the independent effects of different spectrum structure by means of the intensity function and correlation length associated with the propagating waves. Substituting the numerically evaluated S function into equations (3.59)-(3.60), one obtains the desired information for  $I(x,z)$  and  $l$ . Fig. 28a depicts collimated beams propagating thru a random medium with  $H(\xi) = \gamma \xi^2$ . Curve 1 represents the axial intensity and correlation length for the case of wave propagation in free space. Turbulent effects for  $\gamma = 0.5$  and 1 are depicted in curves 2 and 3. (In Figs. 28-31 we use the same curve index for different values of

DIST= 4.37500E-01 WIDTH= 1.00000 AI= 1.00000 GAMMA= 10.0000  
ECTR= 3.00000 GWIG= 2.00000E-01 GAMP= 3.00000E-01 INDEX= 2.00000  
POWER SPECTRUM WITH A GAUSSIAN BUMP

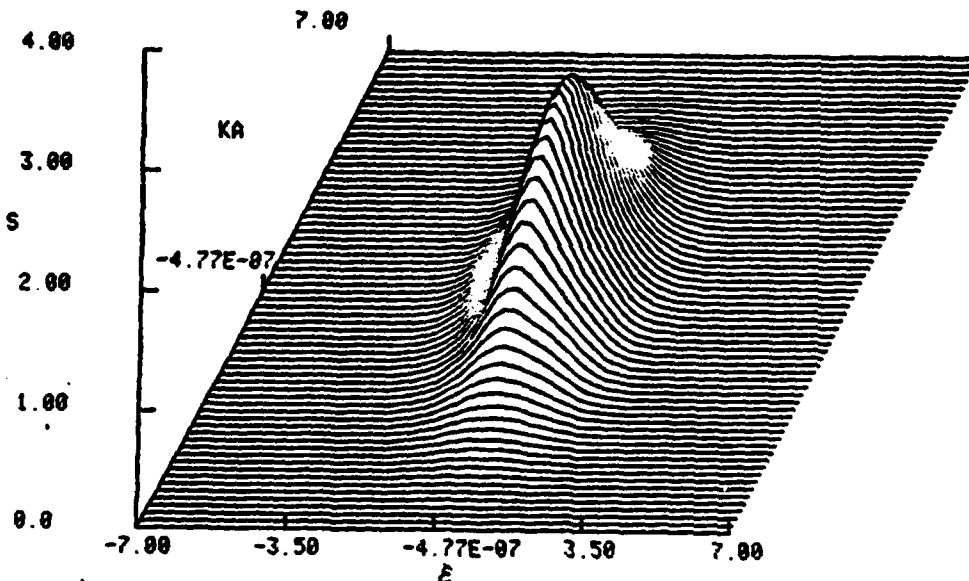


Fig. 24a. S function for a focused beam propagates thru a random medium characterized by spectrum (c);  $k' = -3$ ,  $b = 0.2$ ,  $a = 0.3$ ,  $d_r = d_i = 1$ ;  $z = 0.4375$ .  $\gamma = 10$ .

DIST= 8.75000E-01 WIDTH= 1.00000 AI= 1.00000 GAMMA= 10.0000  
ECTR= 3.00000 GWIG= 2.00000E-01 GAMP= 3.00000E-01 INDEX= 2.00000  
POWER SPECTRUM WITH A GAUSSIAN BUMP

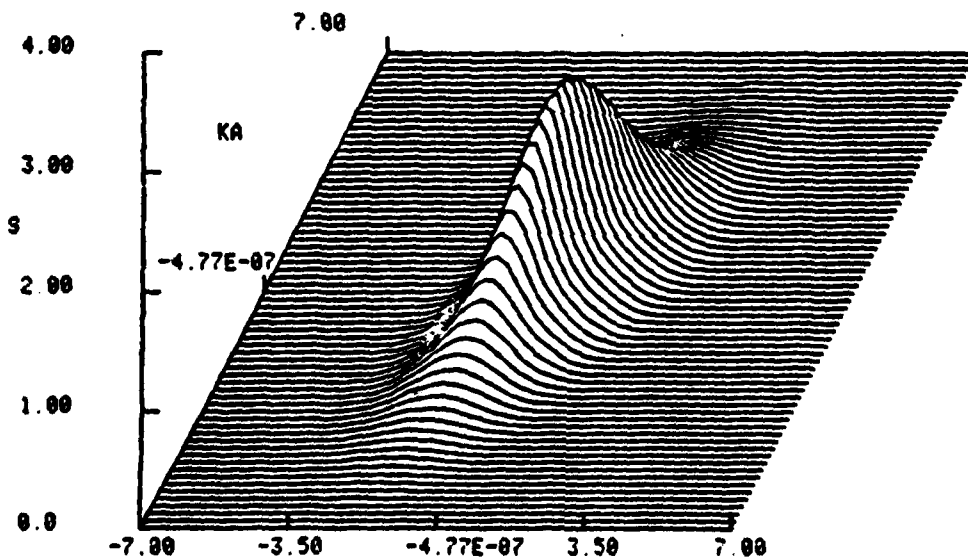


Fig. 24b.  $z = 0.875$ .

DIST= 1.31250    WIDTH= 1.00000    AI= 1.00000    GAMMA= 10.0000  
ECTR= 3.00000    GWID= 2.00000E-01    GAMP= 3.00000E-01    INDEX= 2.00000  
POWER SPECTRUM WITH A GAUSSIAN BUMP

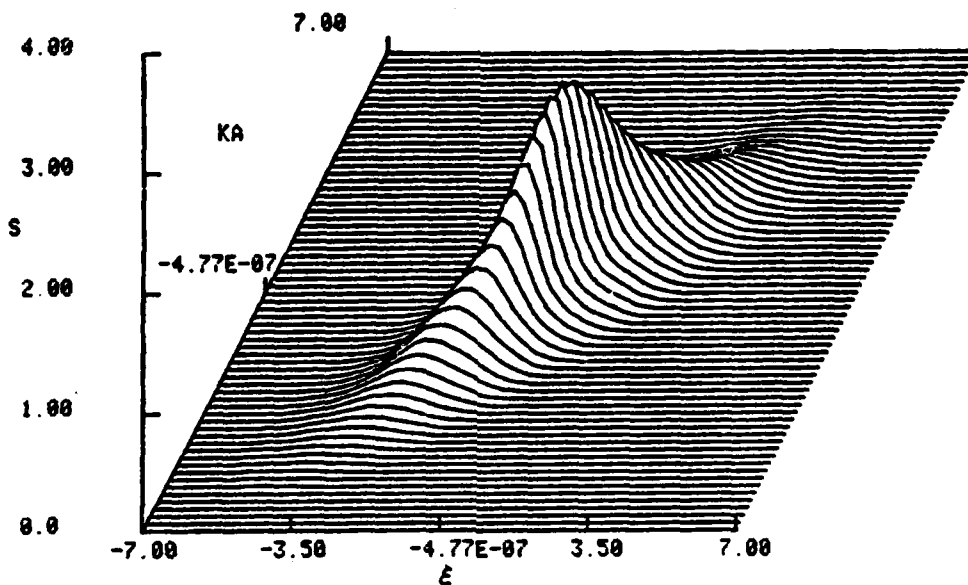


Fig. 24c.    z = 1.3125.

DIST= 1.75000    WIDTH= 1.00000    AI= 1.00000    GAMMA= 10.0000  
ECTR= 3.00000    GWID= 2.00000E-01    GAMP= 3.00000E-01    INDEX= 2.00000  
POWER SPECTRUM WITH A GAUSSIAN BUMP

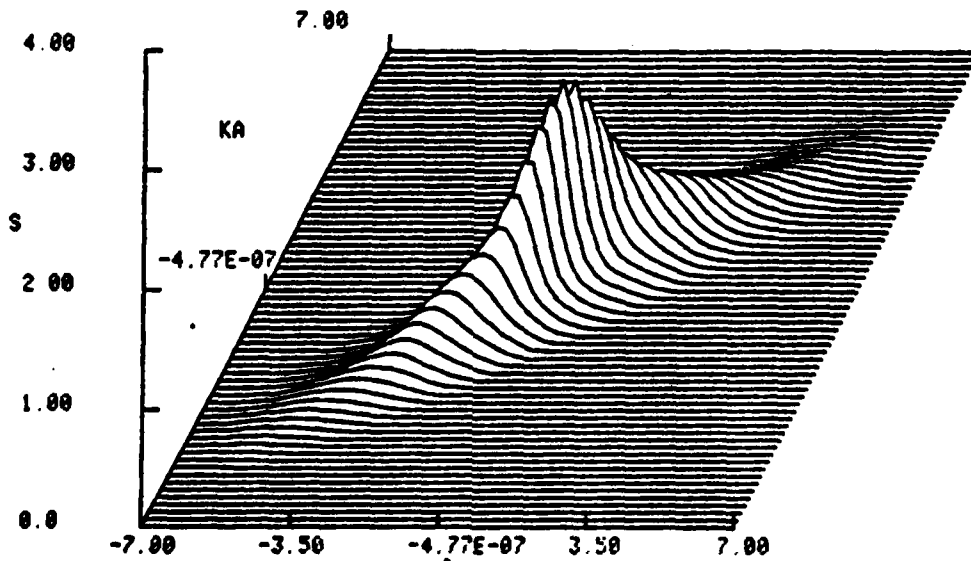


Fig. 24d.    z = 1.75.

DIST= 4.37500E-01 WIDTH= 1.00000 WI= 0.0 GAMMA= 10.0000  
CTR= 1.00000 GWID= 2.00000E-01 GAMP= 3.00000E-01 INDEX= 2.00000  
POWER SPECTRUM WITH A GAUSSIAN BUMP

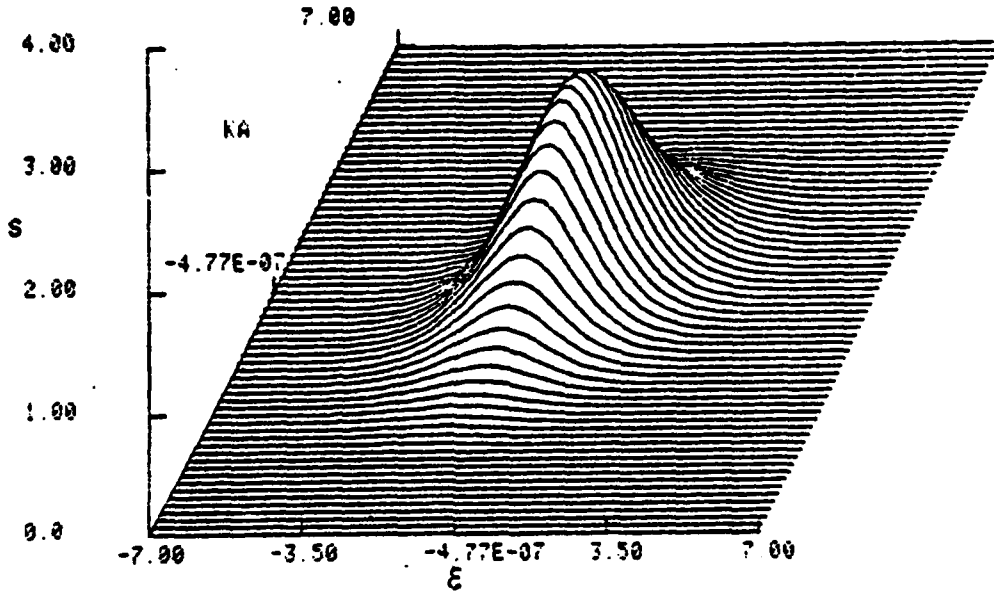


Fig. 25a. S function for a collimated beam propagates thru a random medium characterized by spectrum (c);  $k' = 1$ ,  $a = 0.3$ ,  $b = 0.2$ ,  $p = 4$ ,  $\gamma = 10$ ;  $z = 0.4375$ .

DIST= 3.75000E-01 WIDTH= 1.00000 WI= 0.0 GAMMA= 10.0000  
CTR= 1.00000 GWID= 2.00000E-01 GAMP= 3.00000E-01 INDEX= 3.00000  
POWER SPECTRUM WITH A GAUSSIAN BUMP

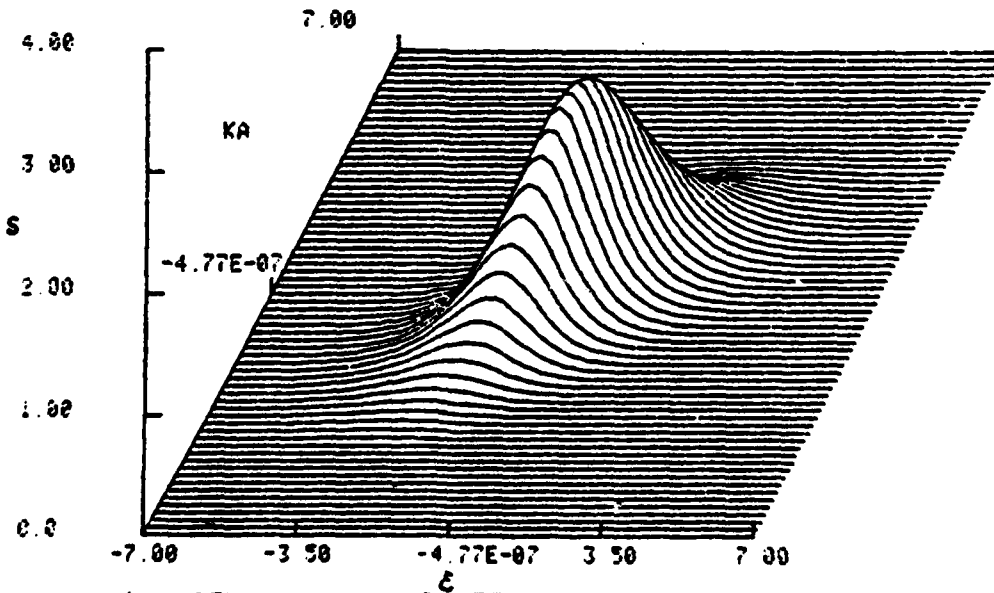


Fig. 25b.  $z = 0.875$ .

DIST= 1.31250    WIDTH= 1.00000    AI= 0.0    GAMMA= 12.0000  
QCTR= 1.00000    GWID= 2.00000E-01    GAMP= 3.00000E-01    INDEX= 2.00000  
POWER SPECTRUM WITH A GAUSSIAN BUMP

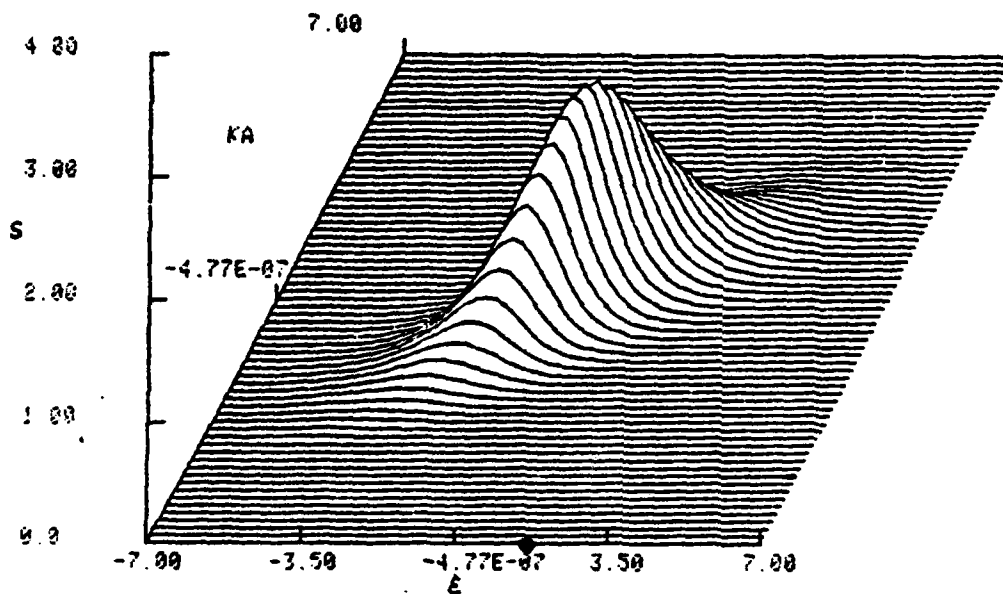


Fig. 25c.    z = 1.3125.

DIST= 1.75000    WIDTH= 1.00000    AI= 0.0    GAMMA= 12.0000  
QCTR= 1.00000    GWID= 2.00000E-01    GAMP= 3.00000E-01    INDEX= 2.00000  
POWER SPECTRUM WITH A GAUSSIAN BUMP

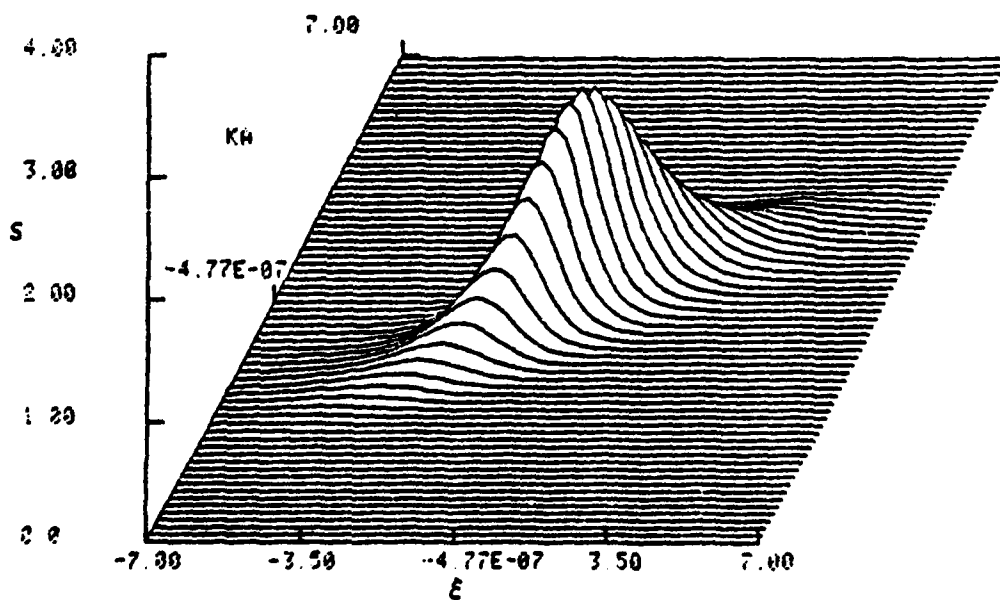


Fig. 25d.    z = 1.75.

DIST= 4.37500E-01 WIDTH= 1.00000 AI= 0.0 GAMMA= 10.0000  
SCTR= 3.00000 GWID= 2.00000E-01 GAMP= 3.00000E-01 INDEX= 2.00000  
POWER SPECTRUM WITH A GAUSSIAN BUMP

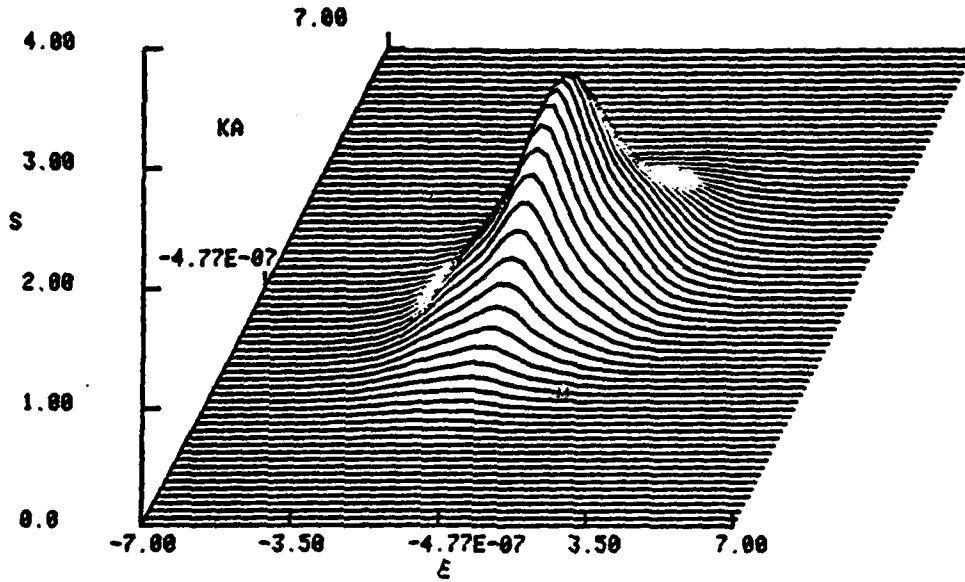


Fig.26a.S function for a collimated beam propagates thru a random medium characterized by spectrum (c);  $k' = 3$ ,  $a = 0.3$ ,  $b = 0.2$ ,  $p = 4$ ,  $\gamma = 10$ ,  $z = 0.4375$ .

DIST= 8.75000E-01 WIDTH= 1.00000 AI= 0.0 GAMMA= 10.0000  
SCTR= 3.00000 GWID= 2.00000E-01 GAMP= 3.00000E-01 INDEX= 2.00000  
POWER SPECTRUM WITH A GAUSSIAN BUMP

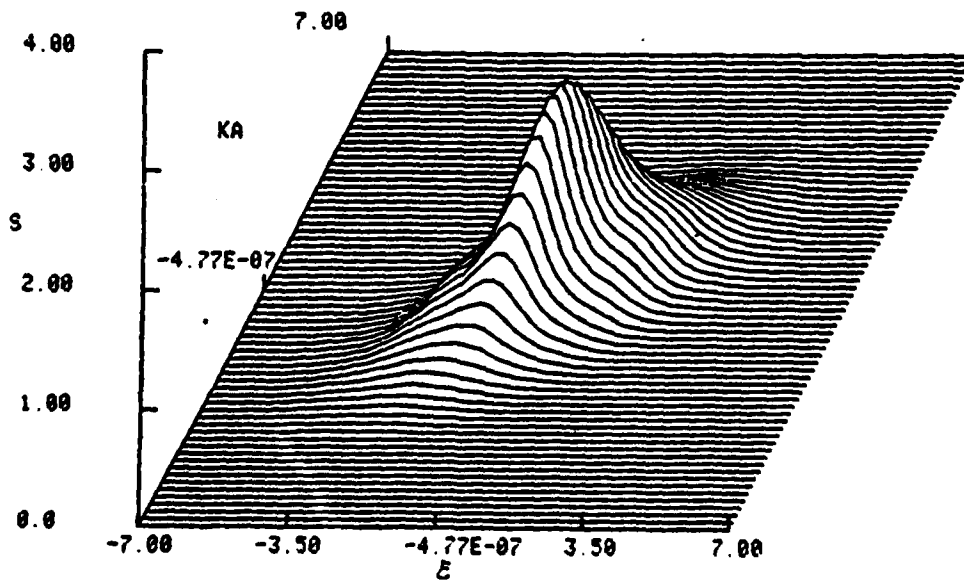


Fig.26b.  $z = 0.875$ .

DIST= 1.31250    WIDTH= 1.00000    AI= 0.0    GAMMA= 10.0000  
CTR= 3.00000    GWID= 2.00000E-01    GAMP= 3.00000E-01    INDEX= 2.00000  
POWER SPECTRUM WITH A GAUSSIAN BUMP

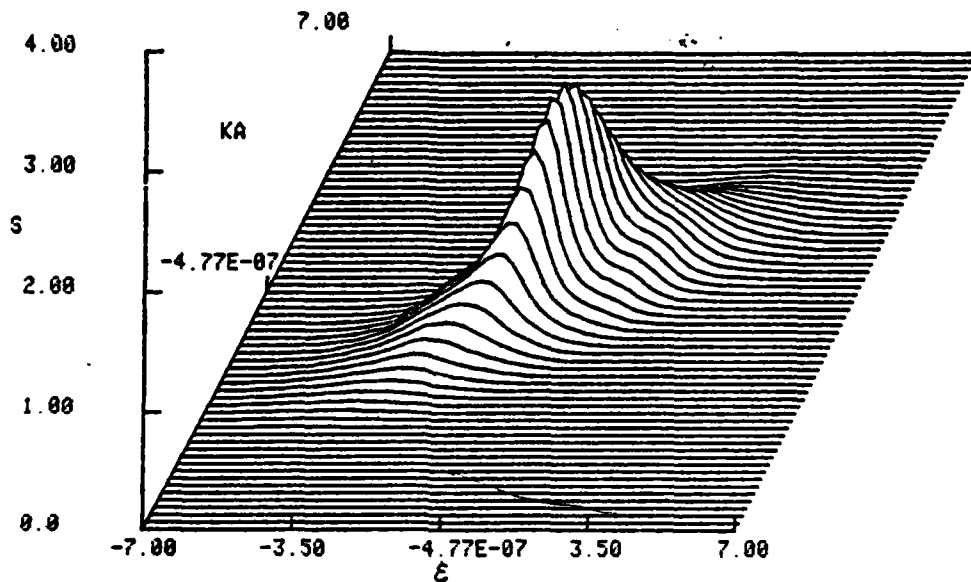


Fig. 26c.    z = 1.3125.

DIST= 1.75000    WIDTH= 1.00000    AI= 0.0    GAMMA= 10.0000  
CTR= 3.00000    GWID= 2.00000E-01    GAMP= 3.00000E-01    INDEX= 2.00000  
POWER SPECTRUM WITH A GAUSSIAN BUMP

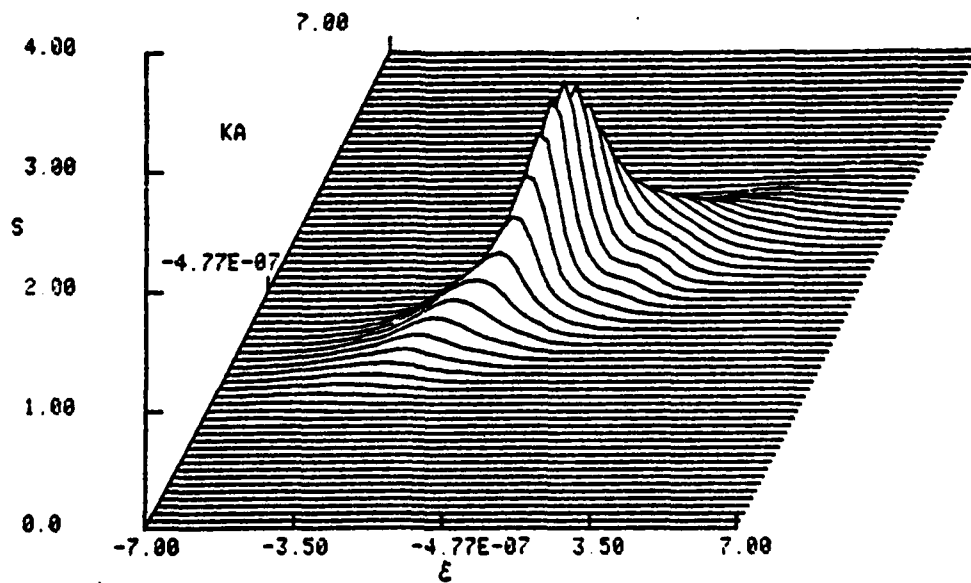


Fig. 26d.    z = 1.75.

AD-A092 720

POLYTECHNIC INST OF NEW YORK FARMINGDALE MICROWAVE R--ETC F/6 4/1

IONOSPHERIC SCINTILLATION (U)

SEP 80 D M WU

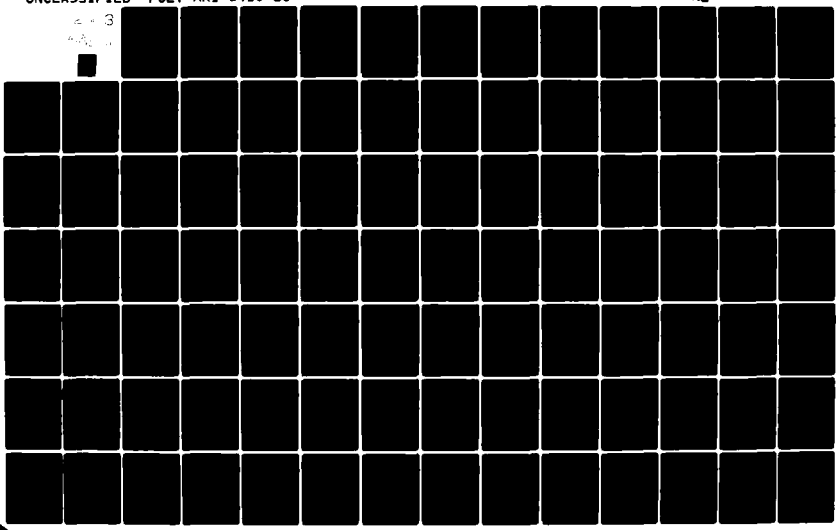
N00014-76-C-0176

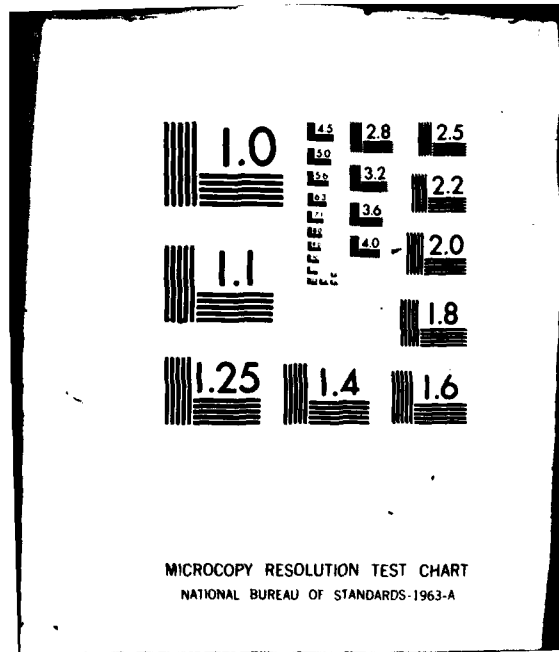
UNCLASSIFIED

POLY-MRI-1410-80

NL

3





MICROCOPY RESOLUTION TEST CHART  
NATIONAL BUREAU OF STANDARDS-1963-A

DIST= 4.37500E-01 WIDTH= 1.00000 AI= 0.0 GAMMA= 10.0000  
CTR= 4.00000 GWID= 2.00000E-01 GAMP= 3.00000E-01 INDEX= 2.00000  
POWER SPECTRUM WITH A GAUSSIAN BUMP

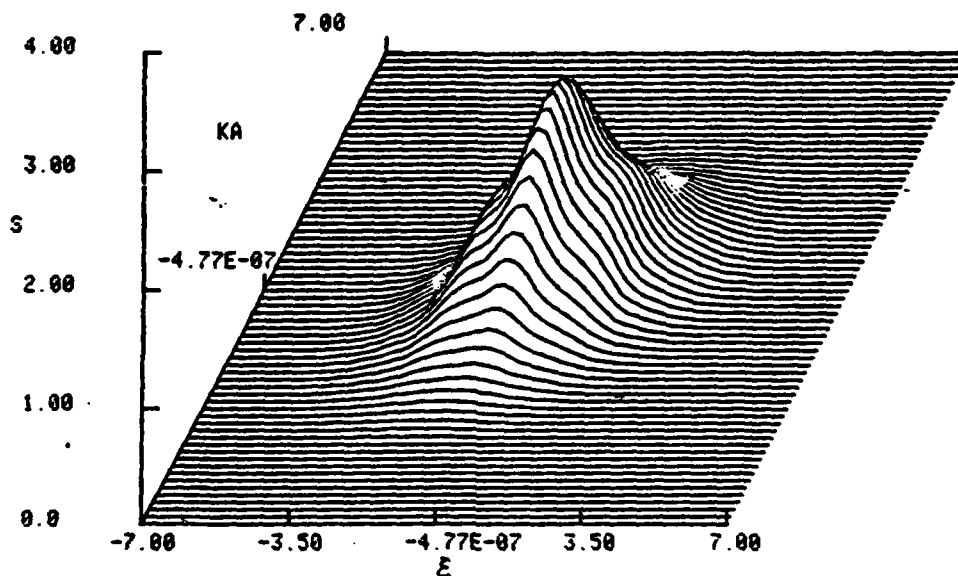


Fig. 27a. S function for a collimated beam propagates thru a random medium characterized by spectrum (c);  $k' = 4$ ,  $a = 0.3$ ,  $b = 0.2$ ,  $p = 4$ ,  $\gamma = 10$ ,  $z = 0.4375$ .

DIST= 3.75000E-01 WIDTH= 1.00000 AI= 0.0 GAMMA= 10.0000  
CTR= 4.00000 GWID= 2.00000E-01 GAMP= 3.00000E-01 INDEX= 2.00000  
POWER SPECTRUM WITH A GAUSSIAN BUMP

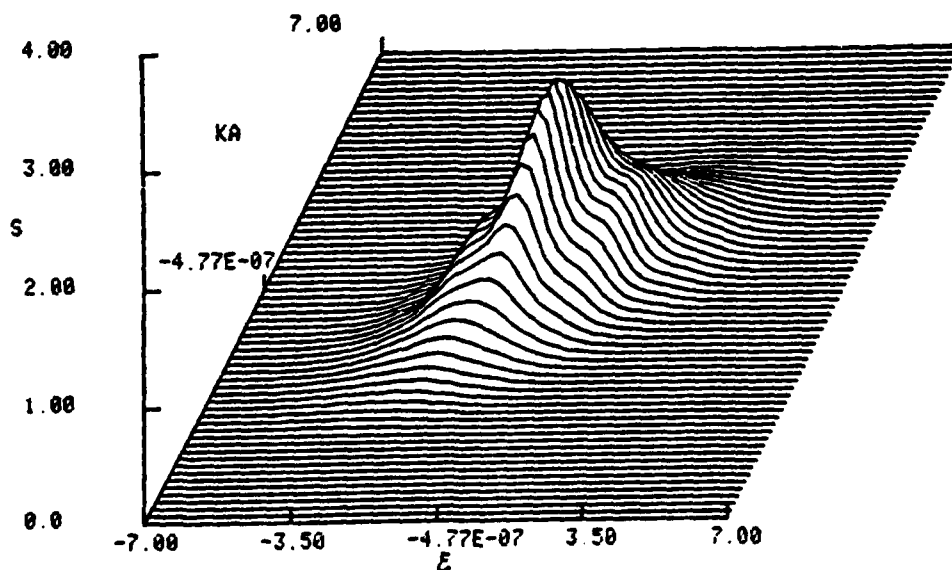


Fig. 27b.  $z = 0.875$ .

DIST= 1.31250    WIDTH= 1.00000    AI= 0.0    GAMMA= 10.0000  
CTR= 4.00000    GWID= 2.00000E-01    GAMP= 3.00000E-01    INDEX= 2.00000  
POWER SPECTRUM WITH A GAUSSIAN BUMP

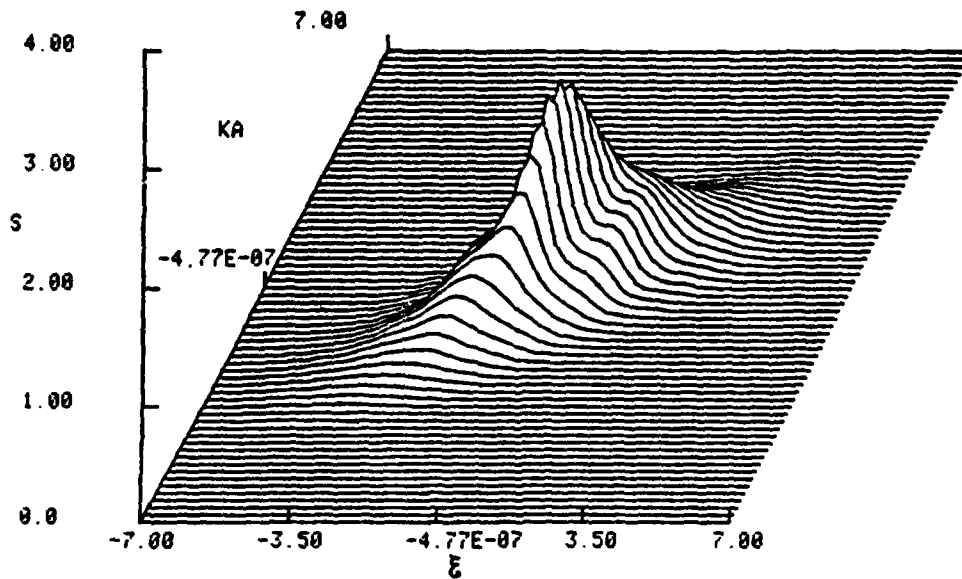


Fig. 27c.     $z = 1.3125.$

DIST= 1.75000    WIDTH= 1.00000    AI= 0.0    GAMMA= 10.0000  
CTR= 4.00000    GWID= 2.00000E-01    GAMP= 3.00000E-01    INDEX= 2.00000  
POWER SPECTRUM WITH A GAUSSIAN BUMP

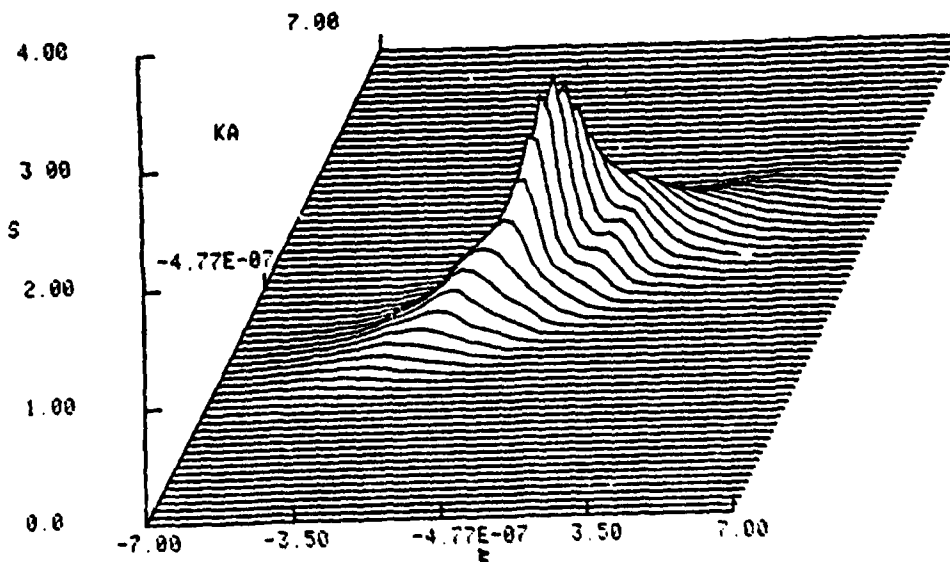


Fig. 27d.     $z = 1.75.$

$\gamma$ ). One observes that the axial intensity  $I(0,z)$  decays as the wave propagates while the correlation length decreases due to turbulent effects until about  $z = 0.3$ ; diffraction effects then become important and coherence is partially restored. After further propagating turbulent effects again dominate and the wave is decorrelated. For a focused beam propagating in free space with  $\alpha_r = 1$ ,  $\alpha_i = 1$ , the intensity at  $z = 0.5$  will reach a maximum and its correlation length a minimum as shown in the curve 1 of Fig. 28b. If a turbulent medium is present, the focal distance is reduced due to the scattering effect imposed by the turbulent medium. Curves 2,3 of Fig. 28b display the decorrelation process contributed by both focusing and turbulent phenomena from  $z = 0$  to  $z \approx 0.4$ . At  $z \approx 1.2$ , the turbulent effect dominates and reduces the correlation length as  $z$  increases. Figs. 29a,b display the same effect for the Gaussian spectrum. Comparing these curves with the square law spectrum, one observes that the Gaussian spectrum has a smaller effect on the wave statistics than the square law spectrum. It is of interest to consider a power law spectrum for the ionospheric random medium. We shall choose the spectrum type (b) with  $p = 4$  and make use of numerical calculations of the  $S$  function to evaluate the axial intensity function  $I(0,z)$  and correlation length  $l$ . The results are depicted in Figs. 30a,b. Fig. 30a displays the case of collimated beam for  $\gamma = 0.5$  and 1. The turbulent effect slightly reduces the intensities (Note that this is a weak turbulence case), and the correlation length decreases compared to the case of free space (curve 1). For the case of focused beams, depicted in Fig. 30b, one finds that scattering effects decrease the focal length; the wave is also diffracted and decorrelated as in the previous case. The spectrum of a real random medium is not a smooth function in general. Experimental results show that the power spectrum could possess a number of "bumps" in various frequency ranges. We shall illustrate the effect of such bumps by simply adding a typical

DIST= 2 13281      WIDTH= 1.00000      A1= 0.0      GAMMA= 0.0  
 GCTR= 0 0      GWID= 1.00000      GAMP= 1.00000      INDEX= 2.00000

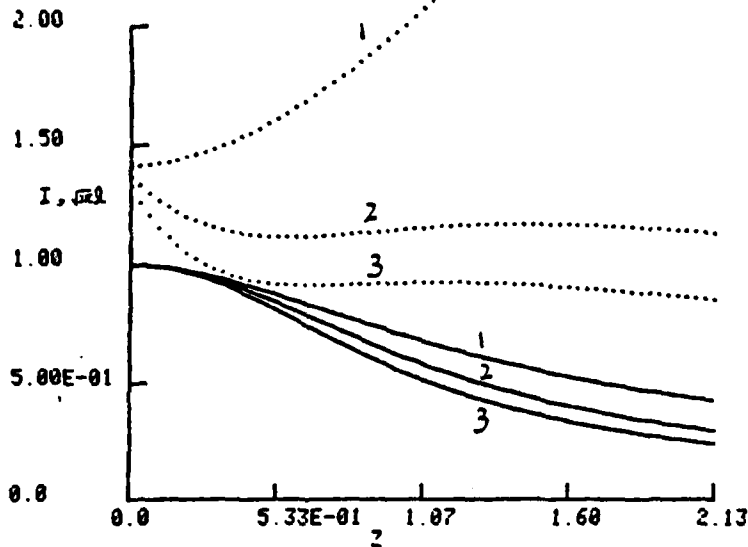


Fig. 28a.  $\sqrt{z}$  vs.  $z$  dotted line;  $I(0,z)$  vs.  $z$  solid line; curve 1; free space; curve 2;  $\gamma = 0.5$ ; curve 3;  $\gamma = 1$ ; collimated beam with  $\alpha_r = 1$ .  
 $H(\xi) = \gamma E^2$ .

DIST= 2 13281      WIDTH= 1.00000      A1= 1.00000      GAMMA= 5.00000E-01  
 GCTR= 0.0      GWID= 1.00000      GAMP= 1.00000      INDEX= 2.00000

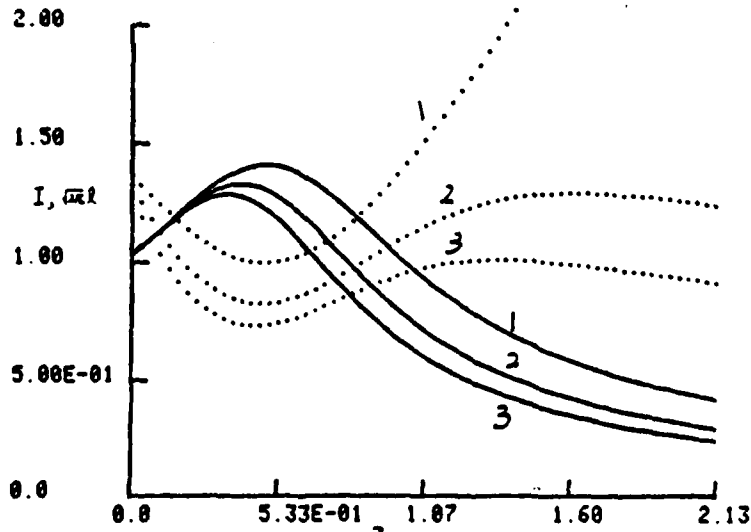


Fig. 28b. focused beam case;  $\alpha_r = \alpha_i = 1$ ,

DIST= 2.13281    WIDTH= 1.00000    AI= 0.0    GAMMA= 0.0  
 GCTR= 0.0    GNID= 1.00000    GAMP= 1.00000    INDEX= 2.00000  
 GAUSSIAN SPECTRUM

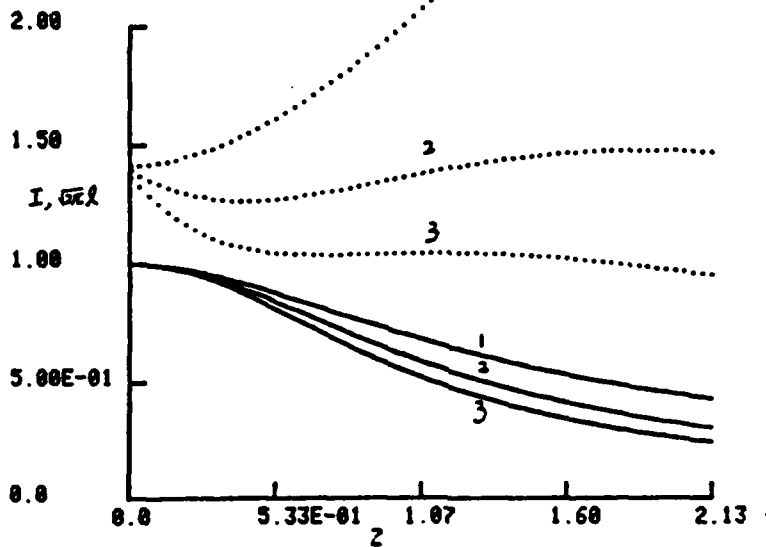


Fig. 29a.  $\sqrt{\lambda}$  1 vs. z dotted line;  $I(0, z)$  vs. z solid line; (1) free space; (2)  $\gamma = 0.5$ ; (3)  $\gamma = 1$ ; Gaussian spectrum,  $k' = 0$ ,  $A = 1$ ,  $b = 1$ .

DIST= 2.13281    WIDTH= 1.00000    AI= 1.00000    GAMMA= 1.00000  
 GCTR= 0.0    GNID= 1.00000    GAMP= 1.00000    INDEX= 2.00000  
 GAUSSIAN SPECTRUM

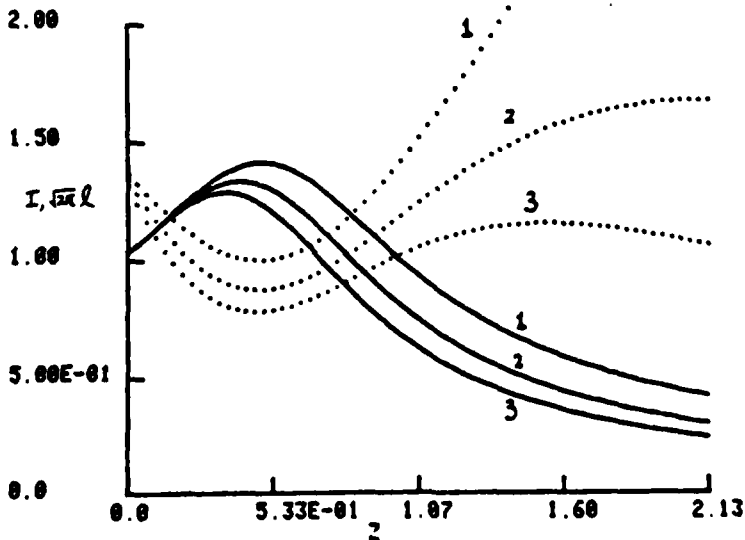


Fig. 29b. focused beam case;  $\alpha_r = \alpha_A = 1$ .

DIST= 2.13281    WIDTH= 1.00000    AI= 0.0    GAMMA= 1.00000  
GCTR= 0.0    GWID= 1.00000    GAMP= 1.00000    INDEX= 2.00000  
POWER LAW SPECTRUM

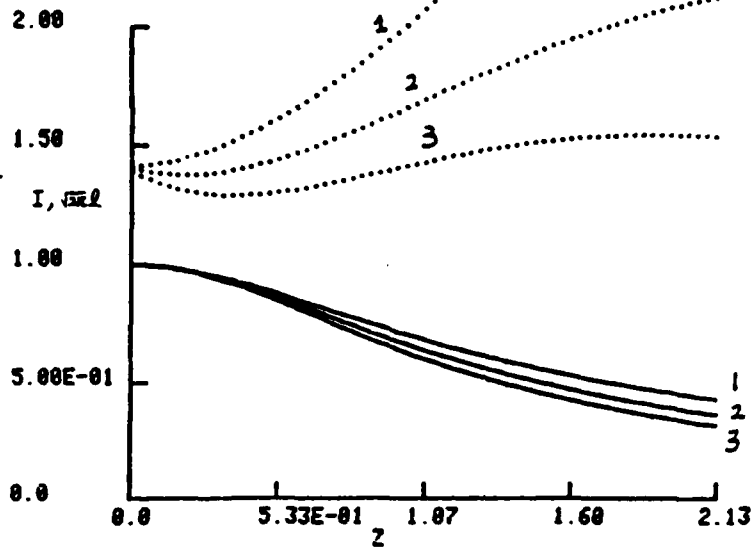


Fig. 30a.  $\sqrt{z} I$  vs.  $z$  dotted line;  $I(0, z)$  vs.  $z$  solid line; (1) free space; (2)  $\gamma = 0.5$ ; (3)  $\gamma = 1$ ; Power law spectrum with  $p = 4$ .

DIST= 2.13281    WIDTH= 1.00000    AI= 1.00000    GAMMA= 0.0  
GCTR= 0.0    GWID= 1.00000    GAMP= 1.00000    INDEX= 2.00000  
POWER LAW SPECTRUM

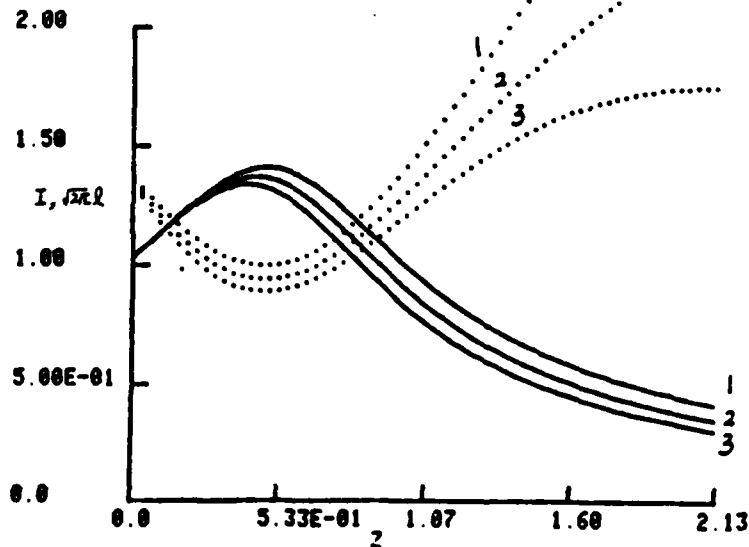


Fig. 30b. focused beam case;  $\alpha_v = \alpha_\lambda = 1$ .

Gaussian bump on the power law spectrum, i.e. a compound spectrum as described in eq. (3.58). Fig. 31a, 31b depict the effect of a Gaussian bump on the axial intensity function and the correlation length for collimated and focused beams respectively. The parameters are chosen as :  $\gamma = 0.5$  and  $1$ .  $GCTR = 1$ ,  $GWID = 0.2$ ,  $GAMP = 0.3$  and  $p = 4$ . The results show that the addition of this Gaussian bump causes strong scattering phenomena. We have presented, for the weak fluctuation cases  $\gamma = 0.5, 1$ , the effects of turbulence in the medium. As a comparison, we shall now display in Figs. 32-33 some results for the strong turbulence case,  $\gamma = 5$  and  $10$ . A collimated beam propagates thru a random medium with a composite spectrum formed by a Gaussian bump located at  $GCTR = 1$ ,  $GWID = 0.2$ ,  $GAMP = 0.3$ , for the cases  $\gamma = 5$  and  $10$ . Curves 2,3 in Fig. 32a represent the intensity and correlation length for  $\gamma = 5$  and  $10$ ; they show that for strong turbulence case the correlation length decreases rapidly and a long tail appears at large  $Z$ . The axial intensity drop appreciably and approaches a small constant value. For the focused beam case, the focal length is greatly reduced for large values of  $\gamma$ . We shall expect, as the turbulent strength is very strong, that the focusing effect will not be present and the wave will decay as  $z$  increases. These results are depicted in Fig. 32b. If a Gaussian bump is located at  $k' = 3$ , the scattering effect is stronger than for the previous case. Figs. 33a and 33b display data for a collimated beam and focused beam propagating thru a random medium described by a composite spectrum with  $k' = 3$ . One observes that decay is much greater for the intensity and that decorrelation phenomena are more evident than for the case  $k'=1$ .

DIST= 2.13281    WIDTH= 1.00000    AI= 0.4    GAMMA= 0.0  
 GCTR= 1.00000    GWID= 2.00000E-01    GAMP= 3.00000E-01    INDEX= 2.00000  
 POWER SPECTRUM WITH A GAUSSIAN BUMP

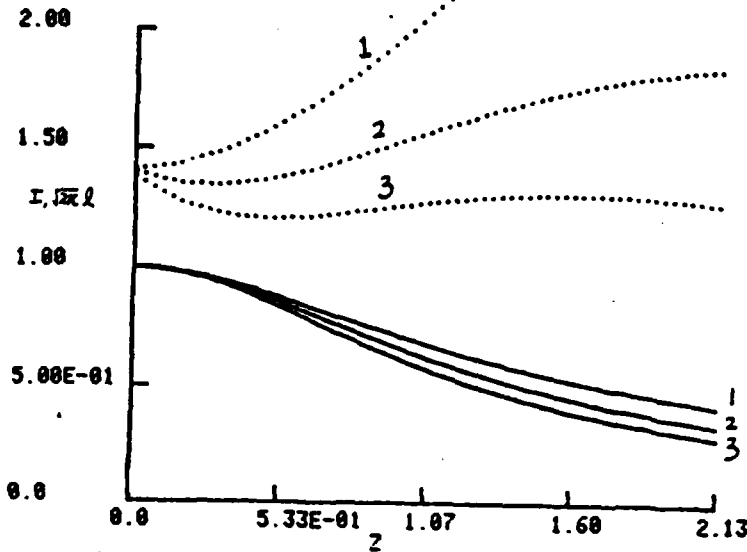


Fig. 31a.  $\sqrt{z} I$  vs.  $z$  dotted line;  $I(0, z)$  vs.  $z$  solid line; (1) free space; (2)  $\gamma = 0.5$ ; (3)  $\gamma = 1$ . Power spectrum with a Gaussian peak,  $k' = 1$ ,  $a = 0.3$ ,  $b = 0.2$ ,  $p = 4$ . collimated beam case.

DIST= 2.13281    WIDTH= 1.00000    AI= 1.00000    GAMMA= 0.0  
 GCTR= 1.00000    GWID= 2.00000E-01    GAMP= 3.00000E-01    INDEX= 2.00000  
 POWER SPECTRUM WITH A GAUSSIAN BUMP

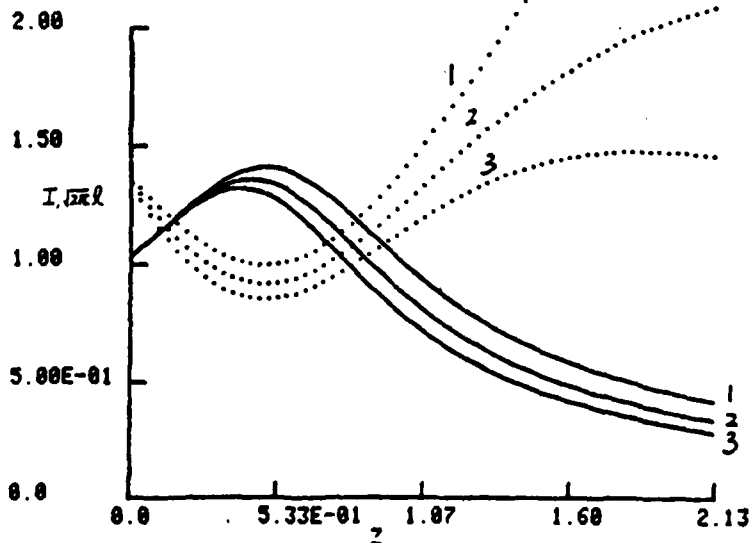


Fig. 31b. focused beam case;  $\alpha_r = \alpha_i = 1$ .

DIST= 2.13281    WIDTH= 1.00000    AI= 0.4    GAMMA= 5.00000  
 GCTR= 1.00000    GWID= 2.00000E-01    GAMP= 3.00000E-01    INDEX= 2.00000  
 POWER SPECTRUM WITH A GAUSSIAN BUMP

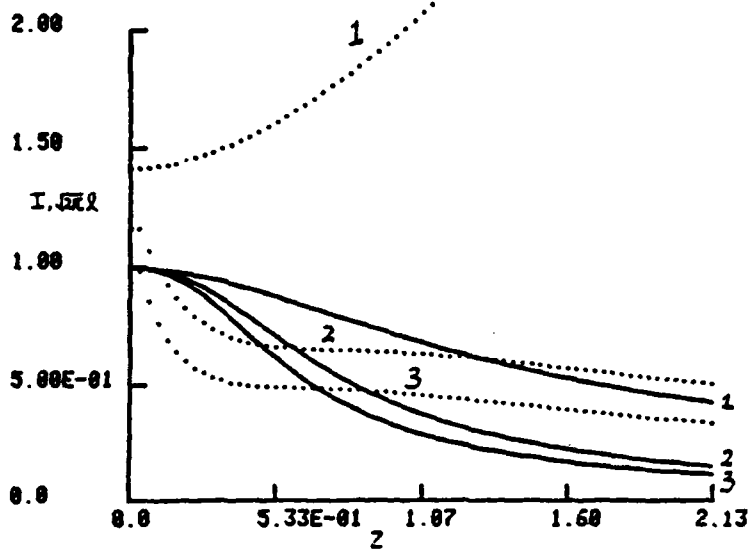


Fig. 32a.  $\sqrt{2\pi}$  I vs. z dotted line;  $I(0,z)$  vs. z solid line; (1) free space; (2)  $\gamma = 5$ ; (3)  $\gamma = 10$ ; Power spectrum with a Gaussian peak,  $k' = 1$ ,  $a = 0.3$ ,  $b = 0.2$ ,  $p = 4$ , collimated beam case.

DIST= 2.13281    WIDTH= 1.00000    AI= 1.00000    GAMMA= 5.00000  
 GCTR= 1.00000    GWID= 2.00000E-01    GAMP= 3.00000E-01    INDEX= 2.00000  
 POWER SPECTRUM WITH A GAUSSIAN BUMP

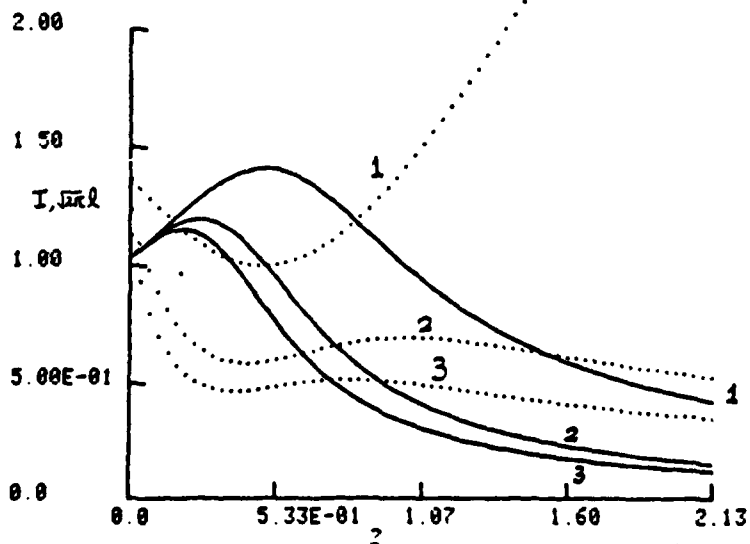


Fig. 32b. focused beam case;  $\alpha_r = \alpha_s = 1$ .

DIST= 2.13281    WIDTH= 1.00000    AI= 0.0    GAMMA= 5.00000  
 GCTR= 3.00000    GWID= 2.00000E-01    GAMP= 3.00000E-01    INDEX= 2.00000  
 POWER SPECTRUM WITH A GAUSSIAN BUMP

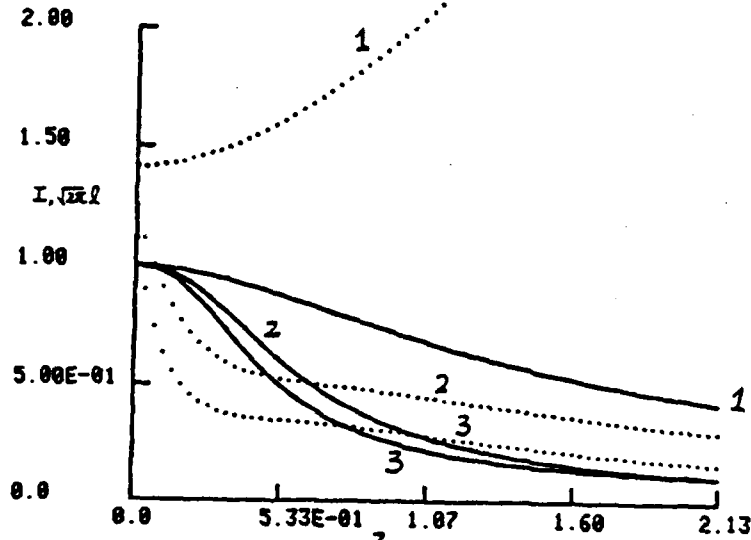


Fig. 33a.  $\sqrt{z} I$  vs.  $z$  dotted line;  $I(0, z)$  vs.  $z$  solid line; (1) free space; (2)  $\gamma = 5$ ; (3)  $\gamma = 10$ ; Power spectrum with a Gaussian peak,  $k' = 3$ ,  $a = 0.3$ ,  $b = 0.2$ ,  $p = 4$ , collimated beam case.

DIST= 2.13281    WIDTH= 1.00000    AI= 1.00000    GAMMA= 0.0  
 GCTR= 3.00000    GWID= 2.00000E-01    GAMP= 3.00000E-01    INDEX= 2.00000  
 POWER SPECTRUM WITH A GAUSSIAN BUMP

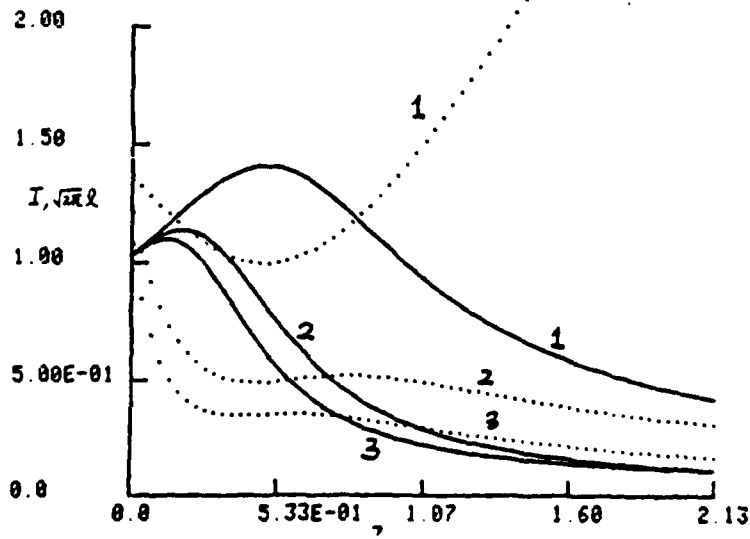


Fig. 33b. focused beam case;  $\alpha_r = \alpha_s = 1$ .

#### IV. Conclusion and Discussion

A wavepacket or beam can be viewed as a finitely extended moving and deforming system of "Quasiparticles". The Fourier transform of the Mutual Coherence Function w.r.t. either the "fast" or "slow" coordinate is defined respectively as the "fast" or "slow" quasiparticle distribution function  $F$  or  $S$ . For wave propagation in a random medium, it is usually more convenient to utilize the "slow quasiparticle" distribution function  $S$ . The knowledge of the  $S$  function provides the desired information for two point statistics of a stochastic wave. For example, the correlation length  $l$  at any value  $z$ , defined in equation (3.61), can be interpreted as the total number of q.p.  $N_S(z)$  divided by the q.p. density at  $\xi = 0$ . Also, the axial intensity  $I(0,z)$  may be represented by the slow q.p. density at  $\xi = 0$ . To obtain the 2 point statistics at any distance  $z$ , one has only to observe the q.p. flow in  $\kappa, \xi$  space as  $z$  increases. For the case of a collimated beam propagating in free space, one considers, at  $z = 0$ , a system of quasiparticles evenly distributed between  $-7 < \xi, \kappa < +7$ . Qualitatively, we shall use the "area" of a circular "point" to represent the number density of slow q.p.; thus at  $z = 0$  the q.p. are distributed in  $\kappa, \xi$  space as shown in Fig. 34. As  $z$  increases, those q.p. with higher  $\kappa$  "move" faster than those with smaller  $\kappa$ . As a result, the q.p. density at  $\xi = 0$  decreases as  $z$  increases and hence the axial intensity  $I(0,z)$  decreases. Since the total number of q.p is conserved in free space propagation, i.e.  $N_S(z)$  is constant, the correlation length increases as q.p. move along the trajectory.

For a focused beam propagating in free space, the q.p. at  $z = 0$  are distributed in  $\kappa, \xi$  space with a maximum along an axis deviating from the  $\xi = 0$  axis as shown in Fig. 35.

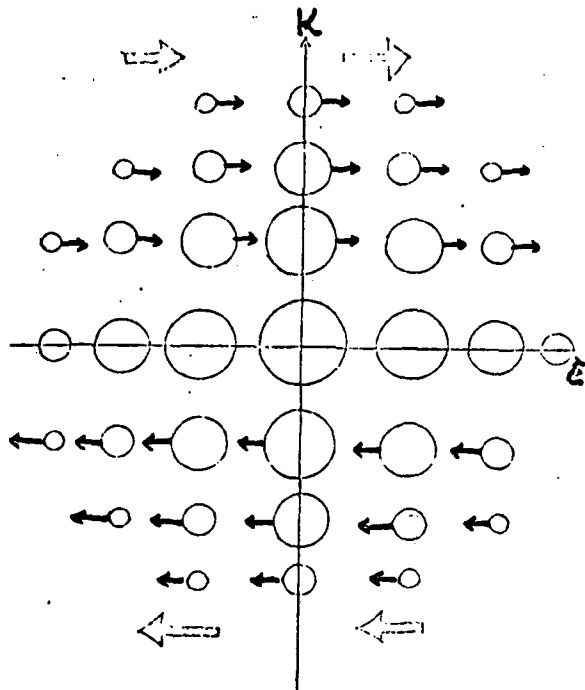


Fig. 34.

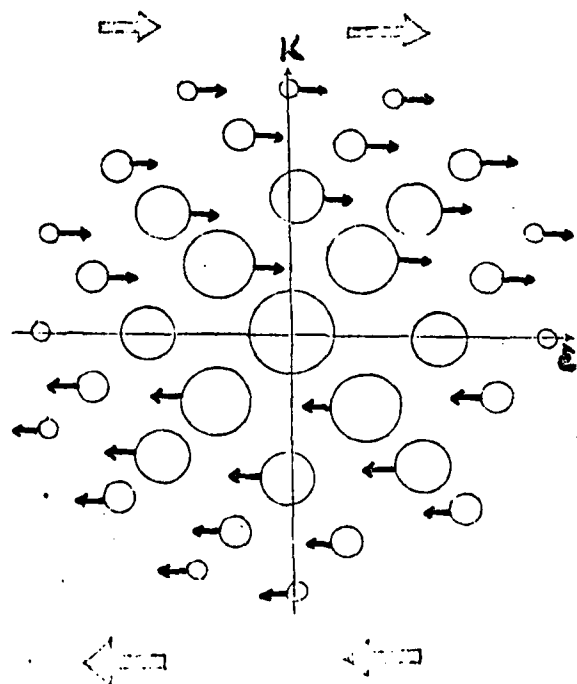


Fig. 35.

Fig. 34. Quantitative representation of slow q.p. distribution function in  $\kappa$ ,  $\xi$  space; collimated beam in free space. Fig. 35. focused beam in free space.

One observes that the q.p. density reaches a maximum at a plane  $z = z_f$ , when those q.p. with larger density reach the center line  $\xi = 0$ . i.e. the axial intensity is maximum at the focal distance  $z_f$ . The conservation of the total number of q.p. in free space then implies a reduction of the correlation length from  $z = 0$  to  $z = z_f$ . As the q.p. flow moves beyond the focal point, those q.p. with lower density move to the center and the axial intensity decreases as  $z$  increases; Correspondingly, this implies an increase in the correlation length.

For a wave propagating in a random medium characterized by the structure function  $H(\xi)$ , one just simply leads to a decay of the wave field in the  $K, \xi$  space as depicted in Fig. 36. The structure function acts as an "absorber" which absorbs part of the q.p. according to its strength. For  $z > 0$ , Fig. 37 depicts for a collimated beam at  $z = 0$ , how the q.p. move in a random medium characterized by  $H(\xi)$ . As  $z$  increases those q.p. with smaller density move toward the center while some of them are absorbed by the structure function. The resulting q.p. density at  $\xi = 0$  is decreased and is smaller than in the case of free space. One notes that the total number of q.p. is not conserved in this case. The ratio of  $N_s(z)$  and  $I(0,z)$ , which determines the correlation length  $l$ , will decrease as  $z$  increases for the strong turbulent case; however, in the weak turbulence case, it will first decrease and then increase as  $z$  increases at least for a short distance (Note that the q.p. at  $K = 0$  will never move). For the case of a focused beam propagating in a random medium, one depicts the q.p. flow thru a random medium characterized by  $H(\xi)$  as in Fig. 38.

Because of turbulence in the medium, the q.p. with larger density are absorbed before reaching the center  $\xi = 0$ .

As a result, the q.p. density at  $\xi = 0$  creates a maximum as a result of q.p. which initially have less density. Thus, the focal length ( $z_f$ ) is smaller compared to the free space case. The correlation length in this case is reduced from  $z = 0$  to  $z = z_f$ . Beyond the focal point, the q.p. density, at  $\xi = 0$ , is reduced and the ratio of  $N_S(z)$  and  $I(0,z)$ , which yields 1, will again decrease for the strong turbulent case or decrease and then increase, as  $z$  increases at least for a short distance, for the weak turbulent case.

The qualitative discussion presented above is suitable for an arbitrary random field. The form of the structure function  $H(\xi)$  will determine the q.p. density profile. To illustrate this effect, we will present some numerical results for a wave propagating in a random medium characterized by the spectrum (C). Fig. 39a depicts the q.p. density function at  $x = 0$  in  $\xi$ -space, i.e.  $M(0, \xi, z)$ , for the case of collimated beams propagating in a turbulent medium with spectrum (C). We choose the parameters  $GCTR = 3$ ,  $GWID = 0.2$ ,  $GAMP = 0.3$  and  $p = 4$ . One notes that the axial intensity decreases as  $z$  increases and the deformation of  $M(0, \xi, z)$  reflects the behavior of the decay field. The normalized correlation function,  $\frac{M(0, \xi, z)}{M(0, 0, z)}$  is shown as a function of  $z$  in Fig. 39b. The area under each curve represents the corresponding correlation length  $l$ . For  $\gamma = 10$ , which represents a strong turbulent case, one sees that the correlation width decreases as  $z$  increases.

The corresponding phenomena for the focused beam case is displayed in Fig. 40a and 40b. One notes the focusing and defocusing effects in Fig. 40a and the associated curves for the normalized MCF in Fig. 40b.

The choice of an symmetric function for the input field

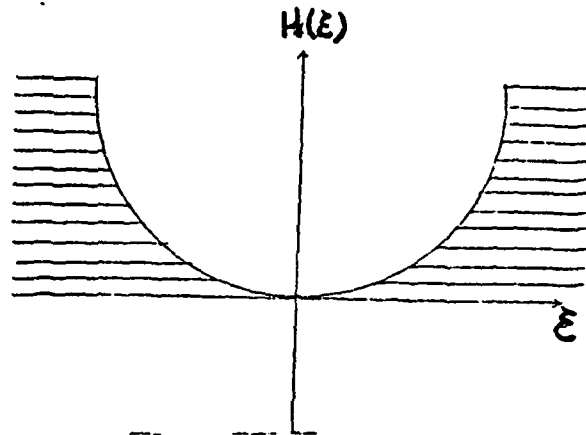


Fig. 36. Quantitative plot of structure function  $H(\xi)$  in  $\xi$  space.

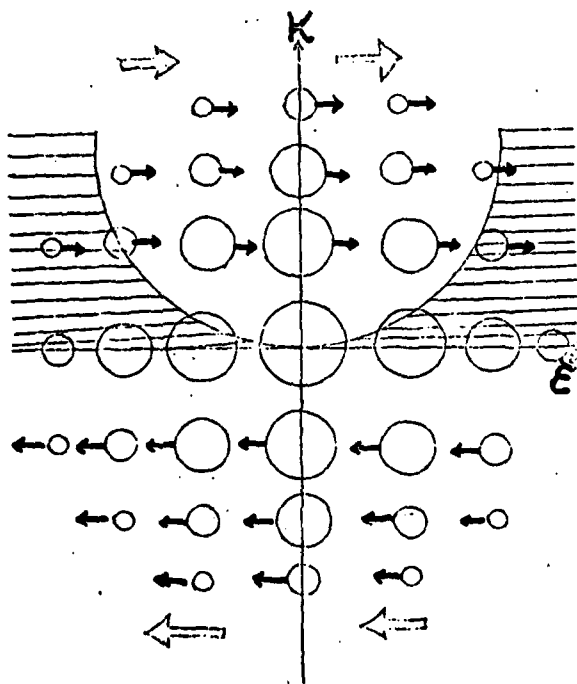


Fig. 37. S function of a collimated beam moves in a random medium.

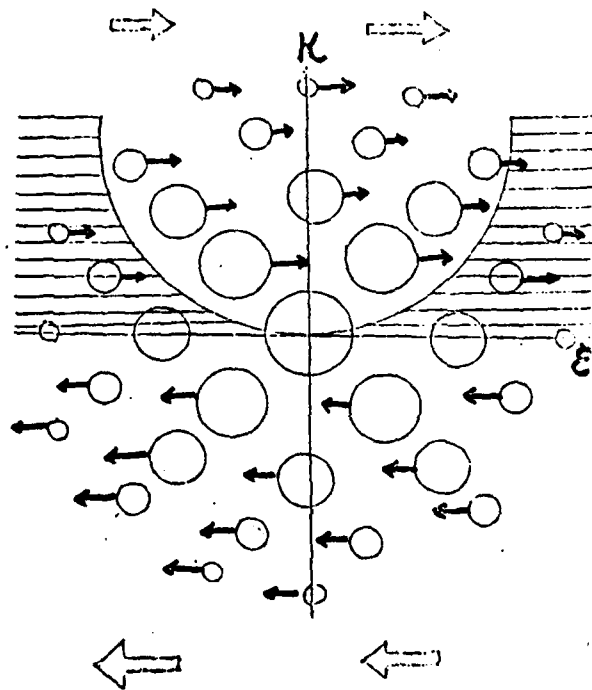


Fig. 38. S function of a focused beam moves in a random medium.

DIST= 1.75000      WIDTH= 1.00000      AI= 0.0      GAMMA= 10.0000  
 GCTR= 3.00000      GWID= 2.00000E-01      GAMP= 3.00000E-01      INDEX= 2.00000  
 POWER SPECTRUM WITH A GAUSSIAN BUMP

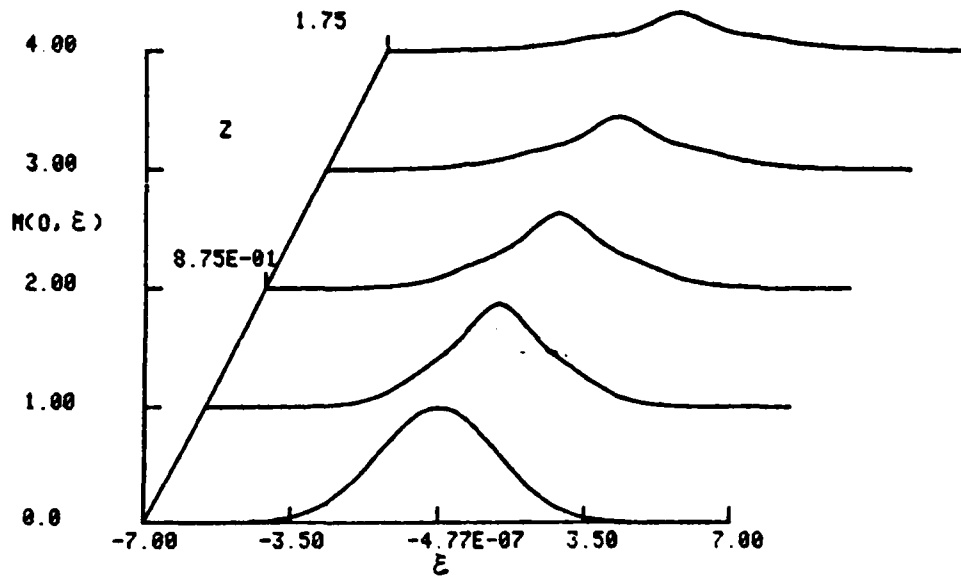


Fig. 39a. q.p. density function, at  $x = 0$ , in  $\xi$  space; plotted as a function of  $\xi$  and  $z$ ; collimated beam propagating thru a random medium with spectrum (c);  $k' = 3$ ,  $a = 0.3$ ,  $b = 0.2$ ,  $p = 4$ ,  $\gamma = 10$ .

DIST= 1.75000      WIDTH= 1.00000      AI= 0.0      GAMMA= 10.0000  
 GCTR= 3.00000      GWID= 2.00000E-01      GAMP= 3.00000E-01      INDEX= 2.00000  
 POWER SPECTRUM WITH A GAUSSIAN BUMP

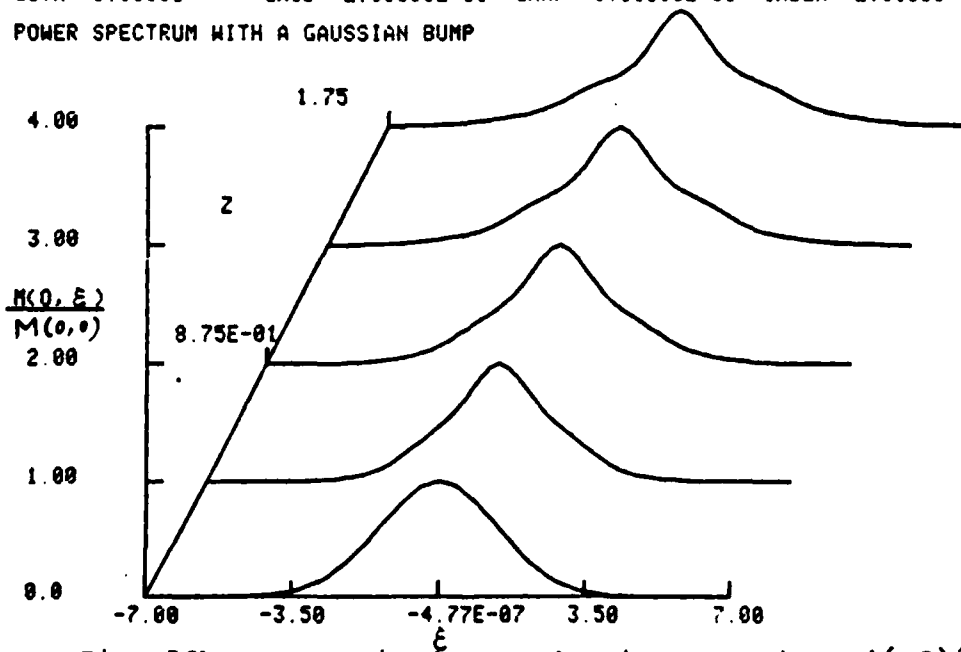


Fig. 39b. Normalized q.p. density function,  $M(0, \xi)/M(0, 0)$  vs.  $\xi$  and  $z$ ; the area under each curve represents the corresponding correlation length 1.

DIST= 1.75000    WIDTH= 1.00000    AI= 1.00000    GAMMA= 10.0000  
GCTR= 3.00000    GWID= 2.00000E-01    GAMP= 3.00000E-01    INDEX= 2.00000  
POWER SPECTRUM WITH A GAUSSIAN BUMP

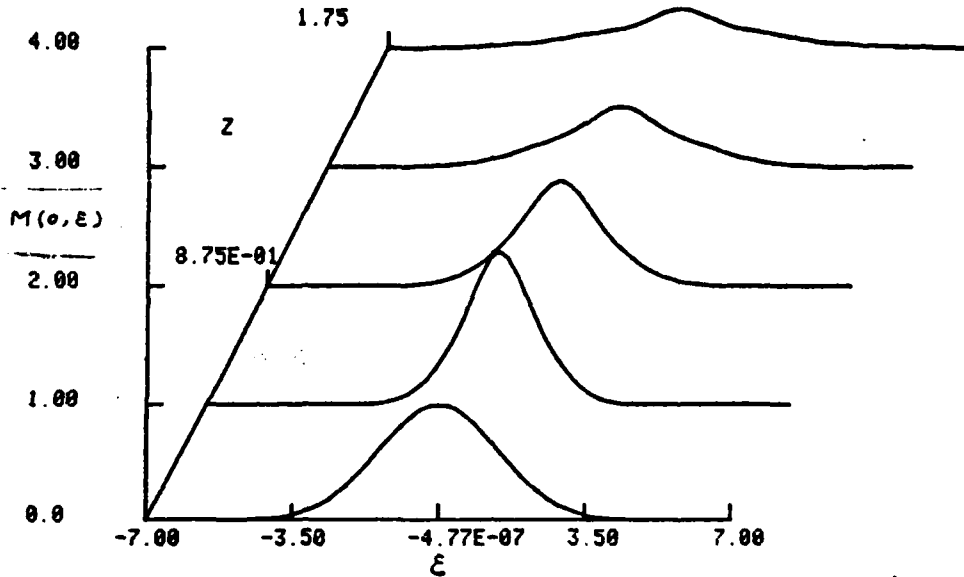


Fig. 40a. q.p. density function, at  $x = 0$ , in  $\epsilon$  space; focused beam propagating thru a random medium with spectrum (c),  $k' = 3$ ,  $a = 0.3$ ,  $b = 0.2$ ,  $p = 4$ ,  $\gamma = 10$ .

DIST= 1.75000    WIDTH= 1.00000    AI= 1.00000    GAMMA= 10.0000  
GCTR= 3.00000    GWID= 2.00000E-01    GAMP= 3.00000E-01    INDEX= 2.00000  
POWER SPECTRUM WITH A GAUSSIAN BUMP

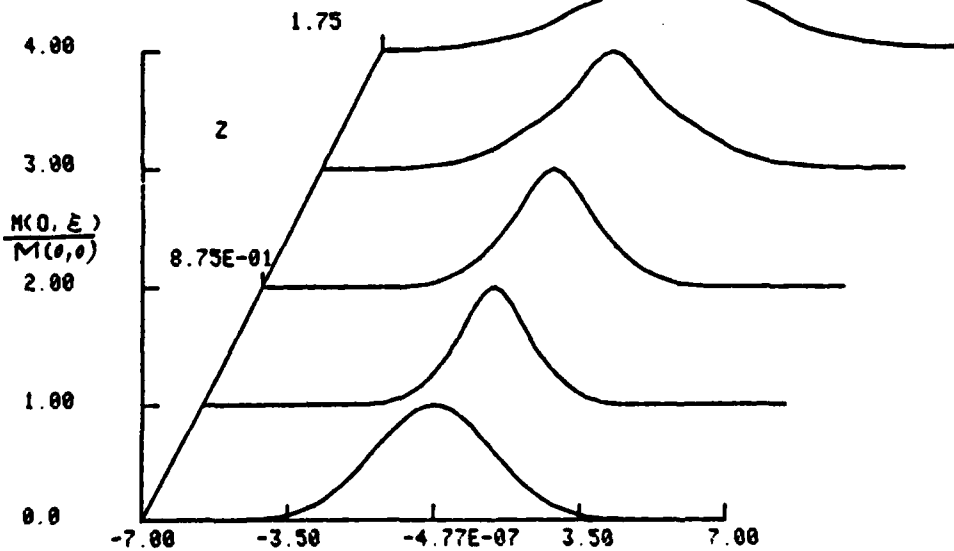


Fig. 40b. Normalized q.p. density function,  $M(0, \epsilon)/M(0, 0)$  vs.  $z$ ; the area under each curve gives 1.

leads to a real S function. It provides a simpler approach to obtaining 2 point statistics especially for numerical evaluations. The exact solution of the Mutual Coherence Function for the case  $H(\xi) = a \xi^2$  is solved and presented in section II. For an arbitrary spectrum, a numerical scheme has been used to evaluate the S function as shown previously in section III.

For simplicity the above analysis has been limited to the two (z,x) dimensional case. The extension to three dimensions is straightforward but requires more computation. For a random medium which is inhomogeneous in z, one simply adds a z dependence to the H function in equation (3.55) and all of the calculational procedures will then be unchanged.

Chapter 4 THE FOURTH ORDER MOMENT AND INTENSITY FUNCTION

I. Formulation of the Fourth Moment Equation:

The parabolic equation for the 4th moment

$$M_4(\underline{r}_1, \underline{r}_2, \underline{r}'_1, \underline{r}'_2) = \langle \hat{\psi}(\underline{z}, \underline{r}_1) \hat{\psi}(\underline{z}, \underline{r}_2) \hat{\psi}^*(\underline{z}, \underline{r}'_1) \hat{\psi}^*(\underline{z}, \underline{r}'_2) \rangle \quad (4.1)$$

may be derived for the case of statistically homogeneous fluctuation as follows: (cf. Tatarskii, 1; Ishimaru, 25)

$$\left\{ \frac{\partial}{\partial \underline{z}} - \frac{i}{2k_0} (\nabla_{\underline{r}_1}^2 + \nabla_{\underline{r}_2}^2 - \nabla_{\underline{r}'_1}^2 - \nabla_{\underline{r}'_2}^2) + \frac{k_0^2}{4} f \right\} M_4 = 0 \quad (4.2)$$

where

$$\begin{aligned} f &= f(\underline{r}_1, \underline{r}_2, \underline{r}'_1, \underline{r}'_2, \underline{z}) \\ &= H(\underline{z}, \underline{r}_1 - \underline{r}'_1) + H(\underline{z}, \underline{r}_2 - \underline{r}'_2) + H(\underline{z}, \underline{r}_1 - \underline{r}'_2) \\ &\quad + H(\underline{z}, \underline{r}_2 - \underline{r}'_1) - H(\underline{z}, \underline{r}_2 - \underline{r}_1) - H(\underline{z}, \underline{r}'_2 - \underline{r}'_1) \end{aligned} \quad (4.3)$$

and

$$\begin{aligned} H(\underline{z}, \underline{r}) &= A(\underline{z}, 0) - A(\underline{z}, \underline{r}) \\ &= 2\pi \int \Phi(\underline{k}, \underline{z}) [1 - \cos \underline{k} \cdot \underline{r}] d\underline{k} \end{aligned} \quad (4.4)$$

Introducing the new variables:

$$\begin{aligned}
 \underline{x}_1 &= \frac{\underline{\rho}_1 + \underline{\rho}'_1}{2} & \underline{R} &= \frac{\underline{x}_1 + \underline{x}_2}{2} \\
 \underline{x}_2 &= \frac{\underline{\rho}_2 + \underline{\rho}'_2}{2} & \underline{\rho} &= \underline{\xi}_1 + \underline{\xi}_2 \\
 \underline{\xi}_1 &= \underline{\rho}_1 - \underline{\rho}'_1 & \underline{\eta}_1 &= \underline{x}_1 - \underline{x}_2 \\
 \underline{\xi}_2 &= \underline{\rho}_2 - \underline{\rho}'_2 & \underline{\eta}_2 &= \frac{\underline{\xi}_1 - \underline{\xi}_2}{2}
 \end{aligned} \tag{4.5}$$

then  $\nabla_{\underline{\rho}'_1}^2 + \nabla_{\underline{\rho}'_2}^2 - \nabla_{\underline{\rho}'_1}^2 - \nabla_{\underline{\rho}'_2}^2 = 2(\nabla_{\underline{R}} \nabla_{\underline{\rho}} + \nabla_{\underline{\eta}_1} \nabla_{\underline{\eta}_2})$  and equation (4.2) takes the form

$$\left\{ \frac{\partial}{\partial \underline{\zeta}} - \frac{i}{k_0} (\nabla_{\underline{R}} \nabla_{\underline{\rho}} + \nabla_{\underline{\eta}_1} \nabla_{\underline{\eta}_2}) + \frac{k_0^2}{4} f(\underline{\zeta}, \underline{\eta}_1, \underline{\eta}_2, \underline{\rho}) \right\} M_A = 0 \tag{4.6}$$

where the function  $f$ , expressed in terms of the new variables, is independent of the center coordinate  $\underline{R}$  and

$$\begin{aligned}
 f(\underline{\zeta}, \underline{\eta}_1, \underline{\eta}_2, \underline{\rho}) &= H(\underline{\zeta}, \underline{\eta}_1 + \frac{1}{2}\underline{\rho}) + H(\underline{\zeta}, \underline{\eta}_1 - \frac{1}{2}\underline{\rho}) \\
 &+ H(\underline{\zeta}, \underline{\eta}_2 + \frac{1}{2}\underline{\rho}) + H(\underline{\zeta}, \underline{\eta}_2 - \frac{1}{2}\underline{\rho}) \\
 &- H(\underline{\zeta}, \underline{\eta}_1 + \underline{\eta}_2) - H(\underline{\zeta}, \underline{\eta}_1 - \underline{\eta}_2)
 \end{aligned} \tag{4.7}$$

Equation (4.6) and (4.7) together with the boundary conditions on  $M_4$  at  $z = 0$  determine the corresponding fourth order statistics of the field in the random medium. To date, no analytical solutions have been derived for equation (4.6), except for the special case  $H(\xi) = a \xi^2$ , which has been solved by Furutsu(13) using functional techniques.

In section 2, we shall extend the "quasiparticle distribution function" concepts to a 4-point correlation spectrum, i.e. the Fourier transform of 4-point correlation function, to obtain an analytical result for the case  $H(\xi) = a \xi^2$ . An approximate solution for arbitrary power spectrum using 4-point. Slow spectrum will be derived in section 3. In the last section of this chapter, we will present a numerical scheme to solve the fourth moment equation (4.6) for an arbitrary power spectrum.

## II. The Exact Solution for the Case $H(\xi) = a \xi^2$

We shall define the F and S functions corresponding to the fourth moment  $M_4$ , viz:

$$F(\underline{k}_R, \underline{k}_f, \underline{r}_1, \underline{k}_{r_2}, \beta) = \int M_4(\underline{R}, \underline{f}, \underline{r}_1, \underline{r}_2, \beta) e^{-i(\underline{k}_f \cdot \underline{f} + \underline{k}_{r_2} \cdot \underline{r}_2)} d\underline{f} d\underline{r}_2 \quad (4.8a)$$

$$S(\underline{k}_R, \underline{f}, \underline{k}_{r_1}, \underline{r}_2, \beta) = \int M_4(\underline{R}, \underline{f}, \underline{r}_1, \underline{r}_2, \beta) e^{-i(\underline{k}_R \cdot \underline{R} + \underline{k}_{r_1} \cdot \underline{r}_1)} d\underline{R} d\underline{r}_1 \quad (4.8b)$$

where  $\underline{R}$  and  $\underline{r}_1$  are denoted as the "slow variables", and  $\underline{p}$  and  $\underline{r}_2$  as "fast variables". One observes that  $F$  and  $S$  form a 4-fold Fourier transform pair with respect to  $\underline{R}$ ,  $\underline{r}_2$  and  $\underline{k}_p$ ,  $\underline{k}_{r_1}$ .

$$S(\underline{k}_p, \underline{p}, \underline{k}_{r_1}, \underline{r}_2, \beta) = \int F(\underline{R}, \underline{k}_p, \underline{r}_1, \underline{k}_{r_2}, \beta) e^{-i(\underline{k}_p \cdot \underline{R} + \underline{k}_{r_2} \cdot \underline{r}_2 - \underline{k}_p \cdot \underline{p} - \underline{k}_{r_1} \cdot \underline{r}_1)} \frac{d\underline{R} d\underline{r}_1 d\underline{k}_p d\underline{k}_{r_2}}{(2\pi)^6} \quad (4.9)$$

Furthermore, the "macroparticle coordinates" can be obtained by the following relation:

$$\frac{\partial^{n_1+n_2+n_3+n_4} S(0,0,0,0,\beta)}{\partial (-i\underline{k}_{R_1})^{n_1} \partial (-i\underline{k}_{r_1})^{n_2} \partial (i\underline{p})^{n_3} \partial (i\underline{r}_2)^{n_4}} = \overline{\underline{R}^{n_1} \underline{r}_1^{n_2} \underline{k}_p^{n_3} \underline{k}_{r_2}^{n_4}} \quad (4.10)$$

For the special case,  $H(\underline{\epsilon}) = a \underline{\epsilon}^2$ , one obtains

$$\begin{aligned} f(\underline{r}_1, \underline{r}_2, \underline{p}, \beta) &= a \left[ (\underline{r}_1 + \frac{1}{2}\underline{p})^2 + (\underline{r}_1 - \frac{1}{2}\underline{p})^2 \right. \\ &\quad \left. + (\underline{r}_2 + \frac{1}{2}\underline{p})^2 + (\underline{r}_2 - \frac{1}{2}\underline{p})^2 \right. \\ &\quad \left. - (\underline{r}_1 + \underline{r}_2)^2 - (\underline{r}_1 - \underline{r}_2)^2 \right] \\ &= a \underline{p}^2 \end{aligned} \quad (4.11)$$

Substituting (4.11) into (4.6) and using (4.8b), we can derive the defining equation for S as:

$$\left\{ \frac{\partial}{\partial \zeta} + \frac{\underline{k}_R}{\underline{k}_0} \cdot \frac{\partial}{\partial \underline{\rho}} + \frac{\underline{k}_{r_1}}{\underline{k}_0} \cdot \frac{\partial}{\partial r_2} + a \underline{\rho}^2 \right\} S(\underline{k}_R, \underline{\rho}, \underline{k}_{r_1}, r_2, \zeta) = 0 \quad (4.12)$$

The characteristic trajectory equations corresponding to equation (4.12) are

$$\begin{aligned} \frac{d \underline{\rho}}{d \zeta} &= \frac{\underline{k}_R}{\underline{k}_0} & , & & \frac{d r_2}{d \zeta} &= \frac{\underline{k}_{r_1}}{\underline{k}_0} \\ \frac{d \underline{k}_R}{d \zeta} &= 0 & , & & \frac{d \underline{k}_{r_2}}{d \zeta} &= 0 \end{aligned} \quad (4.13)$$

Equation (4.12) can be described as the slow quasiparticle distribution function in a two-dimensional phase space spanned by  $\underline{k}_R, \underline{k}_{r_2}, \underline{\rho}, r_2$ . Along the trajectories, the S function obeys

$$S(\underline{k}_R, \underline{\rho}, \underline{k}_{r_1}, r_2, \zeta) = S(\underline{k}_R, \underline{\rho}(0), \underline{k}_{r_1}, r_2(0), 0) \times e^{-\int_0^\zeta a \underline{\rho}^2(\zeta') d\zeta'} \quad (4.14)$$

which is essentially the same expression as described in the 2-point correlation case except that 6-fold spatial directions are involved. For simplicity, we shall consider only the two dimensional case which can be extended to the 6-dimensional

case without great difficulty.

For incident wave at  $z = 0$  of the form

$$\psi(x, 0) = e^{-\frac{1}{2}(\alpha_r + i\alpha_i)x^2}$$

the four point correlation function can be calculated as

$$\begin{aligned} M_4(x_1, x_2, x'_1, x'_2, 0) &= \langle \psi(x_1) \psi(x_2) \psi^*(x'_1) \psi^*(x'_2) \rangle \\ &= e^{-\frac{1}{2}\alpha_r(x_1^2 + x_2^2 + x_1'^2 + x_2'^2) - \frac{1}{2}i\alpha_i(x_1^2 + x_2^2 - x_1'^2 - x_2'^2)} \\ &= e^{-\frac{1}{2}\alpha_r(4R^2 + r_1^2 + \frac{1}{4}\rho^2 + r_2^2) - i\alpha_i(r_1 r_2 + R\rho)} \quad (4.15) \end{aligned}$$

Using (4.8b), one obtains

$$\begin{aligned} S(k_R, \rho, k_{r_1}, r_2, 0) &= \frac{\pi}{\alpha_r} e^{-\frac{1}{2}\alpha_r r_2^2 - \frac{1}{8}\alpha_r \rho^2} \\ &e^{-\frac{(k_R + \alpha_i \rho)^2}{8\alpha_r} - \frac{(k_{r_1} + \alpha_i r_2)^2}{2\alpha_r}} \quad (4.16) \end{aligned}$$

where  $k_R$  and  $k_{r_1}$  are normalized by  $k_0$ . Substituting (4.16) into (4.14) and applying the trajectory equations defined by (4.13), we get

$$\begin{aligned}
 S(k_R, \rho, k_{r_1}, r_2, \beta) = & \frac{\pi}{\alpha_r} \exp \left[ -\frac{1}{2} \alpha_r (r_2 - k_{r_1} \beta)^2 \right. \\
 & - \frac{1}{8} \alpha_r (\rho - k_R \beta)^2 \\
 & - \frac{[k_R + \alpha_i (\rho - k_R \beta)]^2}{8 \alpha_r} \\
 & - \frac{[k_{r_1} + \alpha_i (r_2 - k_{r_1} \beta)]^2}{2 \alpha_r} \\
 & \left. - a (\rho^2 \beta - k_R \rho \beta^2 + \frac{1}{3} k_R^2 \beta^3) \right]
 \end{aligned} \tag{4.17}$$

The fourth moment defined by (4.15) can be derived by substituting (4.17) into (4.8b). For example, let us consider a special case when  $r_1 = \rho = r_2 = 0$ , then

$$S(k_R, 0, k_{r_1}, 0, \beta) = \frac{\pi}{\alpha_r} e^{-A k_{r_1}^2 - B k_R^2} \tag{4.18}$$

where

$$A = \frac{1}{2} \alpha_r \beta^2 + \frac{1}{2 \alpha_r} (1 - \alpha_i \beta)^2$$

$$B = \frac{1}{8} \alpha_r \beta^2 + \frac{1}{8 \alpha_r} (1 - \alpha_i \beta)^2 + \frac{1}{3} a \beta^3$$

and

$$\begin{aligned}
 M_4(R, 0, 0, 0, \beta) &= \frac{\pi}{\alpha_r} \int e^{\frac{-Ak_r^2 - Bk_R^2 + ik_R R}{(2\pi)^2}} dk_R dk_r \\
 &= \frac{1}{4\alpha_r} \sqrt{\frac{1}{AB}} e^{-\frac{R^2}{4B}} \quad (4.19)
 \end{aligned}$$

For the ionospheric propagation case described by Fig.1.1, the S function obtained in equation (4.17) will be used to obtain the distribution function at the bottom of the random slab at  $z = z_1$ . The quasiparticles will redistribute while propagating in free space and obey the following equation:

$$\left\{ \frac{\partial}{\partial \beta} + k_R \frac{\partial}{\partial \rho} + k_r \frac{\partial}{\partial r_2} \right\} S(k_R, \rho, k_r, r_2, \beta) = 0 \quad (4.20)$$

The trajectory equations becomes

$$\begin{aligned}
 \rho(\beta_2) &= \rho(\beta_1) + k_R (\beta_2 - \beta_1) \\
 r_2(\beta_2) &= r_2(\beta_1) + k_r (\beta_2 - \beta_1)
 \end{aligned} \quad (4.21)$$

where  $z_2$  is the location of the receiver on the ground. One notes that

$$S(k_R, \rho(\bar{z}_2), k_{r_1}, r_2(\bar{z}_2), \bar{z}_2) = S(k_R, \rho(\bar{z}_1), k_{r_1}, r_2(\bar{z}_1), \bar{z}_1) \quad (4.22)$$

using (4.17), (4.22) and (4.21), one obtains

$$\begin{aligned} & S(k_R, \rho(\bar{z}_2), k_{r_1}, r_2(\bar{z}_2), \bar{z}_2) \\ &= \frac{\pi}{\alpha_r} \exp \left\{ -\frac{1}{2} \alpha_r [r_2 - k_{r_1} \bar{z}_2]^2 - \frac{1}{8} \alpha_r [\rho - k_R \bar{z}_2]^2 \right. \\ &\quad - \frac{[k_R + \alpha_i (\rho - k_R \bar{z}_2)]^2}{8 \alpha_r} \\ &\quad - \frac{[k_{r_1} + \alpha_i (r_2 - k_{r_1} \bar{z}_2)]^2}{2 \alpha_r} \\ &\quad \left. - a [(\rho - k_R \Delta \bar{z})^2 \bar{z}_1 - (\rho - k_R \Delta \bar{z}) k_R \bar{z}_1^2 \right. \\ &\quad \left. + \frac{1}{3} k_R^2 \bar{z}_1^3 \right\} \end{aligned} \quad (4.23)$$

where  $\Delta z = z_2 - z_1$  is the distance from the bottom of the slab to the ground. For the special case  $\rho = r_1 = r_2 = 0$  the S function can be calculated from (4.23) as:

$$\begin{aligned} & S(k_R, 0, k_{r_1}, 0, \bar{z}_2) \\ &= \frac{\pi}{\alpha_r} \exp \left\{ \left( -\frac{1}{2} \alpha_r k_{r_1}^2 - \frac{1}{8} \alpha_r k_R^2 \right) \bar{z}_2^2 - \frac{k_R^2}{8 \alpha_r} (1 - \alpha_i \bar{z}_2)^2 \right. \\ &\quad - \frac{k_{r_1}^2}{2 \alpha_r} (1 - \alpha_i \bar{z}_2)^2 - a k_R^2 (\bar{z}_2^2 \bar{z}_1 - \bar{z}_2 \bar{z}_1^2 \\ &\quad \left. + \frac{1}{3} \bar{z}_1^3) \right\} \end{aligned} \quad (4.24)$$

and

$$M_4(R, 0, 0, 0, \beta_2) = \int S(k_R, 0, k_{r_1}, 0, \beta_2) e^{i k_R R} \frac{d k_R d k_{r_1}}{(2\pi)^2} \\ = \frac{1}{4\alpha_r} \sqrt{\frac{1}{AB}} e^{-\frac{R^2}{4B}} \quad (4.25)$$

where

$$A = \frac{1}{2} \alpha_r \beta_2^2 + \frac{1}{2\alpha_r} (1 - \alpha_i \beta_2)^2 \\ B = \frac{1}{8} \alpha_r \beta_2^2 + \frac{1}{8\alpha_r} (1 - \alpha_i \beta_2)^2 + a (\beta_1 \beta_2^2 - \beta_1^2 \beta_2 + \frac{1}{3} \beta_1^3) \quad (4.26)$$

One thus concludes that if the 4-point statistics of the wave field is given at  $z = 0$ , the corresponding 4th order statistics at the ground can be obtained from the  $z$  evolution of the quasiparticle distribution function from equation (4.14) and (4.22).

### III. Approximate Solution for 4th Moment

The defining equation for the 4th moment can be rewritten as

$$\left\{ \frac{\partial}{\partial \beta} - \frac{i}{k_0} (\nabla_R \nabla_\rho + \nabla_{r_1} \nabla_{r_2}) + \frac{k_0^2}{4} [H(r_2 + \frac{1}{2}\rho) + H(r_2 - \frac{1}{2}\rho)] \right\} M_4 \\ = - \frac{k_0^2}{4} [H(r_1 + \frac{1}{2}\rho) + H(r_1 - \frac{1}{2}\rho) - H(r_1 + r_2) - H(r_1 - r_2)] \quad (4.27) \\ M_4 .$$

Inserting (4.8b) in (4.27), one obtains

$$\left\{ \frac{\partial}{\partial \beta} + \frac{k_R}{k_0} \cdot \nabla_{\underline{r}} + \frac{k_r}{k_0} \cdot \nabla_{\underline{r}_2} + \frac{k_0^2}{4} [H(\underline{r}_2 + \frac{1}{2}\underline{\rho}) + H(\underline{r}_2 - \frac{1}{2}\underline{\rho})] \right\} S$$

$$= - \frac{k_0^2}{4} \int_{\underline{R}} \int_{\underline{r}_1} J(\underline{r}_1, \underline{r}_2, \underline{\rho}) M_4 e^{-i(k_R \cdot \underline{R} + k_{r_1} \cdot \underline{r}_1)} d\underline{R} d\underline{r}_1 \quad (4.28)$$

where

$$J(\underline{r}_1, \underline{r}_2, \underline{\rho}) = H(\underline{r}_1 + \frac{1}{2}\underline{\rho}) + H(\underline{r}_1 - \frac{1}{2}\underline{\rho}) - H(\underline{r}_1 + \underline{r}_2) - H(\underline{r}_1 - \underline{r}_2)$$

since

$$H(\underline{\rho}) = 2\pi \int \underline{\Phi}(\underline{k}) [1 - e^{i\underline{k} \cdot \underline{\rho}}] d\underline{k} \quad (4.29)$$

one derives from (4.28) after some manipulation

$$J(\underline{r}_1, \underline{r}_2, \underline{\rho}) = 4 \int \underline{\Phi}(\underline{k}) [\cos \underline{k} \cdot \underline{r}_2 - \cos \frac{\underline{k} \cdot \underline{\rho}}{2}] e^{i\underline{k} \cdot \underline{r}_1} d\underline{k} \quad (4.30)$$

and

$$\int J(\underline{r}_1, \underline{r}_2, \underline{\rho}) M_4 e^{-i(k_R \cdot \underline{R} + k_{r_1} \cdot \underline{r}_1)} d\underline{R} d\underline{r}_1$$

$$= k_0^2 \int \underline{\Phi}(\underline{k}') [\cos \underline{k}' \cdot \underline{r}_2 - \cos \frac{\underline{k}' \cdot \underline{\rho}}{2}] S(\underline{k}', \underline{\rho}, \underline{k}' - k_{r_1}, \underline{r}_2, \underline{\rho}) d\underline{k}' \quad (4.31)$$

From (4.28) and (4.31) we readily derive the integral equation for S as:

$$\left\{ \frac{\partial}{\partial \beta} + \frac{k_R}{k_0} \cdot \nabla_{\underline{r}_1} + \frac{k_{r_1}}{k_0} \cdot \nabla_{\underline{r}_2} + \frac{k_0^2}{4} [H(\underline{r}_2 + \frac{1}{2}\underline{\rho}) + H(\underline{r}_2 - \frac{1}{2}\underline{\rho})] \right\} S$$

$$= -k_0^2 \int_{\underline{r}_2, \beta} \Phi(\underline{k}') [\cos \underline{k}' \cdot \underline{r}_2 - \cos \frac{\underline{k}' \cdot \underline{\rho}}{2}] S(\underline{k}_R, \underline{\rho}, \underline{k}' - \underline{k}_{r_1}, \underline{r}_2, \beta) d\underline{k}' \quad (4.32)$$

Equation (4.32) contains an extinction term  $H(\underline{r}_2 + \frac{1}{2}\underline{\rho}) + H(\underline{r}_2 - \frac{1}{2}\underline{\rho})$  which will reduce the quasiparticle distribution function while redistributing it in  $\underline{k}_R, \underline{\rho}, \underline{k}_{r_1}, \underline{r}_2$  space. The "scattering term" on the right hand side of the equation describes the contribution to the total S function at the "momentum coordinates"  $\underline{k}_R, \underline{k}_{r_1}$  from a "momentum coordinates"  $\underline{k}_R, \underline{k}' - \underline{k}_{r_1}$ . The complicated form of equation (4.32) makes it impossible to obtain a solution in analytical form. We shall consider first the simplest case of a plane wave, for which obviously  $\nabla_{\underline{R}} M_4 = 0$ .  $\nabla_{\underline{\rho}} M_4$  can also be eliminated from the equation, ( $\underline{\rho}$  is only a parameter) by setting it to zero because in this case,  $\underline{\rho} = 0$ , the points  $\underline{\rho}_1, \underline{\rho}_1', \underline{\rho}_2, \underline{\rho}_2'$  lie in the plane z at the vertices of a parallelogram centered at the point  $\underline{R}$  and with sides  $\underline{\rho}_1 - \underline{\rho}_1' = \underline{\rho}_2' - \underline{\rho}_2 = \underline{r}_2; \underline{\rho}_1 - \underline{\rho}_2 = \underline{\rho}_1' - \underline{\rho}_2' = \underline{r}_1$ . Therefore equation (4.27) takes the form

$$\left\{ \frac{\partial}{\partial \beta} - \frac{i}{k_0} \nabla_{\underline{r}_1} \cdot \nabla_{\underline{r}_2} + \frac{k_0^2}{4} f(\underline{r}_1, \underline{r}_2, \beta) \right\} M_4 = 0 \quad (4.33)$$

where

$$f(\underline{r}_1, \underline{r}_2, \beta) = 2H(\underline{r}_1) + 2H(\underline{r}_2) - H(\underline{r}_1 + \underline{r}_2) - H(\underline{r}_1 - \underline{r}_2) \quad (4.34)$$

one notes from equation (4.5) that

$$\begin{aligned} r_1 &= \frac{1}{2} [(\beta_1 - \beta_2) + (\beta_1' - \beta_2')] \\ r_2 &= \frac{1}{2} [(\beta_1 - \beta_2) - (\beta_1' - \beta_2')] \end{aligned} \quad (4.35)$$

which suggests that  $\underline{r}_1$  and  $\underline{r}_2$  can be treated as "slow" and "fast" variables respectively. In this case, one encounters the same degree of difficulty using either the "slow spectrum S" or the "fast spectrum F" to solve equation (4.33). In order to maintain the consistency, we shall adopt the "slow spectrum procedure" as described previously.

Following the same steps as in (4.27)-(4.32), one obtains the defining equation for S function for the plane wave case as:

$$\begin{aligned} &\left\{ \frac{\partial}{\partial \beta} + \frac{k_{r_1}}{k_0} \cdot \nabla_{\underline{r}_2} + \frac{k_0^2}{2} H(\beta, \underline{r}_2) \right\} S(\underline{k}_{r_1}, \underline{r}_2, \beta) \\ &= k_0^2 \int_{d\underline{k}'} \Phi(\underline{k}') [1 - \cos \underline{k}' \cdot \underline{r}_2] S(\underline{k}' - \underline{k}_{r_1}, \underline{r}_2, \beta) \end{aligned} \quad (4.36)$$

On the trajectory defined by

$$\frac{dr_2}{d\bar{z}} = \frac{k_{r_1}}{k_0}, \quad \frac{dk_{r_1}}{d\bar{z}} = 0 \quad (4.37)$$

equation (4.36) becomes

$$\begin{aligned} \frac{dS(k_{r_1}, r_2(\bar{z}), \bar{z})}{d\bar{z}} + \frac{k_0^2}{2} H(r_2(\bar{z})) S(k_{r_1}, r_2(\bar{z}), \bar{z}) \\ = J(k_{r_1}, r_2(\bar{z}), \bar{z}) \end{aligned} \quad (4.38)$$

where

$$\begin{aligned} J(k_{r_1}, r_2(\bar{z}), \bar{z}) = k_0^2 \int \Phi(k') [1 - \cos k' \cdot r_2(\bar{z})] \\ S(k_{r_1} - k', r_2(\bar{z}), \bar{z}) dk' \end{aligned} \quad (4.39)$$

The solution of (4.38) has the form

$$\begin{aligned} S(k_{r_1}, r_2(\bar{z}), \bar{z}) = S(k_{r_1}, r_2(0), 0) e^{-\frac{k_0^2}{2} \int_0^{\bar{z}} H(r_2(\bar{z})) d\bar{z}} \\ + \int_0^{\bar{z}} e^{-\frac{k_0^2}{2} \int_{\bar{z}'}^{\bar{z}} H(r_2(\bar{z})) d\bar{z}} J(k_{r_1}, r_2(\bar{z}'), \bar{z}') d\bar{z}' \end{aligned} \quad (4.40)$$

Substituting (4.37) into (4.40), one obtains

$$\begin{aligned}
 S(\underline{k}_r, \underline{r}_2, \underline{z}) &= S(\underline{k}_r, \underline{r}_2 - \frac{\underline{k}_r}{k_0} \underline{z}, 0) \exp\left[-\frac{k_0^2}{2} \int_0^{\underline{z}} \right. \\
 &H(\underline{r}_2 - \frac{\underline{k}_r}{k_0} (\underline{z} - \underline{z}')) d\underline{z}' + \int_0^{\underline{z}} \exp\left[-\frac{k_0^2}{2} \int_{\underline{z}'}^{\underline{z}} \right. \\
 &H(\underline{r}_2 - \frac{\underline{k}_r}{k_0} (\underline{z} - \underline{z}')) d\underline{z}'] J(\underline{k}_r, \underline{r}_2 - \frac{\underline{k}_r}{k_0} (\underline{z} - \underline{z}'), \underline{z}') d\underline{z}'
 \end{aligned} \tag{4.41}$$

Equation (4.41) together with the  $z = 0$  boundary condition,  $S(0, \underline{r}_2, \underline{k}_r) = \delta(\underline{k}_r)$ , gives the solution for the  $S$  function at distance  $z$ . The first approximate solution can be obtained by substituting the  $z = 0$  value of the  $S$  function into equation (4.39), whence one obtains

$$\begin{aligned}
 J(\underline{k}_r, \underline{r}_2 - \frac{\underline{k}_r}{k_0} (\underline{z} - \underline{z}'), \underline{z}') &= k_0^2 \Phi(\underline{k}_r) \times \\
 &[1 - \cos \underline{k}_r \cdot (\underline{r}_2 - \frac{\underline{k}_r}{k_0} (\underline{z} - \underline{z}'))] \tag{4.42}
 \end{aligned}$$

and from equation (4.41)

$$\begin{aligned}
 S(\underline{k}_r, \underline{r}_2, \underline{z}) &= \delta(\underline{k}_r) e^{-\frac{k_0^2}{2} H(\underline{r}_2) \underline{z}} + \\
 &\int_0^{\underline{z}} e^{-\frac{k_0^2}{2} \int_{\underline{z}'}^{\underline{z}} H(\underline{r}_2 - \frac{\underline{k}_r}{k_0} (\underline{z} - \underline{z}')) d\underline{z}'} \times k_0^2 \Phi(\underline{k}_r) \\
 &[1 - \cos \underline{k}_r \cdot (\underline{r}_2 - \frac{\underline{k}_r}{k_0} (\underline{z} - \underline{z}'))] d\underline{z}'
 \end{aligned} \tag{4.43}$$

One notes that the Fourier transform of equation (4.43), which gives the approximate solution of  $M_4$ , is not a symmetric function of  $\underline{r}_1$ ,  $\underline{r}_2$ . This violates the symmetry property of  $M_4$ . Therefore, it is logical to consider the Fourier transformation with respect to  $\underline{r}_2$ , i.e. via the fast spectrum procedure. Let us define

$$F(\underline{r}_1, \underline{k}_{r_2}, \beta) = \int M_4(\beta, \underline{r}_1, \underline{r}_2) e^{-i \underline{k}_{r_2} \cdot \underline{r}_2} d\underline{r}_2 \quad (4.44)$$

One obtains a solution for  $F$  similar to that described in (4.43), except for the interchange  $\underline{r}_2 \leftrightarrow \underline{r}_1$  and  $\underline{k}_{r_2} \leftrightarrow \underline{k}_{r_1}$ . The approximate solution of  $M_4$  can then be written as

$$M_4(\underline{r}_1, \underline{r}_2, \beta) = \frac{1}{2} \left\{ \int S(\underline{k}_{r_1}, \underline{r}_2, \beta) e^{i \underline{k}_{r_1} \cdot \underline{r}_1} d\underline{r}_1 + \int F(\underline{r}_1, \underline{k}_{r_2}, \beta) e^{i \underline{k}_{r_2} \cdot \underline{r}_2} d\underline{r}_2 \right\} \quad (4.45)$$

which maintains the symmetry character of  $M_4$  with respect to  $\underline{r}_1$ ,  $\underline{r}_2$ . (cf. Tatarskii, 1)

#### IV. The Boundary Conditions and Steady State Solution for Plane Wave Case

We note that when the pairs of point  $(\underline{\rho}_1, \underline{\rho}_2')$  and  $(\underline{\rho}_1', \underline{\rho}_2)$  move an infinite distance apart. It is obvious that the fields corresponding to these pairs of points become statistically independent, thus one has

at  $|r_2| \rightarrow \infty$

$$\begin{aligned}
 M_4(\underline{r}_1, \underline{r}_2, \underline{z}) &= \langle \hat{\psi}(\underline{z}, \underline{r}_1) \hat{\psi}^*(\underline{z}, \underline{r}_2') \rangle \langle \hat{\psi}(\underline{z}, \underline{r}_2) \hat{\psi}^*(\underline{z}, \underline{r}_1') \rangle \\
 &= M_2(\underline{z}, \underline{r}_1) M_2^*(\underline{z}, \underline{r}_1) \\
 &= |M_2(\underline{z}, \underline{r}_1)|^2
 \end{aligned}
 \tag{4.46}$$

similarly, we have

at  $|r_1| \rightarrow \infty$

$$M_4(\underline{r}_1, \underline{r}_2, \underline{z}) = |M_2(\underline{z}, \underline{r}_2)|^2
 \tag{4.47}$$

we now consider the properties of the function  $f(\underline{r}_1, \underline{r}_2, z)$  in equation (4.34). One observes that  $f(\underline{r}_1, \underline{r}_2, z)$  is positive everywhere except at  $\underline{r}_1 = 0$  or  $\underline{r}_2 = 0$ ,  $f(\underline{r}_1, \underline{r}_2) = 0$ . We therefore consider the term  $k_0^2/4 f(\underline{r}_1, \underline{r}_2, z)$  as a decaying term which tends to make the function  $M_4$  decay, while the 2nd term in equation (4.33) is a diffraction term which will diffuse the value of  $M_4$  among the transverse coordinates. With the diffraction term only, equation (4.33) can be written as

$$\frac{\partial M_4}{\partial \underline{z}} - i \frac{\partial}{\partial \underline{r}_1} \frac{\partial}{\partial \underline{r}_2} M_4 = 0
 \tag{4.48}$$

the solution of (4.48) can be written as

$$M_4(\underline{r}_1, \underline{r}_2, \underline{z}) = \frac{1}{(2\pi \underline{z})^2} \int M_4(\underline{r}'_1, \underline{r}'_2, 0) e^{\frac{-i(\underline{r}_1 - \underline{r}'_1)(\underline{r}_2 - \underline{r}'_2)}{\underline{z}}} d\underline{r}'_1 d\underline{r}'_2 \quad (4.49)$$

Thus at  $z > 0$  the value of  $M_4$  will be redistributed as described by the above equation.

One also observes that due to the decay term,  $M_4$  will decay to zero when  $z \gg 1$  for all  $\underline{r}_1$  and  $\underline{r}_2$  except near  $\underline{r}_1 = 0, \underline{r}_2 = 0$ . However, because of the diffraction term the value of  $M_4$  near  $\underline{r}_1 = 0$  or  $\underline{r}_2 = 0$  will be redistributed to all other points  $(\underline{r}_1, \underline{r}_2)$  where  $f(\underline{r}_1, \underline{r}_2) = 0$ . Therefore one observes that  $M_4$  will decay to zero for large distance  $z$  unless  $M_4$  is of the form (cf. Lee and Jokipii, 68,69.)

$$M_4(\underline{r}_1, \underline{r}_2, \underline{z}) = m_1(\underline{z}, \underline{r}_1) + m_2(\underline{z}, \underline{r}_2) + m_3(\underline{z}) \quad (4.50)$$

For this range the diffraction term is zero and  $M_4$  will reach an asymptotic solution. In order to satisfy the boundary conditions in equation (4.47), we must have

at  $|\underline{r}_1| \rightarrow \infty$

$$M_4 = |M_2(\underline{r}_2, \underline{z})|^2 = m_1(\underline{z}, \infty) + m_2(\underline{z}, \underline{r}_2) + m_3(\underline{z}) \quad (4.51)$$

therefore

$$\begin{aligned} M_4 &= m_1(\beta, \underline{r}_1) + |M_2(\beta, \underline{r}_2)|^2 - m_1(\beta, \infty) \\ &\quad - m_3(\beta) + m_3(\beta) \\ &= m_1(\beta, \underline{r}_1) + |M_2(\beta, \underline{r}_2)|^2 - m_1(\beta, \infty) \end{aligned} \quad (4.52)$$

at  $|\underline{r}_2| \rightarrow \infty$

$$\begin{aligned} M_4 &= |M_2(\beta, \underline{r}_1)|^2 = m_1(\beta, \underline{r}_1) + m_2(\beta, \infty) \\ &\quad + m_3(\beta) \end{aligned} \quad (4.53)$$

therefore

$$\begin{aligned} m_1(\beta, \underline{r}_1) &= |M_2(\beta, \underline{r}_1)|^2 - m_2(\beta, \infty) - m_3(\beta) \\ m_1(\beta, \infty) &= |M_2(\beta, \infty)|^2 - m_2(\beta, \infty) - m_3(\beta) \end{aligned} \quad (4.54)$$

Substituting (4.54) into (4.52), one obtains

$$\begin{aligned} M_4(\beta \gg 1) &= |M_2(\beta, \underline{r}_1)|^2 + |M_2(\beta, \underline{r}_2)|^2 \\ &\quad - |M_2(\beta, \infty)|^2 \end{aligned} \quad (4.55)$$

For the plane wave case, we obtain the following expression

$$M_4(z \gg 1, \underline{r}_1, \underline{r}_2) = e^{-\frac{k_0^2}{2} [H(\underline{r}_1)] z} + e^{-\frac{k_0^2}{2} [H(\underline{r}_2)] z} e^{-\frac{k_0^2 z}{2} A(0)} \quad (4.56)$$

After the wave leaves the random slab with thickness  $z_1$  and propagates in the free space region, we have the differential equation:

$$\frac{\partial M_4}{\partial z} - \frac{i}{k_0} \nabla_{\underline{r}_1} \cdot \nabla_{\underline{r}_2} M_4 = 0 \quad (4.57)$$

the boundary conditions for  $M_4$  are given by equations (4.46). However,  $M_2$  appearing in equation (4.46) now takes the form

$$M_2(z, \underline{r}) = M_2(z_1, \underline{r}) e^{-\frac{k_0^2 z_1}{2} [A(0) - A(\underline{r})]} \quad (4.58)$$

since in free space  $M_2(z, \underline{r})$  is unchanged.

The solution of (4.57) can be written immediately in terms of the value of  $M_4(z, \underline{r}_1, \underline{r}_2)$ :

$$M_4(\underline{r}_1, \underline{r}_2, \bar{z}) = \left(\frac{k_0}{2\pi\bar{z}}\right)^2 \int M_4(\underline{r}_1', \underline{r}_2', \bar{z}) \times e^{-i\frac{k_0}{\bar{z}}(\underline{r}_1 - \underline{r}_1')(\underline{r}_2 - \underline{r}_2')} d\underline{r}_1' d\underline{r}_2' \quad (4.59)$$

for  $z > 0$ , the value of  $M_4$  is redistributed among the transverse coordinates until it reaches a steady state, if such exists. One finds that at steady state,  $M_4$  obeys

$$M_4 = |M_2(\bar{z}_1, \underline{r}_1)|^2 + |M_2(\bar{z}_1, \underline{r}_2)|^2 - |M_2(\bar{z}_1, \infty)|^2 \quad (4.60)$$

#### V. Numerical Solution for $M_4$ in Plane Wave Case

The general solution of  $M_4$  is too complicated for computation. In order to simplify the problem and still keep the main features of the solution, we shall take the four points  $\underline{r}_1, \underline{r}_2, \underline{r}_1', \underline{r}_2'$  on the  $z = \text{constant}$  plane along a straight line such that  $\underline{r}_1$  and  $\underline{r}_2$  in equation (4.33) become scalar. Introducing the dimensionless variables

$$\bar{\bar{z}} = \frac{\bar{z}}{k_0 l^2}, \quad \bar{r}_1 = \frac{r_1}{l}, \quad \bar{r}_2 = \frac{r_2}{l} \quad (4.61)$$

where  $l$  is a parameter related to the scale size of the irregularities. When written in terms of these variables, eq.(4.33) becomes

$$\left\{ \frac{\partial}{\partial \bar{z}} - i \frac{\partial}{\partial \bar{r}_1} \frac{\partial}{\partial \bar{r}_2} + \frac{1}{4} k_0^3 l^2 A(0) \bar{f} \right\} \bar{M}_4 = 0 \quad (4.62)$$

where

$$\begin{aligned} \bar{f}(\bar{r}_1, \bar{r}_2) = 2 - \frac{1}{A(0)} \left[ 2A(\bar{r}_1) + 2A(\bar{r}_2) - A(\bar{r}_1 + \bar{r}_2) \right. \\ \left. - A(\bar{r}_1 - \bar{r}_2) \right] \end{aligned} \quad (4.63)$$

one observes that  $\gamma = \frac{1}{4} k_0^3 l^2 A(0)$  is a dimensionless quantity. For convenience, we shall drop all the "bars" and rewrite (4.62) as

$$\left\{ \frac{\partial}{\partial z} - i \frac{\partial}{\partial r_1} \frac{\partial}{\partial r_2} + \gamma f(r_1, r_2) \right\} M_4(r_1, r_2, z) = 0 \quad (4.64)$$

Since  $M_4$  is a complex field, it is convenient to divide it into real and imaginary components by writing  $M_4 = M_R + iM_I$ . One obtains two coupled partially differential equations

$$\frac{\partial M_R}{\partial z} = - \frac{\partial}{\partial r_1} \frac{\partial}{\partial r_2} M_i - \gamma f M_R$$

$$\frac{\partial M_i}{\partial z} = \frac{\partial}{\partial r_1} \frac{\partial}{\partial r_2} M_R - \gamma f M_i \quad (4.65)$$

To obtain a unique solution of eq. (4.65), one must specify the boundary condition at  $z = 0$  and the boundary conditions given by equation (4.46), (4.47). In practice, we cannot apply the boundary conditions at  $r_1, r_2 \rightarrow \infty$  because this would require an infinite number of mesh points. One can simply truncate at appropriately large values of  $r_1, r_2$ . The numerical scheme used will be presented in Appendix (VI).

The solution of eq. (4.65) is dependent on the choice of power spectrum  $\Phi(k)$ . A simple and very commonly used form is the Gaussian

$$\Phi(k) = \frac{\langle \tilde{\epsilon}^2 \rangle}{\pi^{3/2} k_l^3} e^{-\frac{k^2}{k_l^2}} \equiv \alpha_0 e^{-\frac{k^2}{k_l^2}} \quad (4.66)$$

then

$$A(0) - A(\rho) = 2\pi^2 \alpha_0 k_l^2 \left[ 1 - e^{-\frac{k_l^2 \rho^2}{4}} \right] \quad (4.67)$$

and

$$A(0) = 2\sqrt{\pi} k_l^{-1} \langle \tilde{\epsilon}^2 \rangle \quad (4.68)$$

however, in situ measurements indicate a more realistic form is given by the modified power law spectrum defined through

$$\Phi(k) = \frac{\langle \tilde{\epsilon}^2 \rangle \Gamma(\frac{p}{2})}{\pi^{3/2} \Gamma(\frac{p-3}{2})} \frac{L_o^3 e^{-\frac{k^2}{k_m^2}}}{(1 + \frac{k^2}{k_{L_o}^2})^{p/2}} \quad (4.69)$$

with  $k_{L_o} \ll k_m$ . This spectrum is flat for  $k < k_{L_o}$ , is a power law with index  $-p$  for  $k_{L_o} < k < k_m$ , and is exponentially decay for  $k > k_m$ .  $L_o = 1/k_{L_o}$  is the outer scale and  $l_o = 1/k_m$  is the inner scale of the irregularities. In the ionosphere case, usually  $2 < p < 4$  and  $p = 11/3$  corresponds to the modified Kolmogorov spectrum (Von-Karman Spectrum).

For the Kolmogorov spectrum, the power spectrum can be written as

$$\Phi(k) = 0.033 C_n^2 L_o^{1/3} (1 + k^2 L_o^2)^{-11/6} e^{-\frac{k^2}{k_m^2}} \quad (4.70)$$

with

$$C_n^2 = 1.9 \langle \tilde{\epsilon}^2 \rangle L_o^{-2/3}$$

if  $L_0 \gg 1$ , one obtains

$$H(\rho) = A(0) - A(\rho) \\ \cong 0.395 \langle \tilde{\epsilon}^2 \rangle L_0 \left[ 1 - \frac{5}{3} \frac{\rho^{5/6} K_{5/6}(\rho)}{2^{5/6} \Gamma(1/6)} \right] \quad (4.71)$$

$$A(0) \cong 0.395 \langle \tilde{\epsilon}^2 \rangle L_0 \quad (4.72)$$

where  $K_{5/6}$  denotes a modified Bessel function of the second kind.

If we choose,  $L_0 = 1 = 300\text{m}$ , and  $\langle \tilde{\epsilon}^2 \rangle = \left(\frac{f_p}{f}\right)^4 \langle \left(\frac{\tilde{N}}{N_0}\right)^2 \rangle \cong \left(\frac{f_p}{f}\right)^4 (0.1)$ , the value of  $\beta = k_0^3 L_0^3 \langle \tilde{\epsilon}^2 \rangle$  ranges from about 8.5 for  $f/f_p = 100$  to about 86.5 for  $f/f_p = 10$ . The value of  $\gamma$  in eq. (4.65) is equal to  $0.0987 \beta$  for the Von Karman spectrum,  $0.16 \beta$  for the power law spectrum with  $p = 4$ , and  $0.2821 \beta$  for the Gaussian spectrum.

We shall adopt the power spectrum given by equation (4.69) with  $p = 4$  and present a numerical solution for the fourth moment. The value of  $\gamma = \frac{1}{2} k_0^3 L_0^3 A(0)$  has been chosen to be 3.5. Fig.41 depicts the normalized function  $f(r_1, r_2)$ , defined by equation (4.63), as a function of  $r_1, r_2$ . One recalls that  $f(r_1, r_2)$  represents a decaying factor which is positive everywhere and equal to zero when  $r_1$  and/or  $r_2 = 0$ . The initial field  $M_4(r_1, r_2, 0) = 1$  is not shown in the figures. The evolution of the 4th moment at  $z = 0.1125, 0.1725$  and  $0.24$  is shown

VON KARMANN SPECTRUM F(R1,R2)

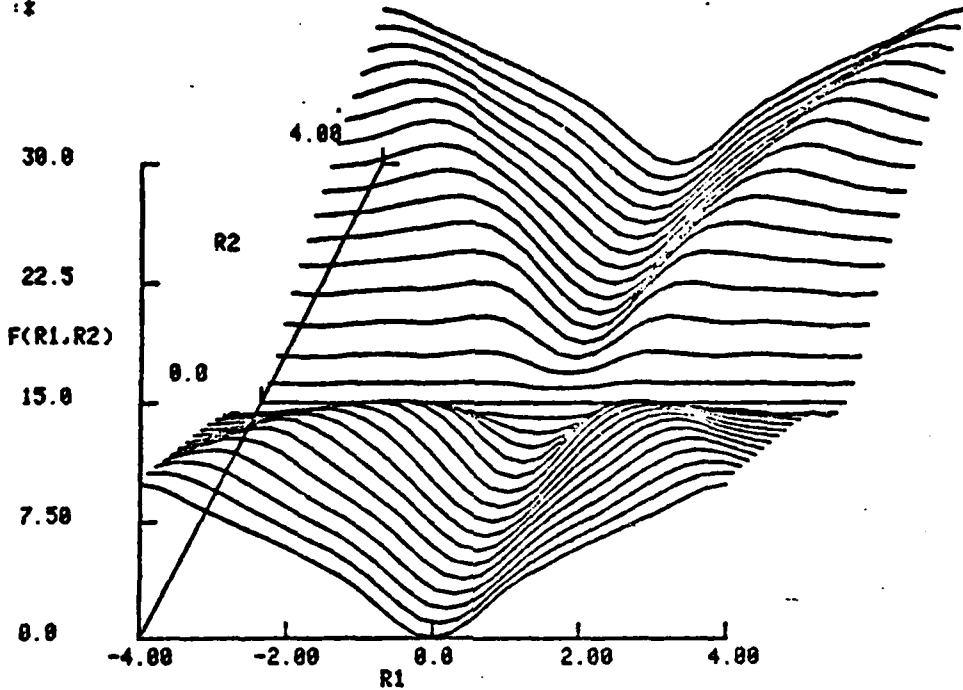


Fig. 41.  $f(r_1, r_2)$  vs.  $r_1$  and  $r_2$ ; Power spectrum with  $p = 4$ .

Z= 1.1250E-01 GAMMA= 3.5000 \*

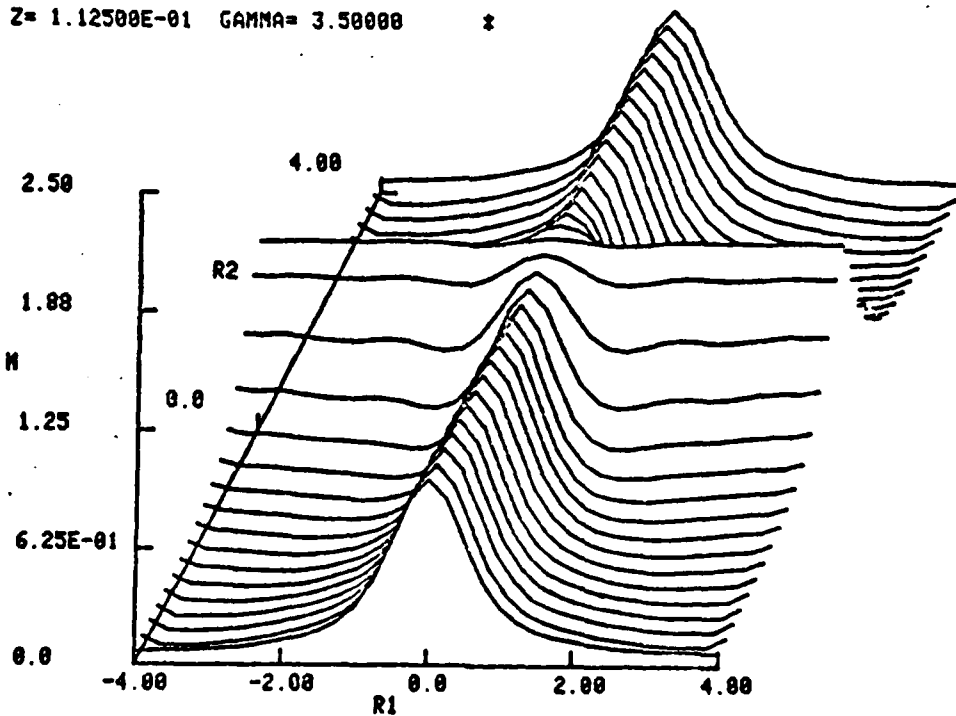


Fig. 42.  $M_4(r_1, r_2, z)$  vs.  $r_1$  and  $r_2$  at  $z = 0.1125$ ; a plane wave propagating in a random medium with a power law spectrum,  $p = 4$ ,  $\gamma = 3.5$ .

Z= 1.72300E-01 GAMMA= 3.50000 \*

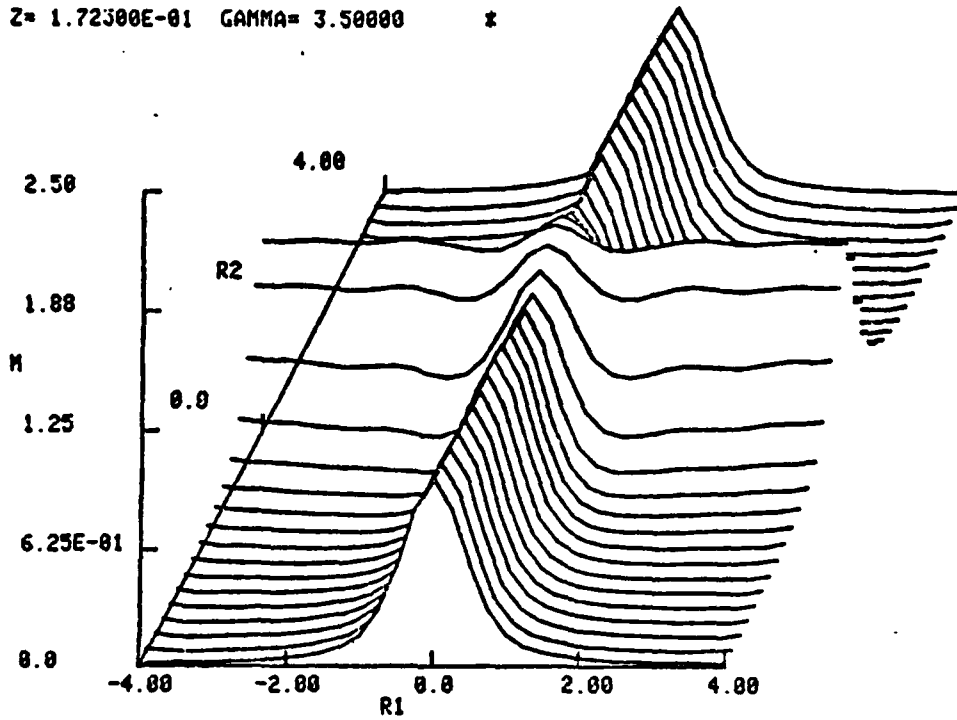


Fig. 43.  $M_4$  vs.  $r_1$  and  $r_2$  at  $z = 0.1725$ .

Z= 2.40000E-01 GAMMA= 3.50000 \*

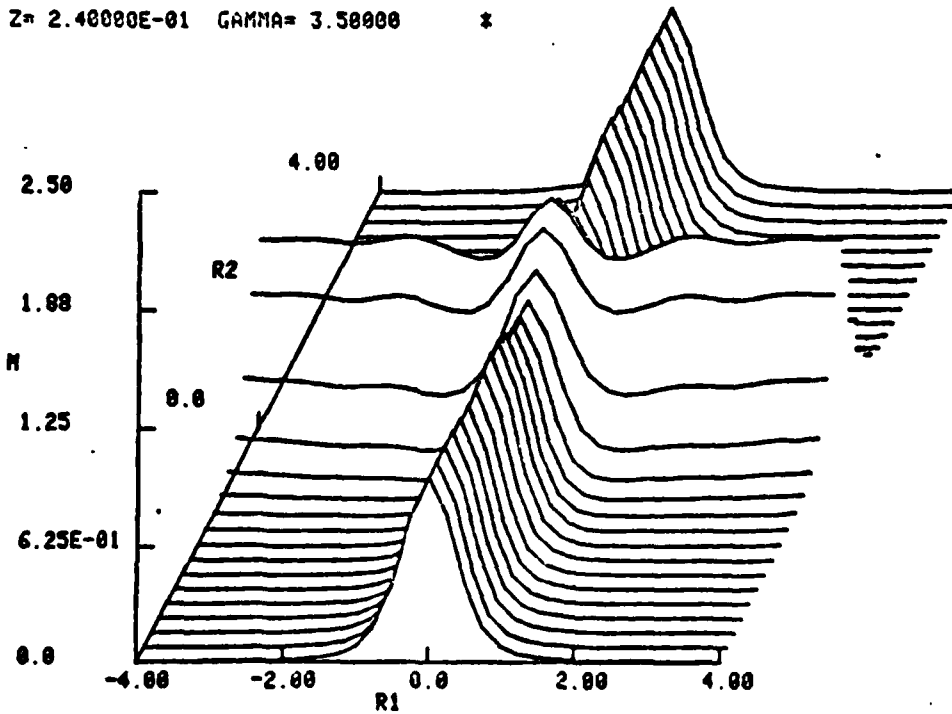


Fig. 44.  $M_4$  vs.  $r_1$  and  $r_2$  at  $z = 0.24$ .

in Fig.42 - Fig.44. One observes that the field decays everywhere except near the neighborhood of  $r_1$  and/or  $r_2 = 0$ . The redistribution phenomena, caused by the 2nd term (diffraction term) in equation (4.64), forces the points near  $r_1$  and/or  $r_2 = 0$  "move" to the decaying region. Therefore, if the evolution continues to a large distance, the final field will tend to reach a steady state as shown by equation (4.55). However, we are not interested in very large distance propagation in this paper. The extent of the normalized random slab will be chosen such that  $L = 0.24$  and the solution will be evaluated at  $z = z'$ , whence the wave will continue to propagate from the bottom of the slab to the ground. Fig.45-48 depict the free space propagation at  $z = 0.4275, 0.6525, 0.8775$  and  $1.1025$ . The diffraction effect, resulting from the interference of the distorted wave front, tends to focus and defocus the field. This focusing and defocusing phenomena will only occur for a strong turbulence case, which will be shown clearer in the next chapter.

## VI. Discussion and Conclusion

The 4 point slow quasiparticle distribution function, defined as the 6 dimensional Fourier transform of the 4 point correlation function w.r.t. the slow coordinates  $R$  and  $r_1$ , is used to obtain the 4 point wave statistics. Pictures of the slow q.p. flow are essentially the same as those in the 2 point correlation case except we are now dealing with a four dimensional phase space  $k_R, R, k_{r_1}, r_1$ . An individual slow q.p. moves along the trajectory defined by eq. (4.13) with "momentum"  $k_R$  in the  $\rho$  direction and  $k_{r_1}$  in the  $r_2$  direction. The structure function is, in general, dependent not only on the "coordinates"  $\rho$  and  $r_2$  but also dependent on the

Z= 4.27500E-01 GAMMA= 0.0

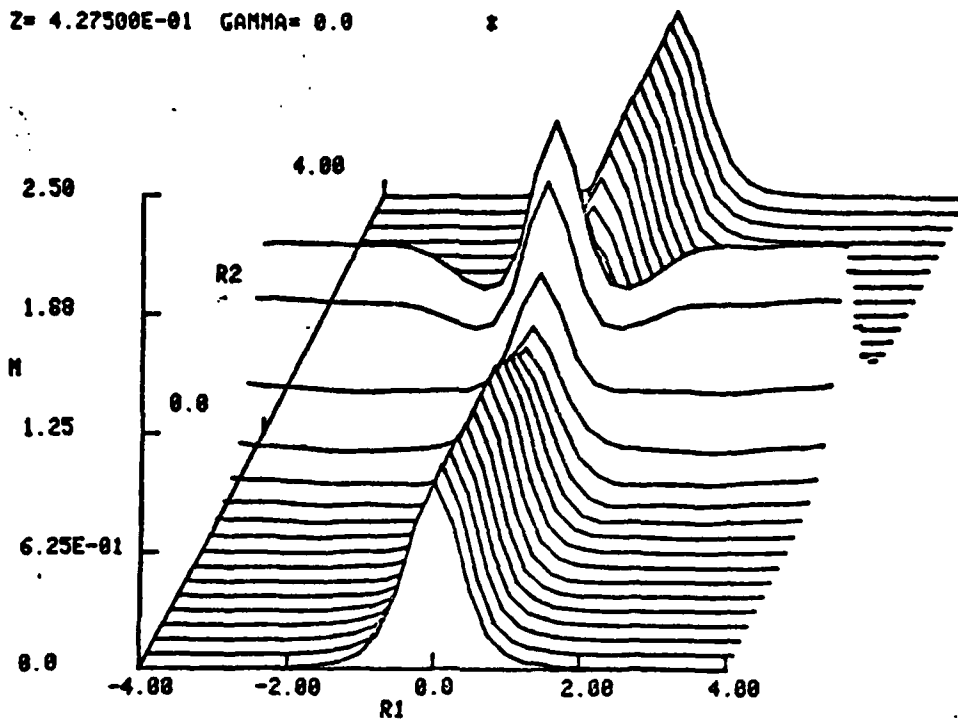


Fig. 45.  $M_4 ( r_1, r_2, z)$  vs.  $r_1$  and  $r_2$  at a distance  $z = 0.4275$  from the bottom of the slab;  $L = 0.24$ .

Z= 6.52500E-01 GAMMA= 0.0

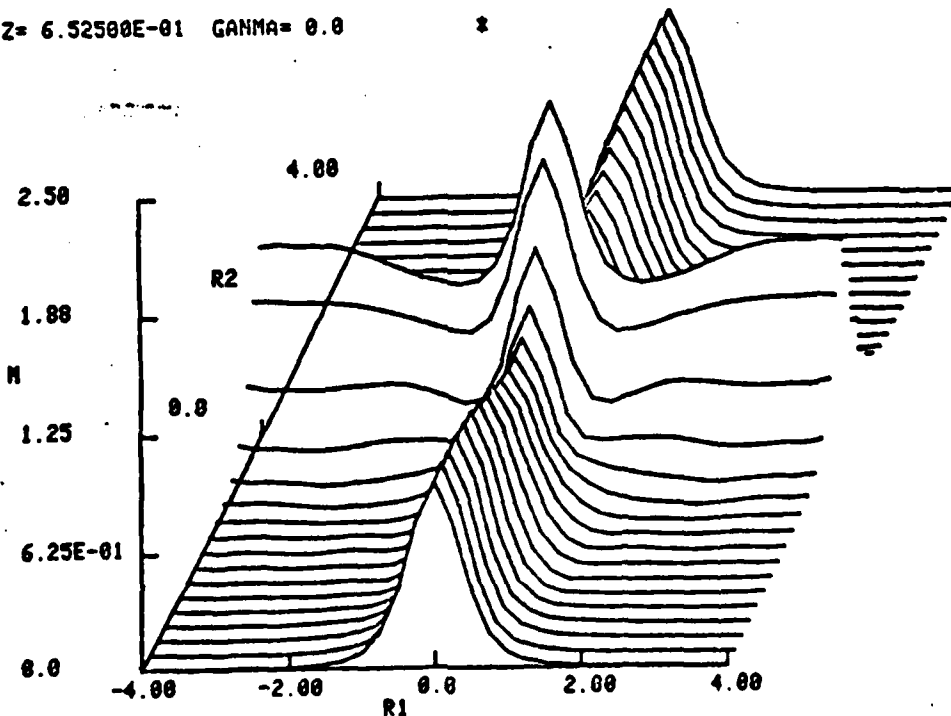


Fig. 46.  $M_4$  vs.  $r_1$  and  $r_2$  at a distance  $z = 0.6525$  from the bottom of the slab.

Z = 8.7750E-01 GAMMA = 0.0

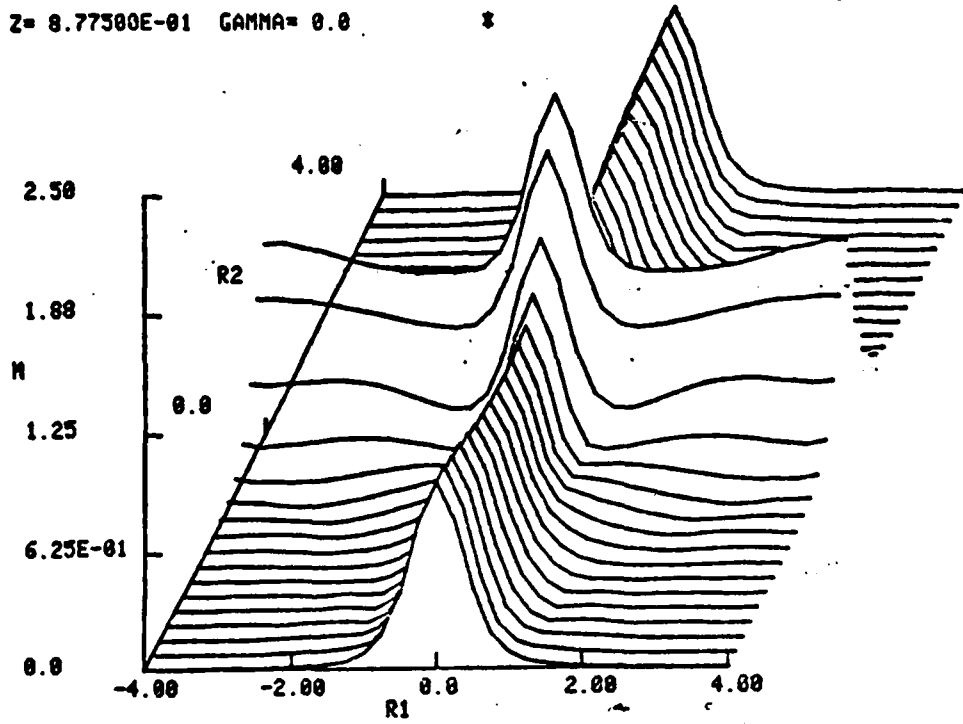


Fig. 47.  $M_4$  vs.  $r_1$  and  $r_2$  at  $z = 0.8775$  from the bottom of the slab.

Z = 1.10259 GAMMA = 0.0

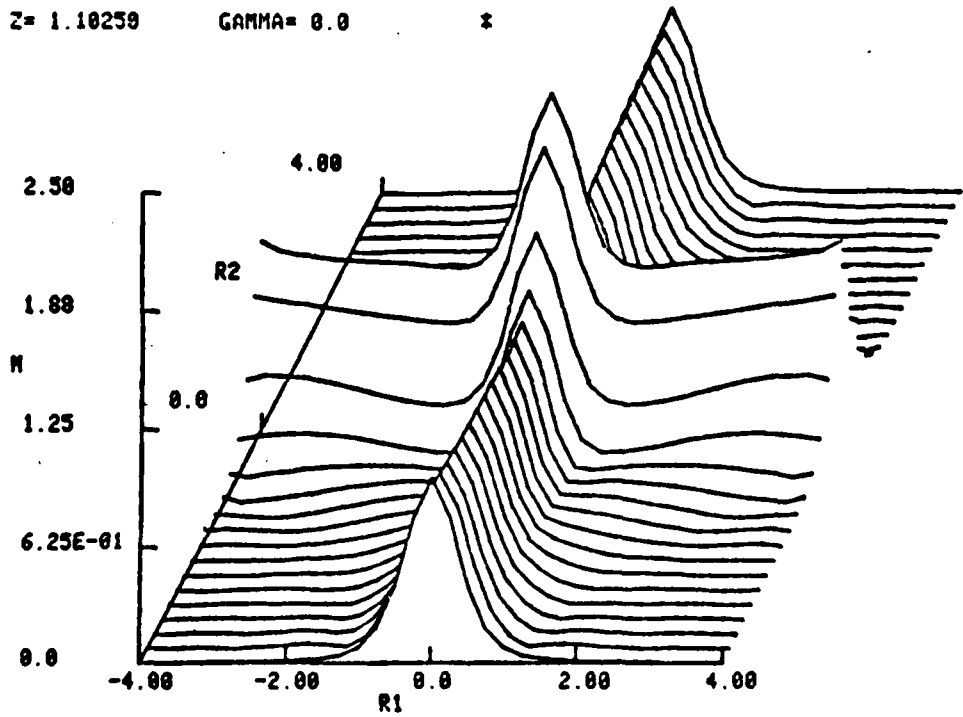


Fig. 48.  $M_4$  vs.  $r_1$  and  $r_2$  at a distance  $z = 1.1025$  from the bottom of the slab.

"coordinate"  $r_i$  associate with the "momentum"  $k_{r_i}$ . For the special case,  $H(\xi) = a \xi^2$ , one finds that the structure function is dependent only on  $\rho$ , and of the form  $f(r_1, r_2, \rho) = a \rho^2$ .

Knowledge of the S function will provide all of the 4 point field statistics. For example, the second moment of the field intensity can be obtained as follows:

$$\langle \hat{I}^2 \rangle = M_4(0,0,0,0,\beta) = \int S(k_R, 0, k_{r_1}, 0, \beta) \frac{dk_R dk_{r_1}}{(2\pi)^2} \quad (4.73)$$

Therefore, the second moment of the intensity can be viewed as the total number of slow q.p.'s located at  $R = r_1 = r_2 = \rho = 0$ .

The 2 point correlation function of the intensity at  $R = 0$  can be obtained as follows:

$$\begin{aligned} \langle \hat{I}(x_1) \hat{I}(x_2) \rangle &= M_4(0,0,r_1,0,\beta) \\ &= \int S(k_R, 0, k_{r_1}, 0, \beta) e^{i k_{r_1} r_1} \frac{dk_R dk_{r_1}}{(2\pi)^2} \quad (4.74) \end{aligned}$$

One notes that when  $\rho = r_2 = R = 0$ , then  $r_1 = x_1 - x_2 = x_1' - x_2'$ .

The Scintillation Index  $S_4$ , defined as the normalized

variance of intensity, i.e.  $S_4 = \langle \hat{I}^2 \rangle - \langle \hat{I} \rangle^2 / \langle \hat{I} \rangle^2$ , can then be obtained from the S function using eqs. (4.73) and (4.74). As an illustration, we shall calculate the 1st and 2nd moments of intensity and the associated  $S_4$  for the case  $H(\xi) = a\xi^2$ , using the S function. Fig. 49 and 50 depict  $\langle \hat{I} \rangle$ ,  $\langle \hat{I}^2 \rangle$  and the corresponding  $S_4$  for a collimated beam propagating in a random medium characterized by  $H(\xi) = a\xi^2$  with  $a = 1$  and  $a = 5$  respectively. (In the following figures, curve 1 stands for  $\langle \hat{I} \rangle$ , curve 2 for  $\langle \hat{I}^2 \rangle$  and curve 3 for  $S_4$ .) One observes that both  $\langle \hat{I} \rangle$  and  $\langle \hat{I}^2 \rangle$  decrease as  $z$  increases, while the scintillation index increases monotonically with  $z$ . The case of a focused beam propagating in a random medium is represented in Figs. 51, 52 with  $\alpha_r = \alpha_i = 1$ ,  $a = 1$  and  $5$  respectively. Focusing and defocusing effects in  $\langle \hat{I} \rangle$  and  $\langle \hat{I}^2 \rangle$  are clearly revealed in these figures. The scintillation index is greater in the case of collimated beams in the range  $z < 2$ , approximately; for  $z \geq 2$ , focused beams display a smaller scintillation index than the collimated beams. One thus concludes that for short distance propagation, a collimated beam is to be preferred while a focused beam is preferable for long distance wave propagation in a random medium.

In ionospheric propagation, we are interested in finding the received signal intensity and its associated  $S_4$  at ground level. A deterministic wave signal is randomly modified by the ionosphere and when the resulting modulated wave front enters the free space, between a random ionospheric slab and the ground, diffraction modifies the wave statistics. In order to show this effect we present results for  $\langle \hat{I} \rangle$ ,  $\langle \hat{I}^2 \rangle$  and  $S_4$ . Figs. 53 and 54 depict the case  $\alpha_r = 1$ ,  $a = 5$  with the thickness of the random slab being  $L = 0.25$  for collimated beams and focused beams respectively. One observes that the focused beam displays saturation at  $z \approx 0.75$ , where  $z$  measures the dis-

1ST AND 2ND MOMENT OF I FOR  $H(XI)=A(XI)^{-2}$   
 $\alpha_r = 1.00000$   $\alpha_l = 0.0$   $\text{GAMMA} = 1.00000$

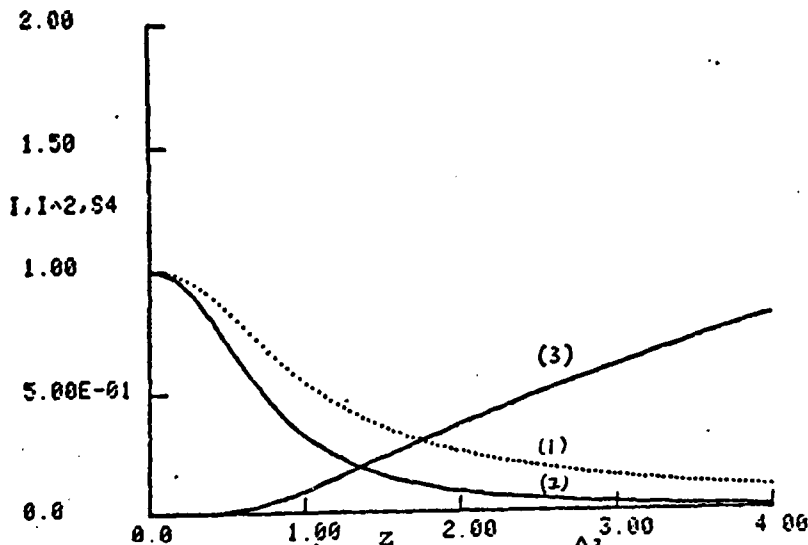


Fig. 49. (1)  $\langle \hat{I} \rangle$  vs.  $z$ ; (2)  $\langle \hat{I}^2 \rangle$  vs.  $z$ ; (3)  $S_4$  vs.  $z$ ;  
 a collimated beam propagating in a random medium,  
 $H(\xi) = a \xi^{-2}$ ,  $a = 1$ ,  $\alpha_r = 1$ .

1ST AND 2ND MOMENT OF I FOR  $H(XI)=A(XI)^{-2}$   
 $\alpha_r = 1.00000$   $\alpha_l = 0.0$   $\text{GAMMA} = 5.00000$

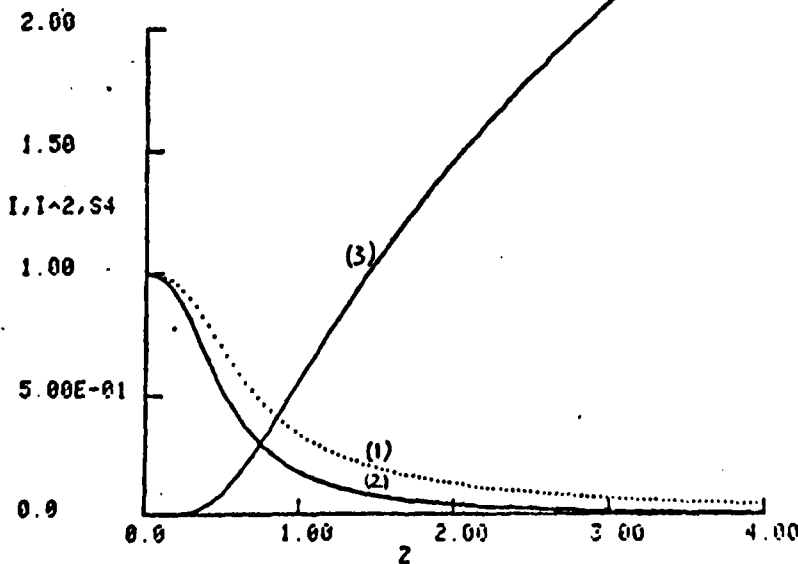


Fig. 50. same as Fig. 49. except  $a = 5$ .

1ST AND 2ND MOMENT OF I FOR  $H(\xi) = a\xi^2$   
 $\alpha_r = 1.00000$      $\alpha_l = 1.00000$      $\text{GAMMA} = 1.00000$

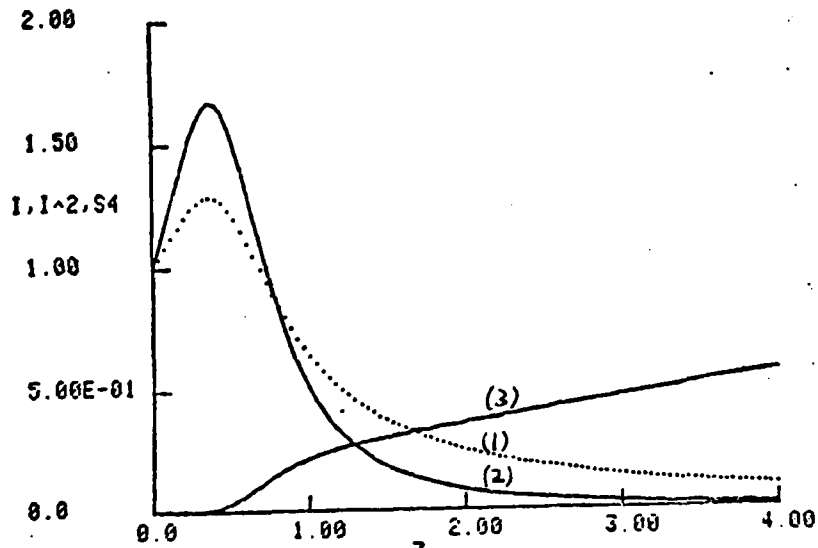


Fig. 51. (1)  $\langle \hat{I} \rangle$  vs.  $z$ ; (2)  $\langle \hat{I}^2 \rangle$  vs.  $z$ ; (3)  $S_4$  vs.  $z$ ; a focused beam propagating in a random medium,  $H(\xi) = a\xi^2$ ,  $a = 1$ ,  $\alpha_r = 1$ .

1ST AND 2ND MOMENT OF I FOR  $H(\xi) = a\xi^2$   
 $\alpha_r = 1.00000$      $\alpha_l = 1.00000$      $\text{GAMMA} = 5.00000$

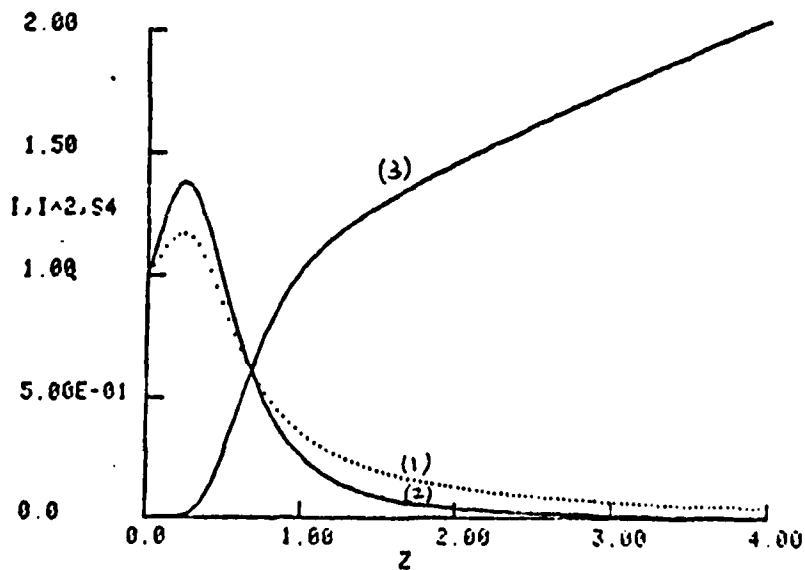


Fig. 52. same as Fig. 51. except  $a = 5$ .

1ST AND 2ND MOMENT OF I FOR  $H(x) = a(x)^2$   
 $\beta = 1.00000$   $\alpha_1 = 0.0$   $\text{GAMMA} = 5.00000$   $\text{SLAB} = 2.50000\text{E-}01$

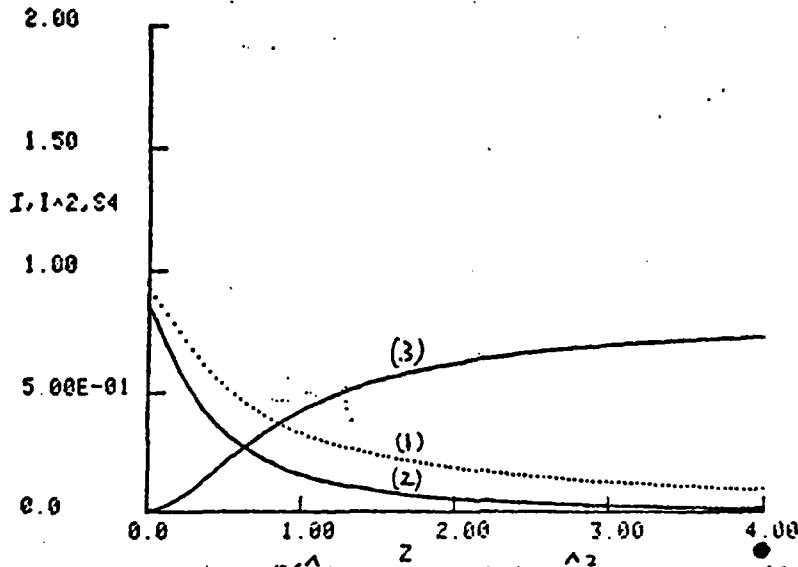


Fig. 53. (1)  $\langle I \rangle$  vs.  $z$ ; (2)  $\langle I^2 \rangle$  vs.  $z$ ; (3)  $S_4$  vs.  $z$ ; a modulated collimated beam propagating in free space;  $L = 0.25$ ,  $a = 5$ ,  $\alpha_r = 1$ .

1ST AND 2ND MOMENT OF I FOR  $H(x) = a(x)^2$   
 $\beta = 1.00000$   $\alpha_1 = 1.00000$   $\text{GAMMA} = 5.00000$   $\text{SLAB} = 2.50000\text{E-}01$

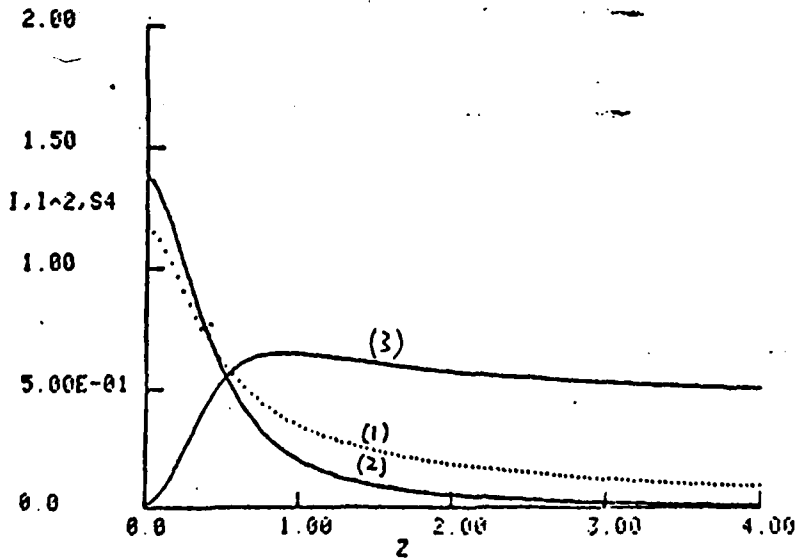


Fig. 54. a focused beam propagating in free space;  $L = 0.25$ ,  $a = 5$ ,  $\alpha_r = \alpha_i = 1$ .

tance from the bottom of the random slab to the receiver. For  $z$  smaller than approximately 1.8, the collimated beam yields a greater  $S_4$  than the focused beam. However, as  $z \approx 1.75$  the focused beam displays a smaller  $S_4$ . Figs. 55 and 56 for  $a = 10$  display the same effects. One obtains a higher scintillation index and observes a saturation at  $z \approx 0.75$  for the focused beam case. It is of interest to plot  $S_4$  vs.  $z$  for different turbulent levels in the ionospheric slab. Figs. 57 and 58 depict  $S_4$  vs  $z$  for  $a = 2$  to 16, in steps of 2, for the collimated beam and the focused beam, respectively. One observes that, for the focused beam,  $S_4$  always saturates at  $z \approx 0.75$ . At  $z \approx 1.75$  the focused beam start to display a higher scintillation index than the collimated beam.

When the slab thickness increases to 0.5, the random wave fields emerging from the bottom of the ionosphere are increasingly more turbulent. The corresponding  $S_4$  in this case is higher than for the case  $L = 0.25$ . Figs. 59-62 depict  $\langle \hat{I} \rangle$ ,  $\langle \hat{I}^2 \rangle$  and  $S_4$  vs.  $z$  for  $a = 5$  and 10 respectively ; one observes that the focused beam saturates at  $z \approx 0.6$  approximately. The focused beam has a smaller  $S_4$  than the collimated beam in the range  $z$  greater than 1.5. The influence of the turbulent strength  $a$  on the scintillation index is shown in Fig. 63 and Fig. 64 for a collimated beam and a focused beam , respectively. The value of  $a$  ranges from 2 to 16 in steps of 2; one notes that at  $z \approx 0.6$  the scintillation index of a focused beam saturates for all values of  $a$ . At a distance  $z \approx 1.5$  the focused beam starts to have a smaller  $S_4$  for all values of  $a$ .

The wave front of the wave emerging from the bottom of the random slab is greatly dependent on slab thickness. As a comparison, we present calculations of  $S_4$  vs.  $z$  for different values of thickness ranging from  $L = 0.125$  to 1 with increments of 0.125 as depicted in Fig. 65 and Fig. 66. One observes that for the focused beam case the saturation distance decreases as

1ST AND 2ND MOMENT OF I FOR  $H(x) = a^2 x^2$   
 $AR = 1.00000$      $AI = 0.0$      $GAMMA = 10.0000$      $SLAB = 2.50000E-01$

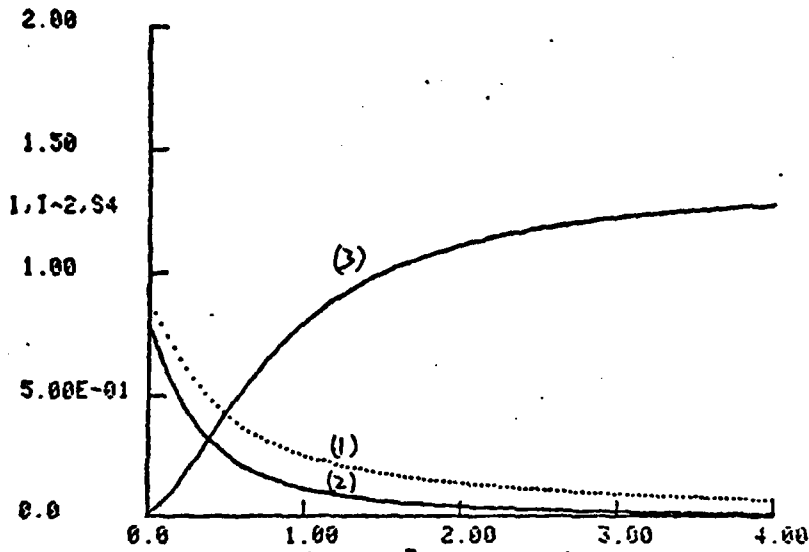


Fig. 55. (1)  $\langle I \rangle$  vs.  $z$  (2)  $\langle I^2 \rangle$  vs.  $z$  (3)  $S_4$  vs.  $z$ ; a modulated collimated beam propagating in free space,  $L = 0.25$ ,  $a = 10$ ,  $\alpha_r = 1$ .

1ST AND 2ND MOMENT OF I FOR  $H(x) = a^2 x^2$   
 $AR = 1.00000$      $AI = 1.00000$      $GAMMA = 10.0000$      $SLAB = 2.50000E-01$

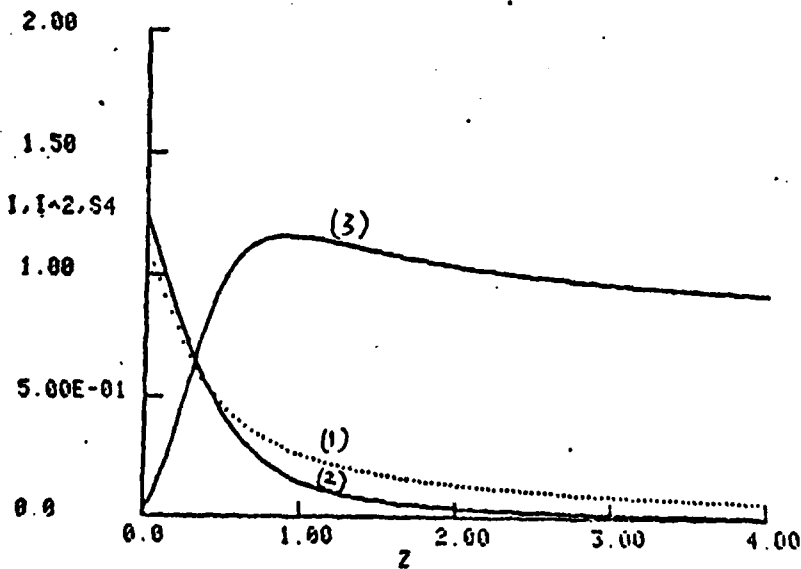


Fig. 56. a modulated focused beam propagating in free space,  $L = 0.25$ ,  $a = 10$ ,  $\alpha_r = \alpha_s = 1$ .

$S_4$  vs.  $z$  FOR  $H(X) = H(X) \sim 2$   
 $AR = 1.00000$   $AI = 0.0$

SLAB = 2.50000E-01

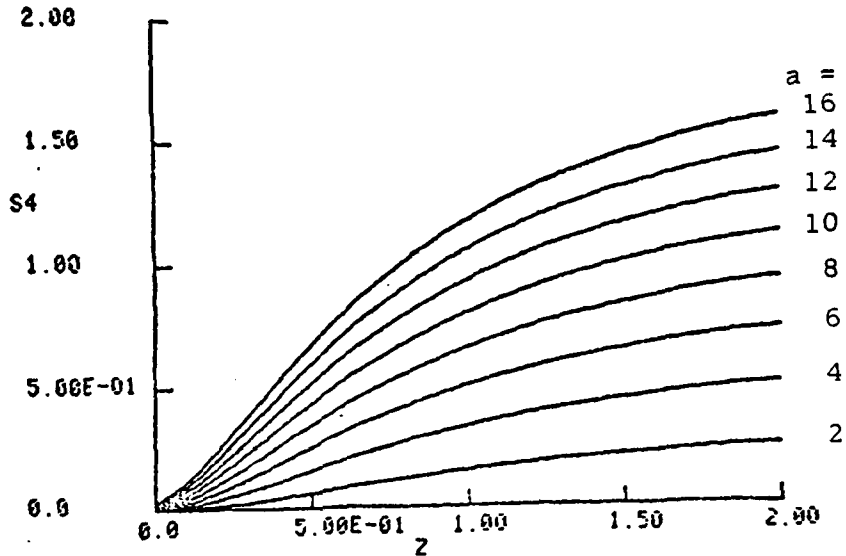


Fig. 57.  $S_4$  vs.  $z$  for  $a = 2$  to 16, in step of 2; a modulated collimated beam propagating in free space,  $L = 0.25$ ,  $\alpha_r = 1$ .

$S_4$  vs.  $z$  FOR  $H(X) = H(X) \sim 2$   
 $AR = 1.00000$   $AI = 1.00000$

SLAB = 2.50000E-01

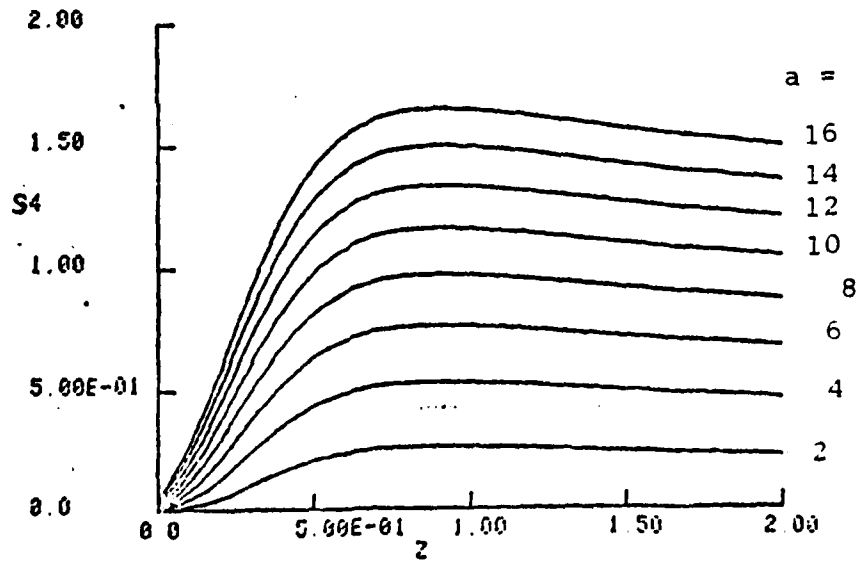


Fig. 58.  $S_4$  vs.  $z$  for  $a = 2$  to 16, in step of 2; a modulated focused beam case.

1ST AND 2ND MOMENT OF I FOR  $H(XI)=A(XI)^2$   
AR= 1.00000 AI= 0.0 GAMMA= 5.00000 SLAB= 5.00000E-01

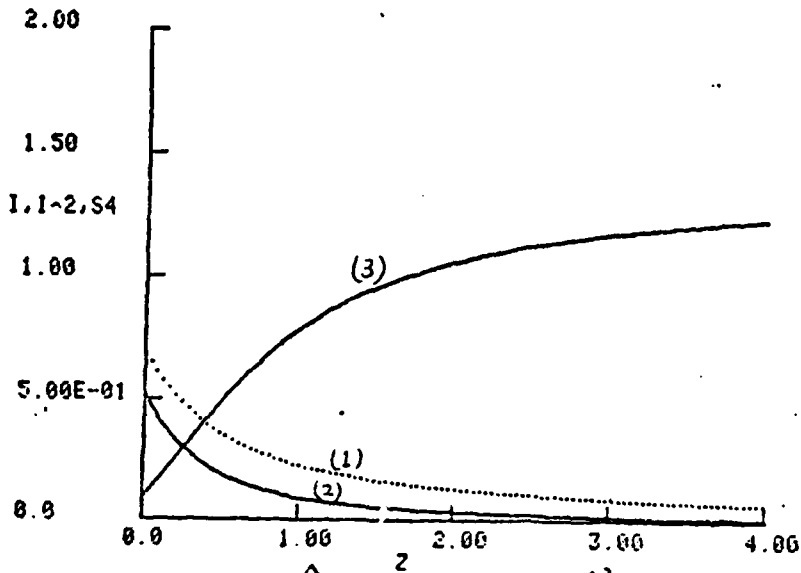


Fig. 59. (1)  $\langle \hat{I} \rangle$  vs. z; (2)  $\langle \hat{I}^2 \rangle$  vs. z; (3)  $S_4$  vs. z; a modulated collimated beam propagating in free space,  $L = 0.5$ ,  $a = 5$ ,  $\alpha_r = 1$ .

1ST AND 2ND MOMENT OF I FOR  $H(XI)=A(XI)^2$   
AR= 1.00000 AI= 1.00000 GAMMA= 5.00000 SLAB= 5.00000E-01

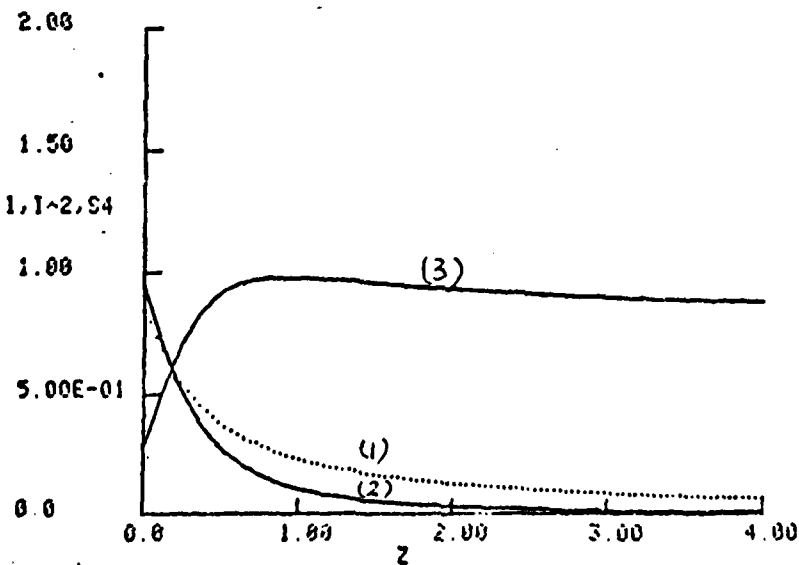


Fig. 60. same as Fig. 59.; a modulated focused beam case.

1ST AND 2ND MOMENT OF I FOR HCNID=ACXID-2  
AR= 1.00000 AI= 0.0 GAMMA= 10.0000 SLAB= 5.00000E-01

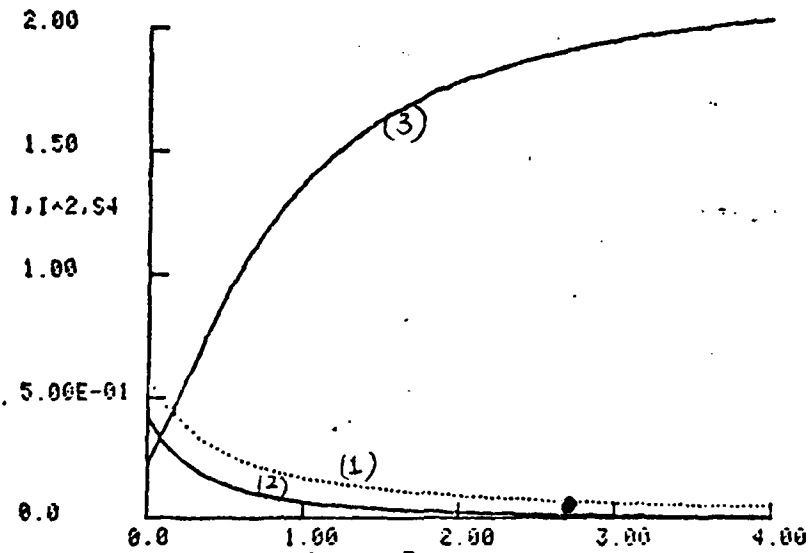


Fig. 61. (1)  $\langle \hat{I} \rangle$  vs.  $z$ ; (2)  $\langle \hat{I} \rangle^2$  vs.  $z$ ; (3)  $S_4$  vs.  $z$ ; a modulated collimated beam propagating in free space,  $L = 0.5$ ,  $a = 10$ ,  $\alpha_r = 1$ .

1ST AND 2ND MOMENT OF I FOR HCNID=ACXID-2  
AR= 1.00000 AI= 1.00000 GAMMA= 10.0000 SLAB= 5.00000E-01

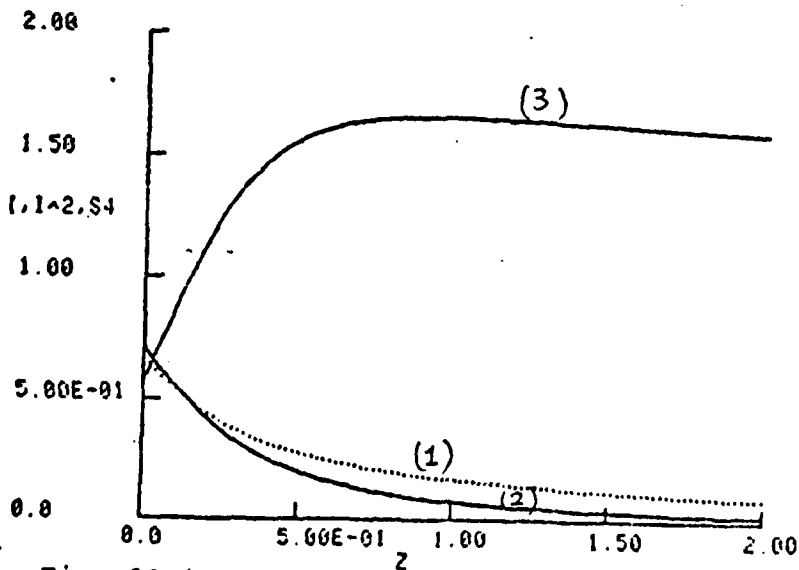


Fig. 62. same as Fig. 61.; a modulated focused beam case.

S4 VS Z FOR HC(XI)=HC(XI)\*2  
AR= 1.00000 AI= 0.0

SLAB= 5.00000E-01

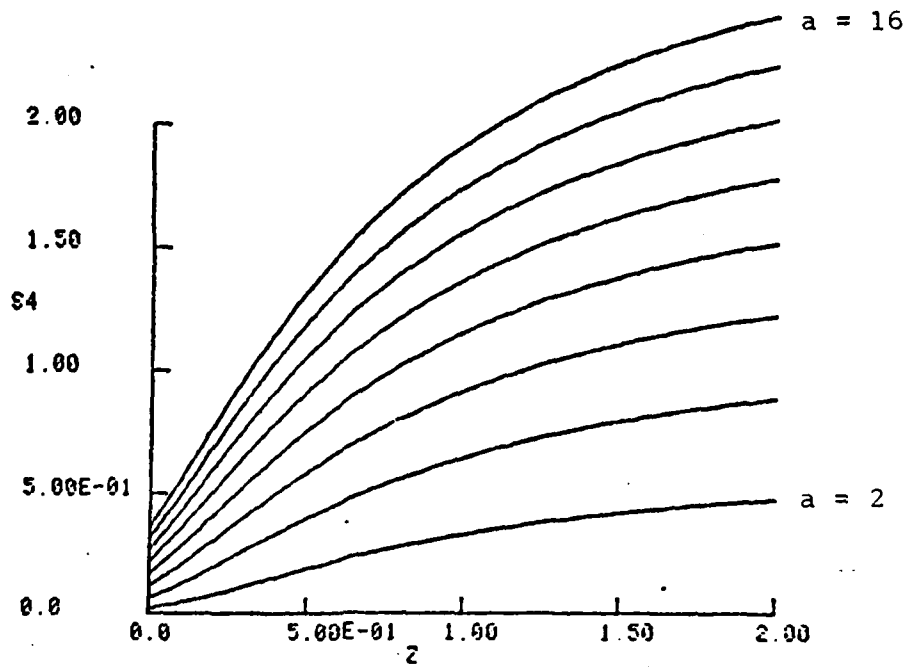


Fig. 63. S4 vs. z for a = 2 to 16, in step of 2; a modulated collimated beam propagating in free space, L = 0.5,  $\alpha_r = 1$ .

S4 VS Z FOR HC(XI)=HC(XI)\*2  
AR= 1.00000 AI= 1.00000

SLAB= 5.00000E-01

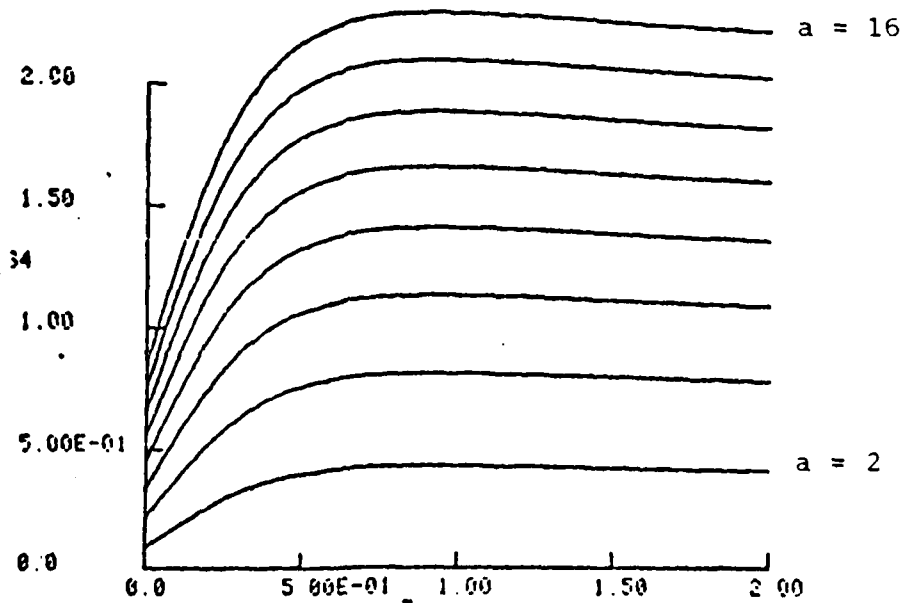


Fig. 64. S4 vs. z for a = 2 to 16, in step of 2; a modulated focused beam propagating in free space, L = 0.5,  $\alpha_r = \alpha_i = 1$ .

L increases. The distance at which the focused beam displays a greater  $S_4$  than the collimated beam decreases as L increases.

The approximate solution for the 4th moment  $M_4$  is presented in Section III. In (4.43), we have replaced the true slow q.p. distribution function  $S(z, r_2, k_r - k')$  on the right in (4.41) by the initial unattenuated q.p. distribution function  $S(0, r_2, k_r - k')$ . It is expected that the solution so obtained will give an exaggerated result for the intensity fluctuation. To illustrate this fact, we shall calculate the scintillation index for the plane wave case and compare it with the exact solution obtained numerically. The random slab will be characterized by a power law spectrum with  $p = 4$ . Fig. 67 depicts the scintillation index calculated from the approximate solution (4.43) for the cases  $L = 0.06, 0.12, 0.24$ . The general behavior of scintillation index agrees with its well known feature. Fig. 68 shows the comparison of the approximate solution (solid line) with the exact solution (dash line). As expected, one observes an overestimated intensity fluctuation in the approximate solution.

Boundary conditions and the steady state solution are discussed in Section 4. We have applied these boundary conditions in the numerical evaluation of the 4th moment as presented in Section 5. The general solution of  $S_4$  is too complicated for computation. In section 5, we computed the solution of  $M_4$  for a special case wherein the 4 points  $x_1, x_1', x_2, x_2'$  lie along a straight line on the  $z = \text{constant}$  plane. The numerical evaluation of  $M_4$ , for a plane wave propagating thru a random slab with  $L = 0.24$  and characterized by a power law spectrum with  $p = 4$ , is presented in Section 5 for  $z = 0.4275, 0.6525, 0.8775$  and  $1.1025$  (Fig. 45-48). One observes that as the field evolution is continuous by extrapolated to a large distance, the final field will tend to reach a steady state as shown by eq. (4.55).

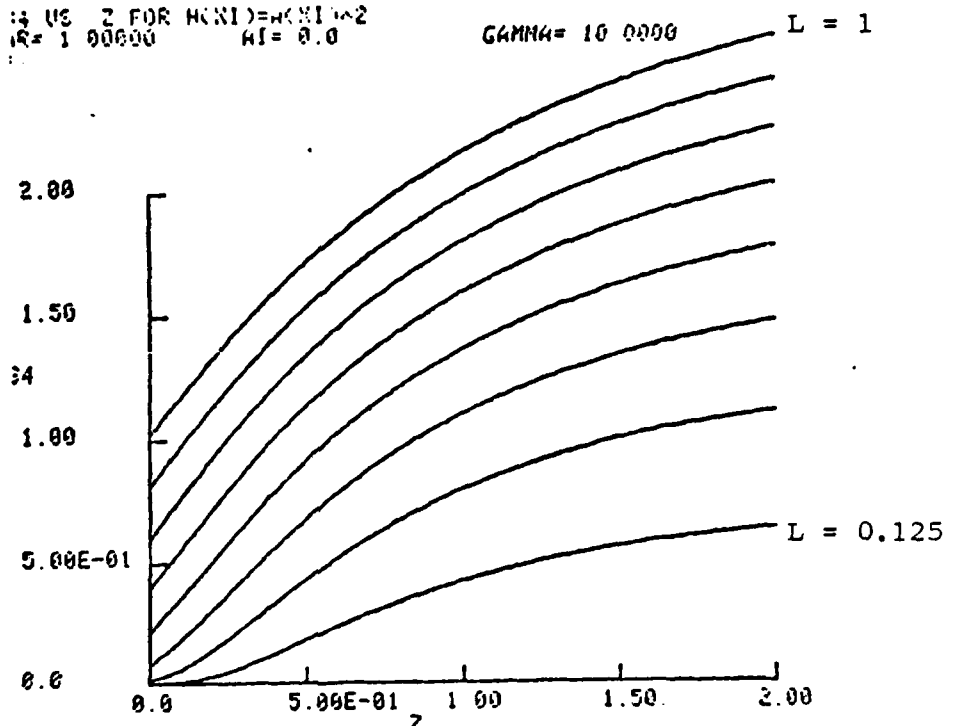


Fig. 65.  $S_4$  vs.  $z$  for  $L = 0.125$  to  $1$ , in step of  $0.125$ ; a modulated collimated beam propagating in free space,  $a = 10$ ,  $\alpha_r = 1$ .

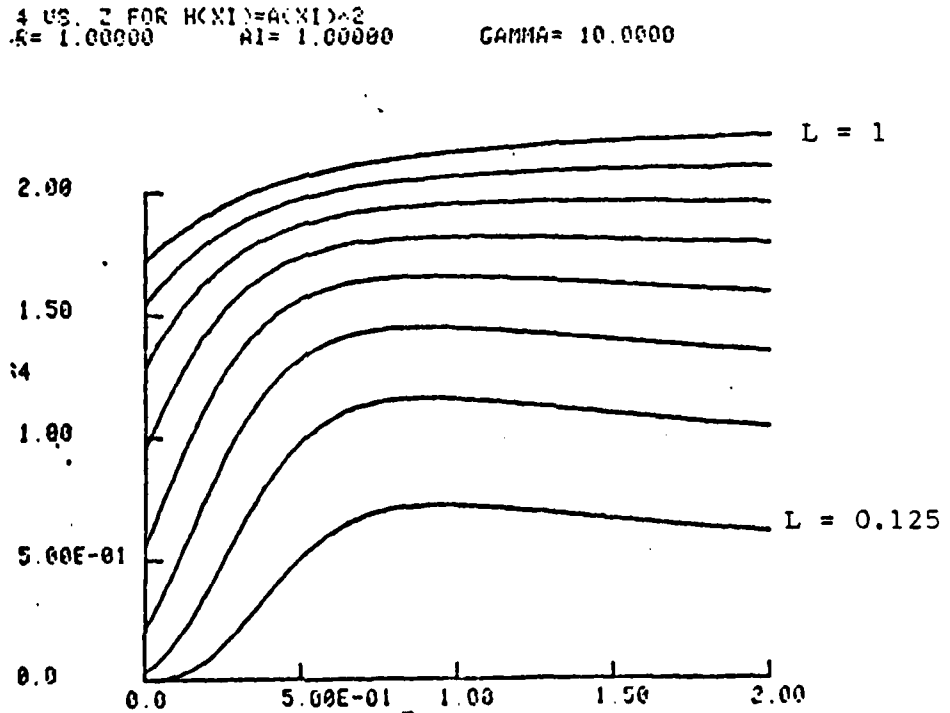


Fig. 66.  $S_4$  vs.  $z$  for  $L = 0.125$  to  $1$ , in step of  $0.125$ ; a modulated focused beam case,  $a = 10$ .

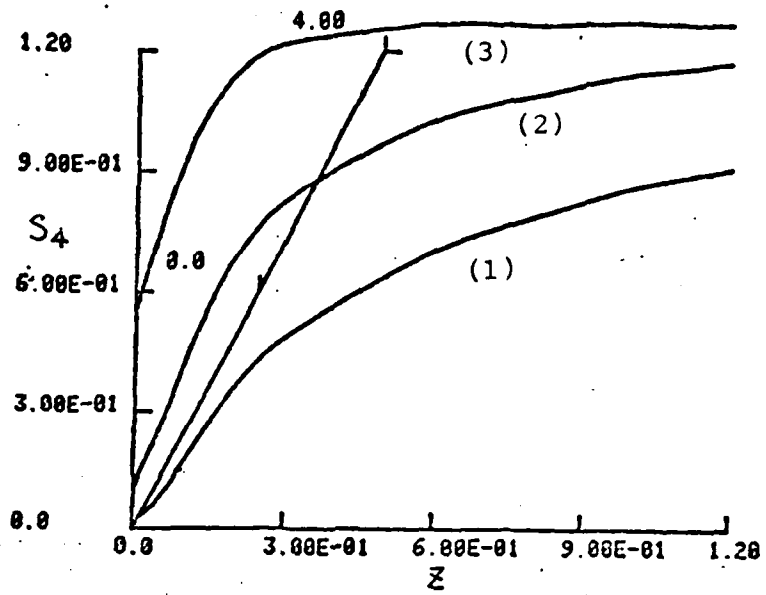


Fig. 67.  $S_4$  vs.  $z$  calculated from the approx. solution (4.43); (1)  $L = 0.06$ ; (2)  $L = 0.12$ ; (3)  $L = 0.24$ .

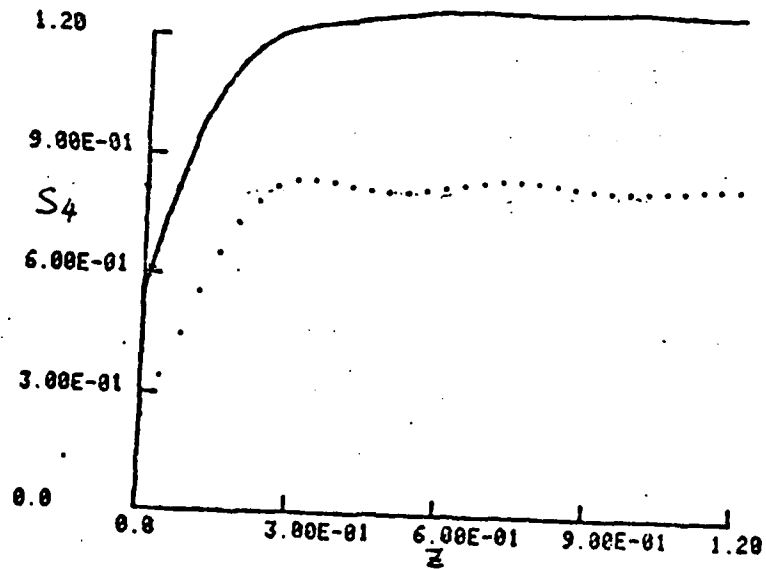


Fig 68.  $S_4$  vs.  $z$ ,  $L = 0.24$ ; solid line: approx. solution; dotted line: exact solution.

Chapter 5 THE INTENSITY FLUCTUATION AND SCINTILLATION INDEX

I. Definition of Intensity Correlation Function and Scintillation Index

If the new variables (4-5) are introduced, the function  $M_4(\underline{r}_1, \underline{r}_2, z)$  is expressed in terms of the wave fields by the formula (for  $\rho = 0$ )

$$M_4(\underline{r}_1, \underline{r}_2, z) = \left\langle \hat{\psi}\left(R + \frac{r_1 + r_2}{2}, z\right) \hat{\psi}\left(R - \frac{r_1 + r_2}{2}, z\right) \hat{\psi}^*\left(R + \frac{r_1 - r_2}{2}, z\right) \hat{\psi}^*\left(R - \frac{r_1 - r_2}{2}, z\right) \right\rangle \quad (5.1)$$

where in this case,  $r_2 = \rho_1 - \rho_1' = \rho_2' - \rho_2$ ,  $r_1 = \rho_1 - \rho_2 = \rho_1' - \rho_2'$ .  
The 2nd moment intensity function is defined by

$$\langle \hat{I}(z, \rho_1) \hat{I}(z, \rho_2) \rangle = \langle \hat{\psi}(z, \rho_1) \hat{\psi}^*(z, \rho_1) \hat{\psi}(z, \rho_2) \hat{\psi}^*(z, \rho_2) \rangle \quad (5.2)$$

which is identical to the fourth moment  $M_4$  when  $\rho_1 = \rho_1'$ ,  $\rho_2 = \rho_2'$  or  $r_2 = 0$ .

One also recalls that

$$M_2(\underline{\beta}, \underline{x}, \underline{\xi}) = \langle \hat{\psi}(\underline{\beta}, \underline{x} + \frac{1}{2}\underline{\xi}) \hat{\psi}^*(\underline{\beta}, \underline{x} - \frac{1}{2}\underline{\xi}) \rangle \quad (5.3)$$

$$M_2(\underline{\beta}, \underline{x}, 0) = \langle \hat{I}(\underline{\beta}, \underline{x}) \rangle \quad (5.4)$$

where  $\underline{x} = \frac{\rho_1 + \rho_1'}{2}$ ,  $\underline{\xi} = \rho_1 - \rho_1'$ . One defines an intensity correlation function as

$$B_I(\underline{\beta}, \rho_1, \rho_2) = \langle \hat{I}(\underline{\beta}, \rho_1) \hat{I}(\underline{\beta}, \rho_2) \rangle - \langle \hat{I}(\underline{\beta}, \rho_1) \rangle \langle \hat{I}(\underline{\beta}, \rho_2) \rangle \quad (5.5)$$

and one observes from equations (4.5) that  $r_2 = 0$ ,  $\rho_1 = R + \frac{r_1}{2}$ ,  $\rho_2 = R - \frac{r_1}{2}$ , and  $\underline{x} = R$ . Therefore

$$\begin{aligned} B_I(\underline{\beta}, \rho_1, \rho_2) &= \langle \hat{I}(\underline{\beta}, R + \frac{r_1}{2}) \hat{I}(\underline{\beta}, R - \frac{r_1}{2}) \rangle \\ &\quad - \langle \hat{I}(\underline{\beta}, R + \frac{r_1}{2}) \rangle \langle \hat{I}(\underline{\beta}, R - \frac{r_1}{2}) \rangle \\ &= M_4(\underline{\beta}, r_1, 0) - M_2(\underline{\beta}, R + \frac{r_1}{2}, 0) M_2(\underline{\beta}, R - \frac{r_1}{2}, 0) \end{aligned}$$

For the plane wave case, one takes into account that  $M_2$  is independent of the slow coordinate and write

$$\begin{aligned} B_I(\beta, \rho_1, \rho_2) &= M_4(\beta, \rho_1, 0) - M_2^2(\beta, 0, 0) \\ &= M_4(\beta, \rho_1, 0) - \langle \hat{I} \rangle^2 \end{aligned} \quad (5.7)$$

Thus,  $M_4(z, r_1, 0)$  enables one to determine the correlation function  $B_I(\tilde{z}, \tilde{\rho}_1, \tilde{\rho}_2) = B(z, r_1)$ .

The scintillation index  $S_4$  is defined as

$$S_4 = \frac{\langle (\hat{I} - \langle \hat{I} \rangle)^2 \rangle}{\langle \hat{I} \rangle^2} = \frac{M_4(\beta, 0, 0) - \langle \hat{I} \rangle^2}{\langle \hat{I} \rangle^2} \quad (5.8)$$

which plays an important role in the scintillation problem and is used as a measure of fluctuation level. For the case  $H(\xi) = a \xi^2$ , one obtains from (5.8) and (4.25)

$$\begin{aligned} M_4(R, 0, 0, 0, \beta_2) &= \frac{1}{4\alpha_r} \sqrt{\frac{1}{AB}} e^{-\frac{R^2}{4B}} \\ M_2(x, 0, \beta_2) &= \frac{1}{2\sqrt{\alpha_r D}} e^{-\frac{x^2}{4D}} \end{aligned} \quad (5.9)$$

where

$$\begin{aligned}
 A &= \frac{1}{2} \alpha_r \beta_2^2 + \frac{1}{2\alpha_r} (1 - \alpha_i \beta_2)^2 \\
 B &= \frac{1}{8} \alpha_r \beta_2^2 + \frac{1}{8\alpha_r} (1 - \alpha_i \beta_2)^2 + a (\beta_1 \beta_2^2 - \beta_2 \beta_1^2 + \frac{\beta_1^3}{3}) \\
 D &= \frac{1}{4} \alpha_r \beta_2^2 + \frac{1}{4\alpha_r} (1 - \alpha_i \beta_2)^2 + a (\beta_1 \beta_2^2 - \beta_2 \beta_1^2 + \frac{\beta_1^3}{3})
 \end{aligned}
 \tag{5.10}$$

the scintillation index can be calculate from (5.8) as

$$\begin{aligned}
 S_4 &= \frac{\langle \hat{I}^2 \rangle - \langle \hat{I} \rangle^2}{\langle \hat{I} \rangle^2} \\
 &= \frac{M_4(0,0,0,0,\beta_2) - M_2^2(0,0,\beta_2)}{M_2^2(0,0,\beta_2)} \\
 &= \sqrt{\frac{D^2}{AB}} - 1
 \end{aligned}
 \tag{5.11}$$

## II. Numerical Solution of Scintillation Index for Arbitrary Power Spectrum

In our computation, we shall first choose a Gaussian power spectrum. The corresponding correlation function is also Gaussian. The main reason for choosing such a spectrum is to check with the results obtained from the thin phase screen approximation (4). For the Gaussian spectrum, the  $\bar{f}(r_1, r_2)$  in equation (4.63) is given by

$$\bar{f}(r_1, r_2) = 2 - 2 \left[ e^{-\frac{r_1^2}{2}} + e^{-\frac{r_2^2}{2}} - \frac{1}{2} e^{-\frac{(r_1+r_2)^2}{2}} - \frac{1}{2} e^{-\frac{(r_1-r_2)^2}{2}} \right] \quad (5.12)$$

Using (5.12) in the numerical calculation to obtain the scintillation index, we shall present some computational results. Fig.69 depicts the behavior of the scintillation index as a function of  $z$  (from the bottom of slab to the receiver) for the case  $\gamma = 10$ . Curves 1,2,3 correspond to slab thickness  $L = 0.06, 0.12, 0.24$  respectively. For  $L = 0.06$ , corresponds to a thin phase screen, we observe that  $S_4$  increases monotonically with  $z$ , and finally reaches a constant value. The results agree very well with the thin phase screen theory. As  $L$  increases, corresponding to a thick random slab, the scintillation index grows. One notes that a focusing phenomenon occurs when  $L = 0.24$ , the scintillation index reaches a maximum before it settles to some saturation level.

It has been indicated that, in the thin phase screen theory, focusing occurs only in the strong turbulence case (rms phase fluctuation  $\phi_0^2 = \gamma L$  in our case). Our results shows the same behavior and should be better, since we take into account the thickness of the slab.

Scintillation index curves as a function of  $z$  for the case  $L = 0.06$  with different values of  $\gamma$ , equal to 5, 10, 30 are shown in Fig.70. The curve on the top indicates that a focusing behavior appears for strong turbulence case even though the random slab is very thin.

GAUSSIAN SPECTRUM  
 $\gamma = 10$

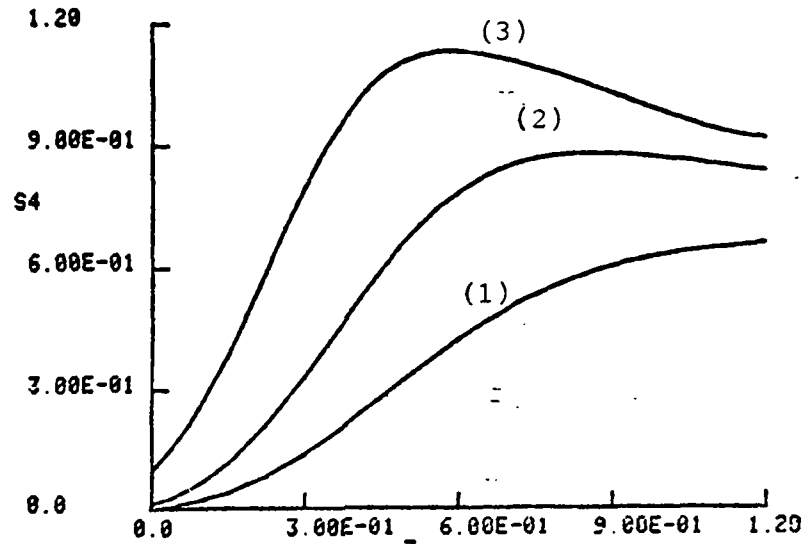


Fig. 69.  $S_4$  vs.  $z$ ; Gaussian spectrum with  $\gamma = 10$ ;  
(1)  $L = 0.06$ ; (2)  $L = 0.12$ ; (3)  $L = 0.24$ .

Gaussian Spectrum  
 $L = 0.06$

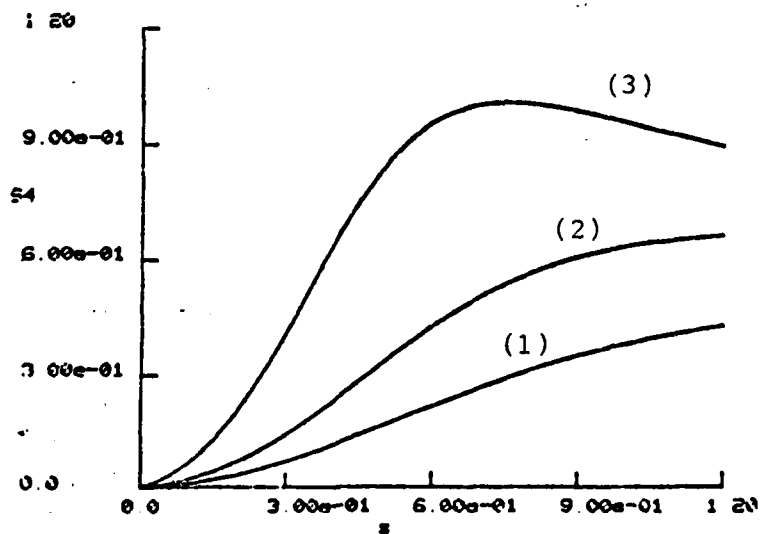


Fig. 70.  $S_4$  vs.  $z$ ; Gaussian spectrum,  $L = 0.06$ ;  
(1)  $\gamma = 5$ ; (2)  $\gamma = 10$ ; (3)  $\gamma = 30$ .

The following types of power spectrum will also be considered

(a) Power law spectrum with power index  $p = 4$

$$\Phi(k) = \frac{\Gamma(2) \langle \tilde{\epsilon}^2 \rangle}{\pi^{3/2} \Gamma(1/2)} \frac{L_0^3}{(1 + k^2 L_0^2)^2} \quad (5.13)$$

(b) Von-Karman spectrum  $p = 11/3$

$$\Phi(k) = \frac{\Gamma(1/6) \langle \tilde{\epsilon}^2 \rangle}{\pi^{3/2} \Gamma(1/3)} \frac{L_0^3}{(1 + k_0^2 L_0^2)^{11/6}} \quad (5.14)$$

(c) Von-Karman spectrum with a Gaussian bump

$$\Phi(k) = \frac{\Gamma(1/6) \langle \tilde{\epsilon}^2 \rangle L_0^3}{\pi^{3/2} \Gamma(1/3)} \left\{ \frac{1}{(1 + k_0^2 L_0^2)^{11/6}} + a e^{-\frac{(k - \bar{k})^2}{\kappa^2}} \right\} \quad (5.15)$$

the calculated function  $\bar{f}(r_1, r_2)$  for cases (a) and (b) are shown in Figs. 71 and 72. Figs. 73, 74 depict the function  $\bar{f}(r_1, r_2)$  of case (c) for  $\bar{k} = 2, \kappa^2 = 0.5, a = 0.5$  and  $\bar{k} = 3, \kappa^2 = 0.5, a = 0.5$  respectively. The scintillation index vs.  $z$  for case (a) is displayed by the dashed curve in Fig. 75 for  $\mathcal{V} = 10/\sqrt{\pi}$ ; the higher curve corresponds to  $L = 0.24$  and the lower curve to  $L = 0.06$ . As a comparison, we also show the corresponding values for the Gaussian power spectrum which are displayed by solid curve in Fig. 75. One notes that the scintillation index associated with the power law spectrum is larger immediately

VON KARMANN SPECTRUM  $F(R_1, R_2)$

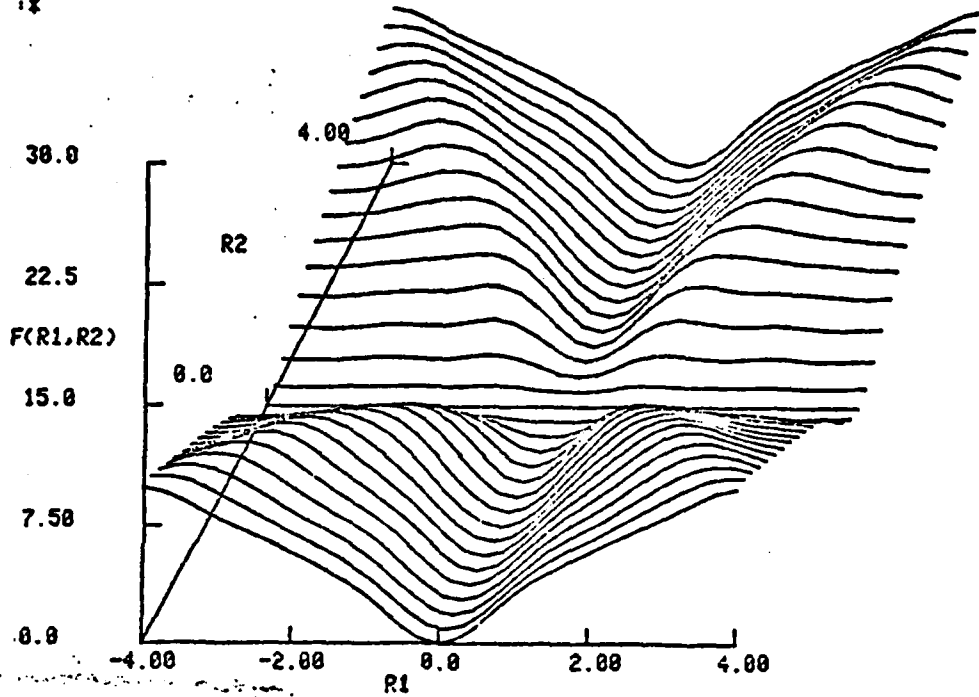


Fig. 71.  $\bar{f}(r_1, r_2)$  vs.  $r_1$  and  $r_2$  ; Power law spectrum with  $p = 4$ .

VON KARMANN SPECTRUM  $F(R_1, R_2)$

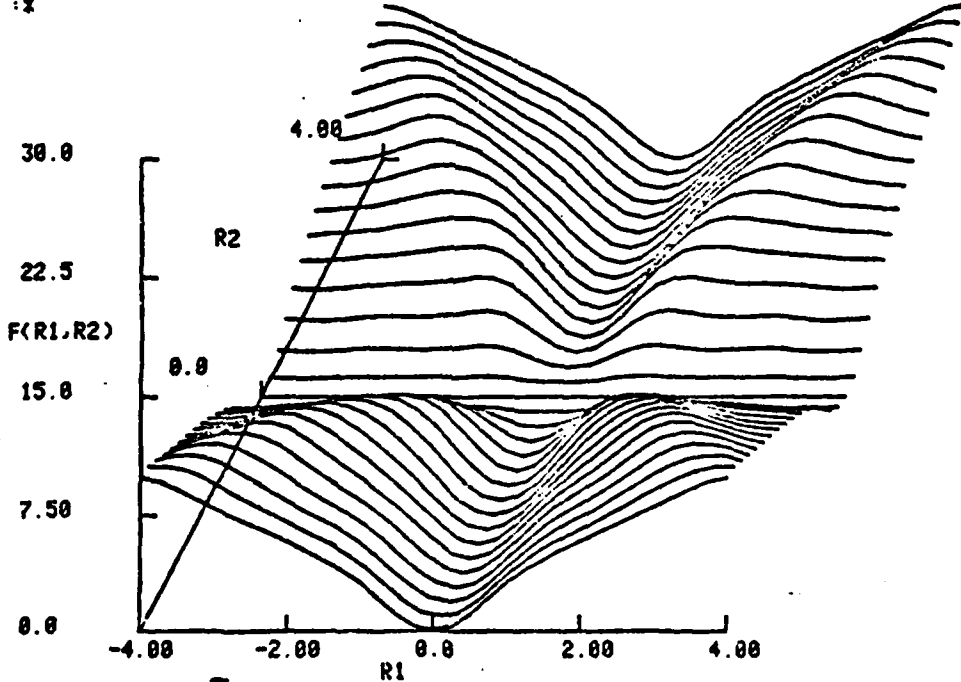


Fig. 72.  $\bar{f}(r_1, r_2)$  vs.  $r_1$  and  $r_2$  ; Von Karmann spectrum with  $p = 11/3$ .

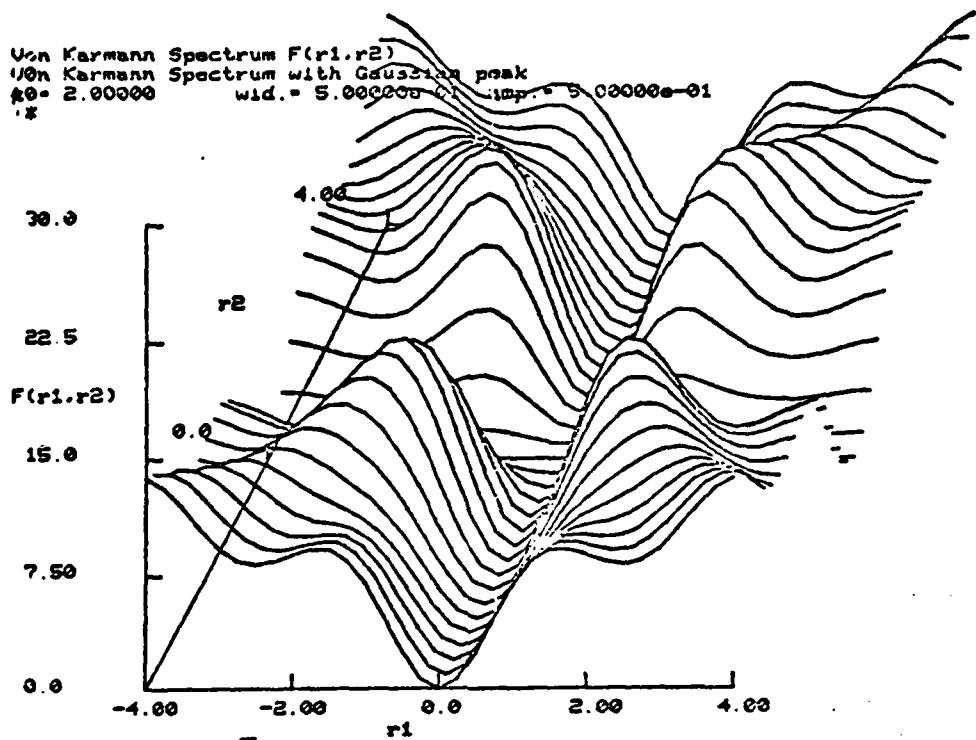


Fig. 73.  $\bar{F}(r_1, r_2)$  vs.  $r_1$  and  $r_2$ ; Von Karmann spectrum with a Gaussian bump,  $\bar{k} = 2, K^2 = 0.5, a = 0.5$ .

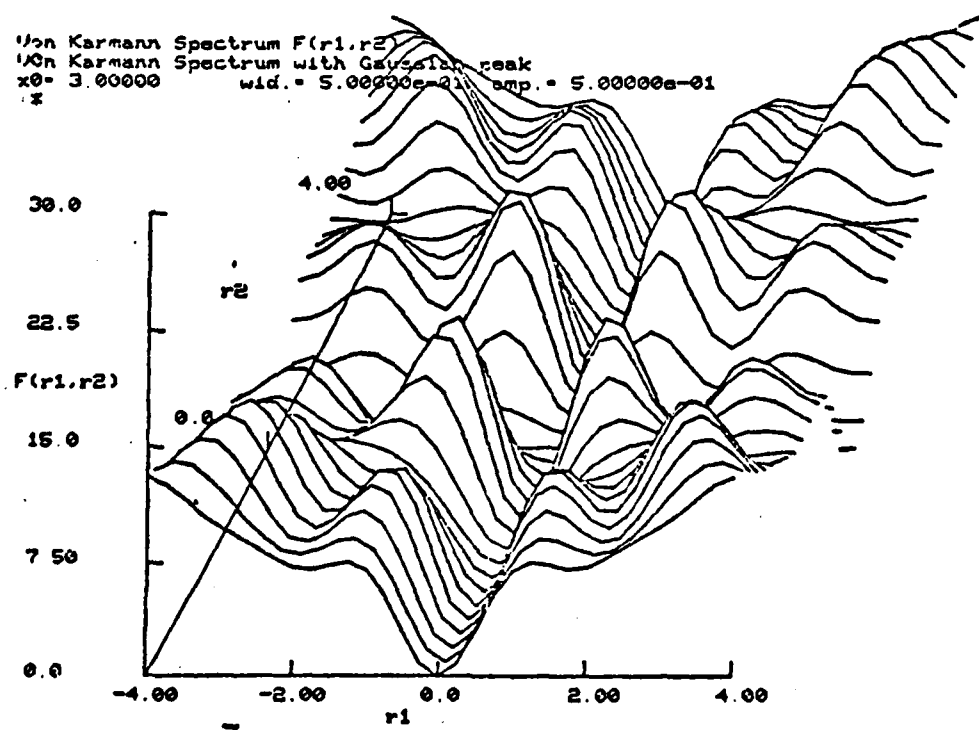


Fig. 74.  $\bar{F}(r_1, r_2)$  vs.  $r_1$  and  $r_2$ ; Von Karmann spectrum with a Gaussian bump,  $\bar{k} = 3, K^2 = 0.5, a = 0.5$ .

below the slab and become smaller at large distance. Fig. 76 shows the scintillation index vs. for case (b) with  $L = 0.12$  and  $\gamma = 5$  (lower curve),  $\gamma = 15$  (higher curve). The distinction between strong and weak turbulence is obviously related by the focusing phenomenon. The Von-Karman spectrum with an additive Gaussian bump greatly changes the behavior of scintillation index and is shown in Fig. 77. Curve 1 depicts the case  $\bar{k} = 3, \gamma = 5, L = 0.12$  and curve 2 displays the case  $\bar{k} = 2, \gamma = 5, L = 0.12$ . One concludes that the location of the Gaussian bump has a significant effect on the scintillation index. The focusing behavior occurs more than once in both curves, which indicates the additive bump increases the distortion of the wavefront emerging from the bottom of the slab. Fig. 78 compares the different behavior of the scintillation index for the case (b) and case (c) and for the parameters  $\gamma = 15, \bar{k} = 2, L = 0.12$ . Focusing occurs in both curves. At  $\beta \rightarrow \infty$ , spectrum (c) has a larger  $S_4$  than spectrum (b). Fig. 79 depicts the behavior of  $S_4$  for case (c) with  $\bar{k} = 2$  and  $\gamma = 5, 15$  respectively. One notes that even for  $\gamma = 5$ , the scintillation index vs.  $z$  shows a focusing phenomenon which is not observed in case (b) with  $\gamma = 5$ . This apparently indicates that the additive Gaussian bump causes a strong scattering effect. In order to show the effect of the power index  $P$ , we observe, for the case  $L = 0.24, k_0^3 L^3 \langle \xi^2 \rangle = 35.44$ , the scintillation index vs.  $z$  for  $p = 4$  and  $p = 11/3$  as displayed in Fig. 80, the solid line being for  $p = 4$  and the dash line for  $p = 11/3$ . One finds that the scintillation index vs.  $z$  has the same character in both cases but increases with the larger power index.

\\F'SPLA54'\\G  
 \\Y+1/2\*1.2MX GFQP

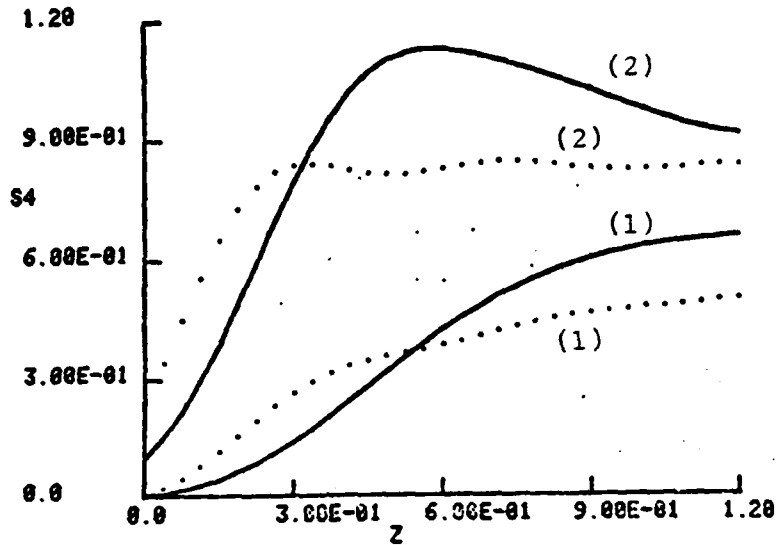


Fig. 75.  $S_4$  vs.  $z$ ; dotted lines: (1) Power law spectrum,  $p = 4$ ,  $L = 0.06$ ; (2) Power law spectrum,  $L = 0.24$ ; solid lines: (1) Gaussian spectrum,  $L = 0.06$ , (2)  $L = 0.24$ .  
 Von Karmann Spectrum  
 F'splal1'G  
 gfk-iv

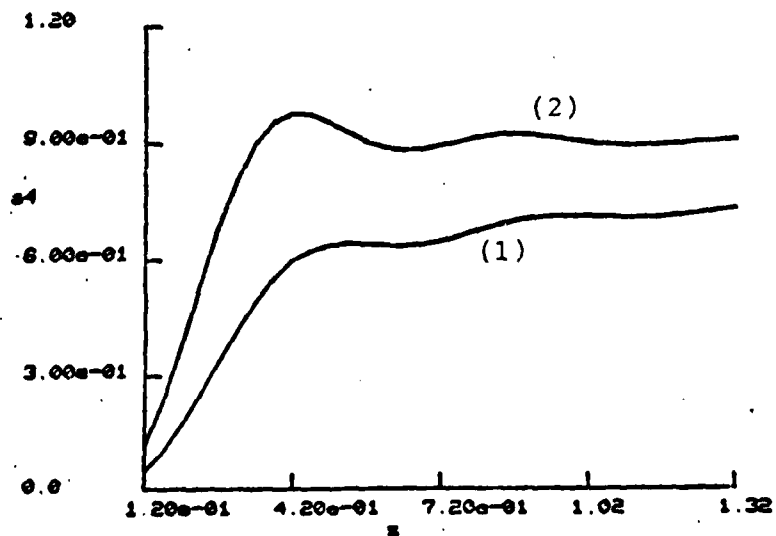


Fig. 76.  $S_4$  vs.  $z$  for Von Karmann spectrum; (1)  $L = 0.12$ ,  $\tau = 5$ ; (2)  $L = 0.12$ ,  $\tau = 15$ .

Scintillation Index vs. Z (Von Karmann Spectrum)  
 Von Karmann Spectrum with Gaussian Peak  
 gamma = 5.00000  
 F'spla28'G

• y+1/2x1.2mx gfk-1v

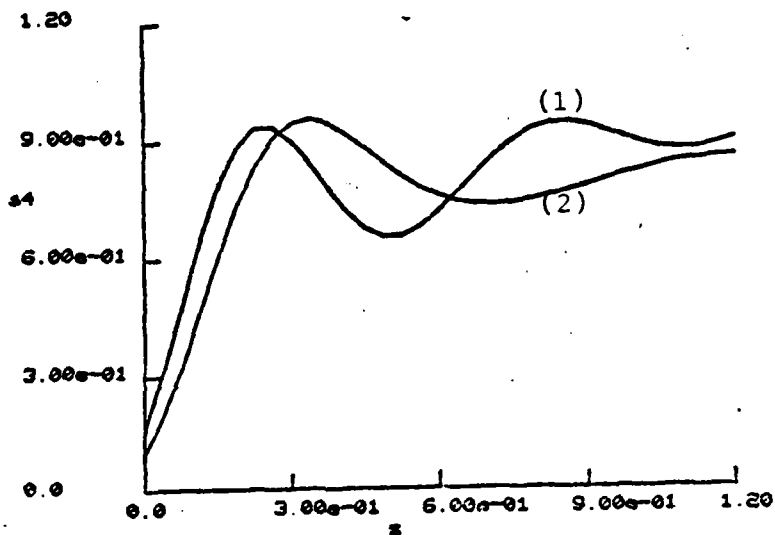


Fig. 77.  $S_4$  vs.  $z$  for Von Karmann spectrum with a Gaussian bump; (1)  $\bar{k} = 3, \gamma = 5, L = 0.12$ ; (2)  $\bar{k} = 2, \gamma = 5, L = 0.12$ .

gamma = 15.0000 wid = 5.00000e-01 ko = 2.00000 tmp = 5.00000e-01  
 F'spla12'G

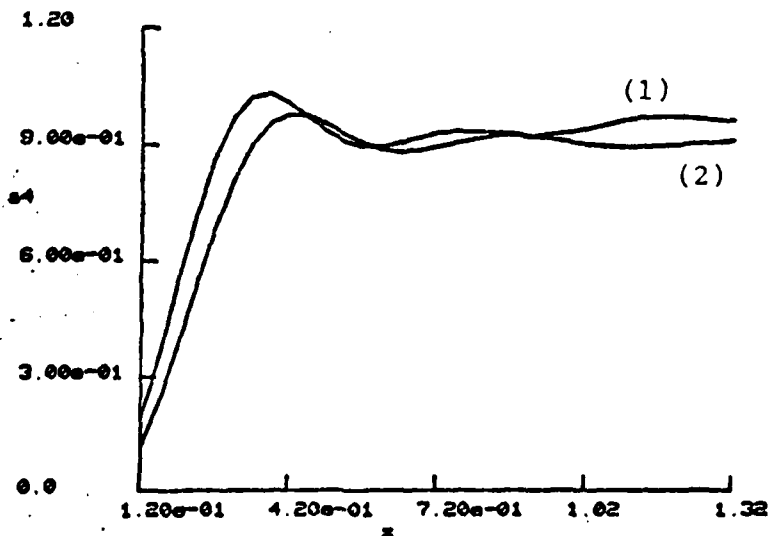


Fig. 78.  $S_4$  vs.  $z$ ; (1) Von Karmann spectrum,  $\gamma = 15, L = 0.12, p = 11/3$ ; (2) Von Karmann spectrum with a Gaussian bump,  $\bar{k} = 2, \gamma = 15, L = 0.12, p = 11/3$ .

K<sub>v</sub> = 2.00000      wid = 5.00000e-01      amp = 5.00000e-01  
 F'splal2'G  
 'gfk-1v

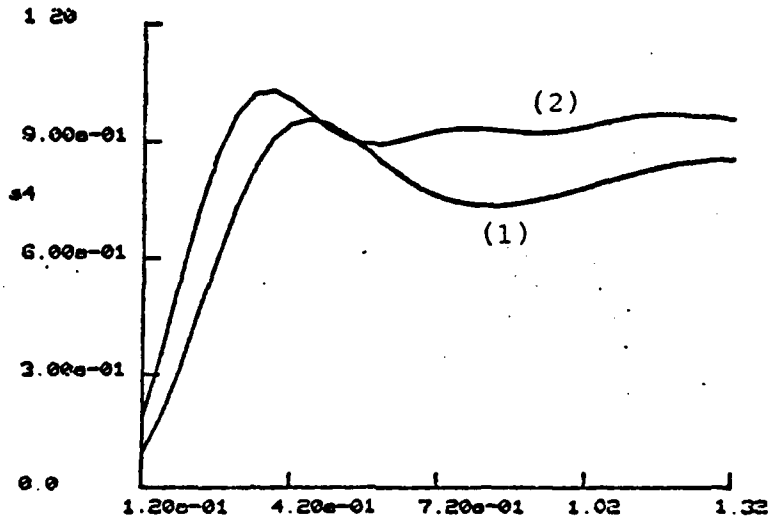


Fig. 79.  $S_4$  vs.  $z$  for Von Karmann spectrum with a Gaussian bump,  $\bar{K} = 2$ ,  $\gamma = 5$ ,  $L = 0.12$ , (curve 1);  $\bar{K} = 2$ ,  $\gamma = 15$ ,  $L = 0.12$ , (curve 2).

'NF'SPLA57'NG  
 'Y+1/2\*1.2MXGFK-1U

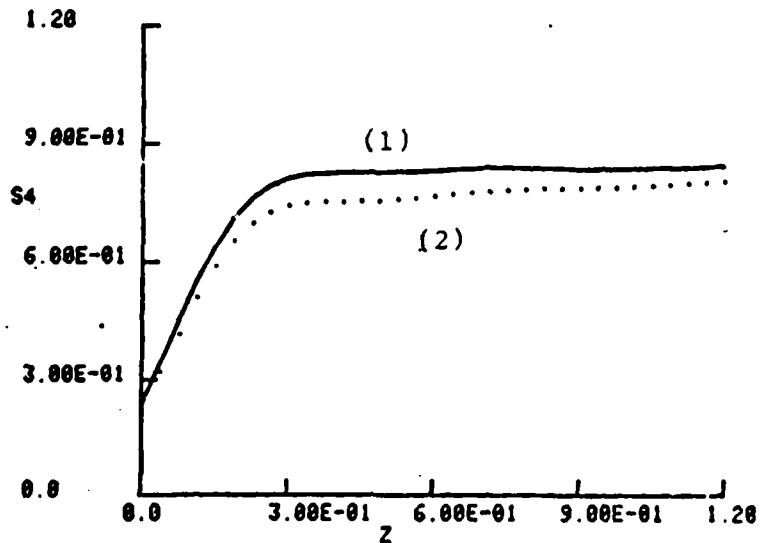


Fig. 80.  $S_4$  vs.  $z$  for power law spectrum; (1)  $L = 0.24$ ,  $\gamma = 8.86$ ,  $p = 4$ ; (2)  $L = 0.24$ ,  $\gamma = 8.86$ ,  $p = 11/3$ .

### III. Application and Discussions

A power spectrum, obtained from the Atmospheric Explorer - E (AE-E) satellite in situ measurements (70), is used to calculate the corresponding  $S_4$  for the night time equatorial scintillation. The variance of  $\tilde{N}/\bar{N}$  is estimated to be 0.207. We have normalized the power spectrum such that the integral of the fluctuation power  $\int \Phi(k) dk$  over the observed frequency range is equal to  $\langle (\tilde{N}/\bar{N})^2 \rangle$ . For computational purposes, we assume a flat spectrum for irregularity wavelength greater than 5 km and truncate the high frequency tail for irregularity scales smaller than 0.4 km. The resulting power spectrum is depicted in Fig. 81. In order to compare the theoretical model with the experimental results, we have chosen an incident wave frequency 137 MHz,  $f_{po} = 9$  MHz and  $l = 600$  m such that the parameter  $\gamma = 1/4 k_0^3 l^2 A(0)$  in equation (4.65) is equal to 52.73. The propagation distance  $z$  is normalized to  $\sim 10^3$  km; i.e. measures distance in  $10^3$  km.

Radar observations suggest that the ionosphere can be replaced by a random slab with an effective thickness  $\sim 200$  km. The distance from the bottom of the random slab to the ground is taken to be about 300 km. Applying these parameters to the defining equation for the fourth moment and using the numerical scheme described in Appendix 6, one obtains a plot of the scintillation index vs.  $z$  as shown in Fig. 82. A scintillation index as high as 0.35 is predicted at the bottom of the random slab. As the wave leaves the random slab and propagates in free space, diffraction phenomena develop. The scintillation index increases, passing through a maximum value at a distance  $\sim 250$  km from the bottom of the slab, and then saturates. At ground ( $z = 300$  km from the bottom of the slab), one obtains a scintillation index of 1.14, which corresponds to a peak to

peak fluctuations of approximately 32 dB.

Experimental results obtained by S. Basu et al. indicate a scintillation index of 0.6 at 137 MHz, which is lower than our analytical results. For a density fluctuation of 20% in the equatorial region, the experimental value,  $S_4 = 0.6$ , seems a little lower than expected. In private communication from Dr. Basu, he has informed us that his experimental result may be too low because of instrument saturation.

Possible explanations of this discrepancy might be:

- (1) The dynamic range of VHF receivers are limited to about 16 dB - 25 dB. A scintillation index as high as 1.14, corresponding to peak to peak fluctuations of 32 dB, is beyond the capacity of such receivers.
- (2) The in situ power spectrum was obtained at an altitude of 250 km. By extrapolation to magnetic field conditions at the scintillation measurement site, Basu et al. suggest an ionospheric structure  $\sim 200$  km in extent about 300 km above the earth. The accuracy of this model assumption is not evident.
- (3) In our theoretical work, we have assumed a flat spectrum for  $\lambda_g > 5$  km and have truncated the tail of the power spectrum for  $\lambda_g < 0.4$  km. This assumed power spectrum is also a possible source for the above discrepancy.
- (4) From the investigation in section II, one concludes that  $S_4$  increases as the thickness of the random slab increases. In the numerical evaluation, we have assumed the thickness of the random slab to be  $\sim 200$  km which may be larger than

the real effective thickness of the ionospheric slab.

In spite of the above discrepancy, one notes that the numerical results for the case of a Gaussian power spectrum are in good agreement with the results obtained by Mercier (4). For the case that  $L = 0.06$  which corresponds to the thin phase screen case, one obtains a saturated  $S_4$  which agrees with the value,  $S_4 = 1 - \exp(-2\phi_0^2)$ , obtained by Mercier (4). Our numerical scheme provides better agreement with thin phase screen theory than the scheme proposed by Liu et al. (60). Therefore, the proposed propagation model and numerical scheme should also provide satisfactory results for the case of an arbitrary power spectrum. The only real difficulties are proper location of the random slab and estimation of its effective thickness.

For further study, we shall apply the theory and numerical scheme presented herein to the multiple frequency, multi-dimensional, inhomogeneous, etc. cases. Consideration of an anisotropic power spectrum and of regime represent nonlinear effects in the strong scattering areas for future investigation and may provide further insights for the theory of ionospheric scintillations.

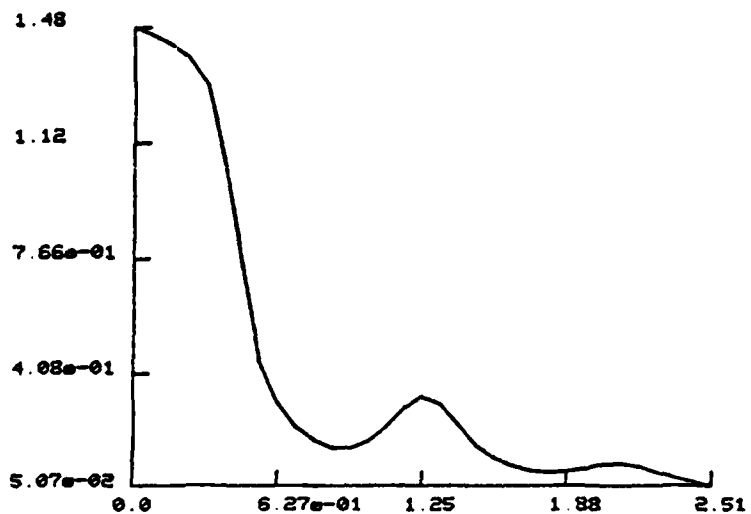


Fig. 81. in situ power spectrum vs.  $k$ ;

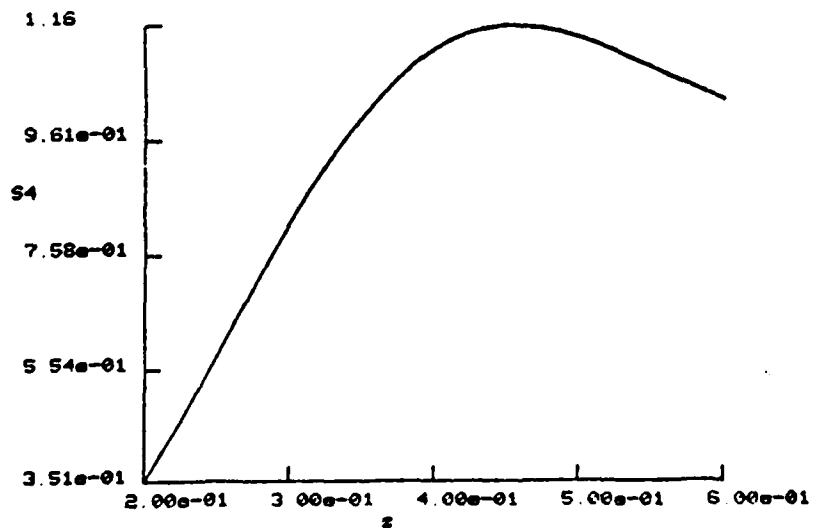


Fig. 82.  $S_4$  vs.  $z$  for a power spectrum depicted in Fig. 81.

APPENDIX 1

Solution of  $(L_0 - \tilde{V}) \hat{f} = 0$  where  $L_0$  is the an unperturbed operator and  $V$  is a random perturbation operator with  $\langle \tilde{V} \rangle = 0$ .

To solve this equation, it is convenient to define a stochastic Green's function:

$$(L_0 - \tilde{V}) \hat{G} = \underline{1} \quad (\text{A1.1})$$

For example, in  $\underline{r}, t$  space

$$\begin{aligned} \hat{G} \hat{f} &\longrightarrow \int \hat{g}(\underline{r}, t, \underline{r}', t') \hat{f}(\underline{r}', t') d\underline{r}' dt' \\ \underline{1} &\longrightarrow \delta(\underline{r} - \underline{r}') \delta(t - t') \end{aligned}$$

For uniqueness, the domain of  $\hat{G}$  will be defined by the requirement:

$$\hat{g}(\underline{r}, t, \underline{r}', t') = 0 \quad \text{for } t < t'$$

It is convenient to introduce the coherent unperturbed operator,  $G_0$ , defined by

$$L_0 G_0 = \underline{1} \quad (\text{A1.2})$$

The perturbation operator in equation (A1.1) can then be treated as the scattering part of the propagation.

By equation (A1.1), we have adjoint operators,  $L_0^\dagger$ ,  $\tilde{V}^\dagger$ ,  $\hat{G}^\dagger$ , which are defined by

$$(L_0^\dagger - \tilde{V}^\dagger) \hat{G}^\dagger = \hat{G}^\dagger (L_0 - \tilde{V}) \quad (\text{A1.3})$$

Therefore,

$$(L_0 - \tilde{V}) \hat{G} = \hat{G} (L_0 - \tilde{V}) = \underline{1} \quad (\text{A1.4})$$

Similarly, we have

$$L_0 G_0 = G_0 L_0 = \underline{1} \quad (\text{A1.5})$$

Multiplying (A1.4) by  $G_0$  and using (A1.5), we obtain

$$G_0 (L_0 - \tilde{V}) \hat{G} = G_0$$

Since  $G_0 L_0 = \underline{1}$ , we have

$$\hat{G} = G_0 + G_0 \tilde{V} \hat{G} = G_0 \hat{T} G_0 + G_0 \quad (\text{A1.6})$$

where we have defined

$$\tilde{V} \hat{G} \equiv \hat{T} G_0 \quad (\text{A1.6a})$$

The operator  $\hat{T}$  represents multiple scattering by the stochastic perturbation  $\tilde{V}$  in the background  $G_0$ . By using (A1.6), we obtain:

$$\hat{G} (1 - G_0 \tilde{V}) = G_0 \quad (\text{A1.7})$$

Substituting (A1.7), into (A1.6a), we obtain

$$\hat{T} = \tilde{V} \hat{G} G_0^{-1} = \tilde{V} (1 - G_0 \tilde{V})^{-1} \quad (\text{A1.8})$$

or

$$\hat{T} = \tilde{V} G_0 (1 + \tilde{V} \hat{G}) G_0^{-1} = \tilde{V} + \tilde{V} \hat{G} \tilde{V} \quad (\text{A1.9})$$

Note that the inverse operator can be expanded in a Neumann series:

$$(1 - G_0 \tilde{V})^{-1} = 1 + G_0 \tilde{V} + G_0 \tilde{V} G_0 \tilde{V} + \dots \quad (\text{A1.10})$$

but it displays secular divergence that limits its range of applicability.

By using (A1.6), (A1.8) and (A1.9), we obtain ensemble average relations as follows:

$$G = G_0 + G_0 V_c G = G_0 + G_0 T G_0 \quad (\text{A1.11})$$

where

$$\begin{aligned} G &= \langle \hat{G} \rangle \\ T &= \langle \hat{T} \rangle \\ V_c G &= T G_0 \end{aligned} \quad (\text{A1.12})$$

where  $V_c$  is a smoothed scattering operator in a background  $G$ .

On using (A1.11), (A1.12), one obtains:

$$\begin{aligned} T &= V_c G G_o^{-1} = V_c (1 - G_o V_c)^{-1} G_o G_o^{-1} \\ &= V_c (1 - G_o V_c)^{-1} \end{aligned} \tag{A1.13}$$

or

$$\begin{aligned} T &= V_c (1 + G_o T) G_o G_o^{-1} \\ &= V_c (1 + G V_c) \\ &= V_c + V_c G V_c \end{aligned} \tag{A1.14}$$

Multiply (A1.11) by  $L_o$  and make use of (A1.5), we obtain

$$\begin{aligned} L_o G - V_c G &= (L_o - V_c) G \\ &= G (L_o - V_c) \\ &= 1 \end{aligned} \tag{A1.15}$$

Equation (A1.15) provides a nonlinear defining equation for  $G$ , the nonlinearity arising from the nonlinear dependence of  $V_c$  on  $G$ . Using (A1.6) and (A1.11), we obtain

$$\hat{G} = G + G_o \tilde{T} G_o \tag{A1.16}$$

where

$$\tilde{T} = \hat{T} - T$$

From (A1.9), we obtain

$$\tilde{T} = \tilde{V} + \tilde{V} \hat{G} \tilde{V} - \langle \tilde{V} \hat{G} \tilde{V} \rangle \quad (\text{A1.17})$$

Using (A1.11) and (A1.12), we have

$$\begin{aligned} G_0 &= G (1 + V_c G)^{-1} \\ &= (1 + G V_c)^{-1} G \end{aligned} \quad (\text{A1.18})$$

Therefore, we can express (A1.16) as follows

$$\hat{G} = G + G (1 + V_c G)^{-1} \tilde{T} (1 + G V_c)^{-1} G \quad (\text{A1.19})$$

$$\hat{G} = G + G \tilde{T}_c G \quad (\text{A1.20})$$

where  $\tilde{T}_c$ , the multiple scattering in the smooth background  $G$ , is defined by

$$\tilde{T}_c = (1 + V_c G)^{-1} \tilde{T} (1 + G V_c)^{-1} \quad (\text{A1.21})$$

On averaging (A1.4), we obtain

$$\begin{aligned} \langle (L_0 - \tilde{V}) \hat{G} \rangle &= \frac{1}{\sim} \\ &= \langle \hat{G} (L_0 - \tilde{V}) \rangle \end{aligned} \quad (\text{A1.22})$$

Comparing with (A1.15), one infers

$$V_c G = \langle \tilde{V} \hat{G} \rangle \quad (\text{A1.23})$$

• From (A1.20), we have

$$\begin{aligned} V_c &= \langle \tilde{V} \hat{G} \rangle G^{-1} \\ &= \langle \tilde{V} G + \tilde{V} G \tilde{T}_c G \rangle G^{-1} \\ &= \langle \tilde{V} G \tilde{T}_c \rangle \end{aligned} \quad (\text{A1.24})$$

We would like to observe the physical meaning of (A1.20) as follows from (A1.4), we can write  $\hat{G}$  in the renormalization from as

$$(L_0 - V_c - \hat{V}_1) \hat{G} = \frac{1}{\sim} \quad (\text{A1.25})$$

Therefore, the scattering is now caused by a stochastic perturbation  $\hat{V}_1 = \tilde{V} - V_c$  of the coherent renormalized back-

ground operator (  $L_0 - V_c$  ). Multiplying (A1.25) by  $G$ , one obtains

$$\hat{G} = G + G \hat{V}_1 \hat{G} = G + G \tilde{T}_c G \tag{A1.26}$$

where we have defined

$$\hat{V}_1 \hat{G} \equiv \tilde{T}_c G \tag{A1.27}$$

On using (A1.26), one obtains

$$\begin{aligned} \tilde{T}_c &= \hat{V}_1 \hat{G} G^{-1} \\ &= \hat{V}_1 (G + G \hat{V}_1 \hat{G}) G^{-1} \\ &= \hat{V}_1 + \hat{V}_1 \hat{G} \hat{V}_1 \end{aligned} \tag{A1.28}$$

or

$$\tilde{T}_c = \hat{V}_1 (1 - G \hat{V}_1)^{-1}$$

From (A1.24), one finds that

$$V_c = \langle \hat{V}_1 G \tilde{T}_c \rangle \tag{A1.29}$$

By using (A1.27), one obtains

$$\begin{aligned} \tilde{T}_c &= \hat{V}_1 + \hat{V}_1 \hat{G} \hat{V}_1 \\ &= \hat{V}_1 + \hat{V}_1 G \hat{V}_1 + \dots \end{aligned} \tag{A1.30}$$

$$V_c = \langle \hat{V}_1 G \hat{V}_1 \rangle + \dots \tag{A1.31}$$

Since

$$\hat{V}_1 = \tilde{V} - V_c$$

Therefore

$$\begin{aligned} \tilde{T}_c &= \tilde{V} + \tilde{V} G \tilde{V} - \langle \tilde{V} G \tilde{V} \rangle \\ &\quad - \tilde{V} G \langle \tilde{V} G \tilde{V} \rangle + \dots \end{aligned} \tag{A1.32}$$

$$\begin{aligned} V_c &= \langle \tilde{V} G \tilde{V} \rangle + \langle \tilde{V} G \tilde{V} \rangle G \langle \tilde{V} G \tilde{V} \rangle \\ &\quad + \dots \end{aligned} \tag{A1.33}$$

On expanding (A1.21) and making use of (A1.20) in (A1.17), we obtain

$$\begin{aligned} \tilde{T}_c &= (1 - V_c G + V_c G V_c G + \dots) \tilde{T} \\ &\quad (1 - G V_c + G V_c G V_c - \dots) \end{aligned} \tag{A1.34}$$

$$\begin{aligned} \tilde{\Gamma} &= \tilde{V} + \tilde{V}G\tilde{V} - \langle \tilde{V}G\tilde{V} \rangle + \tilde{V}G\tilde{T}_cG\tilde{V} \\ &\quad - \langle \tilde{V}G\tilde{T}_cG\tilde{V} \rangle \end{aligned} \tag{A1.35}$$

Substituting (A1.24) in (A1.34) and making use of (A1.35), we obtain

$$\tilde{T}_c = \tilde{V} + \tilde{V}G\tilde{V} - \langle \tilde{V}G\tilde{V} \rangle + \tilde{V}G\tilde{V}G\tilde{V} + \dots \tag{A1.36}$$

$$V_c = \langle \tilde{V}G\tilde{V} \rangle + \langle \tilde{V}G\tilde{V}G\tilde{V} \rangle + \dots \tag{A1.37}$$

APPENDIX 2

In order to find a rapidly convergent series for  $V_c G$ , one considers the following possible expansions;

(1) Expansion a:

$$\begin{aligned} V_c G = & \langle \tilde{V} G \tilde{V} \rangle G + \langle \tilde{V} G \tilde{V} G \tilde{V} \rangle G + \\ & \langle \tilde{V} G \tilde{V} G \tilde{V} G \tilde{V} \rangle G - \langle \tilde{V} G \langle \tilde{V} G \tilde{V} \rangle G \tilde{V} \rangle G \quad (A2.1) \\ & - \langle \tilde{V} G \tilde{V} \rangle G \langle \tilde{V} G \tilde{V} \rangle G + \dots \end{aligned}$$

as described in Appendix 1.

(2) Expansion b:

since

$$V_c = \langle \tilde{V} G \tilde{T}_c \rangle \quad (A2.2)$$

and

$$\tilde{T}_c = (1 + V_c G)^{-1} \tilde{T} (1 + G V_c)^{-1} \quad (A2.3)$$

one obtains

$$V_c = (1 + V_c G)^{-1} \langle \tilde{V} G \tilde{T} \rangle (1 + G V_c)^{-1} \quad (A2.4)$$

where

$$\begin{aligned} \tilde{T} = & \tilde{V} + \tilde{V}G\tilde{V} - \langle \tilde{V}G\tilde{V} \rangle + \tilde{V}G\tilde{T}_cG\tilde{V} \\ & - \langle \tilde{V}G\tilde{T}_cG\tilde{V} \rangle \end{aligned} \quad (A2.5)$$

One multiplies eq. (A2.5) by  $\tilde{V}G$  and takes the ensemble average of this equation. Using equation (A2.3), one then obtains (assume  $\langle \tilde{V}^{2n+1} \rangle = 0$ )

$$\begin{aligned} \langle \tilde{V}G\tilde{T} \rangle = & \langle \tilde{V}G\tilde{V} \rangle + (1+V_cG)^{-1} \langle \tilde{V}G\tilde{V}G\tilde{T}G\tilde{V} \rangle \\ & (1+GV_c)^{-1} \end{aligned} \quad (A2.6)$$

From equations (A2.5) and (A2.3), one observes that

$$\begin{aligned} \langle \tilde{V}G\tilde{V}G\tilde{T}G\tilde{V} \rangle = & \langle \tilde{V}G\tilde{V}G\tilde{V}G\tilde{V} \rangle + (1+V_cG)^{-1} \\ & \langle \tilde{V}G\tilde{V}G\tilde{V}G\tilde{T}G\tilde{V}G\tilde{V} \rangle (1+GV_c)^{-1} \end{aligned} \quad (A2.7)$$

Therefore, one finally obtains the expansion

$$\begin{aligned} V_c = & (1+V_cG)^{-1} \langle \tilde{V}G\tilde{V} \rangle (1+GV_c)^{-1} + \\ & (1+V_cG)^{-2} \langle \tilde{V}G\tilde{V}G\tilde{V}G\tilde{V} \rangle (1+GV_c)^{-2} + \\ & (1+V_cG)^{-3} \langle \tilde{V}G\tilde{V}G\tilde{V}G\tilde{V}G\tilde{V} \rangle (1+GV_c)^{-3} + \\ & \dots \end{aligned} \quad (A2.8)$$

(3) Expansion C:

From equation (A2.3) and (A2.5), one obtains

$$\begin{aligned} \tilde{T}_c = & (1+V_cG)^{-1} (\tilde{V} + \tilde{V}G\tilde{V} - \langle \tilde{V}G\tilde{V} \rangle + \tilde{V}G\tilde{T}_cG\tilde{V} \\ & - \langle \tilde{V}G\tilde{T}_cG\tilde{V} \rangle) (1+GV_c)^{-1} \end{aligned} \quad (A2.9)$$

Therefore, from equation (A2.2) and (A2.9), one has:

$$V_c = \langle \tilde{V} G \tilde{T}_c \rangle = (1 + V_c G)^{-1} \{ \langle \tilde{V} G \tilde{V} \rangle + \langle \tilde{V} G \tilde{V} G \tilde{V} \rangle - \langle \tilde{V} G \langle \tilde{V} G \tilde{V} \rangle \rangle + \langle \tilde{V} G \tilde{V} G \tilde{T}_c G \tilde{V} \rangle - \langle \tilde{V} G \langle \tilde{V} G \tilde{T}_c G \tilde{V} \rangle \rangle \} (1 + G V_c)^{-1} \quad (A2.10)$$

One rewrites equation (A2.10) as

$$V_c = \langle \tilde{V} G \tilde{T}_c \rangle = (1 + V_c G)^{-1} \{ \langle \tilde{V} G \tilde{V} \rangle + \langle \tilde{V} G \tilde{V} G \tilde{V} \rangle \} (1 + G V_c)^{-1} + (1 + V_c G)^{-1} \{ \langle \tilde{V} G \tilde{V} G \tilde{T}_c G \tilde{V} \rangle (1 + G V_c)^{-1} \langle \tilde{V} G \tilde{T}_c \rangle^{-1} \langle \tilde{V} G \tilde{T}_c \rangle \} (1 + V_c G)^{-1} \{ \langle \tilde{V} G \tilde{V} \rangle + \langle \tilde{V} G \tilde{V} G \tilde{V} \rangle \} (1 + G V_c)^{-1}$$

where  $[1 - P_0]^{-1}$

$$P_0 = (1 + V_c G)^{-1} \langle \tilde{V} G \tilde{V} G \tilde{T}_c G \tilde{V} \rangle (1 + G V_c)^{-1} \langle \tilde{V} G \tilde{T}_c \rangle^{-1} \quad (A2.12)$$

The term  $\langle \tilde{V} G \tilde{V} G \tilde{T}_c G \tilde{V} \rangle$  in eq. (A2.12) can be written as:

$$\langle \tilde{V} G \tilde{V} G \tilde{T}_c G \tilde{V} \rangle = (1 + V_c G)^{-1} \{ \langle \tilde{V} G \tilde{V} G \tilde{V} G \tilde{V} \rangle + \langle \tilde{V} G \tilde{V} G \tilde{V} G \tilde{V} G \tilde{V} \rangle - \langle \tilde{V} G \tilde{V} G \langle \tilde{V} G \tilde{V} \rangle G \tilde{V} \rangle \} (1 + G V_c)^{-1} [1 - P_1]^{-1} \quad (A2.13)$$

where

$$P_1 = (1 + V_c G)^{-1} \{ \langle \tilde{V} G \tilde{V} G \tilde{V} G \tilde{T}_c G \tilde{V} G \tilde{V} \rangle - \langle \tilde{V} G \tilde{V} G \langle \tilde{V} G \tilde{T}_c G \tilde{V} \rangle G \tilde{V} \rangle \} (1 + G V_c)^{-1} \langle \tilde{V} G \tilde{V} G \tilde{T}_c G \tilde{V} \rangle^{-1} \quad (A2.14)$$

⋮

In order to reduce the complexity, we shall examine the convergence of  $V_c G$  for the equation of the form

$$i \frac{\partial \hat{\psi}}{\partial z} + \tilde{n} \hat{\psi} = 0 \quad (\text{A2.15})$$

One also assumes that  $\tilde{n}$  is a pure stochastic variable indep. of  $\underline{r}$  and  $z$ . The defining equation for the average Green's function is

$$i \frac{\partial G}{\partial z} + \langle \tilde{n} \hat{G} \rangle = \frac{1}{\sim} \quad (\text{A2.16a})$$

or

$$i \frac{\partial G}{\partial z} + V_c G = \frac{1}{\sim} \quad (\text{A2.16b})$$

Taking the Fourier transform of (A2.16b), one obtains the algebraic equation:

$$(b + i\epsilon - V_c) g = 1 \quad (\text{A2.17})$$

or

$$g = \frac{1}{b + i\epsilon - V_c} \quad (\text{A2.18})$$

In order to evaluate  $g$ , one requires information about  $V_c$ . The most appropriate expansion for  $V_c g$  will be determined via numerical investigation.

(1) For expansion a, we define the following approximations:

$$\text{1st approx.: } V_c g = g^2 \langle \tilde{v}^2 \rangle$$

$$\text{2nd approx.: } V_c g = g^2 \langle \tilde{v}^2 \rangle + g^4 \{ \langle \tilde{v}^4 \rangle - 2 \langle \tilde{v}^2 \rangle^2 \}$$

$$\text{3rd approx.: } V_c g = \{ \text{2nd approx.} \} + g^6 \{ \bigcirc \}$$

$$\text{4th approx.: } V_c g = \{ \text{3rd approx.} \} + g^8 \{ \bigcirc \}$$

For the case that  $\tilde{n} \equiv -\tilde{v}$  is uniformly distributed between  $-a$  and  $a$ , one finds that  $V_c g$  tends to converge as shown by the solid line of Fig. 1. Note that:

$$\text{1st approximation is valid when } g^2 \langle \tilde{v}^2 \rangle = \frac{g^2 a^2}{3} \leq 0.2$$

$$\text{2nd approximation is valid when } g^2 \langle \tilde{v}^2 \rangle \leq 0.6$$

$$\text{3rd approximation is valid when } g^2 \langle \tilde{v}^2 \rangle \leq 0.8$$

(2) We define the following approximations for expansion b:

$$\text{1st approx. } V_c g = (1 + V_c g)^{-2} g^2 \langle \tilde{v}^2 \rangle$$

$$\text{2nd approx. } V_c g = \{ \text{1st approx.} \} + (1 + V_c g)^{-4} g^4 \langle \tilde{v}^4 \rangle$$

$$\text{3rd approx. } V_c g = \{ \text{2nd approx.} \} + (1 + V_c g)^{-6} g^6 \langle \tilde{v}^6 \rangle$$

$$\text{4th approx. } V_c g = \{ \text{3rd approx.} \} + (1 + V_c g)^{-8} g^8 \langle \tilde{v}^8 \rangle$$

as shown by the dotted curves of Fig. 1, one observes that for the case of a uniform distribution, expansion b tends to converge; however, not as fast as expansion a converges.

(3) Approximations for expansion C are:

1st approx.  $V_c g = (1 + V_c g)^{-2} g^2 \langle \tilde{v}^2 \rangle$

2nd approx.  $V_c g = \frac{(1 + V_c g)^{-2} g^2 \langle \tilde{v}^2 \rangle}{1 - \frac{(1 + V_c g)^{-2} \langle g^3 \tilde{v}^4 \rangle}{\langle g \tilde{v}^2 \rangle}}$

3rd approx. \*

4th approx. \*\*

For the case of a uniform distribution, this expansion shows fast convergence. The 3rd approximation falls right between the 3rd and 4th approx. of expansion a, wherein is located the exact solution (Fig.2).

\* 
$$V_c g = \frac{(1 + V_c g)^{-2} g^2 \langle \tilde{v}^2 \rangle}{1 - \frac{(1 + V_c g)^{-2} \langle g^3 \tilde{v}^4 \rangle}{\langle g \tilde{v}^2 \rangle}} \left[ \frac{1 - \frac{(1 + V_c g)^{-2} \langle g^3 \tilde{v}^4 \rangle}{\langle g \tilde{v}^2 \rangle}}{1 - \frac{(1 + V_c g)^{-2} \langle g^5 \tilde{v}^6 \rangle}{\langle g^3 \tilde{v}^4 \rangle}} \right]$$

\*\*

\*\* 
$$V_c g = \frac{(1 + V_c g)^{-2} \langle g^2 \tilde{v}^2 \rangle}{1 - \frac{(1 + V_c g)^{-2} g^3 \langle \tilde{v}^4 \rangle}{g \langle \tilde{v}^2 \rangle}} \left[ \frac{1 - \frac{(1 + V_c g)^{-2} \langle g^3 \tilde{v}^4 \rangle}{\langle g \tilde{v}^2 \rangle}}{1 - \frac{(1 + V_c g)^{-2} \langle g^5 \tilde{v}^6 \rangle}{g^3 \langle \tilde{v}^4 \rangle}} \right] \left[ \frac{1 - \frac{(1 + V_c g)^{-2} \langle g^5 \tilde{v}^6 \rangle}{\langle g^3 \tilde{v}^4 \rangle}}{1 - \frac{(1 + V_c g)^{-2} \langle g^7 \tilde{v}^8 \rangle}{\langle g^5 \tilde{v}^6 \rangle}} \right]$$

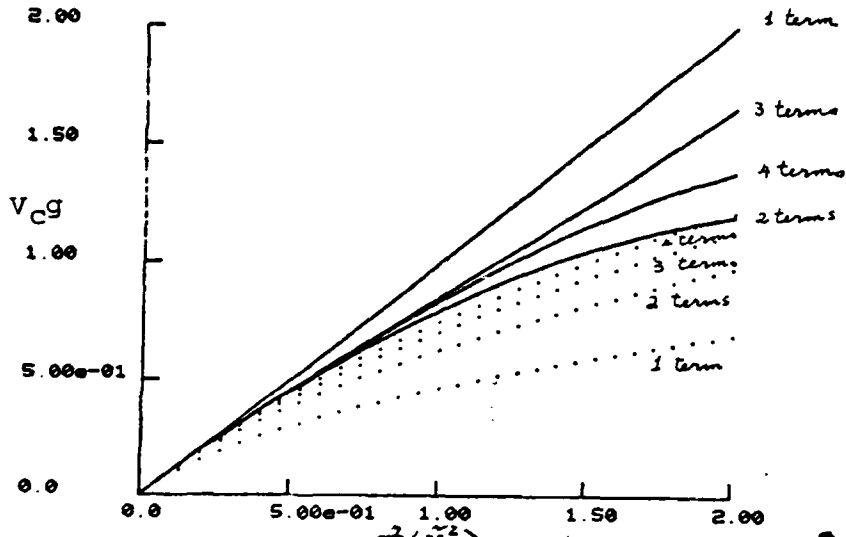


Fig. A2.1.  $V_C g$  vs.  $g^2 \langle \bar{v}^2 \rangle$ ; solid line: expansion a; dotted line: expansion b.

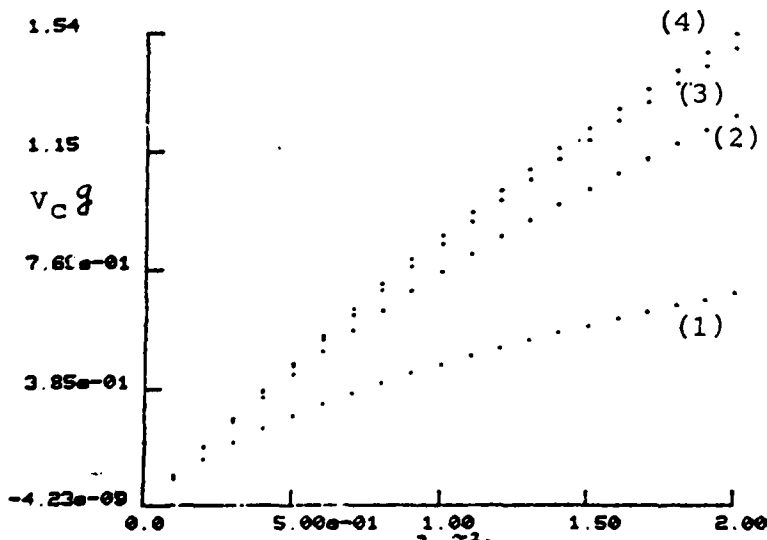
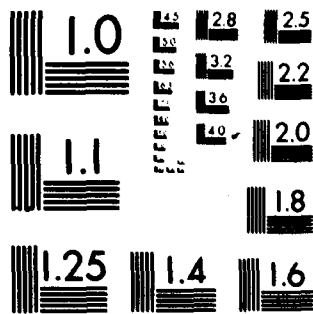


Fig. A2.2.  $V_C g$  vs.  $g^2 \langle \bar{v}^2 \rangle$ ; expansion c; (1) 1st approx.; (2) 2nd approx.; (3) 3rd approx.; (4) 4th approx.;





MICROCOPY RESOLUTION TEST CHART  
 NATIONAL BUREAU OF STANDARDS 1963 A

If  $\tilde{n}$  obeys a Gaussian statistics with a distribution function of the form:

$$f(n) = A e^{-\left(\frac{n}{b}\right)^2}$$

one finds that all expansions described above lead to poor convergence. As an example, we calculate the 1st, 2nd and 3rd approximations for expansion c and depict it in (Fig.3). Let us observe the exact solution of G for equation (A2.15), when  $\tilde{n}$  is Gaussian, we have

$$G = -i \exp \left\{ -\frac{\langle \tilde{n}^2 \rangle (\beta - \beta')^2}{2} \right\}$$

As a power series expansion, one writes

$$G = -i \left[ 1 - \frac{\langle \tilde{n}^2 \rangle (\beta - \beta')^2}{2} + \dots \right]$$

If the series is truncated after a finite number of terms, we have

$$G \rightarrow \infty \quad \text{as} \quad \beta - \beta' \rightarrow \infty$$

The "secular" behavior of G in this case explains somewhat why "moment" expansions for Gaussian statistics are not suitable.

Consider a Gaussian statistics truncated at  $\pm|a|$  namely:

$$f(n) = A e^{-\left(\frac{n}{b}\right)^2} \quad -a < n < a$$

The results of numerical calculations of  $V_c$  are shown in Fig. 4 - Fig. 6. One observes that the convergence of the series expansion is dependent on the ratio  $a^2 / \langle \tilde{n}^2 \rangle$  where  $\langle \tilde{n}^2 \rangle$  denotes the variance of  $\tilde{n}$ . For Fig. 4 to Fig. 6, we use  $a^2 / \langle \tilde{n}^2 \rangle = 4.59796, 3.62336, 3.05054$  respectively, and find that a smaller ratio  $a^2 / \langle \tilde{n}^2 \rangle$  gives a better convergence.

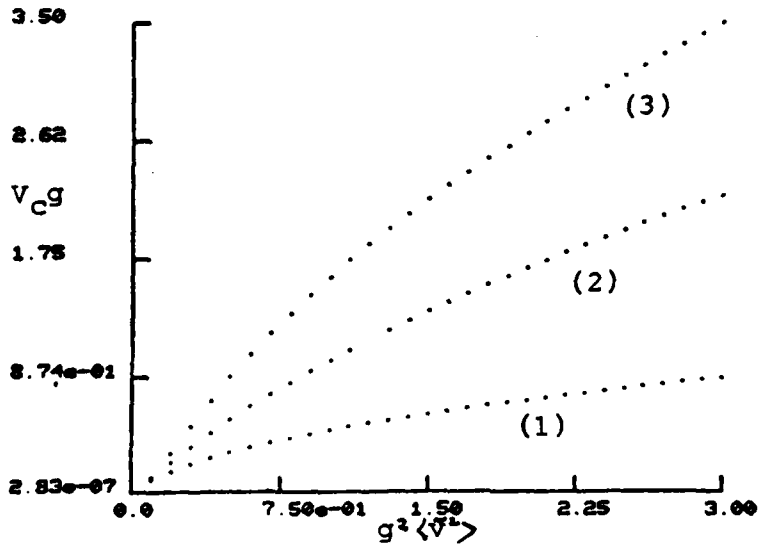


Fig. A2.3.  $V_{Cg}$  vs.  $g^2 \langle \tilde{v}^2 \rangle$ ;  $\tilde{n}$  is Gaussian.  
Expansion c: (1) 1st approx.; (2) 2nd approx.;  
(3) 3rd approx.;

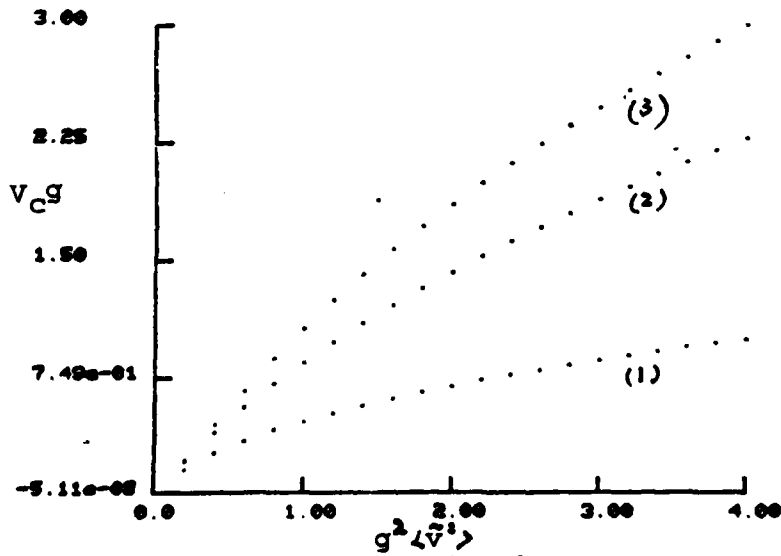


Fig. A2.4  $V_{Cg}$  vs.  $g^2 \langle \tilde{v}^2 \rangle$ ;  $\tilde{n}$  obeys a Gaussian statistics truncated at  $\pm |a|$ ;  $a^2 / \langle \tilde{v}^2 \rangle = 4.598$ . (expansion c)

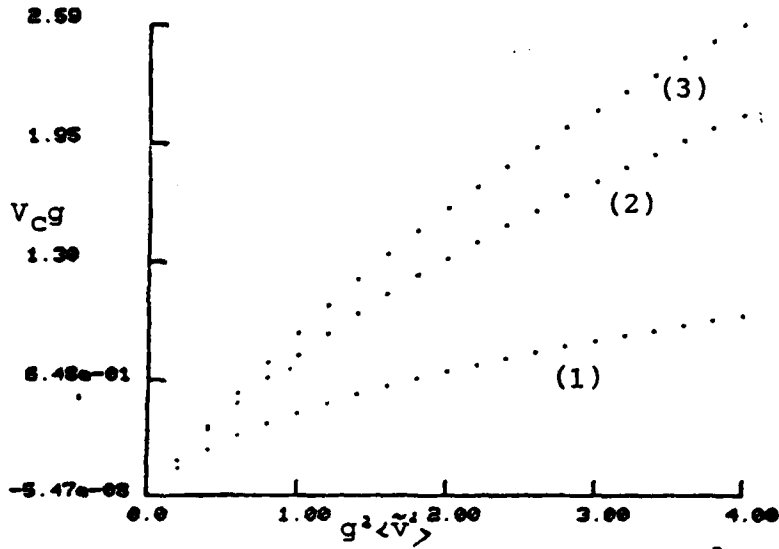


Fig. A2.5. same as Fig. A2.4 except  $a^2 / \langle \tilde{n}^2 \rangle = 3.623$ .

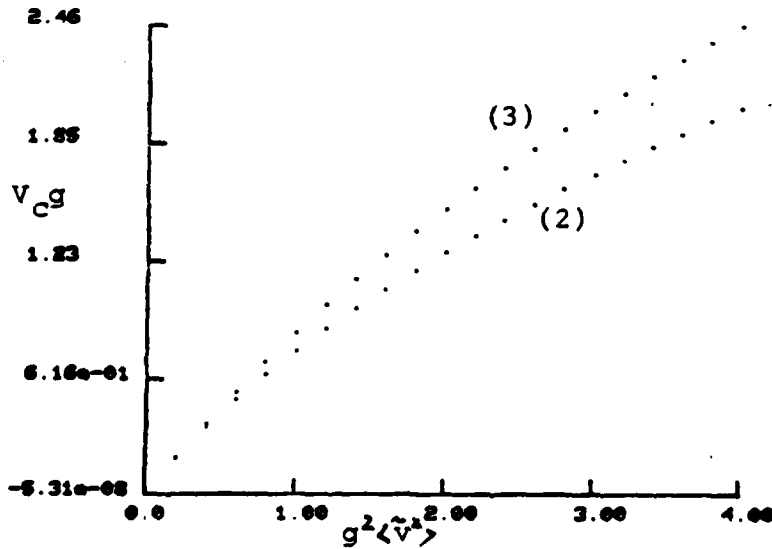


Fig. A2.6. same as Fig. A2.4. except  $a^2 / \langle \tilde{n}^2 \rangle = 3.05$ .

APPENDIX 3

The limit of application of the Markov approximation

Let us consider corrections to the Markov approximation when a finite radius of correlation in the propagating direction is taken into account. Let  $\tilde{\epsilon}(\underline{z}, \underline{r})$  be a sharp peaked function of the argument  $\underline{z}-\underline{z}'$  and  $\langle \tilde{\epsilon}(\underline{z}, \underline{r}) \tilde{\epsilon}(\underline{z}', \underline{r}') \rangle = B(\underline{z}-\underline{z}', \underline{r}-\underline{r}')$ .

The parabolic equation for the random field  $\hat{u}(\underline{z}, \underline{r})$  is written as:

$$2ik_0 \frac{\partial \hat{u}(\underline{z}, \underline{r})}{\partial \underline{z}} + \nabla_{\underline{r}}^2 \hat{u}(\underline{z}, \underline{r}) + k_0^2 \tilde{\epsilon}(\underline{z}, \underline{r}) \hat{u}(\underline{z}, \underline{r}) = 0 \quad (\text{A3.1})$$

Taking the Fourier transform of eq. (A3.1) with respect to and averaging, one obtains

$$\frac{\partial \langle \hat{u} \rangle}{\partial \underline{z}} + \frac{-ik_0^2}{2k_0} \langle \hat{u}(\underline{z}, \underline{r}_p) \rangle - \frac{ik_0}{2} \int \langle \tilde{\epsilon}(\underline{z}, \underline{r}) \hat{u}(\underline{z}, \underline{r}') \rangle e^{i\underline{k} \cdot \underline{r}} d\underline{r} \quad (\text{A3.2})$$

Applying the renormalized series expansion described in Appendix 1, we have

$$\frac{ik_0}{2} \langle \tilde{\epsilon}(\underline{z}, \underline{r}) \hat{u}(\underline{z}, \underline{r}) \rangle \cong -\frac{k_0^2}{4} \int \{ \langle \tilde{\epsilon}(\underline{z}, \underline{r}) G(\underline{z}, \underline{r}, \underline{z}', \underline{r}') \tilde{\epsilon}(\underline{z}', \underline{r}') \rangle + \dots \} \langle \hat{u}(\underline{z}', \underline{r}') \rangle d\underline{z}' d\underline{r}' \quad (\text{A3.3})$$

If the correlation length in the z direction is very small such that the 1st term in the series expansion of eq. (A2.1) dominates, we can approximate (A3.3) as following:

$$\frac{i k_0}{2} \langle \tilde{E}(\underline{z}, \underline{r}) \hat{u}(\underline{z}, \underline{r}) \rangle \cong - \frac{k_0^2}{4} \int B(\underline{z}-\underline{z}', \underline{r}-\underline{r}') G(\underline{z}, \underline{r}, \underline{z}', \underline{r}') \langle \hat{u}(\underline{z}', \underline{r}') \rangle d\underline{z}' d\underline{r}' \quad (\text{A3.4})$$

One rewrites (A3.2) as

$$\left\{ \frac{\partial}{\partial \underline{z}} + \frac{i k_0^2}{2 k_0} \right\} \langle \hat{u}(\underline{z}, k_{\underline{r}}) \rangle + \frac{k_0^2}{4} \int B(\underline{z}-\underline{z}', \underline{r}-\underline{r}') \cdot G(\underline{z}, \underline{r}, \underline{z}', \underline{r}') \langle \hat{u}(\underline{z}', \underline{r}') \rangle e^{i k_{\underline{r}} \cdot \underline{r}} d\underline{z}' d\underline{r}' d\underline{r} = 0 \quad (\text{A3.5})$$

assuming the field  $\tilde{E}(\underline{z}, \underline{r})$  is statistically homogeneous, so that its two dimensional spectral density satisfies the relation:

$$\langle \tilde{E}(\underline{z}, k_{\underline{r}_1}) \tilde{E}(\underline{z}', k_{\underline{r}_2}) \rangle = \delta(k_{\underline{r}_1} + k_{\underline{r}_2}) F(\underline{z}-\underline{z}', k_{\underline{r}_1}) \quad (\text{A3.6})$$

Applying (A3.6) one rewrites (A3.5) after some manipulations, as follows:

$$\left\{ \frac{\partial}{\partial \underline{z}} + \frac{i k_0^2}{2 k_0} \right\} \langle \hat{u}(\underline{z}, k_{\underline{r}}) \rangle + \frac{k_0^2}{4} \iiint_{-\infty}^{+\infty} \underline{z} F(\underline{z}-\underline{z}', k_{\underline{r}_1}) G(\underline{z}, k_{\underline{r}} - k_{\underline{r}_1}, \underline{z}', k_{\underline{r}_1} - k_{\underline{r}_2}) \langle \hat{u}(\underline{z}', k_{\underline{r}_2}) \rangle dk_{\underline{r}_1} dk_{\underline{r}_2} d\underline{z}' \quad (\text{A3.7})$$

Since the function  $F(\underline{z}-\underline{z}', k_{\underline{r}_1})$  is a peaked function of the argument  $\underline{z}-\underline{z}'$ , one infers that the main contribution to the integral over  $\underline{z}'$  lies in the neighborhood of  $\underline{z} \cong \underline{z}'$ . We shall expand the functions  $G$  and  $\langle \hat{u} \rangle$  in powers of  $\underline{z}-\underline{z}'$ , viz:

$$G(\beta, p, \beta', q) = G(\beta, p, \beta, q) - (\beta - \beta') \frac{\partial G}{\partial \beta'} \Big|_{\beta' = \beta} + \frac{(\beta - \beta')^2}{2} \frac{\partial^2 G}{\partial \beta'^2} \Big|_{\beta' = \beta} + \dots$$

$$\langle \hat{u}(\beta', k_p) \rangle = \langle \hat{u}(\beta, k_p) \rangle - (\beta - \beta') \frac{\partial \langle \hat{u}(\beta', k_p) \rangle}{\partial \beta'} \Big|_{\beta' = \beta} \quad (\text{A3.8})$$

$$+ \frac{(\beta - \beta')^2}{2} \frac{\partial^2 \langle \hat{u}(\beta', k_p) \rangle}{\partial \beta'^2} \Big|_{\beta' = \beta} + \dots$$

Substituting (A3.8) into (A3.7), one obtains after some tedious calculations

$$\left\{ \frac{\partial}{\partial \beta} + \frac{i k_p^2}{2 k_0} + \frac{k_0^2}{8} A_{0,0}(\beta) \right\} \langle \hat{u}(\beta, k_p) \rangle$$

$$= \frac{k_0^2}{4} \left\{ \frac{i}{4 k_0} A_{1,2}(\beta) + \frac{k_p^2}{4 k_0^2} A_{2,2}(\beta) + \frac{A_{2,4}(\beta)}{16 k_0^2} + \dots \right. \quad (\text{A3.9})$$

$$\left. \dots \right\} \langle \hat{u}(\beta, k_p) \rangle$$

In the coordinate representation, this equation takes the form

$$\left\{ \frac{\partial}{\partial \beta} - \frac{i}{2 k_0} \nabla_p^2 + \frac{k_0^2}{8} A_{0,0}(\beta) \right\} \langle \hat{u}(\beta, \underline{r}) \rangle$$

$$= \frac{k_0^2}{16} \left\{ i A_{1,2}(\beta) - \frac{A_{2,2}(\beta)}{2 k_0} \nabla_p^2 + \frac{A_{2,4}(\beta)}{4 k_0} + \dots \right. \quad (\text{A3.10})$$

$$\left. \dots \right\} \langle \hat{u}(\beta, \underline{r}) \rangle$$

where

$$A_{\alpha}(\underline{\beta}, \underline{p}) = 2 \int_0^{\underline{\beta}} F(\underline{\beta} - \underline{\beta}', \underline{p}) (\underline{\beta} - \underline{\beta}')^{\alpha} d\underline{\beta}'$$

(A3.11)

$$A_{\alpha, \beta}(\underline{\beta}) = \iint_{-\infty}^{\infty} A_{\alpha}(\underline{\beta}, \underline{p}) |\underline{p}|^{\beta} d\underline{p}$$

(A3.12)

To use the Markov approximation, the terms on the right side in eq. (A3.10) have to be small compared to the corresponding terms on the left in this equation. Thus, one can write these conditions as follows:

$$(1) \quad k_0^2 A_{0,0} \gg A_{2,4}$$

$$(2) \quad A_{22} k_0 \ll 1$$

(A3.13)

A similar analysis can be performed for the higher moment case.

APPENDIX 4

In Appendix 2, we examined several expansions for VcG and used numerical methods to test their convergence. We assumed that the imaginary part of G was very small compared to its real part, i.e. G is approximately real. This is not generally true. Hence all of the results in Appendix 2 only apply to ranges wherein G is real.

Behavior of G w.r.t.  $k_3 (=B+i\epsilon)$ :

We are dealing with the simple case defined by the equation:

$$i \frac{\partial}{\partial \beta} \hat{G} - \tilde{V} \hat{G} = \frac{1}{\tilde{V}} \quad (\text{A4.1})$$

where  $\tilde{V}$  is a random number. Taking the Fourier transform of (A4.1), one obtains the algebraic equation:

$$(B + i\epsilon - \tilde{V}) \hat{g}_k = 1 \quad (\text{A4.2})$$

$$\hat{g}_k = \frac{1}{B + i\epsilon - \tilde{V}} \quad (\text{A4.3})$$

Therefore

Real part of  $\hat{g}_k = \frac{B - \tilde{V}}{(B - \tilde{V})^2 + \epsilon^2} = \hat{g}_{kr} \quad (\text{A4.4a})$

Img. part of  $\hat{g}_k = \frac{-\epsilon}{(B-\tilde{v})^2 + \epsilon^2} = \hat{g}_{ki}$  (A4.4b)

If the probability distribution function  $F(v)$  of  $\tilde{v}$  is given, we can evaluate the average Green's function exactly:

$$\langle \hat{g}_{kr} \rangle = \int_{-\infty}^{\infty} \hat{g}_{kr}(v) F(v) dv$$

and

(A4.5)

$$\langle \hat{g}_{ki} \rangle = \int_{-\infty}^{\infty} \hat{g}_{ki}(v) F(v) dv$$

On the other hand, we can expand  $V_c g_k$  in the following way:

$$\begin{aligned} V_c g_k &= \langle \tilde{v}^2 \rangle g_k^2 + \{ \langle \tilde{v}^4 \rangle - 2 \langle \tilde{v}^2 \rangle^2 \} g_k^4 \\ &+ \{ \langle \tilde{v}^6 \rangle + 7 \langle \tilde{v}^2 \rangle^3 - 6 \langle \tilde{v}^2 \rangle \langle \tilde{v}^4 \rangle \} g_k^6 \quad (A4.6) \\ &+ \dots \end{aligned}$$

The first approximation for  $\langle \hat{g}_k \rangle$  is defined by the following equation:

$$(B + i\epsilon - \langle \tilde{v}^2 \rangle g_k) g_k = 1 \quad (A4.7)$$

The 2nd approximation is defined by:

$$[B + i\epsilon - \langle \tilde{v}^2 \rangle g_k - (\langle \tilde{v}^4 \rangle - 2\langle \tilde{v}^2 \rangle^2) g_k^3] g_k = 1 \quad (\text{A4.8})$$

etc.

We shall examine the approximate solutions of (A4.7) and (A4.8) and compare these solutions with the exact solution (A4.5) by numerical methods.

(a) For the case that  $\tilde{V}$  is uniformly distributed over a range from  $-a$  to  $+a$ , one obtains for the 2nd moment of  $\tilde{V}$ :

$$\langle \tilde{v}^2 \rangle = \frac{a^2}{3}$$

and for the 4th moment of  $\tilde{V}$ :

$$\langle \tilde{v}^4 \rangle = \frac{a^4}{5}$$

Substituting these moments into eq. (A4.7) and (A4.8) and using contour integral techniques, we evaluate  $g_k$  as a function of  $B$  and depicted in Fig.(A4.1) to Fig.(A4.6).

Explanations of Figures:

Fig A4.1:

variance = 0.333

dotted line = 1st approx. of  $g_{kr}$

solid line = 2nd approx. of  $g_{kr}$

Fig. A4.2:

The exact solution of  $g_{kr}$  for  $\langle \tilde{v}^2 \rangle = 0.333$

Fig. A4.3 :

variance = 2.083

dotted line = 1st approx. of  $g_{kr}$

solid line = 2nd approx. of  $g_{kr}$

Fig. A4.4:

The exact solution of  $g_{kr}$  for  $\langle \tilde{v}^2 \rangle = 2.083$

var= 3 33329e-01

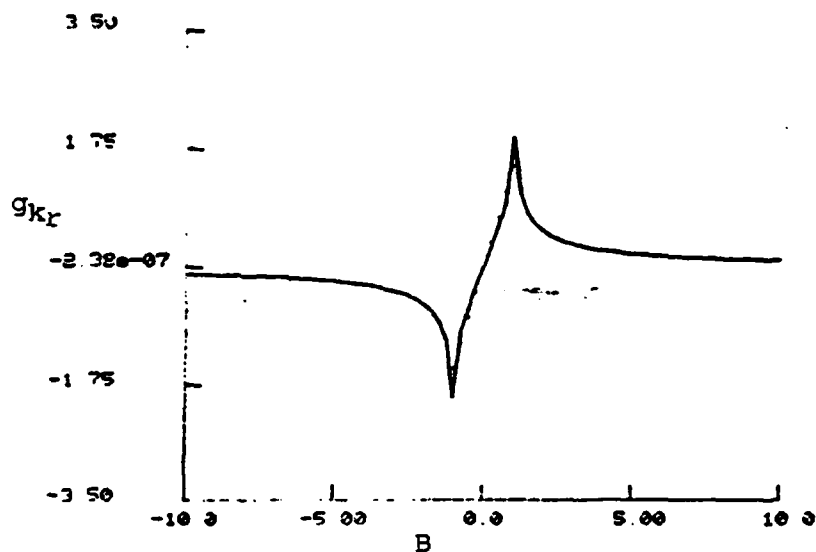


Fig. A4.1.  $g_{kr}$  vs.  $B$ ;  $\tilde{v}$  is uniformly distributed over a range  $(-a, +a)$ ;  $\langle \tilde{v}^2 \rangle = 0.333$ ; 1st approx. dotted line; 2nd approx. solid line.

gfev P'var'.Ko  
var= 3 33329e-01

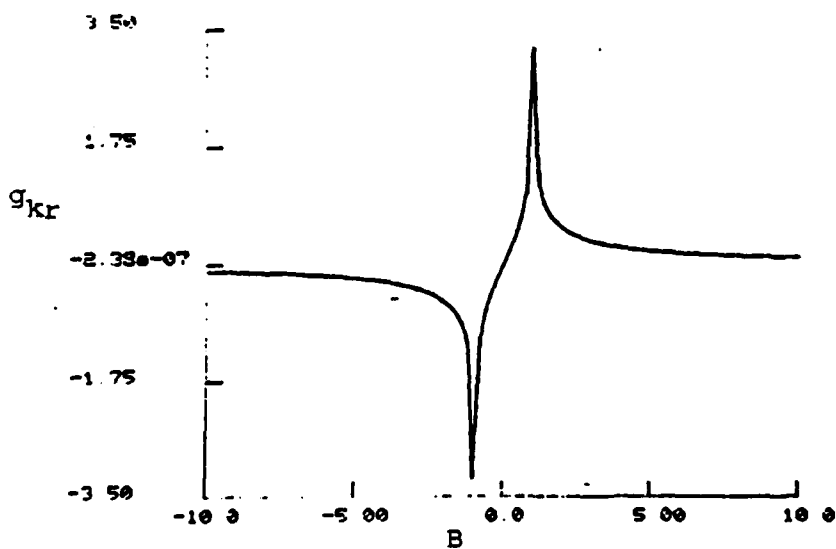


Fig. A4.2. The exact solution of  $g_{kr}$ ;  $\langle \tilde{v}^2 \rangle = 0.333$ .

var = 2.08328

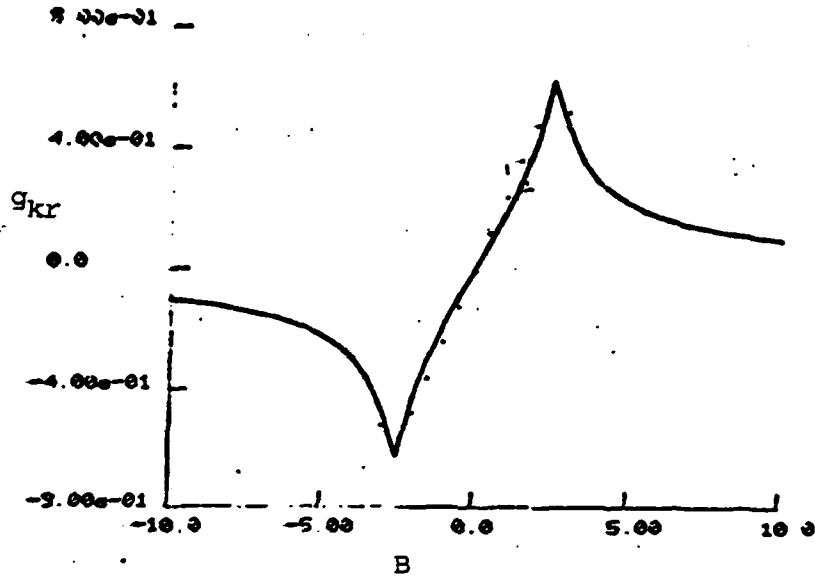
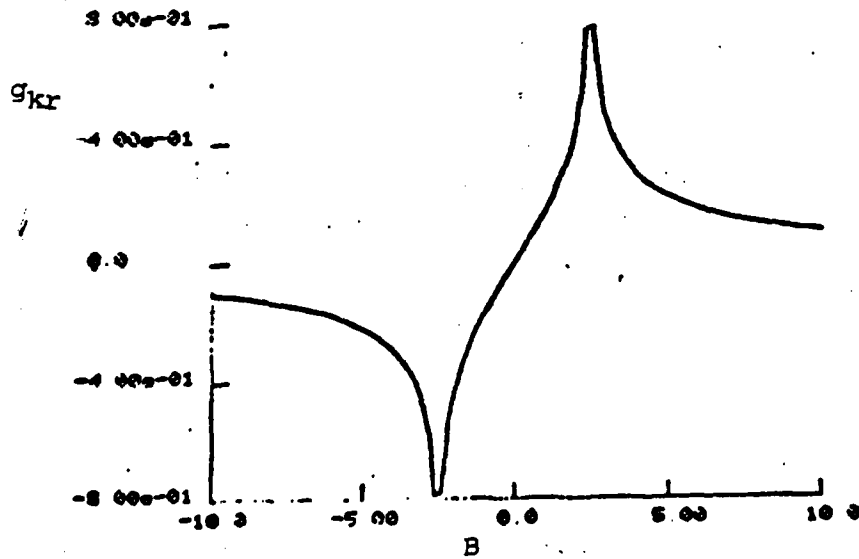


Fig. A4.3.  $g_{kr}$  vs.  $B$ ;  $\tilde{v}$  is uniformly distributed over a range  $(-a, +a)$ ;  $\langle \tilde{v}^2 \rangle = 2.083$ ; 1st approx. dotted line; 2nd approx. solid line.

Fig. A4.4. The exact solution of  $g_{kr}$  for  $\langle \tilde{v}^2 \rangle = 2.083$ .

var = 2.08328



var= 8.33312

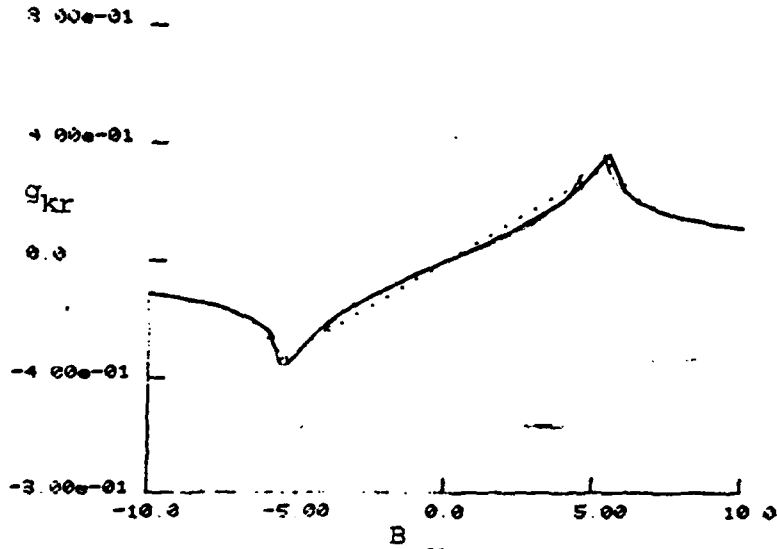


Fig. A4.5.  $g_{kr}$  vs.  $B$ ;  $\tilde{v}$  is uniformly distributed over a range  $(-a, +a)$ ;  $\langle \tilde{v}^2 \rangle = 8.333$ ; 1st approx. dotted line; 2nd approx. solid line.

var= 8.33312

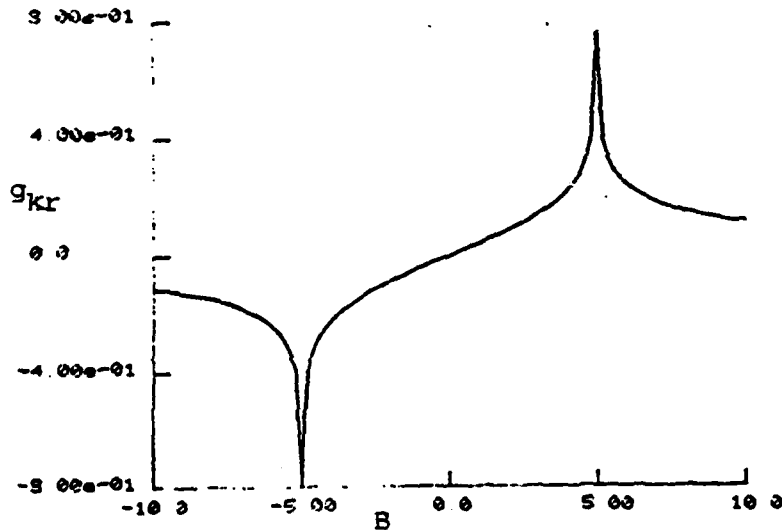


Fig. A4.6. The exact solution of  $g_{kr}$  for  $\langle \tilde{v}^2 \rangle = 8.333$ .

Fig. A4.5:

variance = 8.333

dotted line = 1st approx. of  $g_{kr}$

solid line = 2nd approx. of  $g_{kr}$

Fig. A4.6:

The exact solution of  $g_{kr}$  for  $\langle \tilde{V}^2 \rangle = 8.333$

Conclusion:

For a r.v.  $\tilde{V}$  with a uniform distribution the approximation procedure displays quite good convergence.

(b) For the case that  $\tilde{V}$  obeys a Gaussian statistics, one obtains for the even moments of  $V$ :

$$\langle \tilde{V}^{2n} \rangle = 1 \cdot 3 \cdot 5 \dots (2n-1) \langle \tilde{V}^2 \rangle^n$$

Substituting these moments into (A4.7), (A4.8) and applying the same technique as in (a), we can evaluate  $g_{kr}$  as a function of  $B$ . The results are shown in Fig. (A4.7).

Explanation of Fig. (A4.7):

variance = 1

dotted line = 1st approx of  $g_{kr}$

crossed line (x) = 2nd approx of  $g_{kr}$

solid line = 3rd approx of  $g_{kr}$

thin line = exact solution of  $g_{kr}$

Conclusion:

We observe that these approx. procedures do not show convergence. However, we shall consider some other observation before making any definite conclusions.

Since  $V_c$  can be evaluated exactly from the following integral:

$$V_c g_{kr} = \langle \tilde{V} \hat{g}_k \rangle = \int_{-\infty}^{\infty} v \hat{g}_k(v) F(v) dv \quad (A4.9)$$

We shall compare the real and img. parts of VcG for the 1st, 2nd and 3rd approximations, respectively, with the exact result.

For the case that  $\tilde{V}$  obeys a Gaussian statistics, we display a few plots of these results: ( write  $g_k$  as G )

Fig.A4.8:(exact result)

variance = 1

curve(1) = real part of VcG

curve(2) = img part of VcG

curve(3) = absolute value of VcG

Fig. A4.9:

variance = 1

curve (1) = real part of VcG

curve (2) = img part of VcG

curve (3) = absolute value of VcG

Fig. A4.10:

variance = 1

curve (1) = real part of VcG

curve(2) = img part of VcG

curve (3) = absolute value of VcG

Fig. A4.11:

For variance = 0.25

curve (1) = real part of VcG

curve (2) = img part of VcG

curve(3) = absolute value of VcG

Fig. A4.12:

For  $\langle \tilde{V}^2 \rangle = 0.25$

curve ( 1) = real part of VcG

curve (2) = img. part of VcG

curve (3) = absolute value of VcG

Fig. A4.13:

for  $\langle \tilde{V}^2 \rangle = 0.25$

curve (1) = real part of VcG

curve (2) = img. part of VcG

curve (3) = absolute value of VcG

The above observations show that one can not get a good approx. for VcG by taking a finite number of terms in eq. (A4.6) for a Gaussian statistics. We conclude that the "moment" expansion for VcG is not suitable for a Gaussian statistics.

For the case that  $\tilde{V}$  is uniformly distributed over the range from -0.5 to +0.5, we plot VcG both exactly and for several approximations, viz:

Fig. A4.14: (exact result)

variance =  $8.333 \times 10^{-2}$

curve (1) = real part of VcG

curve (2) = img part of VcG

curve (3) = absolute value of VcG

Fig.A4.15: (1st approx.)

variance =  $8.333 \times 10^{-2}$

curve (1) = real part of VcG

curve (2) = img part of VcG

curve (3) = absolute value of VcG

Fig. A4.16: (2nd approx)

variance =  $8.333 \times 10^{-2}$

curve (1) = real part of VcG

curve (2) = img part of VcG

curve (3) = absolute value of VcG

We observe that eq. (A4.6) provides a rapidly convergent series expansion for VcG when  $\tilde{V}$  obeys a uniform statistics.

var= 9.59986e-01

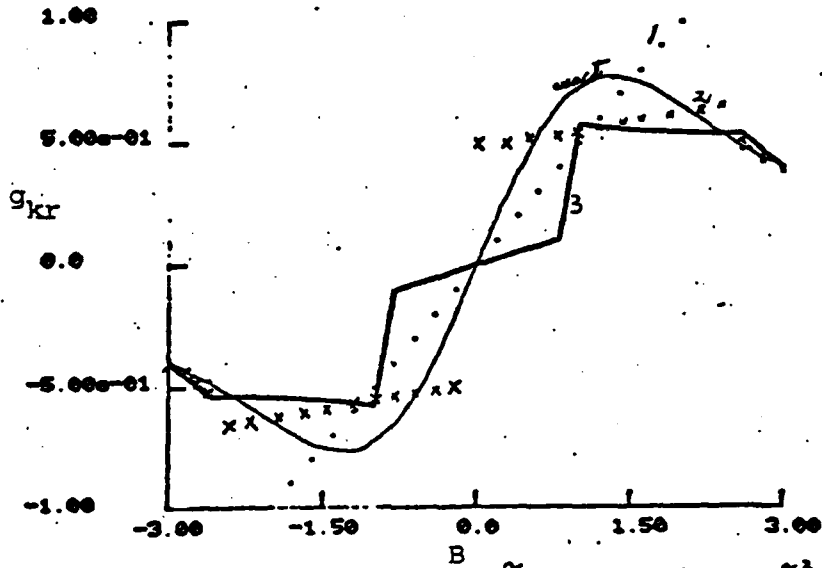


Fig. A4.7.  $g_{Kr}$  vs.  $B$ ;  $\tilde{v}$  is Gaussian;  $\langle \tilde{v}^2 \rangle = 1$ .  
 (1) ... 1st approx.; (2) xxx 2nd approx.;  
 (3) \_\_\_ 3rd approx.; (4) thin line; exact solution.

var= 9.9935e-01  
 $\tilde{v} = +1 \text{ } \tilde{v} = -1 \text{ } \tilde{v}$

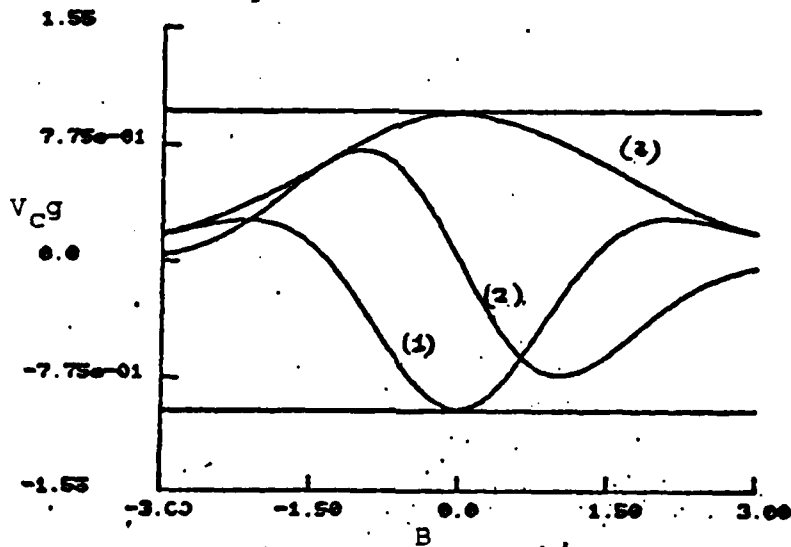


Fig. A4.8.  $\tilde{v}$  is Gaussian;  $\langle \tilde{v}^2 \rangle = 1$ ; (1) real part of  $V_{Cg}$ ; (2) Img. part of  $V_{Cg}$ ; (3) absolute value of  $V_{Cg}$ .

var= 9.90386e-01

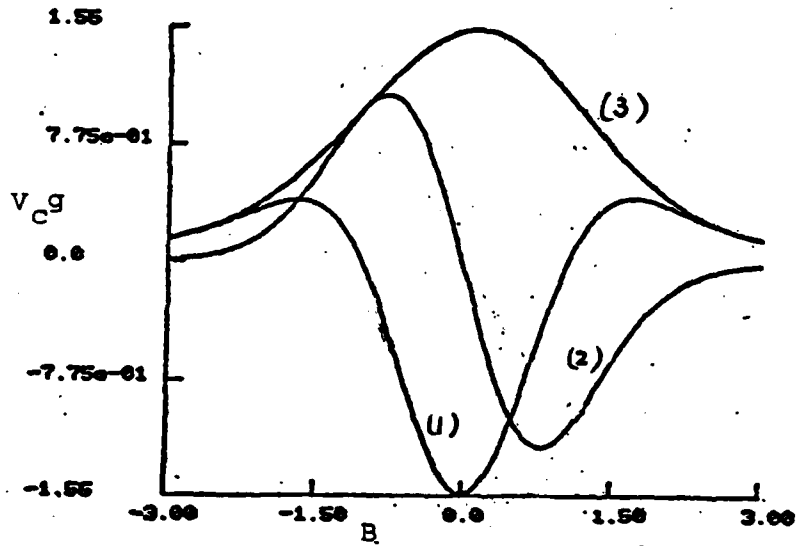


Fig. A4.9. 1st approx. of Fig. A4.8.

P'var=Ko'00P'var=Ko

var= 9.90386e-01

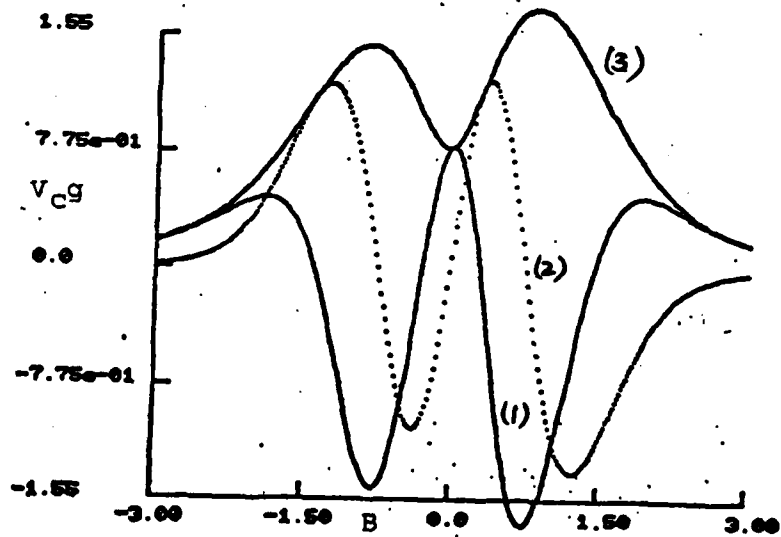


Fig. A4.10. 2nd approx. of Fig. A4.8.

var= 2.50000e-01

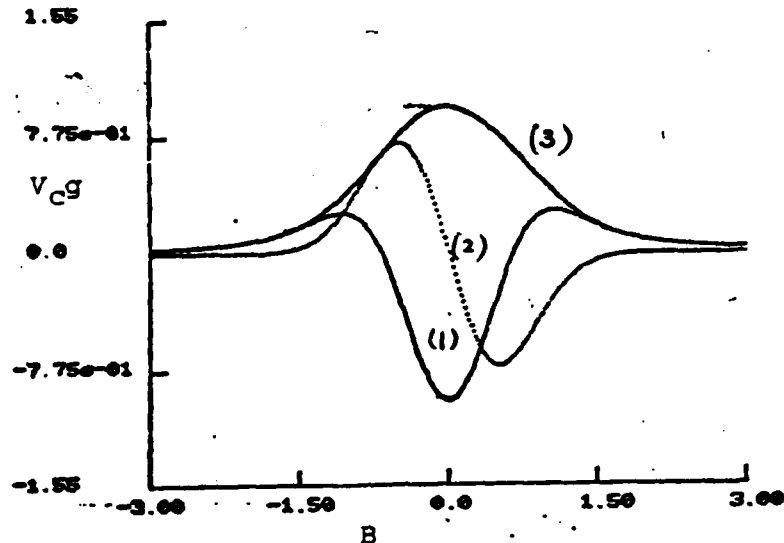


Fig. A4.11.  $v$  is Gaussian; ; (1) real part of  $V_{Cg}$ ; (2) Img. part of  $V_{Cg}$ ; (3) absolute value of  $V_{Cg}$ .  $\langle \tilde{v}^2 \rangle = 0.25$ .

var= 2.50000e-01

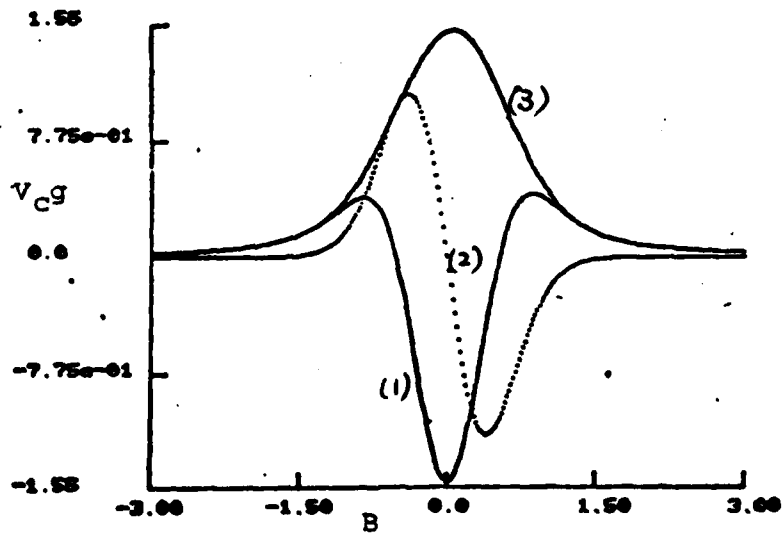


Fig. A4.12. 1st approx. of Fig. A4.11.

var- 2.50000-01

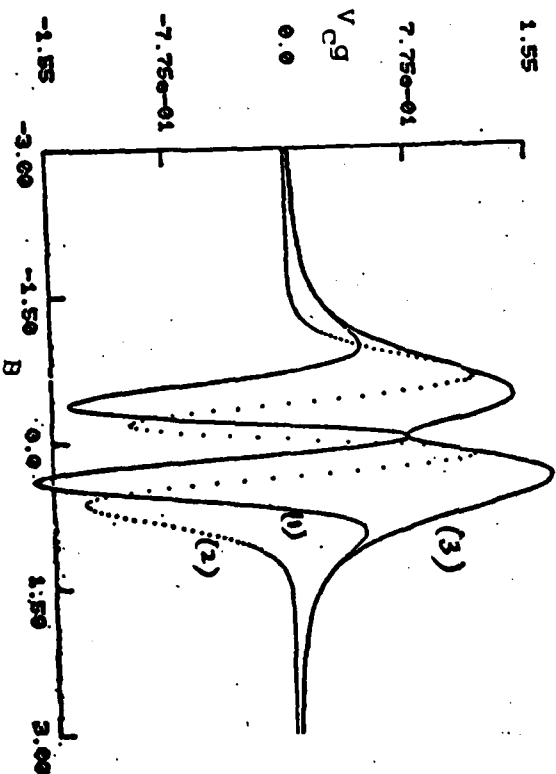


Fig. A4.13. 2nd approx. of Fig. A4.11.

var= 8.33333e-02  
 'S +1 v z -1 v

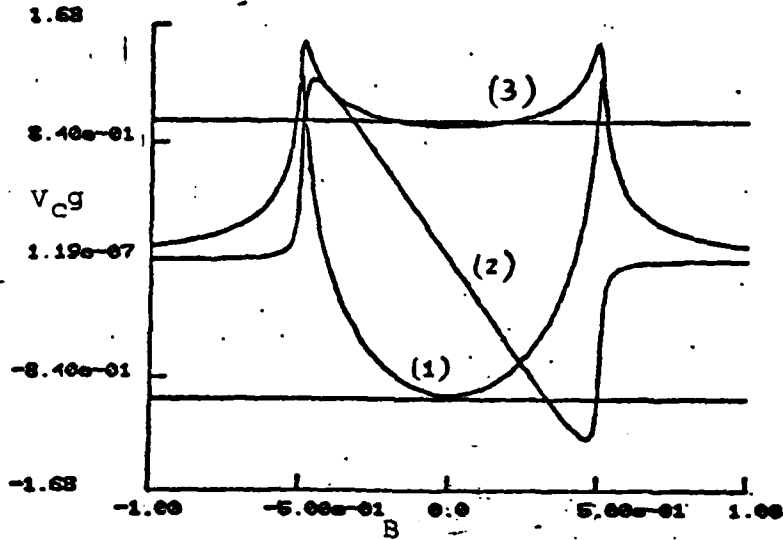


Fig. A4.14.  $V_{cg}$  vs.  $B$ ;  $\tilde{v}$  is uniformly distributed over a range  $(-0.5, +0.5)$ ; (1) real part of  $V_{cg}$ ; (2) Img. part of  $V_{cg}$ ; (3) absolute value of  $V_{cg}$ .

var= 8.33333e-02

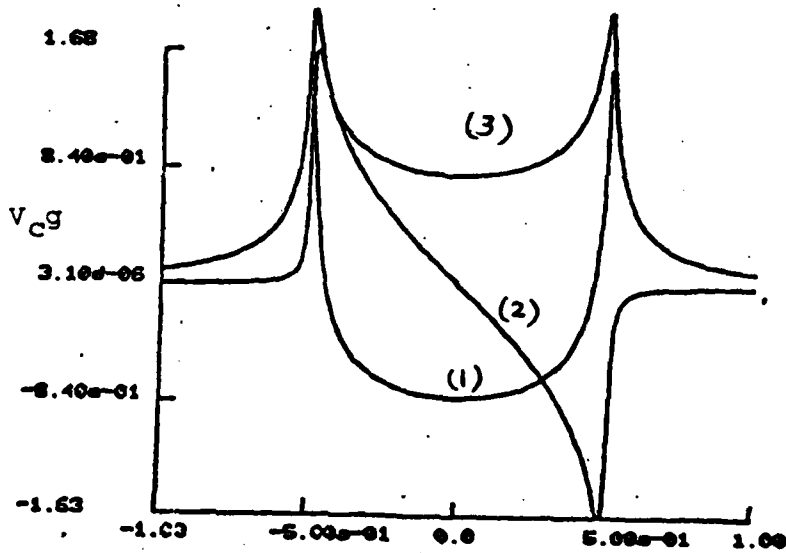


Fig. A4.15. 1st approx. of Fig. A4.14.

WJ 8.33333-08

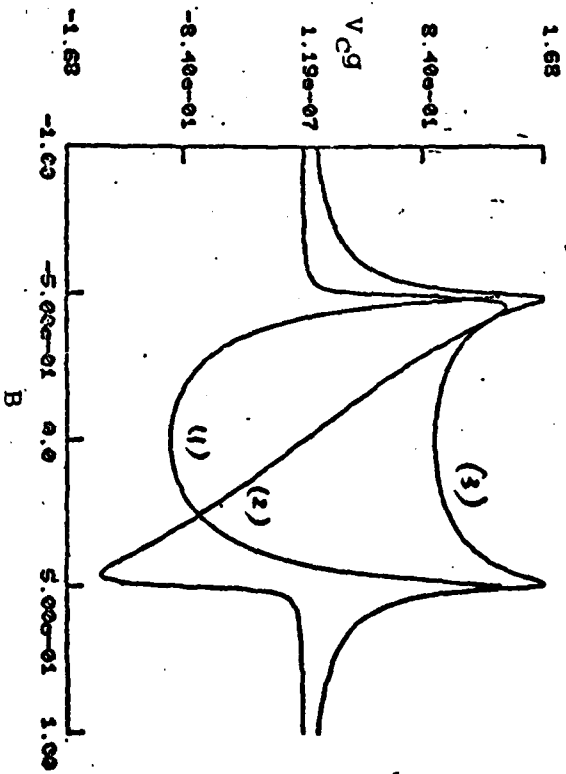


Fig. A4.16. 2nd approx. of Fig. A4.14.

APPENDIX 5

Limits of Application of The Parabolic Equation

The parabolic equation differs from the complete scalar wave equation by a term  $\partial^2 \hat{u} / \partial \bar{z}^2$ . If one treats  $\partial^2 \hat{u} / \partial \bar{z}^2$  as a small perturbation term and writes

$$2ik_0 \frac{\partial \hat{u}}{\partial \bar{z}} + \nabla_{\rho}^2 \hat{u} + k_0^2 \tilde{\epsilon} \hat{u} = - \frac{\partial^2 \hat{u}}{\partial \bar{z}^2} \quad (\text{A5.1})$$

then one expands

$$\hat{u}(\bar{z}, \rho) = \hat{u}_1(\bar{z}, \rho) + \hat{u}_2(\bar{z}, \rho) + \dots \quad (\text{A5.2})$$

and supposes that  $\hat{u}_2$  is of the same order of smallness as  $\partial^2 \hat{u}_1 / \partial \bar{z}^2$ .

Substituting (A5.2) into (A5.1) and equating groups of terms of the same order, one obtains

$$\begin{aligned} 2ik_0 \frac{\partial \hat{u}_1}{\partial \bar{z}} + \nabla_{\rho}^2 \hat{u}_1 + k_0^2 \tilde{\epsilon} \hat{u}_1 &= 0 \\ 2ik_0 \frac{\partial \hat{u}_2}{\partial \bar{z}} + \nabla_{\rho}^2 \hat{u}_2 + k_0^2 \tilde{\epsilon} \hat{u}_2 &= - \frac{\partial^2 \hat{u}_1}{\partial \bar{z}^2} \end{aligned} \quad (\text{A5.3})$$

with the boundary conditions

$$\hat{u}_1(0, \rho) = u_0(\rho) \quad \text{and} \quad \hat{u}_2(0, \rho) = 0$$

one finds on taking the ensemble average of (A5.3)

$$\left\{ 2ik_0 \frac{\partial}{\partial z} + \nabla_{\rho}^2 \right\} \langle \hat{u}_1 \rangle + k_0^2 \langle \tilde{\epsilon} \hat{u}_1 \rangle = 0 \quad (\text{A5.4a})$$

$$\begin{aligned} \left\{ 2ik_0 \frac{\partial}{\partial z} + \nabla_{\rho}^2 \right\} \langle \hat{u}_2 \rangle + k_0^2 \langle \tilde{\epsilon} \hat{u}_2 \rangle \\ = - \frac{\partial^2 \langle \hat{u}_1 \rangle}{\partial z^2} \end{aligned} \quad (\text{A5.4b})$$

Using the renormalization procedure described in Appendix 1, one writes equation (A5.4a) as

$$(L_0 - V_c) \langle \hat{u} \rangle = 0$$

on using of the approximation

$$V_c u \cong \int \langle \tilde{v}(z, \rho) G(z, \rho, z', \rho') \tilde{v}(z', \rho') \rangle u(z', \rho') dz' d\rho' \quad (\text{A5.5})$$

and the assumption that

$$\langle \tilde{\epsilon}(z, \rho) \tilde{\epsilon}(z', \rho') \rangle = \delta(z-z') A(\rho-\rho') \quad (\text{A5.6})$$

One obtains, after some manipulation,

$$\begin{aligned} V_c u &= - \frac{i k_0^2}{4} u(\bar{z}, \rho) \frac{A(0)}{2} \\ &= - \frac{i k_0^2}{8} A(0) u(\bar{z}, \rho) \end{aligned} \quad (\text{A5.7})$$

Therefore, we can rewrite eq. (A5.4a) as follows:

$$2 i k_0 \frac{\partial u_1}{\partial \bar{z}} + \nabla_{\rho}^2 u_1 + \frac{i k_0^3}{4} A(0) u_1 = 0 \quad (\text{A5.8})$$

Similarly, eq. (A5.4b) can be rewritten as

$$2 i k_0 \frac{\partial u_2}{\partial \bar{z}} + \nabla_{\rho}^2 u_2 + \frac{i k_0^3}{4} A(0) u_2 = - \frac{\partial^2 u_1}{\partial \bar{z}^2} \quad (\text{A5.9})$$

Let us consider the case of a plane wave incident upon a random medium such that

$$u_0(\rho) = \text{constant} = u_0$$

One obtains, from equation (A5.4a), that

$$\begin{aligned} u_1(\bar{z}) &= u_0 e^{-\frac{k_0^2 A(0)}{8} \bar{z}} \\ &= u_0 e^{-\frac{1}{2} \alpha \bar{z}} \end{aligned} \quad (\text{A5.10})$$

where

$$\alpha = \frac{1}{4} k_0^2 A(0)$$

equation (A5.4b) then takes form

$$\frac{du_2}{dz} + \frac{k_0^2 A(0)}{8} u_2 = -\frac{\partial^2 u_1}{\partial z^2} = u_0 \left(\frac{1}{4} \alpha^2\right) e^{-\frac{1}{2} \alpha z} \quad (\text{A5.11})$$

The solution of eq. (A5.11) corresponding to the boundary condition  $u_2(0) = 0$  can be calculated as follows:

set

$$u_2 = u_2' e^{-\frac{1}{2} \alpha z} \quad (\text{A5.12})$$

One obtains from eq. (A5.5)

$$u_2'(z) = u_2'(0) + \frac{i k_0^3 A(0) u_0}{128} z \quad (\text{A5.13})$$

Therefore

$$\begin{aligned} u_2(z) &= u_0 e^{-\frac{1}{2} \alpha z} \frac{i k_0^3 A^2(0)}{128} z \\ &= u_1 \frac{i k_0^3 A^2(0)}{128} z \end{aligned} \quad (\text{A5.15})$$

In this case

$$\begin{aligned} u(z) &= u_1(z) + u_2(z) + \dots \\ &= u_0 e^{-\frac{1}{2} \alpha z} \left[ 1 + \frac{i \alpha^2 z}{8 k_0} + \dots \right] \end{aligned} \quad (\text{A5.16})$$

The field  $u_1$  should be considered only in the region where it is marking different from zero, i.e. for  $\lambda \delta \leq 1$ , thus, we obtain the condition for a small correction term,

$$\text{i.e. } \frac{\alpha^2}{k_0} \cdot \frac{1}{\alpha} \ll 1$$

$$\alpha \ll k_0 \quad \text{or} \quad \lambda \alpha \ll 1 \quad (\text{A5.17})$$

If condition (A5.17) is valid then the correction term in eq. (A5.16) will be small compared to its first term. For the higher moment case, the calculation is quite complicate. For example, in the 2nd moment case, one considers the corrections to  $M_2(z, \rho_1, \rho_2) = \langle \hat{u}(z, \rho_1) \hat{u}^*(z, \rho_2) \rangle$ , If  $\hat{u} = \hat{u}_1 + \hat{u}_2 + \dots$ , one has

$$\begin{aligned} M_2(z, \rho_1, \rho_2) &= \langle \hat{u}_1(z, \rho_1) \hat{u}_1^*(z, \rho_2) \rangle + \\ &\quad \langle \hat{u}_1(z, \rho_1) \hat{u}_2^*(z, \rho_2) \rangle + \\ &\quad \langle \hat{u}_2(z, \rho_1) \hat{u}_1^*(z, \rho_2) \rangle + \dots \\ &= M_2^{(1)} + M_2^{(2)} + M_2^{(2)*} + \dots \end{aligned} \quad (\text{A5.18})$$

Applying the Markov approx. and some very tedious calculations, one can obtain equation for  $M_2$ ,  $M_2$ ,  $M_2$  .. as follows:

$$\left\{ 2ik_0 \frac{\partial}{\partial z} + (\nabla_{\rho_1}^2 - \nabla_{\rho_2}^2) + \frac{ik_0^3}{2} [A(0) - A(\rho_1 - \rho_2)] \right\} M_2^{(1)} = 0 \quad (\text{A5.19})$$

$$\left\{ 2ik_0 \frac{\partial}{\partial z} + (\nabla_{\rho_1}^2 - \nabla_{\rho_2}^2) + \frac{ik_0^3}{2} [A(0) - A(\rho_1 - \rho_2)] \right\}$$

$$M_2^{(2)} = \left\{ -\frac{1}{4k_0^2} \nabla_{\rho_2}^4 + \frac{ik_0 A(0)}{8} \nabla_{\rho_2}^2 + \frac{k_0^4 A^2(0)}{64} \right\} M_2^{(1)}$$

(A5.20)

$$\left\{ -2ik_0 \frac{\partial}{\partial z} + (\nabla_{\rho_2}^2 - \nabla_{\rho_1}^2) - \frac{ik_0^3}{2} [A(0) - A(\rho_2 - \rho_1)] \right\}$$

$$M_2^{(2)*} = \left\{ -\frac{1}{4k_0^2} \nabla_{\rho_1}^4 - \frac{ik_0 A(0)}{8} \nabla_{\rho_1}^2 + \frac{k_0^4 A^2(0)}{64} \right\} M_2^{(1)*}$$

(A5.21)

If the parabolic approximation is used, the correction terms  $M_2^{(2)}$  and  $M_2^{(2)*}$  have to be small compared to the 1st term  $M_2^{(1)}$ . One obtains from eq. (A5.20) and (A5.21), let  $M_2^{(2)} + M_2^{(2)*} = M_2^{(2) \prime}$ , the following equation for  $M_2^{(2) \prime}$ :

$$\begin{aligned} & \left\{ 2ik_0 \frac{\partial}{\partial z} + (\nabla_{\rho_1}^2 - \nabla_{\rho_2}^2) + \frac{ik_0^3}{2} H(\rho_1 - \rho_2) \right\} M_2^{(2) \prime} \\ & = \left\{ \frac{1}{4k_0^2} (\nabla_{\rho_1}^4 - \nabla_{\rho_2}^4) + \frac{ik_0 A(0)}{8} (\nabla_{\rho_1}^2 + \nabla_{\rho_2}^2) \right\} M_2^{(1)} \end{aligned}$$

(A5.22)

Let us now consider the case of a plane incident wave, one obtains

$$M_2^{(1)} = |u_0|^2 e^{-\frac{k_0^2}{4} [A(0) - A(\underline{\rho}_1 - \underline{\rho}_2)] \underline{\beta}} \quad (\text{A5.23})$$

In this case

$$M_2^{(2)'}(\underline{\beta}, \underline{\rho}_1, \underline{\rho}_2) = M_2^{(2)'}(\underline{\beta}, \underline{\rho}_1 - \underline{\rho}_2) \quad (\text{A5.24})$$

Moreover

$$\begin{aligned} (\nabla_{\rho_1}^2 - \nabla_{\rho_2}^2) M_2^{(2)'} &= 0 \\ (\nabla_{\rho_1}^4 - \nabla_{\rho_2}^4) M_2^{(1)} &= 0 \\ (\nabla_{\rho_1}^2 + \nabla_{\rho_2}^2) M_2^{(1)} &= 2 \nabla_{\rho_1}^2 M_2^{(1)} \end{aligned} \quad (\text{A5.25})$$

Equation (A5.22) thus takes the form

$$\begin{aligned} \left\{ 2ik_0 \frac{\partial}{\partial \underline{\beta}} + \frac{ik_0^3}{2} H(\underline{\rho}) \right\} M_2^{(2)'}(\underline{\beta}, \underline{\rho}) \\ = \frac{ik_0 A(0)}{4} \nabla_{\underline{\rho}}^2 M_2^{(1)} \end{aligned} \quad (\text{A5.26})$$

from (A5.23), one finds

$$M_2^{(2)'} = M_2^{(1)} \frac{A(0)}{8} \left\{ \frac{k_0^4 \bar{z}^3 [H'(\rho)]^2}{48} - \frac{k_0^2 \bar{z}^2 \nabla_\rho^2 H(\rho)}{8} \right\} \quad (\text{A5.27})$$

Therefore

$$M_2(\bar{z}, \rho) = M_2^{(1)}(\bar{z}, \rho) \left\{ 1 + \frac{A(0)}{8} \left[ \frac{k_0^4 \bar{z}^3 [H'(\rho)]^2}{48} - \frac{k_0^2 \bar{z}^2 \nabla_\rho^2 H(\rho)}{8} + \dots \right] \right\} \quad (\text{A5.28})$$

this leads to the condition:

if  $\left| \frac{A(0)}{8} \left\{ \frac{k_0^4 \bar{z}^3 [H'(\rho)]^2}{48} - \frac{k_0^2 \bar{z}^2 \nabla_\rho^2 H(\rho)}{8} \right\} \right| \ll 1$

then

$$M_2^{(2)'} \ll M_2^{(1)}$$

Appendix 6

The equations to be solved are:

$$\frac{\partial M_R}{\partial \delta} = - \frac{\partial}{\partial r_1} \frac{\partial}{\partial r_2} M_i - \tau f M_R \quad (\text{A6.1})$$

$$\frac{\partial M_i}{\partial \delta} = \frac{\partial}{\partial r_1} \frac{\partial}{\partial r_2} M_R - \tau f M_i \quad (\text{A6.2})$$

One writes

$$\begin{aligned} M_R (\delta + \Delta \delta) &= M_R + \left[ - \frac{\partial}{\partial r_1} \frac{\partial}{\partial r_2} M_i - \tau f M_R \right] \Delta \delta \\ &+ \left[ - \frac{\partial}{\partial r_1} \frac{\partial}{\partial r_2} \left( \frac{\partial}{\partial r_1} \frac{\partial}{\partial r_2} M_R - \tau f M_i \right) - \tau f \right. \\ &\left. \left( - \frac{\partial}{\partial r_1} \frac{\partial}{\partial r_2} M_i - \tau f M_R \right) \right] \frac{(\Delta \delta)^2}{2} + \dots \end{aligned} \quad (\text{A6.3})$$

and

$$\begin{aligned} M_i (\delta + \Delta \delta) &= M_i + \left[ \frac{\partial}{\partial r_1} \frac{\partial}{\partial r_2} M_R - \tau f M_i \right] \Delta \delta \\ &+ \left[ \frac{\partial}{\partial r_1} \frac{\partial}{\partial r_2} \left( - \frac{\partial}{\partial r_1} \frac{\partial}{\partial r_2} M_i - \tau f M_R \right) - \tau f \right. \\ &\left. \left( \frac{\partial}{\partial r_1} \frac{\partial}{\partial r_2} M_R - \tau f M_i \right) \right] \frac{(\Delta \delta)^2}{2} + \dots \end{aligned} \quad (\text{A6.4})$$

The difference equations, to the 2nd order accuracy in  $z$ , are:

$$\begin{aligned}
 M_R(\bar{z} + \Delta\bar{z}) &= M_R - \left[ \frac{d_{r_1}'' d_{r_2}'}{\Delta r_1 \Delta r_2} M_i + \tau f M_R \right] \Delta\bar{z} \\
 &+ \left[ - \frac{d_{r_1}' d_{r_2}''}{\Delta r_1 \Delta r_2} \left[ \frac{d_{r_1}'' d_{r_2}'}{\Delta r_1 \Delta r_2} M_R - \tau f M_i \right] - \right. \\
 &\left. \tau f \left[ - \frac{d_{r_1} d_{r_2}}{4 \Delta r_1 \Delta r_2} M_i - \tau f M_R \right] \right] \frac{(\Delta\bar{z})^2}{2}
 \end{aligned} \tag{A6.5}$$

and

$$\begin{aligned}
 M_i(\bar{z} + \Delta\bar{z}) &= M_i + \left[ \left( \frac{\Delta\bar{z}}{\Delta r_1 \Delta r_2} \right) d_{r_1}'' d_{r_2}' M_R - (\tau f \Delta\bar{z}) M_i \right] \\
 &+ \frac{1}{2} \left\{ \left[ - \left( \frac{\Delta\bar{z}}{\Delta r_1 \Delta r_2} \right) d_{r_1}' d_{r_2}'' \left[ \left( \frac{\Delta\bar{z}}{\Delta r_1 \Delta r_2} \right) d_{r_1}'' d_{r_2}' M_i \right. \right. \right. \\
 &\left. \left. + (\tau f \Delta\bar{z}) M_R \right] - (\tau f \Delta\bar{z}) \left[ \frac{\Delta\bar{z}}{4 \Delta r_1 \Delta r_2} d_{r_1} d_{r_2} - \right. \right. \\
 &\left. \left. (\tau f \Delta\bar{z}) M_i \right] \right\}
 \end{aligned} \tag{A6.6}$$

where

- $d_{r_i}' =$  forward difference operator w.r.t.  $r_i$ .
- $d_{r_i}'' =$  backward difference operator w.r.t.  $r_i$ .
- $d_{r_i} =$  center difference operator w.r.t.  $r_i$ .

The boundary conditions for  $M_4$  are described in equations (4.46) and (4.47).

BIBLIOGRAPHY

1. V. I. Tatarskii, " The Effect of the Turbulent Atmosphere on Wave Propagation," U. S. Dept. of Commerce, TT-68-50464, Springfield, Virginia.
2. E. Collett and R. Alferness, " Depolarization of a laser beam in a turbulent medium," J. Opt. Soc. Amer., vol. 62, 529-533, 1972.
3. H. G. Booker, " Diffraction from an ionospheric screen with application to ionospheric problems," Phil. Trans. Roy. Soc., vol. A242, 579-607, 1950.
4. R. P. Mercier, " Diffraction by a screen causing large random phase fluctuations, " Proc. Cambridge Phil. Soc., vol. 58, 382-400, 1962.
5. B. H. Briggs and I. A. Parkin, " On the variation of radio star and satellite scintillations with zenith angle, " J. Atmos. Terr. Phys., vol. 25, 339-365, 1963.
6. C. L. Rufenach, " Ionospheric scintillation by a random phase screen: spectral approach," Radio Sci., vol. 10, 155-165, 1975.
7. D. de Wolf, "Saturation of irradiance fluctuations due to turbulent atmosphere," J. Opt. Soc. Am. vol. 58, 461-466, 1968.
8. V. Frisch, " Wave propagation in random medium," in " Probabilistic Methods in Applied Math." vol. 1, 76-198, Academic Press, New York.
9. W. P. Brown, "Moment equations for waves propagated in random media," J. Opt. Soc. Am., vol 62, 1, 45-54, 1972a.
10. W. P. Brown, "Fourth moment of a wave propagating in a random medium," J. Opt. Soc. Am., vol. 62, 966-971, 1972b.
11. A. I. Kon, "Focusing of light in a turbulent medium," Radiofizika, vol. 13, 61, 43-50, 1970.
12. S. F. Clifford, "Saturation of optical scintillation by strong turbulence," J. Opt. Soc. Am., vol. 64, 148-154, 1974.

13. K. Furutsu, "Statistical theory of wave propagation in a random medium and the irradiance distribution function," J. Opt. Soc. Am., vol. 62, 240-254, 1972.
14. K. Furutsu, "On the statistical theory of electromagnetic waves in a fluctuation medium (I)," J. of Res. of N.B.S., vol. 67d, 3, 303-323, 1963.
15. Y. N. Barabanenkov, Y. A. Kravtsov, S. M. Rytov, V. I. Tatarski, "Status of the theory of propagation of waves in a randomly onhomogeneous medium," Sov. Phys. Usp., vol. 13, 551-580, 1971.
16. Y. N. Barabanenkov, "Application of the smooth-perturbation method to the solution of general equation of multiple wave scattering theory," Sov. Phys. JETP, vol.27,6, 954-959, 1968.
17. D. de Wolf, "Strong irradiance fluctuations in turbulent air: Plane waves," J. Opt. Soc. Am., vol. 63,2, 171-178, 1973.
18. D. de Wolf, "Strong irradiance fluctuations in turbulent air: Spherical waves," J. Opt. Soc. Am., vol. 63, 10, 1249-1253, 1973.
19. D. de Wolf, "Waves in random media: weak scattering reconsidered," J. Opt. Soc. Am., vol.68, 475-479, 1978.
20. D. de Wolf, "Operator and diagram techniques for solving intensity moment equations in random media: Application to strong scattering," Radio Science, vol. 14, 2, 277-286, 1979.
21. R. L. Fante, "Some new results on propagation of electromagnetic waves in strongly turbulent media," IEEE trans. AP, vol. 23, 3, 382-385, 1975.
22. R. L. Fante, "Some results for the variance of the irradiance of a finite beam in a random medium," J. Opt. Soc. Am., vol. 65, 5, 608-610, 1975.
23. R. L. Fante, "Comparison of theories for intensity fluctuations in strong turbulence," Radio Science, vol. 11, 3, 215-219, 1976.
24. R. L. Fante, "Mutual coherence function and frequency spectrum of a laser beam propagating through atmospheric turbulence," J. Opt. Soc. Am., vol. 64, 5, 592-598, 1974.

25. A. Ishimaru, "Wave propagation and scattering in random media," Academic Press, vol. 1,2, 1978.
26. A. Ishimaru, "Fluctuations of a beam wave propagating through a locally homogeneous medium," Radio Science, vol. 4, 4, 295-305, 1969a.
27. A. Ishimaru, "Fluctuations of a focused beam wave for atmospheric turbulence probing," Proc. IEEE, vol. 57, 4, 407-419, 1969b.
28. A. Ishimaru, "Theory and application of wave propagation and scattering in random media," Proc. IEEE, vol. 65, 1030-1061, 1977a.
29. A. Ishimaru, "Correlation functions of a wave in a random distribution of stationary and moving scatterers," Radio Science, vol. 10, 1, 45-52, 1975.
30. S. A. Bowhill, "The scattering of radio waves by an extended randomly refracting medium," J. of Atmo. and Terr. Phys., vol. 20, 9-18, 1961.
31. S. A. Bowhill, "Statistics of a radio wave diffracted by a random ionosphere," J. of Res. of N.B.S., vol. 65d, 3, 275-292, 1961.
32. H. G. Booker, "The use of radio stars to study irregular refraction of radio waves in the ionosphere," Proc. of IRE, 298-314, 1958.
33. R. Buckley, "Diffraction by a random phase changing screen: A numerical experiment," J. of Atmo. and Terr. Phys., vol. 37, 1431-1446, 1975.
34. H. Bremmer, "General remarks concerning theories dealing with scattering and diffraction in random media," Radio Science, vol. 8, 6, 511-534, 1973.
35. R. K. Crane, "Spectra of ionospheric scintillation," J. of Atmo. and Terr. Phys., vol. 81, 13, 2041-2050, 1976.
36. R. K. Crane, "Ionospheric scintillation," Proc. of IEEE, vol. 65, 2, 180-199, 1977.

37. E. Costa, M. C. Kelley, "Ionospheric scintillation calculations based on the in situ irregularity spectra," Radio Science, vol. 12, 5, 797-809, 1977.
38. S. Basu, "Model of equatorial scintillation from in situ measurements," Radio Science, vol. 11, 10, 821-832, 1976.
39. H. E. Whitney, S. Basu, "The effect of ionospheric scintillation on VHF/UHF satellite communications," Radio Science, vol. 12, 1, 123-133, 1977.
40. S. Basu, R. S. Allen, J. Aarons, "A detailed study of a brief period of radio star and satellite scintillations," J. of Atmo. and Terr. Phys., vol. 26, 811-823, 1964.
41. J. Aarons, R. S. Allen, T. Elkins, "Frequency dependence of radio star scintillations," J. Geophys. Res., vol. 72, 2891-2902, 1967.
42. S. Basu, M. C. Kelley, "A review of recent observations of equatorial scintillations and their relationship to current theories of F region irregularity generation," Radio Science, vol. 14, 3, 471-485, 1979.
43. S. Basu, S. Basu, J. Aarons, J. P. McClure, M. D. Cousins, "On the coexistence of Km and meter scale irregularities in the nighttime equatorial F region," J. Of Geophys. Res., vol. 83, 49, 1978.
44. H. E. Whitney, "Note on the relationship of scintillation index to probability distributions and their uses for system design," AFCRL-TR-74-0004, USAF, Hanscom field, Mass. 01730, 1974.
45. D. G. Singleton, " Power spectra of ionospheric scintillations," J. of Atmo. and Terr. Phys., vol. 36, 113-133, 1974.
46. R. R. Taur, "Ionospheric scintillation at frequencies above 1 GHz," Cosmat Tech. Review, vol. 4, 2, 461-474, 1974.
47. R. R. Taur, "Ionospheric scintillation at 4 and 6 GHz," Cosmat. Tech. Review, vol. 3, 1, 145-163, 1973.

48. R. R. Taur, "Simultaneous 1.5 and 4 GHz ionospheric scintillation measurement," Radio Science, vol. 11, 12, 1029-1036, 1976.
49. L. S. Taylor, C. J. Infosino, "On the strong phase screen theory of ionospheric scintillations," Radio Science vol. 11, 5, 459-463, 1976.
50. L. S. Taylor, "Effects of layered turbulence on oblique waves," Radio Science, vol. 10, 1, 121-128, 1975.
51. C. L. Rino, "Ionospheric scintillation theory," IEEE trans. on AP, vol. 24, 912-915, 1976.
52. C. L. Rino, E. J. Fremouw, "Statistics for ionospherically diffracted VHF/UHF signals," Radio Science, vol. 8, 3, 223-233, 1973.
53. E. J. Fremouw, C. L. Rino, "An empirical model for F-layer scintillation at VHF/UHF," Radio Science, vol. 8, 3, 213-222, 1973.
54. C. L. Rino, "Iterative methods for treating the multiple scattering of radio waves," J. of Atmo. and Terr. Phys., vol. 40, 1011-1018, 1978.
55. C. L. Rino, R. C. Livingston, "Some new results on the statistics of radio waves scintillation 1. Empirical evidence for Gaussian statistics," J. of Geophys. Res., vol. 81, 13, 2051-2057, 1976.
56. C. L. Rino, "Some new results on the statistics of radio waves scintillation 2. Scattering from a random ensemble of locally homogeneous patches," J. Geophys. Res., vol. 81, 13, 2059-2064, 1976.
57. C. L. Rufenach, "Power law wavenumber spectrum deduced from ionospheric scintillation observations," J. of Geophys. Res., vol. 77, 25, 4761-4772, 1972.
58. C. L. Rufenach, "Wavelength dependence of radio scintillation: Ionosphere and interplanetary irregularities," J. of Geophys. Res., vol. 79, 10, 1562-2566, 1974.
59. C. L. Rufenach, "Ionospheric scintillation by a random phase screen," Radio Science, vol. 10, 11, 973-977, 1975.

60. C. H. Liu, A. W. Wernik, K. C. Yeh, M. Y. Youakim, "Effects of multiple scattering on scintillation of transionospheric signals," Radio Science, vol. 9, 599-607, 1974.
61. K. C. Yeh, C. H. Liu, M. Y. Youakim, "A theoretical study of the ionospheric scintillation behavior caused by multiple scattering," Radio Science, vol. 10, 97-106, 1975.
62. V. H. Rumsey, "Scintillation due to a concentrated layer with a power law turbulent spectrum," Radio Science, vol. 10, 107-114, 1975.
63. P. L. Dyson, J. P. McClure, W. B. Hanson, "In situ measurements of the spectral characteristics of F-region ionospheric irregularities," J. Geophys. Res., vol. 79, 1497-1502, 1974.
64. A. W. Wernik, C. H. Liu, "Ionospheric irregularities causing scintillation of GHz frequency radio signal," J. of Atmo. and Terr. Phys., vol. 36, 871-879, 1974.
65. P. E. Serafim, "Ionospheric scintillations," Science Applications, Inc., Virginia 22101, 1976.
66. A. Papoulis, "Probability, random variables, and stochastic process," McGraw Hill, 1965.
67. M. G. Kendall, A. Stuart, "The advanced theory of statistics," Hafner Publishing Co., N.Y., 1969.
68. L. C. Lee, J. R. Jokipii, "Strong scintillation in astrophysics I. The Markov approximation, its application and validity to angular broadening," The Astrophys. J., vol. 196, 695-707, 1975.
69. L. C. Lee, J. R. Jokipii, "Strong scintillation in astrophysics, III. The fluctuations in intensity," The Astrophys. J., vol. 202, 439-453, 1975.
70. S. Basu, J. P. McClure, S. Basu, W. B. Hanson, and J. Aarons, "Co-ordinated study of equatorial scintillation, in-situ and radar observations of nighttime F-region irregularities," J. of Geophys. Res., May 1980.

71. N. Marcuvitz, "Eigenmodes, Quasimodes and Quasiparticles," Philips Res. Rept., vol. 30, 357-375, 1975.
72. N. Marcuvitz, "On quasiparticle descriptions of many particle systems," IEEE trans. on Electron Dev., vol. ED-17, 3, 252-257, 1970.
73. N. Marcuvitz, "On the theory of plasma turbulence," J. of Math. Phys., vol. 15, 6, 1974.
74. N. Marcuvitz, "Quasiparticle view of wave propagation," POLY-MRI-1402-79, 1979.